Functional Characterization of the Nuclear Prolyl Isomerase FKBP25: A multifunctional suppressor of genomic instability

by

David Dilworth
B.Sc., University of Waterloo, 2009

A Dissertation Submitted in Partial Fulfillment of the
Requirements for the Degree of

DOCTOR OF PHILOSOPHY

in the Department of Biochemistry and Microbiology

Functional Characterization of the Nuclear Prolyl Isomerase FKBP25:
A multifunctional suppressor of genomic instability

by

David Dilworth
B.Sc., University of Waterloo, 2009

Supervisory Committee

Dr. Christopher J. Nelson, Supervisor
(Department of Biochemistry and Microbiology)

Dr. Caren C. Helbing, Departmental Member
(Department of Biochemistry and Microbiology)

Dr. Julian Lum, Departmental Member
(Department of Biochemistry and Microbiology)

Dr. Jürgen Ehlting, Outside Member
(Department of Biology)

ABSTRACT

The amino acid proline is unique – within a polypeptide chain, proline adopts either a *cis* or *trans* peptide bond conformation while all other amino acids are sterically bound primarily in the *trans* configuration. In proteins, the isomeric state of a single proline can have dramatic consequences on structure and function. Consequently, *cis-trans* interconversion confers both barrier and opportunity – on one hand, isomerization is a rate limiting step in *de novo* protein folding and on the other can be utilized as a post-translational regulatory switch. Peptidyl-prolyl isomerases (PPIs) are a ubiquitous superfamily that catalyzes the interconversion between conformers. Although pervasive, the functions and substrates of most PPIs are unknown. The two largest subfamilies, FKBPs and cyclophilins, are the intracellular receptors of clinically relevant immunosuppressant drugs that also show promise in the treatment of neurodegenerative disorders and cancer. Therefore, narrowing the knowledge gap has significant potential to benefit human health.

FKBP25 is a high-affinity binder of the PPI inhibitor rapamycin and is one of few nuclear-localized isomerases. While it has been shown to bind DNA and associate with chromatin, its function has remained largely uncharacterized. I hypothesized that FKBP25 targets prolines in nuclear proteins to regulate chromatin-templated processes. To explore this, I performed high-throughput transcriptomic and proteomic studies followed by detailed molecular characterizations of FKBP25's function. Here, I discover that FKBP25 is a multifunctional protein required for the maintenance of genomic stability. In Chapter 2, I characterize the unique N-terminal Basic Tilted Helical Bundle (BTHB) domain of FKBP25 as a novel dsRNA binding module that recruits FKBP25's prolyl isomerase activity to pre-ribosomal particles in the nucleolus. In Chapter 3, I show for the first time that FKBP25 associates with the mitotic spindle apparatus and acts to stabilize the microtubule cytoskeleton. In this chapter, I also present evidence that this function influences the stress response, cell cycle, and chromosomal stability. Additionally, I characterize the regulation of FKBP25's localization and nucleic acid binding activity throughout the cell cycle. Finally, in Chapter 4, I uncover a role for FKBP25 in the repair of DNA double-stranded breaks. Importantly, this function requires FKBP25's catalytic activity, identifying for the first time a functional requirement for *cis-trans* prolyl isomerization by FKBP25.

Collectively, this work identifies FBKP25 as a multifunctional protein that is required for the maintenance of genomic stability. The knowledge gained contributes to the exploration of PPIs as important drug targets.

Contents

List of Tables

List of Figures

ACKNOWLEDGEMENTS

This research is built on the support and ideas of many.

Foremost, I would like to express sincere thanks to my supervisor Dr Christopher Nelson for his guidance. Dr Nelson graciously facilitated many opportunities that fostered my aspiration to pursue meaningful discovery.

I would also like to thank my supervisory committee: Dr Caren Helbing, Dr Julian Lum, and Dr Jürgen Ehlting. Their insightful comments and encouragement throughout my PhD have been invaluable.

The labs of Dr Juan Ausio and Dr Perry Howard have been integral to my research, from the use of laboratory equipment to borrowing reagents for an epiphanic experiment. I thank the members of both labs, past and present.

This research would not have been possible without the input of numerous collaborators. For mass spectrometry studies, members of the UVic Proteomics Centre. For structural NMR work, Dr Cameron Mackereth's group in Bordeaux. For assistance with confocal imaging, Andrew Boyce from Dr Leigh Anne Swayne's Lab in the Dept of Medical Science at UVic. And for laser micro-irradiation studies, Dr Feng Gong from Dr Kyle Miller's lab at the University of Austin at Texas.

I would also like to thank my fellow labmates; Geoff, Andrew, Neda, and Francy. It has been my pleasure to work alongside you over the last several years.

Lastly, I would like to acknowledge the support of my family. Through the success and the failure, my wife Karrie has stuck by me. I am forever grateful for her faithful support. To Karrie's parents, thank you for your kindness and generosity. And to my parents, for your encouragement, continued support, and my proline isomerases - thanks.

Abbreviations

Alt-EJ	alternative end joining.
APC	adenomatous polyposis coli.
b1NRE	b1 nucleolin recognition element.
b2NRE	b2 nucleolin recognition element.
BioID	biotin identification.
BSA	bovine serum albumin.
BTHB	Basic Tilted Helical Bundle.
c-NHEJ	classical non-homologous end-joining.
CDK	cyclin-dependent kinase.
ChIP	chromatin immunoprecipitation.
CLIP	cross-linking immunoprecipitation.
Co-IP	co-immunoprecipitation.
CSK	cytoskeleton buffer.
CyP	cyclophilin.
CyP-A	cyclophilin A.
DAG	diacylglycerol.
DDA	DNA-damaging agent.
DDR	DNA damage response.
DNA-PKcs	DNA-dependent protein kinase catalytic subunit.
DSB	DNA double-strand break.
dsDNA	double-stranded DNA.
dsRBD	dsRNA-binding domain.
dsRNA	double-stranded RNA.
EtBr	ethidium bromide.
FBS	fetal bovine serum.
FKBP	FK506 Binding Protein.

FRT	flippase recognition target.
GO	gene ontology.
GTEx	Genotype-Tissue Expression.
HMG	high-mobility group.
HR	homologous recombination.
IGS	long intragenic spacer.
IL-2	interleukin 2.
ITS	internal transcribed spacer.
LMB	leptomycin B.
MAP	microtubule associated protein.
MAPK	mitogen-activated protein kinase.
MLL1	Mixed Lineage Leukemia 1.
MMEJ	microhomology mediated end-joining.
MNase	micrococcal nuclease.
MRN	Mre11-Rad50-Nbs1 complex.
MT	microtubule.
MTA	microtubule targeting agent.
mTor	mammalian target of rapamycin.
NOR	nucleolar organizing region.
NoRC	nucleolar remodeling complex.
Parp-1	Poly(ADP-ribose) polymerase 1.
PFA	paraformaldehyde.
PI	propidium iodide.
PKC	protein kinase C.
PolI	RNA polymerase I.
PPI	peptidyl-prolyl isomerase.
pre-rRNA	precursor ribosomal RNA.
PTM	post-translational modification.
qPCR	quantitative polymerase chain reaction.
rDNA	ribosomal DNA.
RNA-Seq	RNA sequencing.
RNase A	ribonuclease A.
RNP	ribonucleoprotein.

RPA	replication protein A.
RPKM	Read Per Kilobase of transcript per Million mapped reads.
RRM	RNA recognition motif.
rRNA	ribosomal RNA.
siRNA	short interfering RNA.
snoRNA	small nucleolar RNA.
SSA	single-strand annealing.
TFA	trifluoroacetic acid.
UBF	upstream binding factor.
UT	untransfected.

Chapter 1

Introduction

The landscape of a cell is complex. To survive and thrive, cells depend on the harmonious execution of thousands of molecular events. At its basis, DNA provides the blueprint for all of the components required. However, it is the encoded effector molecules, proteins and RNAs, that bring the cell to life. These cellular constituents function within networks to integrate pulses of information originating both extra and intracellularly. This integration ensures a coordinated effort on behalf of the many active parts within a cell. In the case of proteins, much of this coordination is accomplished through reversible post-translational modifications (PTMs). Once transcribed, there are a variety of chemical moieties that can be added to a protein to alter its localization, protein-protein interactions, enzymatic activity, and stability; these include phosphorylation, acetylation, glycosylation, ADP-ribosylation, methylation, and ubiquitination. Enzymes catalyze the deposition and removal of most PTMs, often referred to as writers and erasers, respectively. In the case of phosphorylation, protein kinases catalyze the transfer of a phosphate group from an ATP donor while phosphatases remove the mark. There is also a collection of protein domains that have evolved to bind specific PTMs, called readers. For example, the bromo domain, which recognizes acetylated residues (Fujisawa and Filippakopoulos, 2017). To date, approximately 600 000 unique PTMs have been identified experimentally (Lu et al., 2013). This vast array of modifications allows the cell to modify its proteome on a physiological time scale to integrate and process complex information (Prabakaran et al., 2012). Thus, the post-translational modification of proteins is an essential mechanism to coordinate the complex interactions that sustain life.

Cellular signaling networks do not act in isolation. Multifunctional proteins bridge the regulation of diverse cellular processes. As well, crosstalk between PTMs integrates information from multiple signaling pathways (Hunter, 2007). Regulation of

the eukaryotic genome by the post-translational modification of chromatin exemplifies this concept (Bannister and Kouzarides, 2011) – it has become clear that chromatin modifying enzymes are required to facilitate all DNA-templated processes; including transcription, replication, and DNA damage repair. It is often the case that a single enzyme is involved in the regulation of more than one of these functions. In eukaryotes, the genome is housed in a complex of DNA and protein known as chromatin. Chromatin consists of ∼147 bp of DNA wrapped around an octamer of histone proteins (two copies each of histone H3, H4, H2A, and H2B) to form the nucleosome-core repeating unit (Luger et al., 1997). Nucleosomal units are then folded into higher-order chromatin fibers. A variety of histone PTMs partitions the genome into distinct chromatin environments coordinating the dynamic usage of genetic information. Certain histone modifications are often found together and act combinatorially to regulate the underlying DNA (Lee et al., 2010). The first example of histone crosstalk showed how phosphorylation of serine 10 on histone H3 (H3pS10) promotes acetylation by the acetyltransferase Gcn5 at histone H3 lysine 14 (H3K14ac) (Cheung et al., 2000; Lo et al., 2000). Gcn5, within the context of the SAGA complex, is known to interact with and influence many histone modifications and is important in the regulation of transcriptional elongation, protein stability, and DNA damage (Koutelou et al., 2010). Since, many more examples of multifunctional chromatin modifying enzymes engaged in crosstalk have been discovered, providing the cell with layered control of its genomic information.

More recently peptidyl-prolyl isomerization, a novel non-covalent PTM has been implicated in the regulation of chromatin (Bannister and Kouzarides, 2011) and cell signaling (Lu et al., 2007). Peptidyl-prolyl isomerases (PPIs) are multifunctional enzymes that regulate both the folding of proteins and their function in the folded state. This thesis sets out to define the functions of the nuclear chromatin-associated prolyl isomerase, FKBP25. I have discovered that this enzyme is a multifunctional protein that localizes with ribosome biogenesis, influences microtubule dynamics, and regulates DNA double-strand break repair. In this capacity, FKBP25 may integrate the regulation of these fundamental cell processes, which are often misregulated in human disease. In this chapter, I will present a collection of published works that describe prolyl isomerization as a regulatory mechanism. Additionally, I will highlight recent findings that support the interconnectivity of functions within the nucleolus, the cellular response to genomic lesions, and microtubule dynamics.

1.1 Peptidyl-Prolyl Isomerization

The amino acid proline is unique – it adopts a *cis* peptide bond conformation at a significantly higher frequency than all other amino acids due to its five-membered ring (Figure 1). In proteins, the isomeric state adopted can influence protein structure and function. Thus prolyl isomerization can act as a regulatory switch (Lu et al., 2007). A well-characterized example is the autoinhibitory mechanism of the signaling adapter protein Crk – the conformation of a single proline dictates the functional activity of this protein (Sarkar et al., 2007, 2011). Isomerization between the *cis* and *trans* state involves a 180° rotation about the imide bond, resulting in a dihedral angle of $\omega = 180°$ in the trans and $\omega = 0°$ in the *cis* conformation (Ramachandran and Sasisekharan, 1968). The *trans* conformation of non-proline amide linkages is strongly favored due to electrostatic interactions of the Cα1 and Hα1 atoms with Cα2 and Hα2 atoms. Due to the symmetry between the Cα and Cδ carbon atoms in proline, *cis* and *trans* isomers are closer in free energy, permitting rotation albeit slowly (on the order of minutes). The occurrence of *cis* conformers in unstructured peptides is ∼10% for any given peptide in solution (Ramachandran and Mitra, 1976). In proteins, the conformation of proline is influenced by the surrounding structural environment, with *cis* proline occurring more frequently in surface exposed bends, turns and coils (Pahlke et al., 2005). A study of 571 protein structures found that 5.21% Xaa-Pro bonds exist in the *cis* conformation in folded proteins (Weiss et al., 1998). However, the authors speculate that this is likely an underestimate due to bias for the *trans* conformation in molecular refinement programs as well as the difficulty in differentiating between states for low-resolution structures.

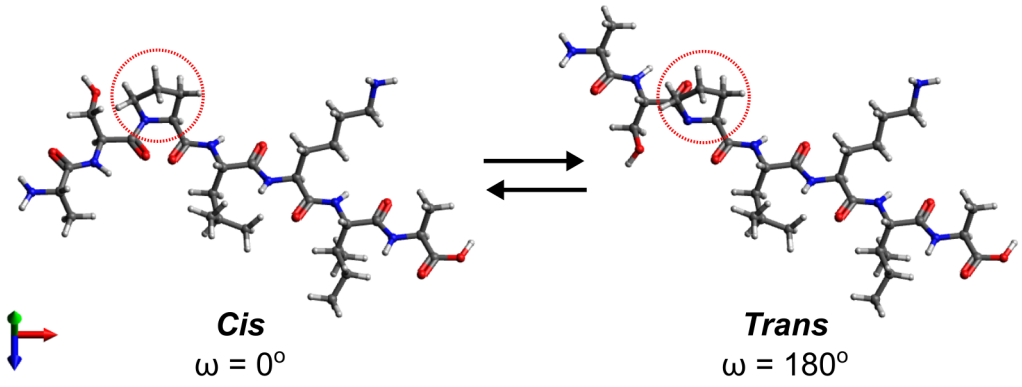

Figure 1. Prolyl *cis-trans* isomerization - In proteins, Xaa-Pro imide bonds can be found in both the *cis* and *trans* conformation altering the structure of the peptide backbone. Depicted here are peptides containing a proline residue (highlighted by a red circle) in either the *cis* or *trans* conformation. Note the "kinked" peptide backbone in the *cis*-Pro containing peptide.

Due to the high energy barrier of the $\omega = 90°$ syn transition state, *cis-trans* isomerization has been recognized as a rate limiting step in protein folding. This was first observed in studies describing the folding kinetics of ribonuclease A (RNase A), which found there existed a kinetically heterogeneous mixture of fast folding (few milliseconds) and slow folding (a few minutes) molecules, both eventually forming active enzymes (Garel and Baldwin, 1973). From these observations the "proline hypothesis" was proposed by Brandts et al. (1975) – stating that slow folding molecules contain non-native proline conformers and that protein folding is limited by the slow isomerization rate of incorrect conformers (Brandts et al., 1975; Cook et al., 1979). In support of this hypothesis, a study of the folding kinetics of RNase A and RNase T1 found that folding and unfolding rates of these proteins were dependent on the number of *cis* prolyl residues present (Kiefhaber et al., 1992).

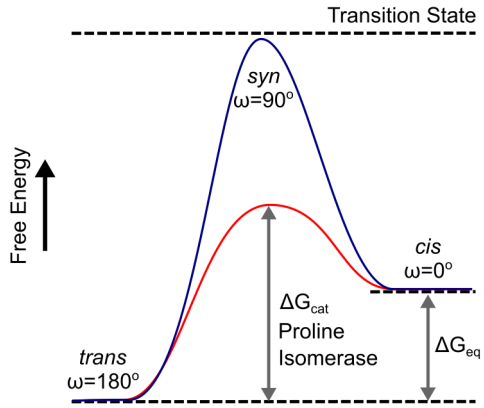

Figure 2. Energy diagram for prolyl *cis-trans* isomerization - Prolyl isomerase enzymes stabilize the syn-90 high-energy transition state lowering the activation energy for interconversion. Figure adapted from Lu et al. (2007)

Peptidyl-prolyl isomerase enzymes have evolved to catalyze this reaction, accelerating protein folding (Schmid, 1995)(Figure2). Enzymatic peptidyl-prolyl isomerase activity was first identified and purified from porcine kidney (Fischer et al., 1984) and was shown to accelerate the folding of a number of substrates; including the immunoglobulin light chain, the S-protein fragment of bovine RNase A, and RNase T1 (Lang et al., 1987; Schönbrunner and Schmid, 1992). It would later be uncovered that the purified enzyme was cyclophilin A, a member of the cyclophilin family of PPIs (Fischer et al., 1989). Since these seminal findings, which highlight the importance of prolyl residues and the enzymes that catalyze their interconversion in *de novo* protein folding, PPIs have also been shown to target folded proteins in the regulation of cell signaling networks.

1.2 Peptidyl-Prolyl Isomerases

PPIs are an evolutionarily conserved ubiquitous superfamily of enzymes categorized into three distinct groups based on protein fold; cyclophilins, FK506-binding proteins (FKBPs), and parvulins (Figure 3). The FKBPs and cyclophilins were first isolated and classified irrespective of prolyl isomerase activity as the intracellular receptors of the immunosuppressant drugs FK506 and cyclosporin, respectively (Siekierka et al., 1989; Harding et al., 1989; Handschumacher et al., 1984). PPIs accelerate the *cis-trans* interconversion of Xaa-Pro bonds in proteins by several orders of magnitude (Kofron et al., 1991). While the three groups are structurally distinct, all contain a central

beta sheet and function as monomers (Ranganathan et al., 1997; Kallen et al., 1991; Van Duyne et al., 1991). Despite the lack of a common fold, the active site structures are quite similar, suggesting a conserved catalytic mechanism (Lu et al., 2007). For all PPIs, an α-helix and β-sheets form a shallow solvent exposed catalytic pocket, at the base an aromatic residue anchors proline residues with additional interactions between enzyme and substrate mediated by a hydrogen bonding network (Dunyak and Gestwicki, 2016). These enzymes operate independently of metal ions, cofactors or post-translational modifications. Many catalytic mechanisms have been proposed, including; substrate desolvation, substrate autocatalysis, preferential transition state binding, and nucleophilic catalysis – yet, there is still no definitive answer as to how these enzymes operate (Fanghänel and Fischer, 2004; Lu et al., 2007). It is however generally accepted that catalysis does not proceed through the breakage of amide bonds, instead by rotation through a twisted amide state (Xu et al., 2011). More recently, an electrostatic handle mechanism has been put forth based on studies of the cyclophilin CyP-A using NMR measurements, molecular dynamics simulations, and density functional theory calculations (Camilloni et al., 2014). Camilloni et. al proposed that an electrostatic field within the catalytic active site turns the electric dipole associated with the preceding carbon atom causing the rotation of the peptide bond. This feature is also present in FKBPs and parvulins. However, the authours conclude that there are likely additional factors that contribute to isomerization, leaving the molecular mechanism still unclear.

While first recognized for their ability to catalyze protein folding, PPI catalyzed *cis-trans* isomerization can also act as a regulatory switch within folded proteins. The substrates of PPIs are known to be involved in human disease, including cancer and neurodegenerative disorders, and potent small molecule inhibitors exist. Thus, there is significant interest in further defining the biological functions of these proteins and their potential as points of therapeutic intervention.

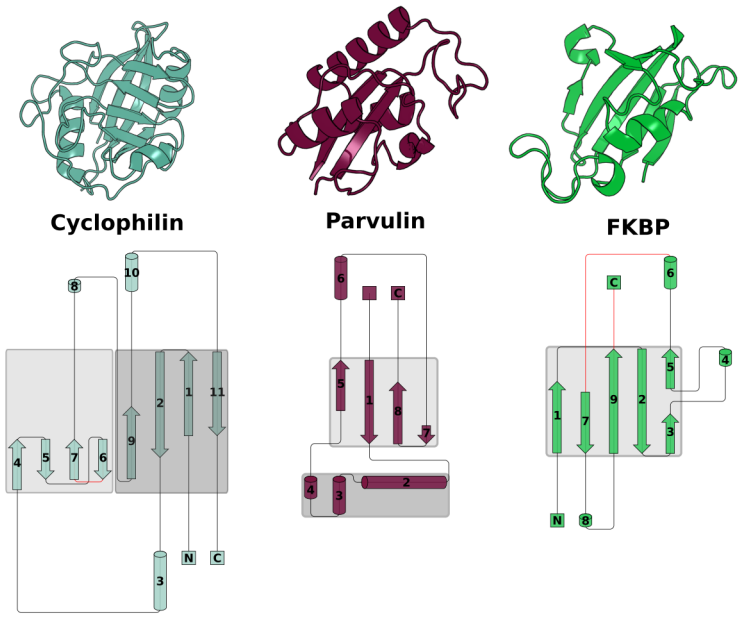

Figure 3. Prolyl isomerase families - Crystal structures of prolyl isomerase domains representing the three families; cyclophilins (CyP-A - PDB ID: 3K0N), FKBPs (FKBP12 - PDB ID: 2PPN), and parvulins (Pin1 - PDB ID: 1NMW). Structures also presented as topology diagrams below, created using the Pro-origami webserver (Stivala et al., 2011)

1.2.1 Parvulins

Members of the parvulin family of PPIs are ubiquitously expressed in both prokaryotes and eukaryotes. Unlike the FKBPs and cyclophilins, parvulins are not characterized by the binding of immunosuppressant drugs; instead, they receive their distinction based on homology to a small prokaryotic PPI, originally described in *E.coli* (lat.: parvulus, very small)(Rahfeld et al., 1994). The human genome encodes two parvulin proteins, Pin1 and Pin14, as well as a Pin14 isoform Pin17 (Mueller et al., 2006). The initial discovery of Pin1 by Hunter and colleagues came as the result of a yeast two-hybrid screen to identify proteins that interact with the mitotic kinase NIMA in *Aspergillus nidulans* (Lu et al., 1996). Deletion of Pin1 resulted in a mitotic arrest in HeLa cells, whereas overexpression prompted arrest in G2, indicating Pin1 was essential for cell cycle regulation (Lu et al., 1996). Many cell-proliferative abnormalities characteristic of cyclin D1 deficient mice were also found in Pin1 null mice, including decreased body weight, and testicular and retinal atrophies (Liou et al., 2002). It is now known that Pin1 regulates cyclin D1 through its interaction with many upstream factors by prolyl isomerization of pS/T-Pro motifs. These discoveries were

the first to mechanistically confirm prolyl isomerization in processes beyond *de novo* protein folding, shifting the paradigm of PPIs from mere chaperones to regulators of cell signaling.

The parvulins are the only class of PPIs that exhibit precise substrate specificity. Initially, Pin1 was shown to display a preference for an acidic residue N-terminal to the isomerized proline bond. This raised the possibility of phosphorylation-mediated ligand recognition by Pin1, with the implication that Pin1 acts downstream of proline-directed cyclin-dependent kinase (CDK) and mitogen-activated protein kinase (MAPK) signaling (Ranganathan et al., 1997). The work of several groups successively showed that Pin1 selectively binds and isomerizes phosphorylated Ser-Pro or Thr-Pro motifs, validating this hypothesis (Verdecia et al., 2000; Yaffe, 1997; Lu et al., 1999; Landrieu et al., 2001). Two phospho-specific domains of Pin1 facilitate these properties: an N-terminal WW protein interaction domain and C-terminal PPI domain (Ranganathan et al., 1997). The former enables these enzymes to associate with Ser/Thr-Pro phosphorylated motifs, and the latter displays PPI activity towards similarly phosphorylated epitopes. Precisely how Pin1 might transfer substrate from the WW to catalytic domain remains unclear. However, as many Pin1 targets are phosphorylated at several Ser/Thr-Pro motifs, it remains possible, for at least some substrates, that the binding and catalytic domains interact with separate phospho-epitopes on a substrate. Collectively, these findings link Pin1, and therefore peptidyl-prolyl isomerization, to phosphorylation-dependent signal transduction. The larger implication is that the isomerization of proline switches regulates processes beyond *de novo* protein folding. Since these initial studies, there has been a significant number of Pin1 substrates identified – far too many to adequately describe in this introduction. For a summary of the transcription factors targeted by Pin1, a table is presented in the appendix of this thesis (Table A1). For those interested, I also suggest a review by Zhou and Lu (2016), which aptly details Pin1's substrates and role in cancer.

1.2.2 Cyclophilins

The cyclophilins (CyPs) are characterized by the presence of a structurally conserved prolyl isomerase domain that binds the immunosuppressive drug, cyclosporine. CyPs are ubiquitous – present in all cell types across both prokaryotes and eukaryotes (Wang and Heitman, 2005). In humans there are sixteen cyclophilins, *Arbidopsis* has up to 29, and yeast eight. Cyclophilin A (CyP-A) has the distinction of being the first PPI to be isolated. In 1984, it was purified from bovine thymocytes as a

high-affinity binder of cyclosporin (Handschumacher et al., 1984). The isolation of CyP-A was followed by its characterization as a prolyl isomerase, implicating this class of protein in *de novo* protein folding (Fischer et al., 1989). Over the years the functional repertoire of CyPs has expanded to include the regulation of viral replication (Chatterji et al., 2009; Watashi et al., 2005), splicing (Mesa et al., 2008), and transcription (Wang et al., 2010b; Park et al., 2010; Li et al., 2007).

Unlike parvulins, cyclophilins do not act on a defined sequence motif. Instead, additional accessory domains and cellular localizations direct their prolyl isomerase activity. CyP-A, the founding member, consists of only a CyP domain and is highly abundant in the cytoplasm, contributing upwards of 0.1-0.6% of the total cytoplasmic protein pool (Nigro et al., 2013). Here, it is presumably engaged primarily in protein folding. Further understanding of its cellular functions is warranted as it has been implicated in cardiovascular disease, neurodegeneration, and cancer (Nigro et al., 2013). CyP-40 is directed to mitochondria by a signal sequence at its N-terminus (Andreeva and Crompton, 1994; Tanveer et al., 1996). Here it is involved in the formation and regulation of the mitochondrial permeability transition pore, which promotes cell death – suggesting CyP-40 is an important mediator of the stress response (Andreeva et al., 1999). Additionally, CyP-40 disaggregates neurotoxic amyloids, indicating its importance in preventing neurological disorders (Baker et al., 2017). CyP-33 contains a RNA binding domain and localizes to the nucleus. It is the first description of a protein containing both RNA binding and prolyl isomerase activities (Mi et al., 1996). Here it is involved in the regulation of chromatin modifying enzymes (Park et al., 2010; Wang et al., 2010b). There are many more examples of CyPs participating in the regulation of folded proteins that unfortunately cannot be addressed in the scope of this introduction. Studies to date have established the cyclophilins as a functionally diverse family of proteins. However, the molecular mechanisms and substrates of cyclophilin-mediated regulation remain largely elusive.

1.2.3 FK506 Binding Proteins (FKBPs)

Like cyclophilins, FK506 Binding Proteins (FKBPs) were first identified based on their binding to an immunosuppressant drug. In 1989, the Sigal and Schreiber labs separately identified the intracellular receptor for the immunosuppressant FK506 as a small 12 kDa peptidyl-prolyl isomerase (Siekierka et al., 1989; Harding et al., 1989). FKBP12, consisting of only an isolated FKBP domain, is the primary receptor for FK506 and the FKBP12-FK506 complex inhibits T cell proliferation (Bierer et al., 1990). In humans, eighteen proteins contain FKBP domains (Galat, 2004). They differ in their overall domain architecture and cellular localizations, and like CyPs rely on ancillary domains and signaling sequences to direct their function and localization (Figure 4). In mammals, at least six FKBPs contain multiple tetratricopeptide repeat (TPR) domains. TPR domains act to mediate protein-protein interactions (Cortajarena and Regan, 2006), likely to target FKBPs to distinct protein complexes. The accessory domain of FKBP25 is a unique protein fold termed a basic tilted helical bundle domain (BTHB), whose only known structural homologue is a subdomain of the E3 ubiquitin ligase HectD1 (Helander et al., 2014). How this unusual fold may act to direct FKBP25 activity remains to be determined.

FKBPs have been shown to have roles in cell signaling, protein folding, apoptosis, and the regulation of chromatin, with implications in human diseases like cancer (Yao et al., 2011). FKBP12, aside from being the primary receptor for FK506 and rapamycin, has also been shown to bind and stabilize the closed state of the ryanodine receptor (RyR) in a calcium-dependent manner (Chelu et al., 2004). RyRs are calcium release channels that are required for excitation-contraction coupling process in skeletal and cardiac muscle (Fill and Copello, 2002). Disruption of FKBP12 and RyR is thought to be a mechanism of skeletal (Reiken et al., 2003) and cardiac muscle heart failure (Wehrens et al., 2004). Mitochondrial membrane-associated FKBP38 is pro-apoptotic, it is activated by increased cellular calcium through the formation of a complex with calmodulin, in its activated form FKBP38 inhibits the function of the anti-apoptotic protein Bcl-2 (Edlich et al., 2005). This regulation may be particularly important in the brain, as the specific FKBP38 inhibitor, DM-CHX, was shown to have neuroprotective and regenerative properties in a rat brain ischemia model (Edlich et al., 2006). Recent studies have also highlighted FKBPs for their roles in cancer and as potential biomarkers (Solassol et al., 2011; Yao et al., 2011). The large FKBPs, FKBP51 and FKBP52, function as co-chaperones for Hsp90 and regulate the activity of steroid hormone receptors (Storer et al., 2011). Disruption of steroid hormone signaling is a contributing factor in several forms of cancer and endocrine

therapies, like aromatase inhibitors, are a common treatment for hormone-dependent cancers. Supporting a role for these FKBPs, FKBP51 expression has been shown to be activated in prostate cancer cells (Makkonen et al., 2009) and FKBP52 was found to be significantly elevated in breast cancer tissues relative to normal breast tissue (Ward et al., 1999). Collectively, these findings demonstrate the importance of FKBPs in human health and may provide the basis for future treatment strategies. However, a better understanding of the cellular functions of these enzymes, in particular, uncharacterized members of the FKBP family, is still required.

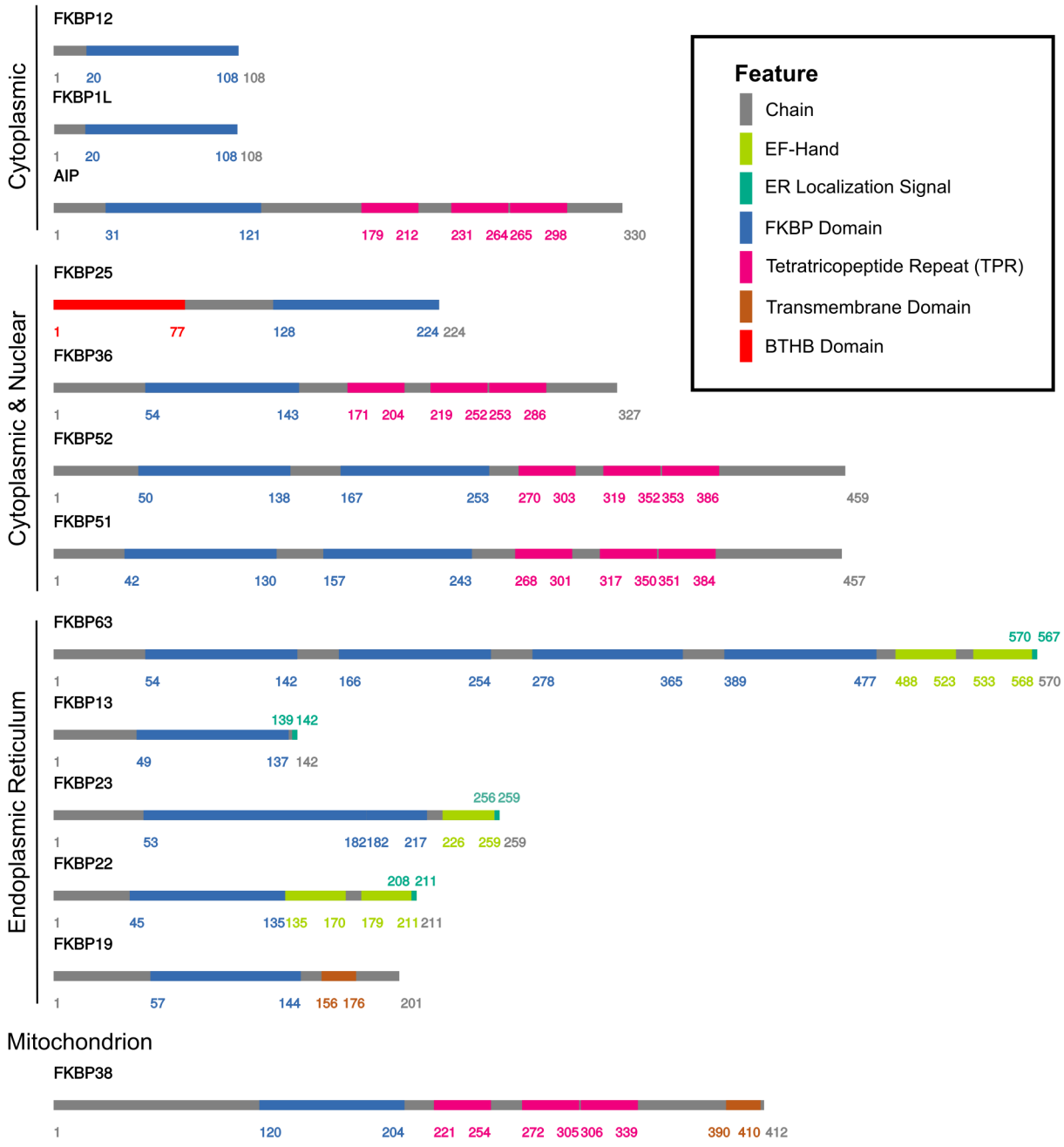

Figure 4. Localization and domain architecture of several members of the FKBP family. Domains and signal sequences are indicated in the legend. Domain features were retrieved from the UniProt Knowledgebase (Apweiler, 2004).

1.2.4 Prolyl Isomerases as the Intracellular Targets of Immunosuppressant Drugs

Cyclophilins and FKBPs are classified based on their binding to the clinically relevant immunosuppressive drugs cyclosporin and FK506/rapamycin, respectively (Fischer et al., 1989; Takahashi et al., 1989; Siekierka et al., 1989; Kallen et al., 1991; Van Duyne et al., 1991). These initial studies found that immunosuppressant drugs bind to the active site of prolyl isomerases and inhibit their activity. A discovery that precipitated a flurry of excitement in the field, implicating prolyl isomerase enzymes as novel regulators of immune function. However, the excitement was short-lived. It soon became apparent that the immunosuppressant activity of these compounds was unrelated to the enzymatic activity of PPIs. Rather, the immunoinhibitory properties resulted from the formation of a drug dependent ternary complex with calcineurin, in the case of cyclosporin/FK506, and the nutrient sensor mammalian target of rapamycin (mTor), in the case of rapamycin (Heitman et al., 1992; Ho et al., 1992; Heitman et al., 1991; Liu et al., 1991). Oddly, through independent mechanisms both calcineurin and mTor inhibition act to suppress transcription of interleukin 2 (IL-2), halting the development and proliferation of T-cells. Regardless of the mechanism, these drugs have become important clinical tools to suppress the immune system, and have found application in stem cell and organ transplantation as well as suppression of graft-versus-host-disease (Diehl et al., 2016). Realization of their potential in the treatment of aging-associated diseases, including several neurological disorders and cancers, has reignited interest in defining the molecular functions of PPIs. Due to their significant clinical history, repositioning theses molecules for the treatment of disease may expedite the transition from discoveries at the bench to drugs in the clinic.

Several studies have shown that FK506 and cyclosporin are effective in the treatment of neurodegenerative disease in animal models (Sinigaglia-Coimbra et al., 2002; Domañska-Janik et al., 2004; Avramut et al., 2001; Gold et al., 1995; Gold, 1999; Jost et al., 2000). Interestingly, non-immunosuppressive analogues of FK506, rapamycin, and cyclosporin have been shown to retain their neurotrophic activity (Soto and Sigurdsson, 1998). Dissociation of their neurotrophic activities from immunosuppressive qualities suggests that these drugs act through the targeting of a prolyl isomerase and not the immune system. Furthermore, a study that tested direct inhibitors of calcineurin function concluded that the neuroregenerative and neuroprotective qualities of FK506 are independent of its inhibition of either calcineurin or JNK (Klettner

et al., 2001) – lending additional support to this hypothesis. While the exact mechanism of their action is not well defined, it highlights the promise for the use of these inhibitors in the treatment of neurodegenerative disorders. In the case of FKBPs, multiple proteins are likely to contribute to the effect (Chattopadhaya et al., 2011). Thus, these findings support the argument for a more thorough functional characterization of these proteins.

Rapamycin is a potent allosteric inhibitor of mTOR signaling, which controls cell growth, proliferation, and metabolism. Increased activity of mTOR has been identified in numerous cancers, through mutations in upstream oncogenes and tumor suppressors (Li et al., 2014a). Derivatives of rapamycin have been approved for the treatment of advanced renal carcinoma and progressive neuroendocrine tumors and clinical trials are taking place for other cancers (Li et al., 2014a). Rapamycin, like cyclophilin and FK506, is also known to provide neuroprotection in several experimental models of neurodegenerative disease (Bové et al., 2011). As well as, extending lifespan in yeast, nematodes, fruit flies, and mice (Powers et al., 2006; Vellai et al., 2003; Kapahi et al., 2004; Jia et al., 2004; Kaeberlein, 2005; Harrison et al., 2010). Of note, there is also an ongoing longitudinal study in place evaluating the effect of rapamycin on the life span of companion dogs (Urfer et al., 2017). Much of rapamycin's anti-cancer and neuroprotective effects have been considered only in the light of its inhibition of mTOR. However, the catalytic activities of FKBPs are also targeted. How these side effects influence the efficacy of mTOR inhibition is largely unknown. In the very least, there is a correlation between expression levels of FKBPs and the efficacy of rapamycin targeting of mTOR (Schreiber et al., 2015). As FKBP12 can be functionally replaced by the large FKBP51 or FKBP52, and likely FKBP25 (März et al., 2013; Lee et al., 2016), characterizing how these proteins are regulated and their functions is necessary to fully appreciate rapamycin's mechanisms of action.

Although there has been a significant inquiry into the drug dependent immunological and anti-caner functions of these enzymes, relatively little is known about their natural biological roles. Given the broader potential of these immunosuppressant compounds in the treatment of disease, it is important to improve our understanding of these enzymes. Exploring their individual roles will enhance understanding of how immunosuppressants work as neuroprotective and anti-cancer drugs, potentially leading to novel therapeutic designs in the treatment of these diseases.

1.2.5 PPIs in the Nucleus

Interestingly, several prolyl isomerases have been found to reside in the nucleus, suggesting their activity is important in regulating nuclear processes, such as the regulation of chromatin and transcription. Epigenetic control of transcriptional programs is intertwined with the development and progression of cancer (Morgan and Shilatifard, 2015). Thus, understanding how PPIs function in this respect is important. Regulation by PPIs has been shown to affect the transcription machinery itself, histone proteins, and chromatin modifying proteins. Pin1, for example, regulates transcription directly through isomerization of the CTD of RNA polymerase II during the transcription cycle (Xu and Manley, 2007). While, the yeast prolyl isomerase Fpr4 directly binds the amino tails of histone H3 and H4 and isomerizes prolines 16, 30, and 38 of histone H3 *in vitro*, with crosstalk between Set2 methylation of H3K36, which is tri-methylated in the coding region of actively transcribed genes (Nelson et al., 2006; Monneau et al., 2013). Structural details of the JMJD2 demethylase, responsible for removal of the methyl mark, revealed that bending of the H3 tail at either a glycine or proline may be necessary for the active site to accommodate its substrate; hinting at the potential importance of prolyl isomerization in both the addition and removal of H3K36 methyl marks (Chen et al., 2006). Indirect regulation of histones through prolyl isomerization of chromatin modifiers has also been reported (Dilworth et al., 2012). An especially interesting example is CyP-33 mediated regulation of Mixed Lineage Leukemia 1 (MLL1). It was found that CyP-33 regulates the conformation of MLL1 through the isomerization of a single proline resulting in binding of CyP-33's RNA recognition motif (RRM) domain, transitioning MLL1 from an activator of transcription to a repressor (Wang et al., 2010b). Given these first glimpses into how prolyl isomerases influence gene expression through associations with the chromatin template, a more comprehensive view of PPIs in the nucleus is warranted.

1.3 The Nuclear FK506 Binding Protein FKBP25

FKBP25, the mammalian orthologue of yeast Fpr4, is a nuclear PPI hypothesized to be involved in the regulation of chromatin and ribonucleoprotein complexes. However, little is known about the functions of this protein in cells. FKBP25 is composed of a structurally unique hydrophilic Basic Tilted Helical Bundle (BTHB) domain at its N-terminus (aa 1-77)(Helander et al., 2014) and a structurally conserved FKBP PPI domain (aa 108-224)(Liang et al., 1996) at its C-terminus – these domains are

connected by an intervening unstructured polypeptide linker (Figure 5). FKBP25 was first discovered by the Schreiber lab in 1992 as a result of a systematic effort to isolate additional members of the FKBP family that bound rapamycin (Galat et al., 1992). Interestingly, they found FKBP25 contained an N-terminal domain unrelated to any known protein at the time and a putative nuclear localization signal, which looped out from its FKBP catalytic domain, suggesting residency in the nucleus (Galat et al., 1992; Jin et al., 1992). Subsequently, FKBP25 was shown to localize to the cytoplasm and nucleus, where it forms interactions with the multifunctional nucleolar protein nucleolin and binds DNA (Rivière et al., 1993; Jin and Burakoff, 1993). FKBP25's nuclear localization and interactions with nucleolin and DNA provided some of the first hints that PPIs were likely to have functions beyond their described roles in *de novo* protein folding.

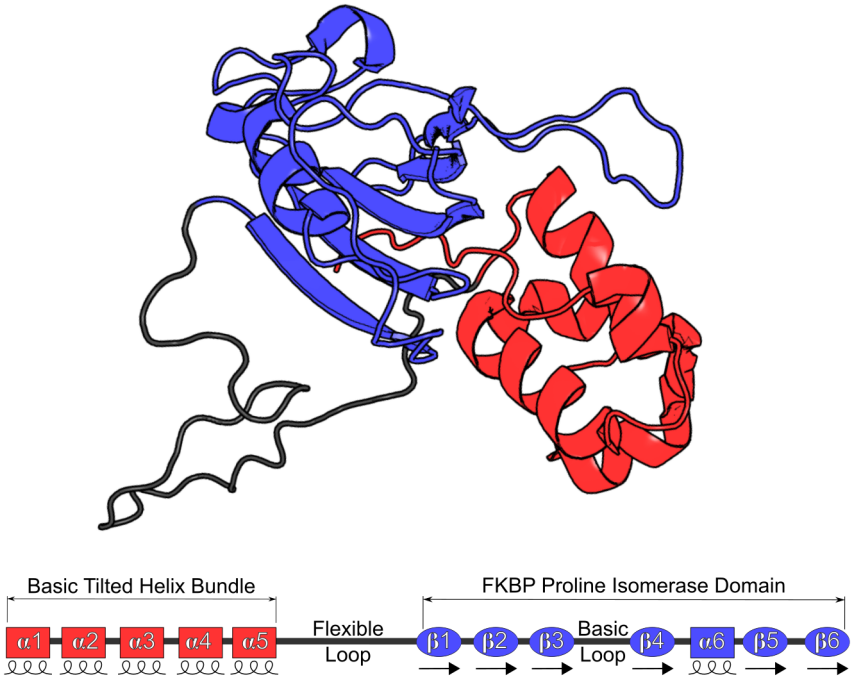

Figure 5. Structure of FKBP25 - Full length in solution NMR structure of FKBP25 (PDB ID: 2MPH) solved by Prakash et al. (2016). Shown below is a corresponding depiction of FKBP25's domain architecture

1.3.1 Involvement of FKBP25 in the Regulation of Chromatin and Transcription

The first indication that FKBP25 was chromatin-associated came as result of biochemical fractionation experiments to identify FKBP25's interacting partners. These researchers found that native FKBP25 associates with high-mobility group (HMG) II proteins (Leclercq et al., 2000). HMG proteins influence structural features of chromatin by binding and bending DNA to regulate the assembly of nucleoprotein complexes (Paull et al., 1993). In this way, they regulate many DNA-related processes; including transcription, replication, recombination, and repair (Reeves, 2010). More recently, FKBP25 was also shown to co-fractionate with the HMG I proteins HMGB1 and HMBG3, and interact with core histones (Galat and Thai, 2014; Foulger et al., 2012), supporting the notion that FKBP25 is chromatin-associated. FKBP25 is also known to interact with the histone deacetylases HDAC1 and HDAC2 and regulates the DNA binding of the transcription factor YY1, promoting its association with DNA (Yang et al., 2001). This activity is independent of the prolyl isomerase domain and is mediated by the BTHB domain of FKBP25 (Yang et al., 2001). A recent structural characterization of full-length FKBP25 characterized its DNA binding activity and mapped the YY1 binding site on FKBP25, providing some mechanistic details for FKBP25's regulation of YY1 (Prakash et al., 2016). The authors suggest that FKBP25's DNA binding activity is critical in mediating the formation of an FKBP25-DNA-YY1 ternary complex, which stabilizes YY1 interactions with DNA (Prakash et al., 2016). Many of the studies describing a function for FKBP25 on chromatin have been performed *in vitro* with purified proteins. Therefore, how FKBP25 may regulate chromatin in cells is still unclear.

FKBP25 may also regulate transcription indirectly by influencing the protein levels of the tumor suppressor p53. p53 is a transcription factor that coordinates the cell stress response by promoting senescence and in some cases apoptosis to suppress tumor formation (Bieging et al., 2014). FKBP25 was shown to interact with the ubiquitin ligase MDM2, which regulates the proteosome-dependent degradation of p53, promoting MDM2 autoubiquitination and degradation; thereby relieving proteasomal pressure from p53 (Ochocka et al., 2009). As with FKBP25's regulation of YY1, this interaction is independent of FKBP25's prolyl isomerase activity. However, the full-length protein is required to reduce MDM2 levels efficiently (Ochocka et al., 2009) – the role of FKBP25's catalytic activity in the regulation of chromatin and transcription remains elusive. Interestingly, it was also shown that FKBP25 is targeted by p53

mediated repression (Ahn et al., 1999). Collectively, these results suggest a role for FKBP25 in mediating the cellular response to stress via p53.

1.3.2 A Putative Role for FKBP25 in RNA Metabolism

Several published reports have linked FKBP25 to RNA metabolic processes. In fact, one of the earliest descriptions of FKBP25 identified nucleolin as a major interacting partner, suggesting a putative role for FKBP25 in ribosome biogenesis (Jin and Burakoff, 1993). Nucleolin is an abundant nucleolar RNA-binding protein – its expression is correlated with ribosomal output and it is thought to regulate transcription, modification, and processing of ribosomal RNA (Tajrishi et al., 2011). FKBP25 has also been described to interact with polyribosomes, clusters of actively translating ribosomes, supporting a putative role in ribosome biogenesis (Galat and Thai, 2014). Further, FKBP25 orthologous proteins in *S. cerevisiae* and *A. thaliana* are required for silencing of ribosomal chromatin (Li and Luan, 2010; Kuzuhara and Horikoshi, 2004). While these results are highly suggestive of FKBP25's involvement in ribosome biogenesis, the exact function and mechanisms still need to be determined.

Providing further links between FKBP25 and RNA metabolism, a systematic screen for defining the mRNA interactome identified FKBP25 as an mRNA binding protein (Castello et al., 2012). In support, FKBP25 has also been shown to co-purify with RNA granules in the brain (Elvira, 2005). RNA granules are ribonucleoprotein (RNP) complexes that are involved in neuronal RNA transport, the formation of P bodies, and the storage of mature mRNA in response to cellular stress (Kiebler and Bassell, 2006). The mechanisms of how FKBP25 associates with mRNA and its function have not yet been characterized.

The described protein interactions of FKBP25 provide a strong link to the nucleolus, transcriptional regulation, and chromatin biology. While intriguing, these findings prompt more questions than answers. This thesis sets out to answer these questions – exploring FKBP25's roles in ribosome biogenesis and chromatin biology, characterizing the significance of its nucleic acid binding activities, and determining the function of its mysterious N-terminal domain.

1.4 The Nucleolous

The nucleolus is a membrane-less sub-nuclear compartment that coordinates the transcription of ribosomal RNA (rRNA) and early processing events in ribosomes biogen-

esis. It is further subdivided into a tripartite structure visible by electron microscopy – these three regions moving outward from the center are known as the fibrillar center, dense fibrillar component, and granular component. Nucleoli also have important roles beyond ribosome biogenesis, including the assembly of signal recognition particles, regulation of growth and proliferation, in the cellular response to stress, and DNA replication and repair (Boisvert et al., 2007). Malfunctions in nucleolar function have been implicated in several diseases, including multiple genetic disorders and cancers (Boisvert et al., 2007). Nucleoli assemble around tandem repeating units of ribosomal gene clusters, known as nucleolar organizing regions (NORs), a concept first put forth by Barbara McClintock from here studies in *Zea mays* a decade before DNA had even been discovered (McClintock, 1934). The presence of nucleoli in eukaryotic cells had been well documented by this point – due to its density the nucleolus was one of the first organelles discovered and characterized by early microscopists (Montgomery, 1898). In the 1960s, the nucleolus became defined for what it is best known, the site of ribosome biogenesis (Pederson, 2011). It was also at this time that the nucleolus would give researchers the first glimpse of transcription by electron microscopy, a now iconic view of elongating rRNA extending out from ribosomal DNA (rDNA), known as Miller spreads (Miller and Beatty, 1969). For a more detailed and entertaining read on the history of the nucleolus, I recommend a review by Pederson (2011).

1.4.1 Ribosome Biogenesis

Ribosomes are large macromolecular complexes, containing both protein and RNA, which are responsible for the translation of mRNA to protein. In eukaryotes, ribosomal rRNA is transcribed by RNA polymerase I as a single polycistronic 47S precursor from clusters of repetitive transcriptional units at the interface of the fibrillar center and the dense fibrillar component of the nucleolus (excluding the 5S rRNA, which is transcribed outside of the nucleolus by RNA polymerase III). A single mammalian cell can contain upwards of 10 million ribosomes, with numbers correlating with proliferation (Cooper, 2014). Early processing of the 47S rRNA precursor, which includes scores of PTMs and nucleolytic processing steps, occurs as rRNA moves out of the nucleolus and through the granular component. Additional modifications and assembly steps take place within the nucleosol, which yields pre-ribosomal subunits, before export to the cytoplasm, where the ribosome undergoes the final maturation and assembly steps to become translationally competent (Figure 6). The assembly and

maturation of ribosomes involves greater than 200 transiently associated assembly factors and many small nucleolar RNA (snoRNA) (Thomson et al., 2013; Tafforeau et al., 2013). It is a complex and tightly regulated affair, ensuring the accurate synthesis of core cellular machinery.

In humans there are an estimated 300-400 copies of the 43 kb rDNA repeating unit arrayed in tandem in NORs, with the sequence encoding precursor ribosomal RNA (pre-rRNA) being separated by long intragenic spacers (IGSs) (Gonzalez and Sylvester, 1995). Ribosomal genes exist in two distinct epigenetic states that promote either silencing or activation of rDNA transcription (McStay and Grummt, 2008). Thus, regulation of rRNA transcription can occur in two ways, increased transcription from euchromatin repeats or altering the ratio of epigenetically active to silent repeats. Patterns of DNA methylation, specific histone modifications, and nucleosomal positioning distinguish these chromatin environments. The transcription termination factor TTF-1 is essential for Pol I transcription and the maintenance of the epigenetic state of rDNA through cell division. It binds both downstream of the transcribed region to mediate transcriptional termination and at the promoter-proximal terminator T0, influencing the establishment and maintenance of the appropriate chromatin environment (Längst et al., 1998; Bartsch et al., 1988; Henderson and Sollner-Webb, 1986). TTF-1 recruits the repressive nucleolar remodeling complex (NoRC), which is composed of the remodelers TIP5 and SNFh2 (Strohner et al., 2001). NoRC induces nucleosome sliding, shifting the promoter-bound nucleosome into a position that represses RNA polymerase I transcription, indicating that TTF-1 is a bifunctional protein regulating both activation and repression of rDNA (Li et al., 2006). Similarly to protein-coding genes, the transcriptional status of rDNA is also dictated by histone modifications, such as the repressive methyl mark at H3K9 and the activating mark H3K4me3 at promoters. TTF-1 recruitment of NoRC results in DNA methylation, deacetylation of H4, and di-methylation of H3K9 at the promoter, silencing expression (Feng et al., 2010). While H3K9 methylation is typically associated with a repressive state, the methyltransferase G9a was shown to di-methylate H3K9 residues in the coding region of rDNA providing a binding surface for HP1γ and increasing ribosomal expression (Yuan et al., 2007). This finding supports the idea that specific modifications cannot be directly associated with a particular transcriptional output. However, it is the context in which these marks exist that dictates function – a sentiment first proposed by Strahl and Allis (2000). Also, these studies show the importance of epigenetic regulation at ribosomal DNA, suggesting, prolyl isomerases, which target chromatin and localize to the nucleolus, may be important

mediators of the epigenetic regulation of ribosome production.

During ribosome biogenesis, assembly of the processing machinery begins co-transcriptionally. rRNA is modified at a number of conserved sites by methylation and pseudo- uridylation by small nucleolar ribonucleoprotein complexes. The timing of post-translational modification and nucleolytic processing events can differ among organisms and cell types (Henras et al., 2015). In mammals, the first step is the removal of the 3′ ETS followed by cleavage at the A2 site in the internal transcribed spacer (ITS) 1, separating the maturing large and small subunits of the ribosome. These pre-ribosomal species are further processed to give rise to the 18S, 5.8S and 28S pre-rRNA, which will undergo further maturation and assembly in the nucleus before export.

For pre-ribosomes to fully mature they must undergo export from the nucleus to the cytoplasm. This is an active process involving the nuclear pore complex. The karyopherin Crm1 is a receptor for both the large and small ribosomal subunits and controls export in a Ran-GTP-dependent manner (Zemp and Kutay, 2007). In the case of the 60S subunit, the shuttling adaptor protein NMD3 acts a gatekeeper, ensuring immature or defective ribosomal particles are not exported (Sengupta et al., 2010). Export is a highly regulated affair and serves as a checkpoint, ensuring defective ribosomes do not clog up the translation machinery in the cytoplasm. In the cytoplasm, final maturation involves the release of several ribosomal proteins from the 60S and 40S, as well as rRNA dimethylation of the 40S subunit (Zemp and Kutay, 2007).

From start to finish, ribosome biogenesis is a complex process coordinated by many RNA molecules and proteins – the potential involvement of FKBP25 is intriguing. However, how it may participate is entirely unknown. Given that FKBP25 has been shown to interact with polyribosomes (Galat and Thai, 2014), nucleolin (Jin and Burakoff, 1993), and chromatin (Galat and Thai, 2014), it may be involved at multiple stages of ribosome biogenesis. Further complicating the matter is the fact that the nucleolus also has roles beyond strictly producing ribosomes; many nucleolar factors moonlight in other processes and others seem not to be directly involved in ribosome biogenesis at all (Pederson and Tsai, 2009). Thus, FKBP25's association with the nucleolus may not necessarily translate to a direct function in ribosome biogenesis – it is clear that further characterization is required.

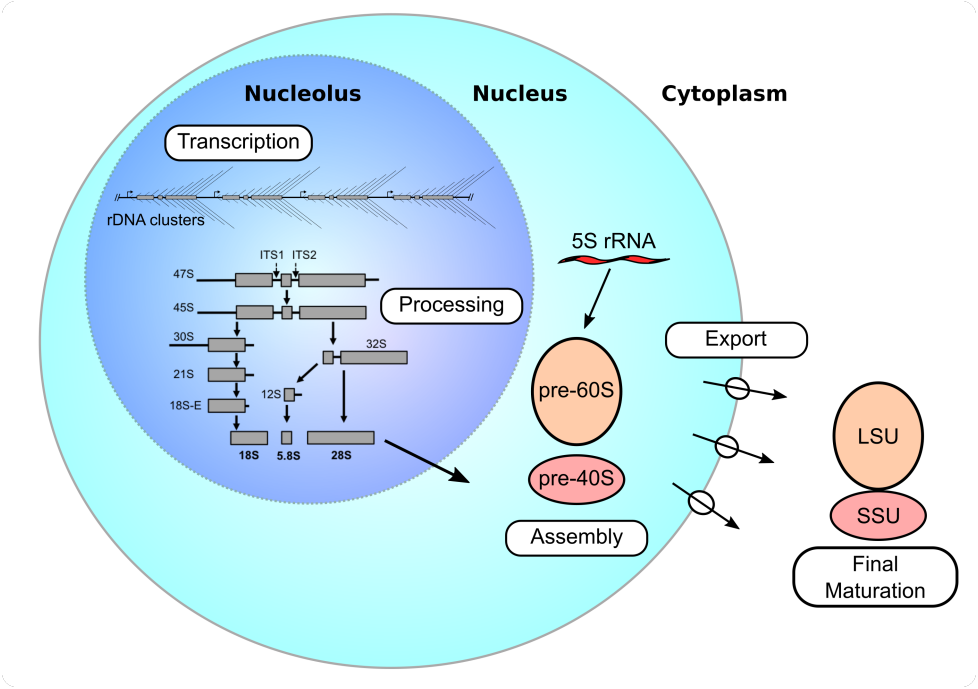

Figure 6. Ribosome Biogenesis - Ribosomal RNA is transcribed by RNA polymerase I from clusters of active ribosomal genes generating a 47S pre-rRNA transcript. The 47S transcript is processed in the nucleolus to generate the 28S, 18S, and 5.8S. In the nucleolus, the pre-60S and pre-40S subunits are assembled for export to the cytoplasm, where they undergo the final steps of maturation.

1.4.2 The Nucleolar Response to Stress

Under stress, the nucleolar proteome reorganizes through an exchange of proteins between the nucleolus and nucleus (Figure 7)(Boulon et al., 2010). During the stress response the Pol I machinery is targeted directly by the stress-activated kinase c-Jun, which phosphorylates and inactivates the Pol I-specific transcription factor TIF-IA (Mayer et al., 2005). Shut down of 47S rRNA transcription leads to the release of several ribosomal proteins from the nucleolus, which can directly interact with MDM2 to prevent ubiquitin-dependent repression of p53 (Zhang and Lu, 2009). While 47S transcription is attenuated, non-coding RNAs become transcribed from the IGS and act to sequester factors, such as MDM2, which repress the stress response under normal conditions (Audas et al., 2012). The NPM1-p14ARF-p53 pathway mediates a similar phenomenon. Under normal conditions, NPM sequesters p14ARF, a negative regulator of MDM2, in the nucleolus. When the stress response is activated, both NPM and p14ARF are released into the nucleosol, where p14ARF serves to both promote p53 activity through the regulation of MDM2 and inhibit TTF-1 nuclear

translocation to reinforce the block on rRNA transcription (Korgaonkar et al., 2005; Lessard et al., 2010). Through these redundant pathways, the nucleolus ensures a coordinated and robust response to cellular stress.

Interestingly, proteomic studies of the nucleolus have shown that only ∼30% of nucleolar residents have a direct role in ribosome biogenesis – of the rest, a significant number of proteins are directly involved in the DNA damage response (DDR) (Andersen et al., 2005). This observation suggests that the nucleolus plays a much broader role in cell biology than simply producing ribosomal subunits. While once considered as distinct disciplines, it is now recognized that considerable crosstalk between the DDR and ribosome biogenesis factors exists (Ogawa and Baserga, 2017; Larsen and Stucki, 2016). Nucleolin and NPM1, for example, relocate from the nucleolus to the nucleus in response to DNA damage and participate in the repair of different forms of damage (Scott and Oeffinger, 2016). Similar to other forms of cellular stress, the shutdown of rRNA transcription triggers their relocalization. DNA damage-dependent ATM signaling targets TTF-1, as well as several nucleolar regulators, to shut down rRNA transcription in the event of prolonged and sustained double-strand breaks (Harding et al., 2015; Kruhlak et al., 2007; Larsen and Stucki, 2016). This requires Poly(ADP-ribose) polymerase 1 (Parp-1), which functions in both ribosome biogenesis and DNA repair (Dejmek et al., 2009; Wei and Yu, 2016). The full extent of crosstalk between the nucleolus and the DDR is not known – it is likely further exploration will continue to expose the relationship between these two fundamental processes.

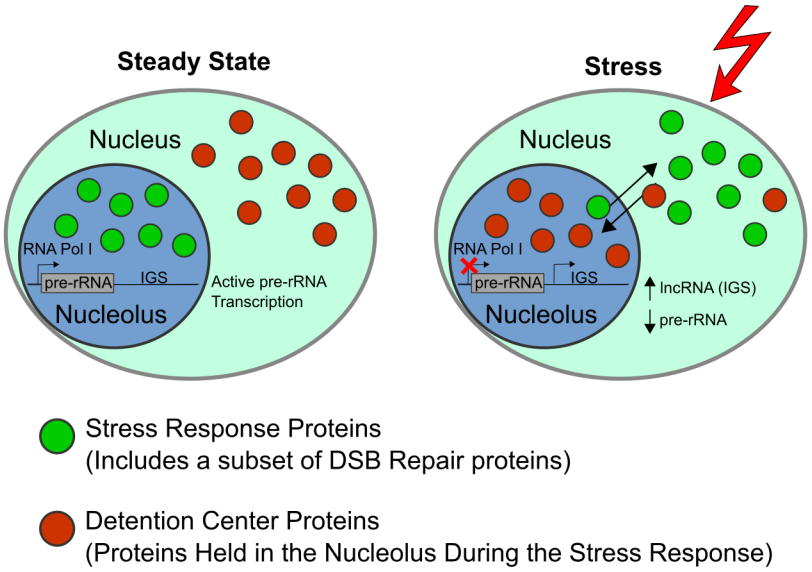

Figure 7. The nucleolar stress response - A schematic representation of the nucleolar response to cellular stress. The nucleolus plays a critical role in regulating the response to cell stress. Some stress response proteins localize to the nucleolus and are redeployed to the nucleus to facilitate the stress response. In contrast, proteins that temper the stress response under steady state conditions become detained in the nucleolus impairing their function. This co-ordinated effort temporarily halts rRNA transcription by RNA pol I until conditions return to normal.

1.5 DNA Double-Strand Break Repair

DNA double-strand break (DSB) are the most dangerous cytotoxic lesions – failure to properly repair these breaks results in genomic instability (Yu and McVey, 2010). DSBs can be induced by environmental sources such as ionizing radiation, as a result of DNA replication stress, or as programmed breaks during V(D)J recombination. Cells have evolved complex signaling networks that recognize and repair such lesions to maintain the integrity of DNA. This is a highly coordinated response, integrating pathways that control transcription, chromatin, ribosome biogenesis, and the cell cycle. There are four independent pathways that can resolve DSBs: homologous recombination (HR), classical non-homologous end-joining (c-NHEJ), alternative end joining (Alt-EJ), and single-strand annealing (SSA). c-NHEJ and HR are the major repair pathways – if they become impaired Alt-EJ and SSA provide alternative routes of repair. The degree of DNA-end resection, which is coordinated by cell cycle-dependent regulation of repair factors, largely dictates the repair path-

way utilized (Figure 8)(Kakarougkas and Jeggo, 2014). End resection is primarily carried out by the DNA endonuclease CtIP in a cell cycle-dependent manner (Yu and McVey, 2010). The DDR in all cases is initialized by activation of the apical kinases ATM/ATR/DNA-PKcs, which phosphorylate and activate downstream effectors, including H2Ax at serine 139, known as γH2Ax (Burma et al., 2001; Stiff et al., 2004; Ward and Chen, 2001). γH2Ax provides a chromatin anchored platform for the recruitment of repair factors that spread to cover a 2 Mbp region surrounding the break (Burma et al., 2001). Briefly described here are the general mechanisms of DSB repair and how chromatin influences the repair process. For more detailed description I suggest the review by Ceccaldi et al. (2016).

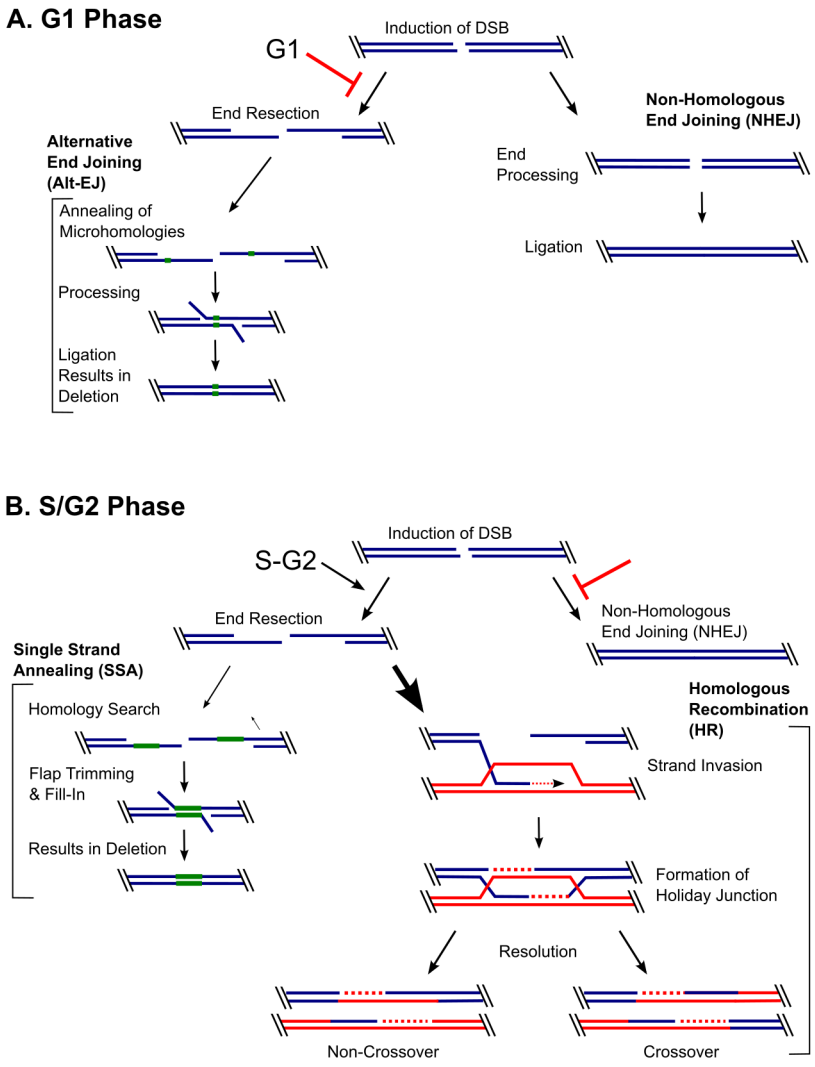

Figure 8. The cellular response to DNA double-strand breaks - (A) During G0/G1 end resection of DNA DSBs is impaired promoting repair by NHEJ. (B) During S and G2 phases of the cell cycle, when a homologous DNA template is available for repair, end resection proceeds resulting in repair predominately by HR. In the absence of a capable HR repair pathway, end resection will result in repair by SSA or Alt-EJ.

1.5.1 Non-Homologous End Joining and Alternative End-Joining

End joining pathways can be classified into two types, c-NHEJ and Alt-EJ. They are characterized by the ligation of DNA ends and can result in insertions, deletions, point mutations, and chromosomal rearrangement – this is especially true in the case of Alt-EJ. c-NHEJ repairs breaks through direct ligation of DNA ends with minimal

end-processing and does not require regions of homology for repair. Therefore, it is the primary repair pathway utilized during G1 of the cell cycle and in non-cycling cells. c-NHEJ is also employed in V(D)J recombination and immunoglobulin class switching, playing a critical role in the function of the immune system (Yu and McVey, 2010). During c-NHEJ, DSB breaks are quickly recognized by the Ku heterodimer (Ku70 and Ku80), which forms a ring to encircle DNA, self-association results in a physical tethering of broken DNA strands (Walker et al., 2001; Cary et al., 1997). In the absence of damage, Ku proteins partially localize to the nucleolus, this fraction relocalizes to the nucleus when DSBs are detected (Britton et al., 2013; Dejmek et al., 2009). A critical regulator of c-NHEJ is the reader protein 53BP1, which represses end resection in G1 (Zimmermann et al., 2013). The assembled Ku-DNA complex then recruits DNA-dependent protein kinase catalytic subunit (DNA-PKcs), which through the phosphorylation of several substrates promotes downstream repair events, including the formation of γH2Ax chromatin domains (Cary et al., 1997). Finally, DNA ends are processed by different enzymes depending on the nature of the break, such as the nuclease ARTEMIS, before ligation by the XRCC4-DNA ligase IV complex. For a more detailed review of the factors that facilitate c-NHEJ, I direct interested readers to the review by Mahaney et al. (2009).

Alt-EJ is mutagenic and is typically suppressed in cells by c-NHEJ – if c-NHEJ is disrupted, Alt-EJ can be activated independently of Ku and Lig4 activity. As such, Alt-EJ was first recognized as a residual end-joining pathway in Ku80, Ku70 or Lig4 yeast mutants and characterized by a dependence on regions of microhomology at junctions (Wilson et al., 1997; Boulton and Jackson, 1996). Due to this feature, the pathway was initially referred to as microhomology mediated end-joining (MMEJ) and thought to be mechanistically similar to SSA. However, Alt-EJ functions independently of Rad52, a critical mediator of SSA, and relies on much shorter regions of homology (Bennardo et al., 2008). It was later discovered that MMEJ is not dependent on exposing microhomologous templates, non-templated nucleotide insertion by TdT-like polymerase activity of polμ (McElhinny et al., 2005), or templated insertion by polθ (Yu and McVey, 2010) may provide an alternative route to generating the microhomologies required for base pair matching and ligation. Thus, Alt-EJ has become the preferred term for this type of repair. The complete mechanism and proteins involved in this process have not yet been fully characterized. However, it is believed that the Mre11-Rad50-Nbs1 complex (MRN) may be required for the initial activation of the response and tethering of broken ends, followed by CtIP mediated end resection to expose regions of microhomology, processing by polymerases, and

ligation by DNA ligase 1 or 3 (For a more detailed review see Yu and McVey (2010)). Recruitment of MRN is mediated by Parp-1, which competes with Ku for binding to free ends of DNA (Haince et al., 2008; Wang et al., 2006). In the absence of Ku, Parp-1 can promote the accumulation of the nuclease activity of MRN and subsequently CtIP to facilitate end-resection in G1. While CtIP is typically inactive during G1, it can be phosphorylated in G1 on Ser327 by Polo-like kinase 3 to mediate an interaction with BRCA1, which promotes its activity (Yu and McVey, 2010).

1.5.2 Homologous Recombination and Single-Strand Annealing

During S and G2 phases of the cell cycle, DSBs are accurately repaired by homologous recombination utilizing the sister chromatid as a template. Cell cycle control is critical as unscheduled recombination events can result in gross chromosomal rearrangements – tight regulation of HR is largely dictated by end resection. Mutations in HR genes are also common causes of hereditary forms of cancer, for example, inactivating mutations in the BRCA genes are associated with hereditary breast and ovarian cancers (Powell and Kachnic, 2003). During HR, DSBs are first recognized by Parp-1 and MRN, which tethers the broken ends of DNA and activates the kinase ATM, initializing a signaling cascade. Mre11 also possess both endo- and exonuclease activities that initiate end resection and are required for repair by HR (Chen et al., 2013). During S phase and G2, CtIP is activated in part by CDK phosphorylation (Yu and McVey, 2010). This phosphorylation enhances CtIP's interaction with BRCA1, which promotes CtIP end resection activity (Cruz-García et al., 2014). Increases in BRCA1 expression further enhance this relationship during S phase (Chen et al., 2013). The coordinated effort of these nucleases inhibits binding by Ku, preventing c-NHEJ (Chanut et al., 2016), and committing to homology-mediated repair. Furthermore, BRCA1 antagonizes 53BP1 phosphorylation-mediated activation during S and G2 phases (Feng et al., 2015b). As end resection proceeds, the exposed $3'$ ssDNA tails are initially stabilized by binding of replication protein A (RPA) (Chen et al., 2013). A critical step in the commitment to HR repair is the displacement of RPA by Rad51 to form the Rad51-ssDNA nucleofilament. Rad51 nucleofilament formation is required for efficient homology search and strand invasion (Uchida et al., 2012). This process is promoted by the tumor suppressor BRCA2 (Liu et al., 2010). During strand invasion, a displacement loop (D-loop) is formed, and a polymerase extends the invading $3'$ strand, synthesizing new DNA and resulting in a structure called a

Holiday junction. From here, the Holiday junction is resolved by one of two pathways; double-strand break repair (DSBR) or synthesis-dependent strand annealing (SDSA). For a more in-depth description of repair by HR, I suggest the following review Krejci et al. (2012).

SSA is somewhat similar to Alt-EJ, in that they both primarily repair breaks through the annealing of CtIP exposed repetitive regions resulting in a deletion mutation between repeats (Bhargava et al., 2016). However, these repair events are mechanistically distinct and likely differ in the degree of end-resection required. As end-resection is activated during S phase and G2, SSA may become the more prevalent alternative repair pathway outside of G1. SSA also requires the ssDNA binding protein Rad52, which is dispensable for Alt-EJ (Bennardo et al., 2008). Rad52 is a ssDNA binding protein that mediates homology search and annealing of repeats through rearrangements of the ssDNA-Rad52 complex (Rothenberg et al., 2008). Following annealing, the 3′ ssDNA tail is removed by the ERCC1/XPF complex (Motycka et al., 2004). Remaining gaps are filled and ends ligated by uncharacterized proteins. It is still unclear in what context a healthy cell would choose SSA over HR. It may serve primarily as a backup in the absence of an intact HR pathway. A critical step in the decision is Rad51 turnover of Rad52-RPA bound ssDNA, Rad51 and Rad52 compete to establish repair conditions for either HR or SSA (Gibb et al., 2014). Disruption of Rad51, or Rad51 mediator proteins such as BRCA2, causes a substantial increase in the frequency of SSA (Stark et al., 2004). Thus, targeting of SSA is now being investigated in the treatment of BRCA/HR-deficient cancers and inhibitors of Rad52 have shown promise in this respect (Chandramouly et al., 2015).

1.5.3 DSB Repair in the Context of Chromatin

It is important to consider that DSBs occur within the context of chromatin. On the one hand, presenting a barrier to repair, on the other, an opportunity to coordinate signaling events through chromatin modifications. As such, there are many histone PTM writers/readers and chromatin remodelers that function in DSB repair. For example, histone ubiquitination has been shown to be important in many steps in the repair of DSBs, including both histone eviction and recruitment of repair factors (Schwertman et al., 2016). There also several remodeling factors and chaperones that get recruited to DSBs to promote a chromatin environment amenable for repair. The FKBP25 interacting partner nucleolin, for example, has histone chaperone activity and is involved in histone turnover at DSB sites creating a more open chromatin

environment (Goldstein et al., 2013). Interestingly, complexes associated with the formation of higher order chromatin structures and heterochromatin have also been shown to be critical for DSB repair. This includes the rapid and transient accumulation of members of the repressive NuRD remodeling complex (Smeenk et al., 2010; Chou et al., 2010). Its activity is required for downstream ubiquitination DSB signaling events (Smeenk et al., 2010). While it is not entirely clear, the transient formation of heterochromatin domains surrounding DSB sites seems to be important for coordinating early DSB signaling events. What is now clear, is that chromatin is not merely an obstacle for repair, but an active participant.

1.5.4 Targeting the DDR in the Treatment of Cancer

Cancer is among the leading causes of death worldwide – in 2012, approximately 8.2 million people succumbed to the disease (Ferlay et al., 2015). There is a significant need to improve both understanding of the disease and the failings of current treatments. A vital component of cancer treatment today is the use of cytotoxic chemotherapeutic drugs, which act to kill cancer cells and reduce tumor growth by targeting fundamental cell processes. The first rationally designed chemotherapeutics came from the research of Dr. Sidney Farber on folate analogs for the treatment of children with acute lymphoblastic leukemia (Farber et al., 1948). While not known at the time, these antifolate compounds have since been shown to kill cancer cells through DNA-damaging properties. There exists a long clinical history of DNA-damaging agents (DDAs) being used in the chemotherapeutic treatment of cancer (Cheung-Ong et al., 2013), these include anti-cancer compounds such as cisplatin, carboplatin, methotrexate, and doxorubicin. DNA repair pathways are involved in both the formation of cancer and resistance to treatment by DDAs, thus inhibitors that directly target repair may be valuable when used in combination with DNA-damaging chemotherapeutics or the case of cancers with oncogenic mutations in DDR proteins as single-agent therapies (Biffi and Tuissi, 2017). Indeed, Parp-1 inhibitors are now in use in the clinic for the treatment of BRCA-associated hereditary forms of breast and ovarian cancer (Feng et al., 2015a). Researchers are also actively looking for ways to further exploit the potential of precision medicines aimed at the DDR by finding synergistic compounds that each target a distinct repair pathway. This approach may extend the utility of these drugs to HR-competent cancers as well.

Chemotherapeutics that target DNA are often used in combination regimens with microtubule targeting agents (MTAs) to achieve greater efficacy. MTAs were first

developed in the 1950s, following the wave of new cytotoxic drugs discovered to have anti-cancer properties, like the DDAs. Initially, it was thought that MTAs worked by disrupting mitosis, preventing the formation of the mitotic spindle (Horton et al., 1988). However, drugs that specifically target mitosis have not found the same success in the clinic as MTAs, suggesting the mechanism of MTAs in cancer may include microtubule-mediated processes in interphase as well (Komlodi-Pasztor et al., 2011). Interestingly, the disruption of the MT network is known to interfere with the trafficking of DNA repair proteins to the nucleus, with increased localization to the cytoplasm of DNA damage repair proteins DNA-PKcs, NBS1, MRE11, and 53BP1 when cells were treated with MT-disrupting agents (Poruchynsky et al., 2015). Microtubules may also be important in regulating the mobility of chromatin containing a double-strand break, which is required for efficient repair (Miné-Hattab and Rothstein, 2013). It has been proposed that DNA breaks may need to be relocalized to repair centers in the nucleus (Neumaier et al., 2012). Indeed, it has been shown that dynamic microtubules are required for the mobility of and repair of damaged chromatin in both yeast (Villoria et al., 2017) and mammalian systems (Lottersberger et al., 2015). Collectively, these findings describe a clear relationship between microtubule dynamics and DNA repair processes. Further characterization of this relationship may improve the way chemotherapeutics are administered and our understanding of the synergy between drugs that seem to target seemingly distinct cellular components. Again, like ribosome biogenesis and DNA damage repair, there is a connection between these seemingly independent cellular events, arguing for an integrated systems-level approach to understanding cell biology as well as a better understanding of multifunctional proteins that may bridge these divides.

1.6 The Microtubule Cytoskeleton

Microtubules (MTs) are cylindrical polar structures approximately 25 nm across with a 5 nm wide hollow central core, composed primarily of α and β tubulin heterodimers (Figure 9). They constitute one of three major structural components of the cytoskeleton, the remaining two being actin microfilaments and intermediate filaments. MTs are critical to many fundamental cellular processes, including cell motility, intracellular trafficking of cargo, supporting the structure of the cell, and coordinating segregation of chromosomes and abscission during cell division. A defining property of MTs is dynamic instability, first discovered by Mitchison and Kirschner (1984). Dynamic instability refers to the ability to alter between phases of polymerization and

depolymerization at their plus end. The minus end is typically linked by γ-tubulin to a capping complex, such as the centrosome. The stability of MTs can be influenced by a number of microtubule associated proteins (MAPs).

Dynamic instability of MTs is well demonstrated during mitosis, as the interphase MT network rapidly disassembles to form the mitotic spindle apparatus, a large macromolecular complex that is responsible for the segregation of chromosomes during cell division (Walczak and Heald, 2008). The structure of the mitotic spindle and its actions during mitosis are captivating, and have been appreciated by microscopists for over 50 years (Schmidt, 1939; Inoué and Bajer, 1961; Swann, 1951). As mitosis begins, the nuclear envelope disassembles and chromatin condenses. Bi-polar arrays of microtubules extend inward, emanating from two recently duplicated centrosomes and attaching to chromosomes at defined genomic loci called centromeres. Once all of the chromosomes are properly attached to the spindle, release from the spindle assembly checkpoint allows the migration of sister chromatids to opposing poles. The nuclear envelope begins reforming around each set of chromosomes that now begin decondensing, while a remaining bundle of microtubules, called the midbody, coordinates the final stages of cytokinesis, resulting in abscission and two genetically identical daughter cells.

Given the pivotal role of the mitotic spindle in cellular division, the MT network has become an established target in the pharmacological treatment of cancer as a means to halt proliferation (Dumontet and Jordan, 2010). For example, the vinca alkaloids and taxanes, anti-mitotic agents that function by suppressing microtubule dynamics, are currently administered in the treatment of both solid tumors and hematological malignancies. Several MAPs are also known to play a role in chemotherapeutic resistance and tumor growth (Bhat and Setaluri, 2007). Over-expression of the MAP tau, an MT stabilizer, is correlated with poor outcome in breast cancer (Neal and Yu, 2006) and low tau expression is a general indicator that a patient will respond well to paclitaxel (Smoter et al., 2011). Additionally, MAP2, stathmin, survivin, BRCA1, and VHL have been implicated in cancer progression and resistance to MT-targeting chemotherapies (Parker et al., 2014). Hence, improved understanding of MT dynamics and the mechanisms by which this process is regulated is important.

In mature neurons, which are terminally differentiated, the microtubule network is utilized as an architectural element and not for cell division (Matamoros and Baas, 2016). Arrays of microtubules promote axonal outgrowth and provide neurons with a platform for the transport of molecular cargo along their axons and dendrites. Reduced microtubule stability and impaired long-distance transport, often as a con-

sequence of impaired MAP function, has been associated with a number of neurodegenerative diseases (Dubey et al., 2015). The MAP tau has been well studied in this regard – the formation of tau aggregates in paired helical filaments and neurofibrillary tangles, which inactivates its MT-stabilizing activity and disrupts axonal transport, is a pathological hallmark of Alzheimer's disease and related neurodegenerative disorders, coined tauopathies (Wang and Mandelkow, 2015). Strikingly, the *cis-trans* conformational state of a single proline in tau is indicative of either the pathogenic or biologically active state (Nakamura et al., 2012), and monoclonal antibodies recognizing the two distinct states show promise for the early diagnosis, prevention, and treatment of tauopathies (Iqbal et al., 2016). In cells, the *cis-trans* conformers of tau are regulated by PPI enzymes (Cao and Konsolaki, 2011; Blair et al., 2015; Koren et al., 2011). More generally, PPIs have emerged as critical regulators of the MT network and as potential therapeutic targets for the treatment of MT-associated diseases.

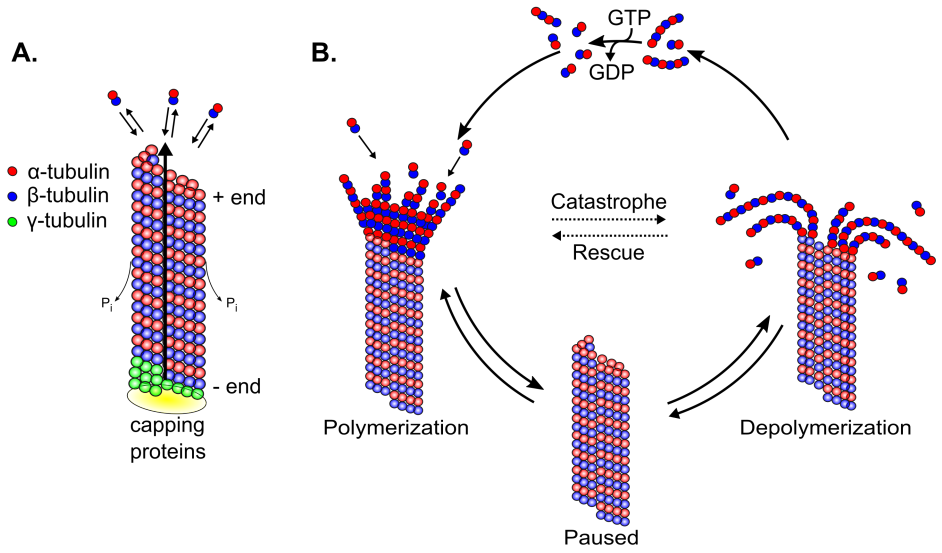

Figure 9. Microtubule Dynamics - (A) Microtubules, composed primarily of α-tubulin and β-tubulin heterodimers, are polarized structures within the cell with reduced stability at their fast-growing end (plus end) relative to the slow growing end (minus end) resulting in directional growth. Microtubules are nucleated by capping proteins, such as the centrosomal proteins, through a linkage provided by γ-tubulin. (B) Microtubules switch between phases of growth, pausing, and shrinkage in a process known as dynamic instability. Recruitment of a GTP-bound heterodimer to the growing end of microtubules promotes GTP hydrolysis of the previous subunit, providing a GTP cap that stabilizes the microtubule structure at the plus end. The rapid loss of GDP-bound tubulin heterodimer subunits characterizes depolymerization.

1.6.1 Intracellular Transport

MTs facilitate movement, both by promoting morphological changes that aid navigation through the external environment and as a platform for the intracellular transport of cargo. Most cargo is bound simultaneously by the prototypical plus-end directed kinesin motors and minus-end dynein motors. Engaged in a back and forth tug of war – these movements have an overall net directionality towards the intended destination in a process known as bidirectional transport (Hancock, 2014). This process ensures proteins, vesicles, organelles, and ribonucleoprotein (RNP) complexes arrive at their intended destination while being able to still navigate any potential roadblocks along the way. Kinesins are a superfamily, with up to 25 members, each member sharing a common but divergent cargo-binding tail domain, which allows the recognition of different forms of cargo (Miki et al., 2005). In stark contrast, there is only one major form of dynein which transports many different types of cargo (Pfister et al., 2006). Thus, dynein-mediated transport requires an accessory complex, known as dynactin, to load various forms of cargo (Schroer, 2004). This may also include the use of other proteins to aid in the recognition and attachment of different types of cargo. Interestingly, several FKBPs seem to play this role, as discussed below.

1.6.2 Regulation of the MT Network by Prolyl Isomerases

Recently, members of all three families have been shown to regulate MT architecture either directly or through the modulation of MAP activity. Pin1, a member of the parvulin family, recognizes phosphorylated S/T-proline motifs and restores misfolded *cis* proline containing tau (Lu et al., 1999; Nakamura et al., 2012). Another parvulin, Par17, interacts with tubulin in a GTP-dependent manner and its catalytic activity promotes polymerization (Thiele et al., 2011). In contrast, the FKBP, FKBP52 destabilizes microtubules through direct binding of tubulin independently of its catalytic domain (Chambraud et al., 2007). It has also been shown to regulate the MAP tau and may be a therapeutically relevant target for the treatment of Alzheimer's disease (Chambraud et al., 2010). Several of the hsp90-associated immunophilins are known to interact with the microtubule network through the motor complex dynein via their isomerase domains, with implications for the transport of cargo and MT stability. These include: CyP-A (Galigniana et al., 2004), CyP-40 (Galigniana et al., 2002), FKBP52 (Galigniana et al., 2004; Wochnik et al., 2005), FKBP51 (Wochnik et al., 2005), and FKBPL (McKeen et al., 2008). FKBP15 has also been shown to be involved in the MT-dependent intracellular transport of early endosomes, however lit-

tle is known with regards to its mechanism (Viklund et al., 2009). And as mentioned, the immunomodulatory drug FK506, which targets the catalytic pocket of FKBPs, has been shown to have neuroprotective and regenerative qualities (Hausch, 2015). While these reports suggest an intimate relationship between prolyl isomerases and MT dynamics, the full contribution of this family of enzymes to the regulation of the MT network is unclear as the biological function of most members remains uncharacterized. Thus, understanding the individual contributions of each FKBP will improve the rational design of drugs in the treatment of MT-associated disease.

1.7 Crosstalk between Regulatory Networks - Moving toward a systems-level understanding of cellular biology

The reductionist approach to understanding cellular biology has been to break down cellular systems into individual parts, identify core components that execute a particular cell function and study them in their simplest form. While this has been incredibly valuable in unraveling and establishing the fundamental requirements of a cell, it underestimates the complexity and interconnectedness of phenomenon in cellular biology. The concepts presented in this introduction would have at one time been thought of as discrete processes and studied as individual disciplines. However, with the advent of next-generation "omic" technologies, a systems-level view of the cell is taking shape and the connections are becoming clearer. Understanding how the individual parts of the cell come together through crosstalk via PTMs and multifunctional proteins will support a better understanding of the internal wiring of cells in health and sickness. Thus, identifying and studying proteins that moonlight in different aspects of cell biology will greatly benefit our overall understanding of the interconnected cell.

1.8 Research Objectives

Since their discovery, prolyl isomerase enzymes have proven to be much more than simple protein folding chaperones. Prolyl isomerization catalyzed by PPIs is also an important mechanism in the regulation of folded proteins within the context of biological signaling networks. While there have been significant advances in our understanding of these enzymes to support this view, a knowledge gap remains; the functions and substrates of most PPIs remain unknown. This information is particularly relevant given the widespread use of the immunosuppressant drugs FK506 and rapamycin and the potential for these drugs in the treatment of disease. Thus, a comprehensive understanding of how these enzymes operate, will not only begin to elucidate the anti-cancer and neurotrophic properties of these established pharmaceuticals but may also identify novel drug targets.

The overarching objective of my research has been to characterize the cellular function of the nuclear prolyl isomerase FKBP25 in the context of biological networks. When I began this research, there were few accounts in the published literature regarding FKBP25's functions. It was known to be one of the few FKBPs that localized to the nucleus (Jin and Burakoff, 1993) and had been shown to associate with several factors involved in transcriptional regulation and ribosome biogenesis, these included; core histones (Galat and Thai, 2014), HMG proteins (Foulger et al., 2012), HDAC1 (Yang et al., 2001), YY1 (Yang et al., 2001), MDM2 (Ochocka et al., 2009), and nucleolin (Jin and Burakoff, 1993). Therefore, my initial hypothesis was that FKBP25 targets proline residues in nuclear proteins associated with ribosome biogenesis and transcription to regulate their function. While a putative role for FKBP25 in these processes had been proposed, suggesting FKBP25 may be a multifunctional protein, direct evidence had been lacking. To test this, my research plan was to utilize recent advances in "omics technologies to identify the protein-protein interactions of FKBP25 and its influence on gene transcription without bias, on a systems-level. Using a broad proteomics approach, I believed we would be able to narrow down and follow up on putative functions and substrates, following a 'guilt by association' approach. Through next-generation sequencing of RNA isolated from FKBP25 depleted cells, I hoped to further characterize the protein's role in the regulation of chromatin, transcription, and RNA metabolism. Based on the outcome of these experiments, I would derive hypotheses regarding putative functions to be investigated by biochemical, cell biology, and molecular biology experiments. Thus, the primary research objectives of this project were as follows;

1. Define the protein-protein interactions FKBP25 participates in to identify putative functions and substrates for further exploration.

2. Investigate FKBP25 mediated regulation of transcription using high-throughput sequencing.

3. Utilize the information garnered from high-throughput proteomic and transcriptomic screens to functionally explore FKBP25's role in the cell using biochemical and cell biology techniques.

4. Identify putative FKBP25 substrates.

1.9 Agenda

Chapter 1 - Introduction. Here I have outlined both the rational for studying FKBP25 and several aspects of cell biology that will be important for interpreting the results presented in data chapters two through four. Also, I hope this chapter presents the reader with a sense of just how integrated signaling networks are within eukaryotic cells and the importance of multifunctional proteins.

Chapter 2 - The BTHB Domain of FKBP25 is a dsRNA Binding Module. In this chapter I have performed a proteomic analysis to identify FKBP25's interacting partners and putative substrates, finding FKBP25 interacts with a significant number of RNA binding and ribosome biogenesis proteins. This led to the discovery that most of FKBP25's physical interactions are dependent on RNA and that the BTHB domain of FKBP25 is a novel dsRNA binding module. Further, I explore potential roles for FKBP25 in the transcription and processing of ribosomal RNA. This chapter describes experiments that have been both published and submitted for publication, as a co-first and first author paper, respectively.

Chapter 3 - FKBP25 Regulates Microtubule Stability. In Chapter 3 I set out to characterize the transcriptional consequences of FKBP25 depletion in HEK293 cells. These results led me to a detailed characterization of FKBP25's regulation of the cell cycle and the discovery that FKBP25 is a novel microtubule-associated protein required for the maintenance of chromosome stability. I further explored mechanisms of FKBP25's regulation during mitosis on its microtubule and nucleic acid binding properties. The experiments described here are currently in preparation for submission as a first author paper.

Chapter 4 - FKBP25 Participates in the Repair of DNA DSBs. In this final data chapter, I follow up on novel FKBP25 protein-protein interactions with DSB factors identified in Chapter 2. I show that FKBP25 regulates DSB repair in a catalytic dependent fashion. Also presented, is preliminary evidence that targeting FKBPs may be beneficial in the treatment of BRCA-proficient cancers by Parp inhibition. This story is in preparation for submission, with several additional experiments in progress.

Chapter 5 - Discussion & Future Exploration. I will discuss the significant findings of my Ph.D. work and how they relate to broader biological questions and future directions for the study of FKBP25.

Chapter 2

The BTHB Domain of FKBP25 is a dsRNA Binding Module

This chapter was adapted from the following publications:

Gudavicius G‡, **Dilworth D**‡, Serpa JJ, Sessler N, Petrotchenko EV, Borchers CH, & Nelson CJ (2014) The prolyl isomerase, FKBP25, interacts with RNA-engaged nucleolin and the pre-60S ribosomal subunit. RNA 20 (7): 1014-22.

Dilworth D‡, Upadhyay SK‡, Bonnafous P, Bibi Edoo A, Bourbigot S, Pesek-Jardim F, Gudavicius G, Serpa JJ, Petrochenko EV, Borchers CH, Nelson CJ, & Mackereth CD. The basic tilted helical bundle domain of the prolyl isomerase FKBP25 is a novel double-stranded RNA binding module. *Submitted.*

‡ equally contributed to the manuscript.

Contributions: Experiments and data analysis performed by **DD** under the supervision of CJN with the following exceptions: SKU, PB, ABE, SB, and CDM performed NMR experiments, recombinant protein production, and molecular modeling; GG, JJS, NS, EVP, and CHB were involved in mass spectrometry sample preparation and instrument operation; GG performed Co-IP and silver staining in Figure 11A; FPJ purified biotinylated proteins by streptavidin capture for mass spectrometry analysis. The paper was written by **DD**, CDM, and CJN.

2.1 Abstract

Prolyl isomerases are defined by a catalytic domain that possesses prolyl *cis-trans* isomerase activity. In the case of FKBP proteins, their activity is not directed by a defined sequence motif. Instead, substrate specificity is achieved through accessory domains, which can also serve to broaden their functional repertoire. Here we report that the N-terminal BTHB domain of the human prolyl isomerase FKBP25 confers specific binding to double-stranded RNA (dsRNA). This binding is selective over DNA as well as single-stranded oligonucleotides. We find that an FKBP25-RNA association is required for its nucleolar localization and the vast majority of its protein interactions, including those with 60S pre-ribosome and early ribosome biogenesis factors. We further investigate a putative role in transcription and processing of rRNA, showing FKBP25's activity in these early events of ribosome biogenesis is limited.

2.2 Introduction

Information on the substrates of peptidyl prolyl isomerases is unfortunately lacking or incomplete for most family members, and the molecular basis for their target selectivity is unclear. It is assumed that protein-protein interactions, usually mediated by accessory domains, direct these enzymes to discrete subcellular locations and substrates (Schiene-Fischer, 2015). For example, while FKBP12 is a 12 kDa single domain cytosolic protein, the 25 kDa FKBP25 is predominantly found in the nucleus (Jin and Burakoff, 1993). Here it interacts with nucleolin (Jin and Burakoff, 1993), MDM2 (Ochocka et al., 2009), and the histone deacetylases HDAC1/HDAC2 (Yang et al., 2001). Recently, the N-terminal accessory domain of FKBP25 was found to adopt a novel basic BTHB domain fold (Helander et al., 2014), which mediates its interaction with the transcription factor YY1 (Yang et al., 2001). A combined interface made by the BTHB and FKBP domains was also reported to bind to DNA, albeit with low-affinity (Prakash et al., 2016). Although the interaction with YY1, and possibly DNA, can explain some of the targets of FKBP25, what is missing is a defining property that would account for the remaining putative substrates and most notably the proteins associated with the ribosome.

Here we demonstrate that FKBP25 localization and protein interactions are each RNA-dependent and mediated by a direct and specific interaction between the BTHB domain and dsRNA. In support of this model, we show that proteins that associate

with FKBP25 *in vivo* are enriched in RNA-binding proteins, ribosome subunits and maturation factors, as well other chromatin-associated proteins. The direct association of the BTHB of FKBP25 with dsRNA brings this FKBP to a discrete substrate clientele of proteins in ribonucleoprotein complexes. The discovery of the BTHB domain as a new dsRNA-binding domain also adds a new member to the small number of domain folds known to recognize dsRNA.

2.3 Results

2.3.1 RNA mediates most of FKBP25's protein-protein interactions

To better understand the biological function of FKBP25 and to identify putative substrates, I decided first to obtain information on proteins that come into close physical contact with FKBP25 in the cell. To this end, we used a proximity-dependent biotin identification (BioID) strategy to provide a historical snapshot of neighboring proteins. BioID utilizes a protein fusion to the promiscuous biotin ligase BirA to enable biotinylation of exposed primary amines, predominately lysines, on closely associated proteins in the presence of exogenous biotin (Figure 10A)(Roux et al., 2012). Biotin-tagged proximal interactors are then selectively purified via streptavidin capture and the digested peptides subsequently identified by mass spectrometry. I generated U2OS cell lines stably expressing either an FKBP25-BirA fusion protein or BirA alone. Cells were incubated for 24 h with biotin to allow labeling of proximal interactors and biotinylated proteins were purified by streptavidin capture under denaturing conditions (Figure 10B). Unbiased mass spectrometry protein identification revealed 73 proteins enriched in the FKBP25-BirA sample relative to the BirA control (Figure 10C). Gene ontology (GO) analysis of proximal interactors with the DAVID webserver (Huang et al., 2009) showed a strong enrichment for RNA binding and ribosome biogenesis factors, including 22 ribosomal proteins and several proteins involved in the early maturation events of ribosome production (a full list of identified proteins is presented in Table A.2 of the appendix). Apart from proteins related to the ribosome, there is an additional enrichment of other RNA-binding functions including proteins implicated in binding to polyA RNA, double-stranded RNA and mRNA 5′ UTRs (Figure 10D). The common aspect of RNA-binding behavior to most of the identified FKBP25 interactors suggests that RNA molecules may be a key mediator of FKBP25's protein interactome.

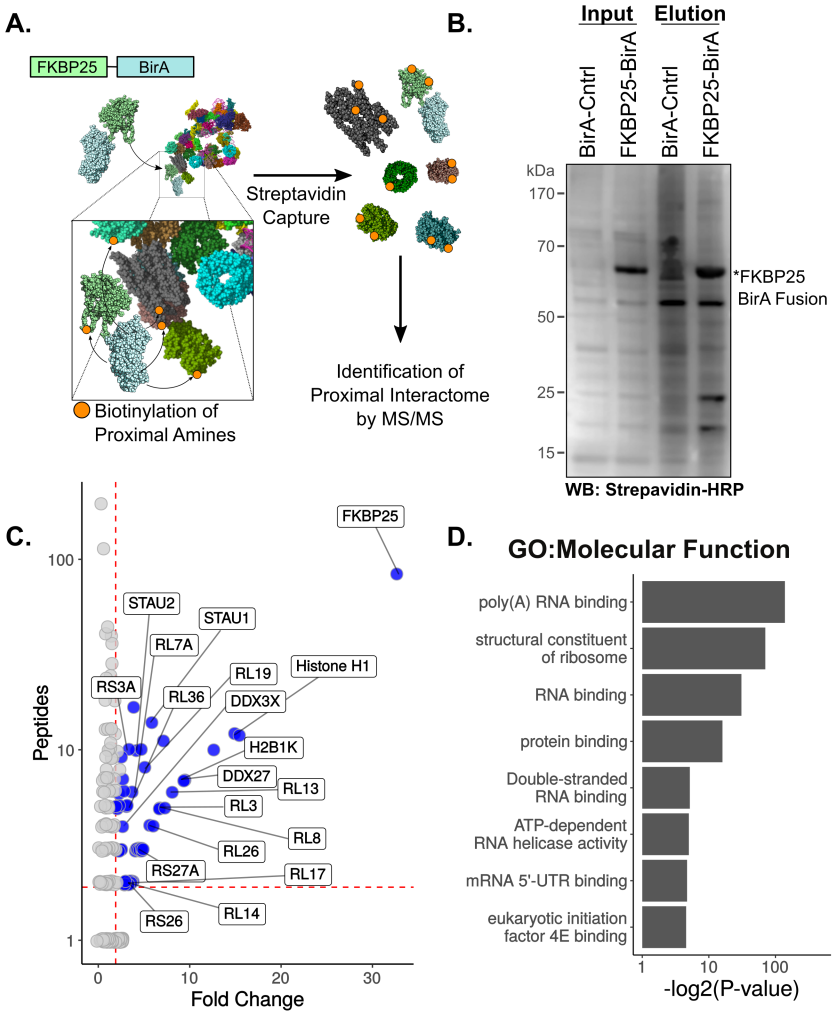

Figure 10. Identification of ribosomal and RNA binding proteins as proximal FKBP25 interacting partners by BioID. (A) Schematic of BioID-based identification of cellular proteins proximal to FKBP25. (B) Streptavidin-HRP western blot of whole cell extracts and streptavidin capture from U2OS cells stably expressing an FKBP25 biotin ligase fusion or biotin ligase control, incubated for 24 h in media containing 50 µM biotin. (C) Mass spectrometry identification of biotinylated proteins enriched in FKBP25-BirA streptavidin purifications relative to BirA control. The number of significant peptides identified relative to fold change is shown. (n=1) (D) Enriched GO by molecular function.

To test this hypothesis, we performed co-immunoprecipitation (Co-IP) of FLAG-tagged FKBP25 from HEK293 nuclear extract with and without pre-treatment with RNase A to deplete cellular RNAs. Silver staining of the immunoprecipitated material showed a clear reduction in co-purifying proteins to near background levels with RNase A pre-treatment (Figure 11A). These samples were then analyzed by mass spectrometry to precisely identify the RNA-dependent interactome of FKBP25 (Figure 11D; a full list of identified proteins can be found in Table A.3 of the appendix). Again, we identified a significant number of ribosome biogenesis factors and RNA binding proteins as FKBP25 interactors. We show that RNaseA treatment disrupts these interactions – this is highlighted by the GO analysis of interacting proteins identified in the presence or absence of RNase A treatment (Figure 11D).

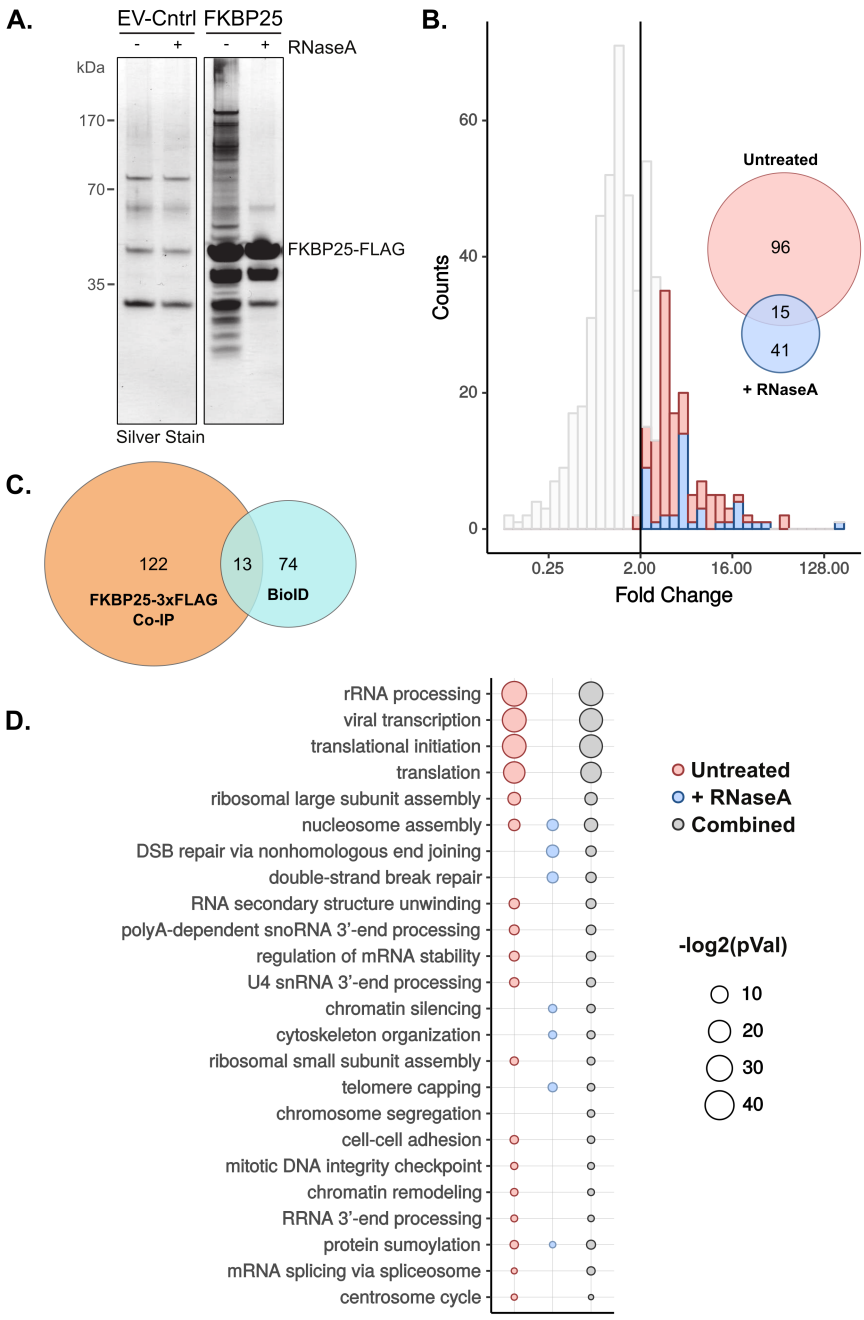

Figure 11. FKBP25 associates with ribosome biogenesis factors and other proteins in an RNA-dependent manner. (A) FKBP25 3xFLAG-tagged co-immunoprecipitated material with and without pre-treatment with RNase A analyzed by SDS-PAGE and visualized by silver stain. Empty vector cell lines are shown as a control. (B) Mass spectrometry analysis of proteins enriched in the FKBP25-FLAG sample relative to control, for samples either untreated or pre-treated with RNase A. (n=1) (C) Overlap in identified proteins between the BioID and FLAG Co-IP experiments. (D) Summarized GO analysis by biological process.

The overlap of proteins identified by the BioID and RNA-dependent Co-IP reveals a list of 12 common targets (Figure 11C; Table 2.1) with a noticeable cluster of 9 subunits of the 60S ribosome (RPL13, RPL15, RPL24, RPL27, RPL27A, RPL28, RPL3, RPL36, RPL8) and two subunits of the 30S ribosome (RPS23, RPS3A). An analysis of the complete FKBP25 interactome utilizing protein-protein interaction data from the Agile Protein Interactomes Dataserver (APID) (Alonso-López et al., 2016) highlights the published interactions between proteins involved in different biological processes and that these interactions cluster around ribosome biogenesis factors (Figure 12). In addition to the RNA associated proteins described, our proteomics screen to uncover FKBP25 protein-protein interactions also identified a number of DNA double strand break repair proteins and proteins associated with the cytoskeleton. Functional studies following up on a putative role for FKBP25 in the regulation of cytoskeleton dynamics and the DNA damage repair response are presented in Chapter 3 and Chapter 4 of this thesis, respectively. These interactions are also supported by a recent global proteomic study of protein complexes, which analyzed the protein content of over 1000 biochemical fractionations to identify soluble protein complexes (Havugimana et al., 2012). Gene ontology analysis of fractions containing at least five FKBP25 peptides shows that FKBP25 biochemically co-purifies with RNA metabolic factors and DNA repair enzymes, supporting the findings of our mass spec screen (the results of this analysis are shown as Figure A1 in the Appendix).

I independently validated several of these interactions by FLAG co-immunoprecipitation (Figure 13C), confirming that all interactions tested require intact RNA. The second observation from these studies is that inclusion of a canonical nuclear localization signal improves the capture of proteins from the BioID and proteomic screens (Figure 13AB). In keeping with previous results from our lab (Gudavicius et al., 2014), this finding shows that the majority of FKBP25 protein-protein interactions occur within the nucleus and that RNA-dependent interactions mainly derive from the nuclear pool of FKBP25.

Table 2.1. FKBP25 interacting proteins identified in both BioID and FKBP25-FLAG Co-IP proteomic screens

Uniprot Accession	**Gene Name**	**RNA Dependent?**
P08779	KRT16	No
P26373	RPL13	Yes
P39023	RPL3	Yes
P46776	RPL27A	Yes
P46779	RPL28	Yes
P61247	RPS3A	Yes
P61313	RPL15	Yes
P61353	RPL27	Yes
P62266	RPS23	Yes
P62917	RPL8	Yes
P83731	RPL24	Yes
Q8NC51	SERBP1	Yes
Q9Y3U8	RPL36	Yes

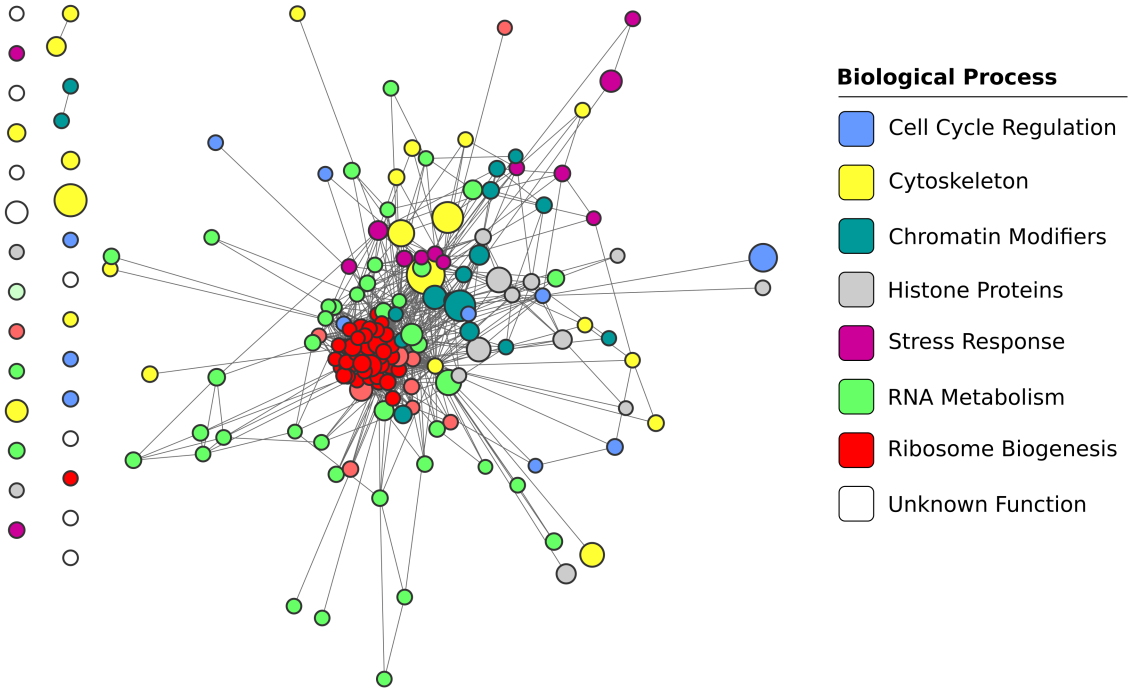

Figure 12. The FKBP25 interactome. Shown is a network analysis of FKBP25 interacting proteins identified by BioID or FLAG affinity capture. Network edges represent experimentally validated physical protein interactions contained within the Agile Protein Interactomes DataServer (Alonso-López et al., 2016)

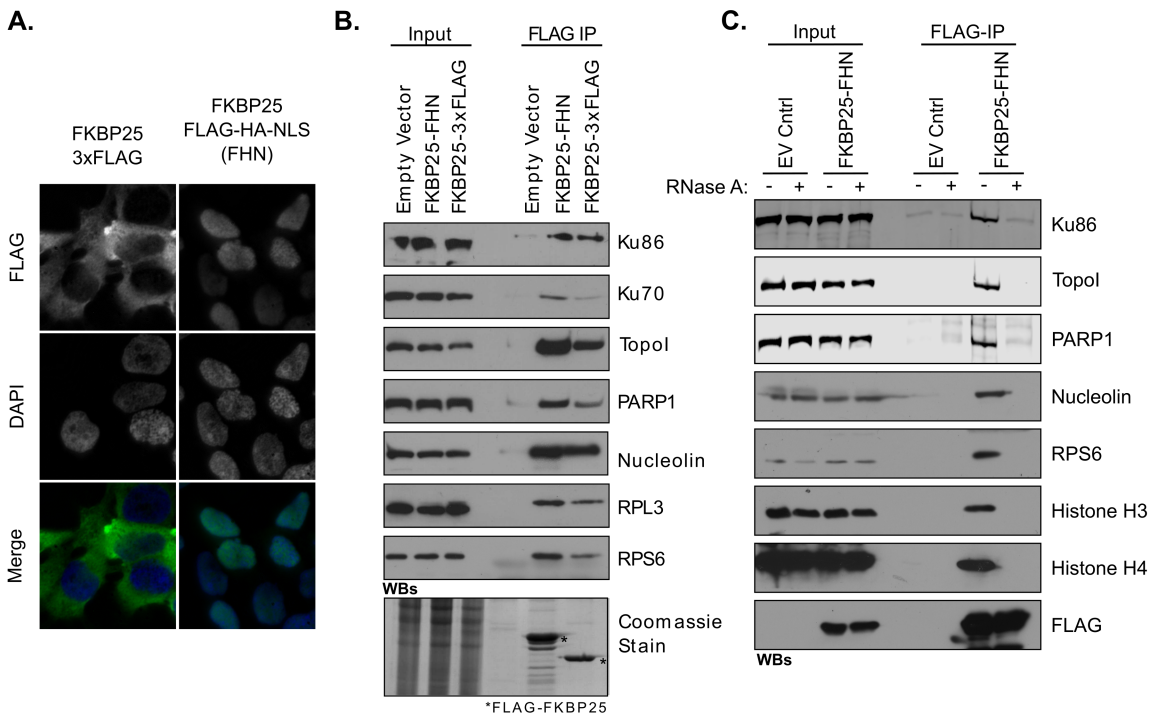

Figure 13. Validation of select proteins identified as interacting with FKBP25 by BioID and RNA-dependent co-immunoprecipitation. (A) Immunofluorescence of cells expressing FKBP25-3xFLAG and FKBP25-FLAG-HA-NLS. The addition of a canonical nuclear localization signal forces the transgene product into the nucleus. (B) Western blot validation of FKBP25 interacting proteins identified in the mass spectrometry protein interaction screens. The inclusion of a nuclear localization signal enhances recovery of co-purifying proteins. (C) Independent validation of protein interactions dependence on RNA. Whole cell extracts were either incubated in the presence or absence of RNase A before immunoprecipitation with FLAG antibodies. All protein interactions independently validated require RNA.

2.3.2 Nucleolar localization requires RNA

Given the abundance of nucleolar factors identified as FKBP25 associated, I wanted first to confirm that FKBP25 does indeed localize to the nucleolus. Thus, I performed a biochemical cellular fractionation that revealed FKBP25 localizes to the cytoplasmic, nuclear, and nucleolar fractions (Figure 14A). In support of this, FKBP25 has an exposed nuclear localization signal (NLS) and accumulates in the nucleus upon treatment with the nuclear export inhibitor leptomycin B (LMB) (Ochocka et al., 2009). Additionally, I performed chromatin immunoprecipitation (ChIP) using affinity purified antibodies raised against the N-terminus of FKBP25, confirming the presence of FKBP25 on rDNA repeats (Figure 14B). FKBP25 showed similar occupancy as

observed for nucleolin (Figure 14B-E). The presence of FKBP25 in the nucleolus is intriguing and supports the interaction data showing an association with nucleolar factors. It also supports a putative role in ribosome biogenesis, as previously suggested (Jin and Burakoff, 1993), demonstrating for the first time a nucleolar localization for FKBP25.

To investigate a cellular link between RNA and nuclear FKBP25, I first performed *in situ* subcellular fractionations by incubating cells with a mixture of detergent and buffered sucrose known as cytoskeleton buffer (CSK) (Figure 14F); a technique commonly used to release soluble proteins prior to immunofluorescence to facilitate the visualization of proteins associated with large macromolecular complexes in the nucleus (Maison et al., 2002; Javed et al., 2004). I then visualized *in situ* fractionated U2OS cells by confocal immunofluorescence microscopy. Pre-washing of cells with CSK alone, leaving cellular membranes intact, shows that FKBP25 is primarily localized to the nucleus in U2OS cells, with a lesser fraction present in the cytoplasm (Figure 14F). In contrast, the addition of Triton, which permeabilizes cell membranes, eliminates the soluble cytoplasmic and nuclear FKBP25 signal, leaving only the chromatin-associated fraction. I observe a distinctive pattern of FKBP25 within the nucleus that is reminiscent of nucleoli, the nuclear substructures where early events in ribosome production take place (Boulon et al., 2010; McStay and Grummt, 2008). Indeed, colocalization with the rRNA transcription factor upstream binding factor (UBF) confirms a nucleolar enrichment of FKBP25 (Figure 14F). This localization is efficiently disrupted with treatment by RNase A, whereas UBF, which is incorporated into nucleolar chromatin, remains intact. Further, I show that upon low dose treatment with the RNA polymerase I inhibitor actinomycin D, the nucleolar localization of FKBP25 becomes impaired (Figure 14G). Lastly, when FKBP25-FLAG-HA-NLS immunoprecipitated material is run on a 1% denaturing formaldehyde agarose gel, I show a clear enrichment for an RNA species that migrates similarly to 28S ribosomal RNA (Figure 15). Since the FKBP25-FLAG-HA-NLS construct is exclusively nuclear localized and FKBP25's protein-protein interactions are predominately nuclear in origin, this is likely an immature pre-60S ribosomal species. Together, these results strongly indicate that FKBP25 is recruited to sites of nascent rRNA transcription through an interaction with RNA. Given the importance of RNA in mediating protein-protein interactions and the dependence of RNA in nucleolar localization, I wondered if FKBP25 could in fact directly associate with RNA.

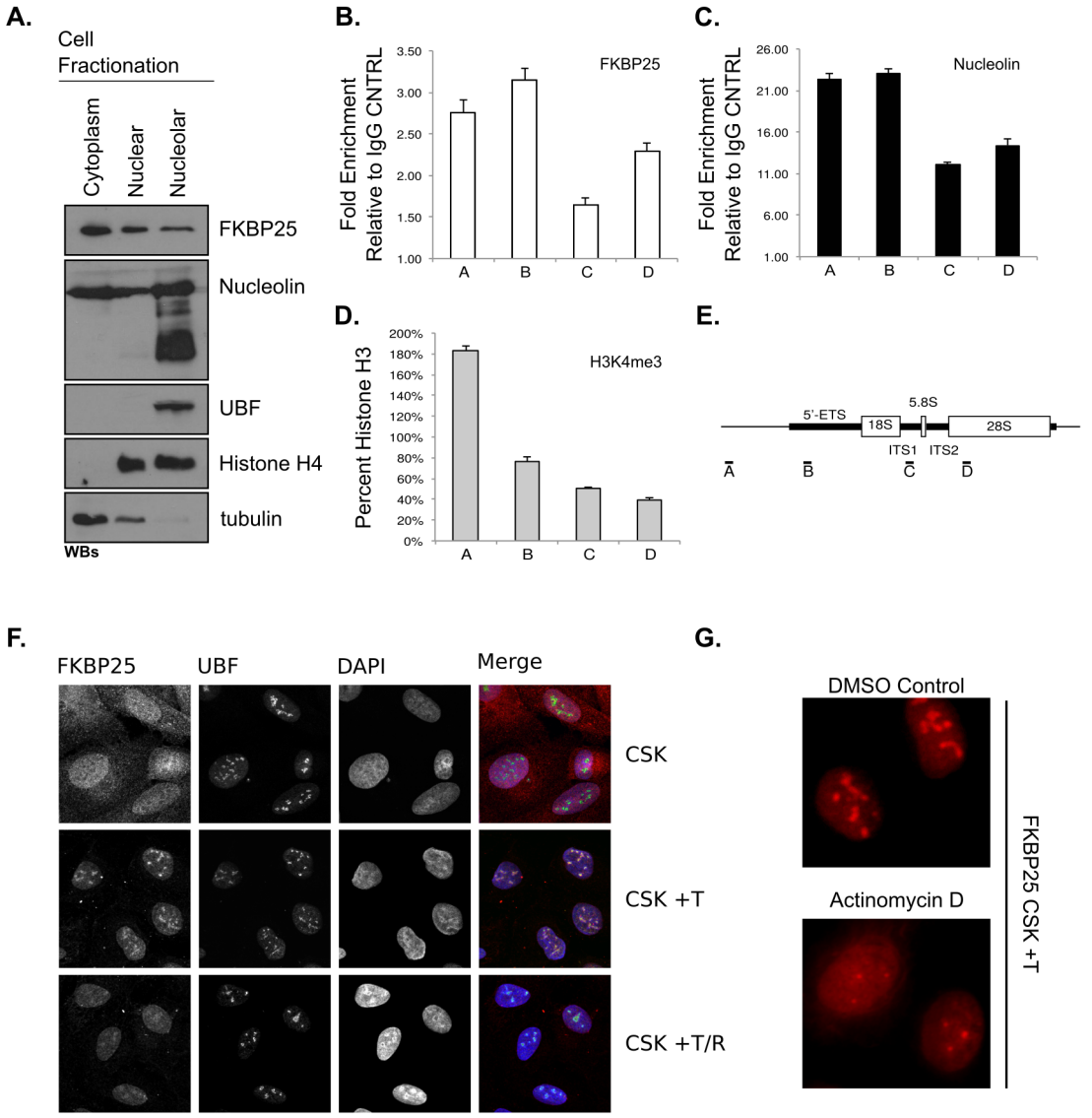

Figure 14. FKBP25 requires RNA for nucleolar localization. (A) Cellular fractionation of HEK293 cells displaying the localization of FKBP25 by western blot. αTubulin is a cytoplasmic marker, H4 is a nuclear/nucleolar marker, upstream binding factor (UBF) is a nucleolar marker, and nucleolin is known to localize to all three compartments of the cell. (B-D) ChIP of FKBP25, nucleolin, and H3K4me3 on rDNA repeats analyzed by quantitative polymerase chain reaction (qPCR). A = 1000 kb upstream start-site, B = 5' ETS, C = ITS1, and D = 28S. Shown as ± SD of three technical replicates. (E) Schematic indicating the location of amplicons on the rDNA repeat. (F) Confocal microscopy of FKBP25 and the nucleolar-specific upstream binding factor (UBF). Cells were either incubated in CSK alone, pre-extracted with CSK containing Triton (CSK+T), or pre-extracted with CSK containing Triton and treated with RNaseA (CSK+T+R) before fixation. (G) Epi-fluorescence microscopy of FKBP25 in cells treated with the RNA polymerase I inhibitor actinomycin D (10 nM for 4 h) and pre-extracted with CSK+T.

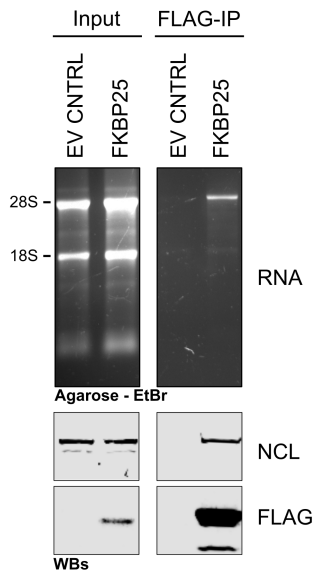

Figure 15. FKBP25 binds 28S ribosomal RNA in cells. Trizol extracted total RNA from FLAG immunoprecipitation of HEK293 cells expressing FKBP25-FLAG-HA-NLS or an empty vector control electrophoresed on a 1% denaturing formaldehyde-agarose gel and western blotting for FKBP25 and nucleolin.

2.3.3 FKBP25 directly binds to RNA

Past studies have described the direct binding of FKBP25 to DNA using a variety of techniques (Yang et al., 2001; Prakash et al., 2016; Galat and Thai, 2014; Rivière et al., 1993) – we first decided to replicate these findings by NMR spectroscopy. Using a 23 bp double-stranded DNA (dsDNA) ligand based on the transcription factor YY1 binding site (Yang et al., 2001), we observed movement of several amide crosspeaks in a series of 2D ^{15}N-HSQC spectra collected with increasing amounts of DNA indicating residue-specific proximity to the ligand (Figure 16). This is in agreement with the recent report on DNA binding by FKBP25 (Prakash et al., 2016).The modest shift for a subset of amide crosspeaks demonstrated weak but specific binding to residues in both the N-terminal (e.g. K22, K23, K48) and C-terminal (e.g. K154) domains. Given the importance of RNA in the function of FKBP25, we next repeated this experiment with a double-stranded RNA (dsRNA) version of the 23 bp ligand. Strikingly, we saw a robust and specific association of the N-terminal region of FKBP25 to this ligand. Note that amide crosspeaks corresponding to the N-terminal domain of FKBP25 are broadened and undetected upon binding to the large dsRNA ligand, whereas the linker and C-terminal domain remain visible with the same weak interac-

tion to dsRNA as with dsDNA. To confirm a domain-specific interaction with dsRNA, we repeated the titrations with the isolated N-terminal BTHB domain from FKBP25 (residues 1-74). A strong interaction with dsRNA was indeed maintained for the isolated BTHB domain, with a weak interaction to dsDNA identical in magnitude as for the full-length protein (Figure 16B). Titrations with the isolated C-terminal FKBP peptidyl-prolyl isomerase domain from FKBP25 (residues 108-224) also recapitulated the finding from the full-length protein and the weak interaction to both dsDNA and dsRNA (Figure 16C). Together, these results point to a selective recognition of dsRNA by the BTHB domain of FKBP25. This specific binding is in contrast to the more modest interaction to dsDNA by both domains. Also evident is a clear independence of the two domains on nucleic acid binding, and similar binding behavior between the isolated domains and the full-length protein.

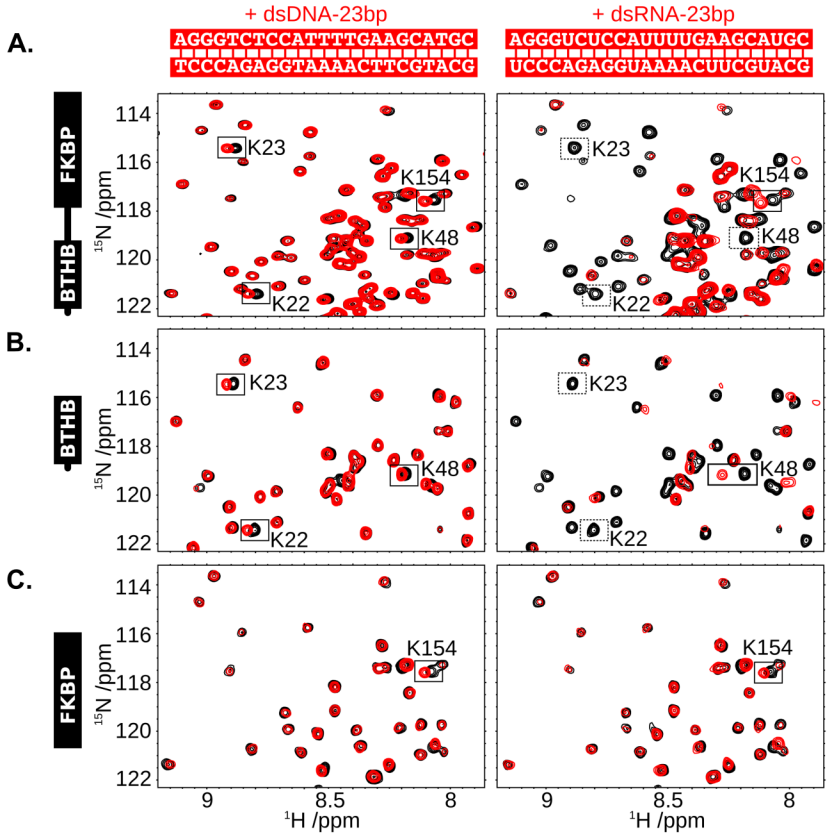

Figure 16. The BTHB domain displays a binding preference for dsRNA over dsDNA. (A)^{15}N-HSQC spectra regions corresponding to 100 µM ^{15}N-labelled full-length FKBP25 (in black) superimposed by the spectra with 100 µM added 23-bp dsDNA (left, in red) or 100 µM added 23-bp dsRNA (right, in red). Crosspeaks corresponding to three lysine residues from the BTHB domain (K22, K23, K48) and one from the FKBP domain (K154) have been annotated. Most crosspeaks corresponding to the BTHB domain broaden below detection upon addition of dsRNA-23bp. (B-C) Similar analysis with the isolated BTHB domain (residues 1-74) and the isolated FKBP domain (residues 108-224).

2.3.4 The BTHB domain is selective for dsRNA

The apparent selectivity of the BTHB for dsRNA over dsDNA prompted us to further probe the binding preferences of this domain with a variety of RNA and DNA oligonucleotides. Using the same approach as in Figure 16B we added increasing amounts of an oligonucleotide to ^{15}N-labelled FKBP25$_{(1-74)}$ and monitored binding-induced changes in residue-specific NMR crosspeak positions or signal disappearance due to broadening (ligand sequences and selected spectra regions shown in Figure 17). To minimize size-dependent signal loss in the NMR spectra for the bound BTHB we first

used a short 8bp ligand. Notably, this ligand (dsRNA-8) was bound by most of the residues sensitive to the addition of the dsRNA-23bp. Specificity is also retained in the 8 bp ligand since the DNA version, dsDNA-8, did not result in any noticeable interaction. We then tested BTHB interactions with the single-stranded oligonucleotides ssRNA-8 and ssDNA-8, neither of which showed signs of binding. Finally, we found that an RNA-DNA duplex, RNA/DNA-8, was recognized by FKBP25 to almost the same degree as for dsRNA-8. Collectively these results show that the BTHB binds to short dsRNAs and to a lesser extent an RNA-DNA duplex. However, does not bind to ssRNA, ssDNA, or dsDNA.

To investigate if the BTHB has any sequence specificity for dsRNA binding, we designed two new 8 bp ligands with varying palindromic sequences. dsRNA-8b interacted to the same extent as the initial 8 bp ligand, whereas dsRNA-8c still bound but with a significant reduction in crosspeak movement. In particular, the perturbation of the Asn46 side chain amide is almost entirely lost. Therefore, although there is a general binding to 8 bp dsRNAs, the BTHB may possess a degree of sequence or shape preference that could target a distinct set of RNA targets.

Given that FKBP25 interacts with 28S ribosomal RNA (Figure 15) we speculated that regions of double-stranded rRNA represent likely physiological ligands for the BTHB. The 28S rRNA has numerous dsRNA segments within stemloop structures, and we selected two examples for which NMR spectroscopy data are already available,b1 nucleolin recognition element (b1NRE) and b2 nucleolin recognition element (b2NRE) (Finger et al., 2003). The b1NRE stemloop interacted with the BTHB domain to a similar degree as the dsRNA-8 ligand (Figure 17). A comparable interaction was also observed with the b2NRE stemloop ligand (Figure 17). Both stemloops were initially studied due to their interaction with nucleolin, and nucleolin was previously found in FKBP25-containing complexes (Jin and Burakoff, 1993). We, therefore, prepared a second b2NRE ligand pre-bound to the first and second RRM domains of hamster nucleolin (residues 299-459). The presence of nucleolin on the b2NRE stemloop did not appear to affect the ability to bind to FKBP25 (Figure17). We conclude that dsRNA within the context of nucleolin-associated stemloops provides one possible cellular target of the FKBP25 BTHB domain.

Finally, we asked if BTHB-dsRNA affinity is based on the length of the dsRNA. From the NMR spectroscopy titrations, it was already shown that the 8 bp dsRNA ligand caused less perturbation as compared to the original dsRNA-23bp. We, therefore, tested an additional series of four palindromic ligands from 6 bp to 18 bp (Figure 17). The NMR spectra indicate that the two longest sequences, dsRNA-18 and dsRNA-14,

bound most strongly to FKBP25. Binding to dsRNA-10 was somewhat reduced. In contrast, dsRNA-6 had only minimal effect on the BTHB amide signals. It appears that binding affinity is sensitive to the length of the dsRNA, and that association with FKBP25 requires a dsRNA ligand longer than 6 bp.

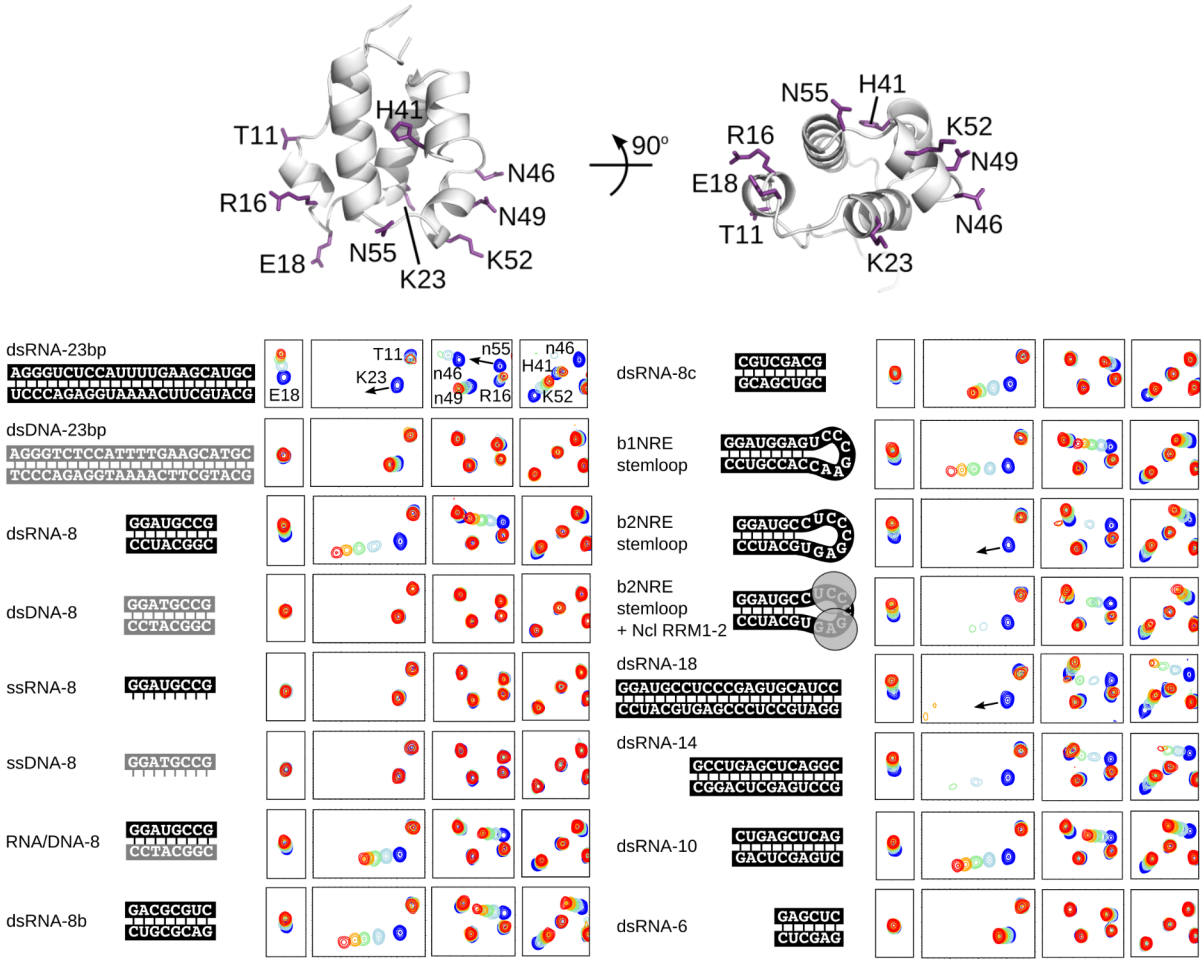

Figure 17. Binding preference for the isolated BTHB domain. Regions of NMR spectra following titration of various ligands into 100 µM ^{15}N-labelled FKBP25$_{(1-74)}$. The unbound spectra are shown in blue, and the spectra following the addition of 25 µM, 50 µM, 75 µM and 100 µM ligand are colored light blue, light green, orange and red, respectively. The location of residues from the BTHB with annotated crosspeaks are indicated (top panel; atomic coordinates from PDB ID 2KFV). Annotations with a small letter n correspond to the asparagine sidechain amide crosspeaks.

2.3.5 RNA-binding ability is required for *in vivo* interactions of FKBP25

Our NMR studies provide information of the surface residues of the BTHB domain that are in proximity to the dsRNA (Figure 18A; Figure 19A). This includes a pair of key lysine residues, K22/K23. With an aim to design mutants for *in vivo* studies, we constructed two variants of FKBP25 targeting these lysine residues implicated in RNA binding. Lysine to methionine mutations were selected as such substitutions remove the positive charge with minimal disruption to side chain length. We show that the double mutations K22M/K23M do not affect the folding of the BTHB domain as evident by their NMR spectra (Figure 18B). Using the dsRNA-10 ligand, we titrated the K22M/K23M mutant and followed the binding using NMR spectroscopy, showing significant inhibition of dsRNA binding (Figure 19B).

To confirm that FKBP25 does indeed interact directly with RNA in cells, I performed UV cross-linking immunoprecipitation (CLIP) experiments using both wild-type FKBP25 and the K22M/K23M mutant. UV cross-linking of cells results in irreversible covalent bonds between RNA binding proteins and their bound RNA, allowing stringent purification (König et al., 2011; Konig et al., 2011). I utilized FLAG-tagged tetracycline inducible constructs to temper over-expression of the FKBP25 transgenes to limit the potential of a false positive interaction with RNA (Figure 19C). Using increasing dilutions of RNase A treatment before immunoprecipitation as well as pre-treatment with excess DNase, shows that the interacting nucleic acids, which are visualized by radiolabelling with ^{32}P-labelled ATP, are in fact RNA (Figure 19E). Further, the K22M/K23M mutant shows a significant reduction in the amount of directly bound RNA, highlighting the importance of these residues in mediating dsRNA-binding activity. Finally, I utilized this construct in Co-IP experiments and show a reduction in several FKBP25 binding partners relative to the wild-type sequence (Figure 19D).

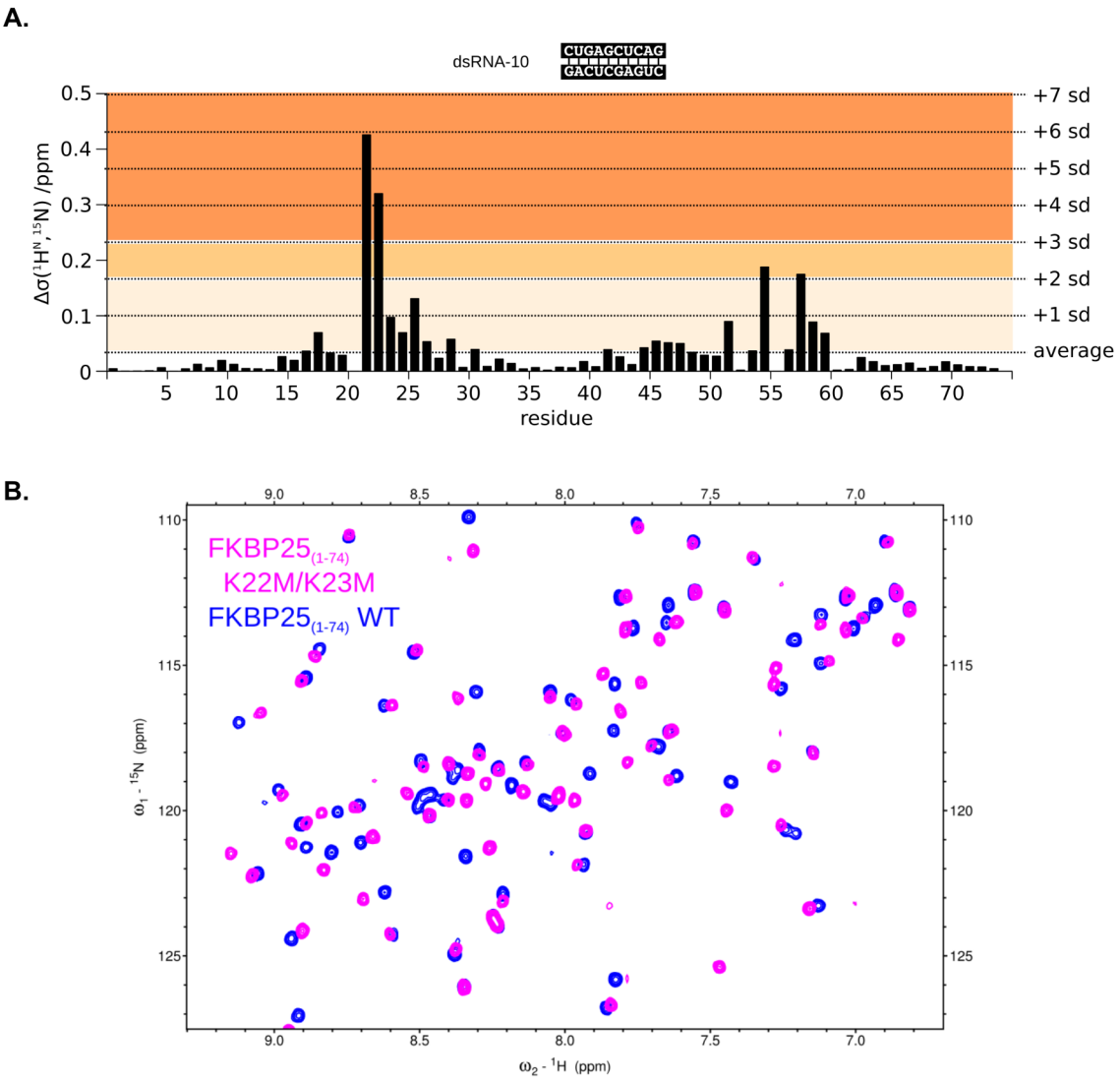

Figure 18. Identification of K22/K23 of the BTHB domain as key lysine residues involved in mediating FKBP25 dsRNA binding *in vitro*. (A) Chemical shift perturbation ($\Delta\delta$) measured by $^{1}H^{N}$ and ^{15}N changes in amide crosspeak positions for 100 µM ^{15}N-labelled FKBP25$_{(1-74)}$ in 20 mM sodium phosphate (pH 6.5) and 160 mM NaCl, without and with 300 µM dsRNA-10. The colour threshold values above the average are the same as in Figure 17a. (B) ^{1}H, ^{15}N-HSQC spectra of K22M/K23M mutant (magenta) and wildtype (blue) ^{15}N-labelled FKBP25$_{(1-74)}$.

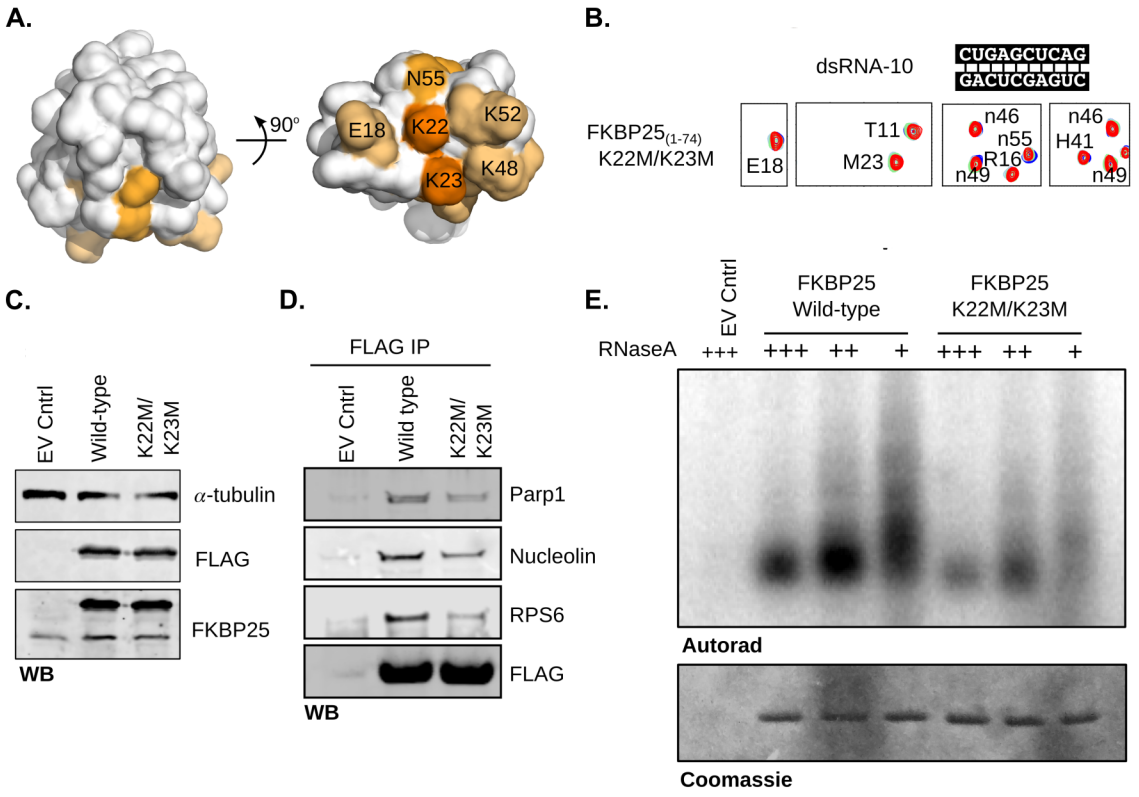

Figure 19. Mutation of key lysine residues reduces *in vitro* and cellular RNA-binding. (A) Structural model depicting key residues involved in FKBP25 binding of dsRNA *in vitro*. (B) NMR spectra following titration of dsRNA-10 into 100 µM ^{15}N-labelled FKBP25$_{(1-74)}$ with the K22M/K23M mutations. Colors as in Figure 17. (C) Western blot analysis of FLAG-tagged FKBP25 constructs (wild-type and the K22M/K23M mutant) relative to endogenous FKBP25 (empty vector control) in HEK 293 cells. Antibodies against α-tubulin, FLAG-tag, and FKBP25 correspond to the loading control, detection of FKBP25 constructs, and detection of both endogenous and FKBP25 constructs, respectively. (D) FLAG-affinity capture of cells expressing an empty vector control, wild-type FKBP25, or the K22M/K23M mutant with analysis by western blot using antibodies against the FKBP25-interacting proteins Parp1, nucleolin, and RPS6. FKBP25 construct expression verified by antibodies against the FLAG tag. (E) RNA cross-linking IP (CLIP) experiment with wild-type FKBP25 or the K22M/K23M mutant in HEK293 cells, with DNAse pre-treatment coupled with variable amounts of RNase A.

2.3.6 FKBP25 does not affect steady-state levels of ribosomal RNA

Given FKBP25's association with numerous ribosome biogenesis factors, likely through direct RNA binding of a pre-ribosomal RNA species, I next wanted to test whether FKBP25 may affect the transcript levels or processing of rRNA. I first looked at a potential role in RNA polymerase I (PolI) transcript levels of rRNA by disrupting FKBP25 function in HEK 293 cells with short interfering RNA (siRNA) and measuring total rRNA (RN18S) and unprocessed pre-rRNA levels (pre-rRNA) by qPCR (Figure 20A). I did not detect a significant difference in expression relative to a non-targeting siCNTRL, indicating FKBP25 is unlikely to regulate ribosomal transcript levels directly. Next, I was interested in exploring a potential role downstream of transcription in processing of pre-rRNA into its mature form. To explore this, I performed northern blots on total RNA isolated from HEK293 cells depleted of FKBP25 by siRNA (Figure 20). I detected no significant difference in any intermediary rRNA species upon knockdown of FKBP25 (Figure 20B). Thus, the presence of FKBP25 is not essential for the processing of rRNA. Similarly, I observed no major differences in transcript levels of any processed stage upon overexpression of FKBP25 in comparison to the control (Figure 20C). Similar experiments were also performed in U2OS cells with no obvious defect in transcript levels or processing of rRNA detected (data not shown), indicating this negative result is unlikely to be due to a cell type specific phenomenon.

As a control to ensure that I could detect changes in rRNA processing, I treated cells with rapamycin, which is well documented to affect rRNA processing through mTOR (Iadevaia et al., 2012). Consistent with previous reports (Iadevaia et al., 2012), I observe a rapamycin-induced accumulation of the 30S transcript (Figure 4D). Thus, I conclude that FKBP25 is not required to maintain the steady-state levels of pre-rRNA species. Neither the depletion or overexpression of FKBP25 had any effect on processing; thus, FKBP25's role within the nucleolus remains elusive.

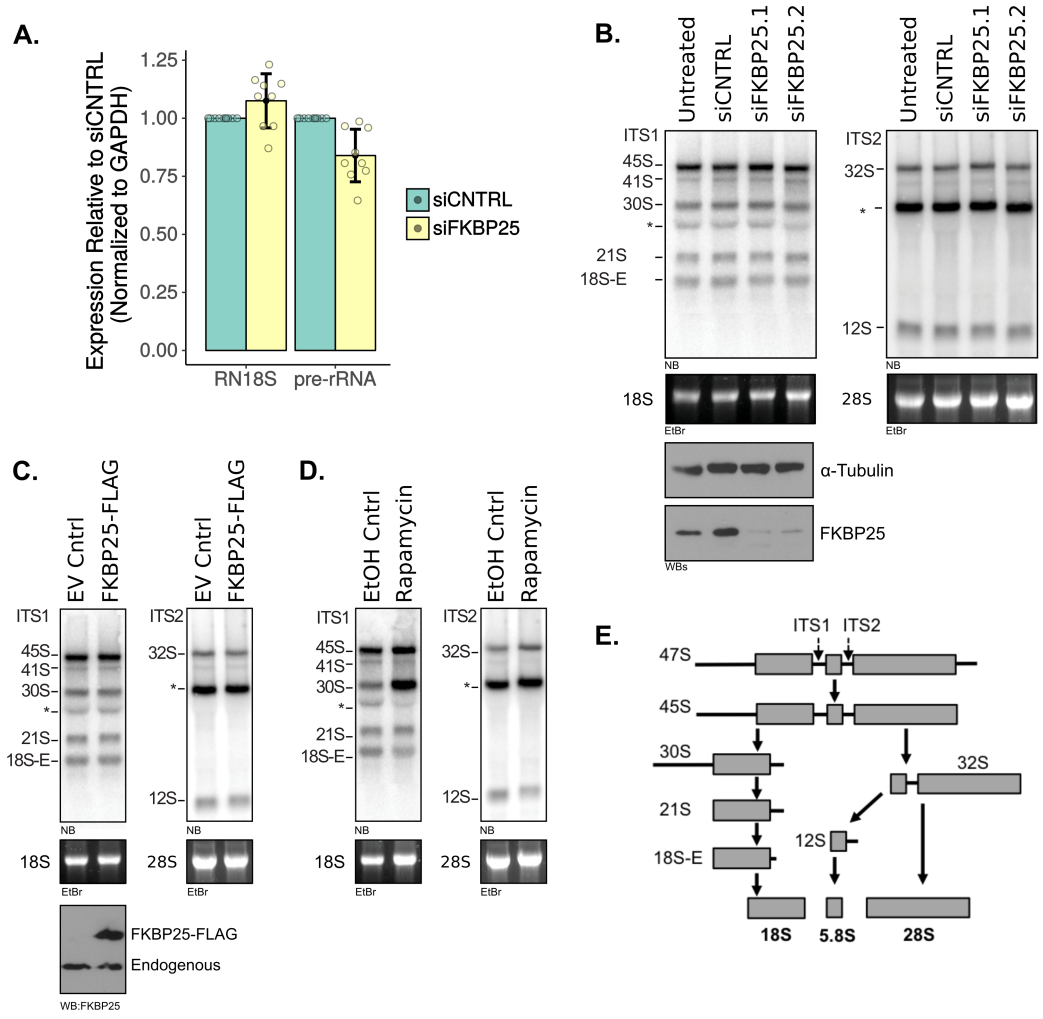

Figure 20. FKBP25 does not affect the expression or processing of ribosomal RNA. (A) qPCR measuring the expression of 18S processed rRNA (RN18S) and 47S pre-rRNA relative to an RNA Pol II transcribed GAPDH control in HEK293 cells depleted of FKBP25 or transfected with a non-targeting control. Results shown as the mean ± SD of three technical replicates from three independent experiments. (B) Northern blot of RNA extracted from untransfected HEK293 cells or HEK293 cells transfected with control siRNA or FKBP25-targeting siRNA. Blots were probed for ITS1 (left) or ITS2 (right). Extracts western blotted for FKBP25 to verify knockdown. (C) Northern blot of RNA extracted from HEK293 from control and cells overexpressing FLAG-FKBP25. Blots were probed for ITS1 (left) or ITS2 (right). (D) Northern blot of HEK293 cells treated with vehicle or rapamycin probed for ITS1 (left) or ITS2 (right). (E) Schematic of rRNA processing steps. (∗)Indicates non-specific probe binding.

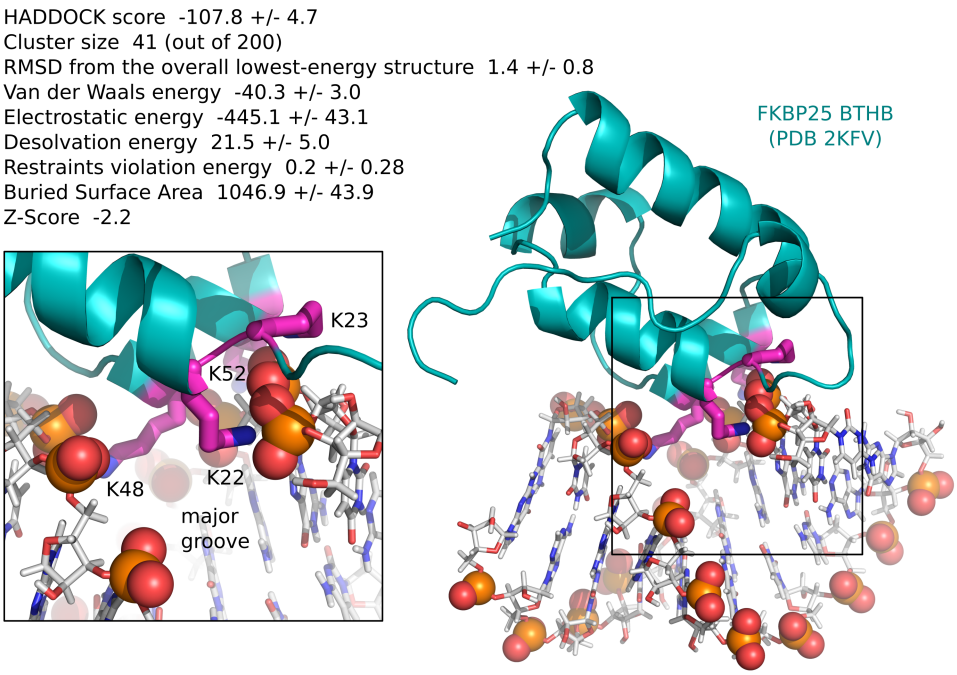

Figure 21. Putative model of dsRNA binding by the BTHB domain. (A) Lowest energy docking model of the FKBP25 BTHB domain (PDB ID: 2KFV) with an A-form dsRNA based on the dsRNA-10 sequence. The key lysines shown in Figure 17 are labeled and the sidechains shown in magenta. The phosphate groups along the dsRNA backbone are shown as spheres with the phosphorous and oxygen colored orange and red, respectively. The HADDOCK energies for the cluster of 41 models are also provided.

2.4 Discussion

We have used a variety of techniques to demonstrate an RNA-dependent interaction of FKBP25 with several proteins involved in RNA metabolism; these include ribosome biogenesis and chromatin regulatory factors. We observe cytoplasmic, soluble nuclear, insoluble RNA-dependent nucleolar localization, and chromatin association of FKBP25, which would be consistent with a function of this protein in pre-ribosome assembly. However, we were unable to identify a direct role for FKBP25 in the earliest events of ribosome biogenesis, transcription or processing of the 47S rRNA transcript. Using a collection of NMR techniques, we show that this novel property of a prolyl isomerase is conferred by its N-terminal BTHB domain, which can directly and selectively bind to dsRNA. These results identify FKBP25 as a peptidyl-prolyl isomerase recruited to ribonucleoprotein complexes through direct binding of dsRNA.

Protein domains that specifically bind to dsRNA are not common. The most prominent example is the family of dsRNA-binding domain (dsRBD) proteins. The dsRBD is a small domain (usually 65-70 amino acids) containing both α-helices and β-strands in an α-β-β-β-α architecture (Masliah et al., 2013). This domain is found in proteins that edit and process rRNA, tRNA, siRNA, and miRNAs (Masliah et al., 2013). In general, recognition of dsRNA by dsRBD is guided by the shape features unique to dsRNA. Compared to the canonical B-form dsDNA, dsRNA is typically found in the A-form with a narrower and deeper major groove and a wider and shallower minor groove (Dickerson et al., 1982). The dsRBD straddles contiguous minor-major-minor grooves, with shape recognition predominating the interaction but with some dsRBD members displaying sequence specificity with base pairs in the minor grooves. A central region of the dsRBD-dsRNA interface involves residues that contact phosphate groups on opposing sides of the major groove.

In our study of dsRNA binding by FKBP25, we show that a minimum length of 8 bp is required for association with the BTHB domain (Figure 17). A comparison of A-form dsRNA models explains this preference: it is evident that 8 bp and 10 bp ligands are sufficient in length to display phosphates on opposite sides of the major groove, whereas a dsRNA ligand of 6 bp is too short. As a result, it is likely that the BTHB domain uses this feature of the major groove to recognize dsRNA specifically. Indeed, by using the dsRNA-10 ligand sequence and binding contribution by the critical lysines K22, K23, K48 and K52, a docking-based (HADDOCK2.2)(Van Zundert et al., 2016; Dominguez et al., 2003; Wassenaar et al., 2012) model illustrates that the BTHB can efficiently interact with phosphates on both sides of the major groove (Figure 21).

The discovery of direct RNA-binding by FKBP25 provides an explanation for the dependence of RNA on protein-protein association and cellular localization. A significant fraction of FKBP25 colocalizes with UBF, which is found only within active rDNA clusters, and its expression levels determine the number of transcriptionally active rRNA (Sanij et al., 2008). As well, FKBP25's localization to the nucleolus is dependent on active Pol I transcription. This localization supports a role of FKBP25 in ribosome biogenesis in the nucleolus. Although we did not identify a function for FKBP25 in rRNA processing, the presence of a prolyl isomerase in ribosome biogenesis is intriguing. Fpr4, the *S. cerevisiae* ortholog of FKBP25, also associates with some ribosomal proteins and regulators (Ho et al., 2002; Saveanu et al., 2003; Krogan et al., 2006); however, the role of Fpr4 in ribosome biogenesis has yet to be explored. Moreover, *S. pombe* FKBP39, a related prolyl isomerase to FKBP25

and Fpr4, acts as a histone chaperone for ribosomal DNA silencing (Kuzuhara and Horikoshi, 2004). The involvement of FKBP25 orthologs in ribosome biogenesis, combined with the data presented in this report, strongly suggests a function of FKBP25 in the maturation of ribosomes. FKBP25 may play a role in later stages of ribosomal processing, including the chaperoning the assembly of ribosomal proteins post-processing or export to the cytoplasm.

Importantly, the high concentration of ribosomes may make RPL-FKBP25 interactions the most detectable in proximity labeling and IP- mass spectrometry methods we have used. However, it is likely that other processes and protein complexes are also regulated by FKBP25. It will, therefore, be important to determine if FKBP25 regulates other ribonucleoprotein complexes and cellular processes where dsRNA is involved. The GO enrichments categories of chromatin regulation, DNA repair, and some cytoskeletal processes in our proteomics screens provide some direction for these future investigations. This thesis will address functions in both DNA damage in Chapter 4 and regulation of the cytoskeleton in Chapter 3.

While there are several reports of cyclophilin and parvulin isomerases being linked to mRNA splicing (Mesa et al., 2008), FKBP25 is so far the only FKBP family member that has demonstrated direct binding to RNA and is the only prolyl isomerase shown to bind dsRNA. Interestingly, two cyclophilin prolyl isomerases can bind ssRNA due to an auxiliary RRM domain. The RRM domain of the nuclear human CyP-33/PPIE directly binds to single-stranded AU-rich RNA sequences (Hom et al., 2010; Mi et al., 1996), found in mRNA, but does not bind to rRNA or tRNA (Wang et al., 2008). An overlapping interaction surface on the RRM domain also recognizes the third plant homeodomain (PHD3) of mixed lineage leukemia (MLL) protein, and the binding of MLL is thought to displace RNA (Hom et al., 2010). The second RNA-binding cyclophilin is CYP59/PPIL4 from *Arabidopsis thaliana*, which functions in pre-mRNA processing (Gullerova et al., 2006) and has both an RRM and zinc-knuckle domain. A binding preference for a G-U/C-N-G/A-C-C-A/G motif was determined, a sequence found in 70 % of *Arabidopsis* protein-coding genes (Bannikova et al., 2013). There are no parvulin proteins that display RNA-binding behavior. However, similar to FKBP25, human Par14/PIN4 has been implicated in ribosome biogenesis (Fujiyama-Nakamura et al., 2009; Fujiyama et al., 2002). Knockdown of cellular Par14 levels results in a decrease in the ribosome processing rate (Fujiyama-Nakamura et al., 2009). In this case, the localization of Par14 appears to be due to association with nucleophosmin B23 or direct binding to DNA (Fujiyama-Nakamura et al., 2009; Saningong and Bayer, 2015). Collectively, it seems that several prolyl isomerases

are recruited to RNA-containing complexes, and this suggests that *cis-trans* prolyl isomerization of RNA proximal proteins is critical for their dynamic functions.

Regarding cellular localization, we note that most of the identified FKBP25 interactions (Figure 12) are in keeping with a predominantly nucleolar presence. However, it is also evident that FKBP25 is present within other regions of the cell. In the cytoplasm, FKBP25 may interact with a separate cohort of protein factors and perform different roles. Nevertheless, the ability to bind to regions of dsRNA could still represent a major factor in target recognition by FKBP25. For example, the identification of FKBP25 as an mRNA-binding protein (Castello et al., 2012) may represent interaction with regions of dsRNA such as stem-loop structures in cytosolic mRNA. Finally, it appears from the co-immunoprecipitation data that FKBP25 may also interact with a small number of proteins in an RNA-independent manner. In this regard, other protein-protein interactions, or indeed the lower affinity of FKBP25 to DNA, may serve a more important role.

Although each FKBP family member likely has a limited target repertoire, a clear preference for amino acids around the proline substrate has not been identified. This property is true for all three prolyl isomerases (Schmidpeter et al., 2011; Zoldák et al., 2009), except for the protein Pin1 which recognizes a phosphorylated serine or threonine before the proline residue (Yaffe, 1997). Instead, cellular targets appear to be defined by domains such as the BTHB that limit the protein to a particular location or biomolecular complex. In this report, we reveal that FKBP25 is directed to ribonucleoprotein complexes via a novel dsRNA-binding domain. The continued characterization of these auxiliary domains will, therefore, help to identify the cellular targets of each prolyl isomerase and enable a clearer understanding of their biological roles. This information will also provide a more detailed appreciation of the cellular processes and protein complexes that may be affected by immunosuppressive drugs of the cyclosporin and FK506/rapamycin families. A potential limitation of these drugs is that they target the catalytic domain, the part of the prolyl isomerase that displays reduced variation within each family. Such additional, and possibly undesired, targets of these drugs could help explain unwanted side-effects. Instead of just targeting the shared isomerase domains, it is possible that auxiliary domains such as the BTHB may serve as useful and more precise targets of regulation.

The catalytic action of prolyl isomerases is important for the proper folding and function of proteins. Although we cannot entirely rule out that FKBP25 may regulate the kinetics of rRNA processing, given the "foldase" action of FKBPs, we speculate that FKBP25 likely functions to chaperone proteins, or the numerous protein-rRNA

interactions within the nascent pre-60S ribosomal subunit. Identifying the proline targets within this vast nucleoprotein complex is now an important question to address to understand the biological function of FKBP25 in ribosome biogenesis.

2.5 Materials & Methods

Plasmids

Expression vectors containing flippase recognition target (FRT) sites for stable integration in Flp-In cell lines, and tetracycline-inducible expression, were generated by sub-cloning a synthesized FKBP25-3xFLAG-His_6 gene (GenScript) into a modified pcDNA5/FRT/TO vector (Thermo Fisher). FKBP25-FLAG-NLS vectors were constructed by PCR amplification of an FLAG-HA-NLS (FHN) tag from pcDNA4-FHN-4ICD (kindly provided by N. Yamaguchi, Chiba University) (Ishibashi et al., 2013). The FHN tag was then cloned into the pcDNA5 vector, replacing the 3x-FLAG-6xHis tag. To create BirA fusion products, FKBP25 was cloned into pcDNA3.1 mycBioID (Addgene # 35700) and pcDNA3.1 MCS-BirA(R118G)-HA (Addgene # 36047) vectors. Site-directed mutagenesis of the pcDNA5 vector was accomplished by PCR with mutagenic primers. Expression vectors for recombinant production of human FKBP25 in *E. coli* were made by inserting constructs into NcoI/Acc65I sites in a modified pET-9d plasmid containing an N-terminal His_6 purification tag followed by a tobacco etch virus (TEV) protease cleavage site. Inserts include full-length $FKBP25_{(1-224)}$, as well as the isolated BTHB $domain_{(1-74)}$ and FKBP $domain_{(108-224)}$. The first two RRM domains from hamster $nucleolin_{(299-459)}$ were expressed from a pET-15b plasmid (kindly provided by P. Bouvet, Ecole Normale Superieure de Lyon). Mutant proteins were created by using PCR amplification with a set of oligos overlapping the mutation site. All constructs were validated by sequencing.

Cell culture, plasmid transfection, and generation of stable cell lines

U2OS (ATCC HTB-96) and Flp-In T-Rex HEK293 (Thermo Fisher) cells were grown in a 5% CO_2 humidified incubator at 37 ℃ in DMEM media supplemented with 10% (v/v) fetal bovine serum (FBS) (Sigma) and antibiotics (10 µg/ml penicillin and 10 units/ml streptomycin, Thermo Fisher). Generally, all experiments were performed when cells reached 80% confluency. Transfection of DNA for both transient and stable expression was performed using Lipofectamine 3000 (Thermo Fisher) following the manufacturer's instructions. To generate stable cells expressing tagged FKBP25, Flp-In T-Rex HEK293 cells were transfected with a 9:1 ratio of pOG44 (Thermo Fisher) to pcDNA5 integration vector and allowed to recover for 24 h before selection with hygromycin (InvivoGen). Stable clones were pooled and tested for expression with the addition of 1 µg/mL tetracycline (Sigma) for 24 h. U2OS stable cell lines expressing BirA fusion proteins were created by transfection and clonal isolation fol-

lowing G418 selection (A.G. Scientific). Clones were screened by western blotting with streptavidin-horse radish peroxidase (Thermo Fisher).

Rationale for cell line selection

The cell lines utilized in this chapter are common throughout biomedical research as generalized models for human cell biology. The HEK293 Flp-In cell line was selected for its integrated FRT loci downstream of a tetracycline-inducible CMV promoter allowing rapid and efficient generation of inducible transgenic cell lines. Tetracycline induction also provided control of gene expression. This allowed either over or endogenous matched expression levels of transgenes. Characteristics of the human osteosarcoma U2OS cell line, including relatively strong adherence and rapid proliferation, made it useful for *in situ* fractionation and immunofluorescence experiments. These cell lines were also used for BioID experiments as they are easily transfected and amenable for stable cell line generation by antibiotic marker selection.

Statistics

All numerical results are reported as mean ± standard deviation (SD). The number of replicates, technical or biological, are indicated in corresponding figure legends. P-values associated with gene ontology enrichment were calculated by the David web server (Huang et al., 2009) using the Fishers exact test.

Affinity capture of biotinylated proteins

Purification of biotinylated proteins was performed as outlined by Roux et al. (2012). U2OS cells stably expressing an FKBP25-BirA-HA fusion protein or Myc-tagged BirA control were incubated for 24 h in complete DMEM media supplemented with 50 µM biotin (Sigma) in 15 cm^2 dishes. Cells were then washed three times in PBS and lysed directly on the plate with 1 mL Lysis Buffer (50 mM Tris pH 7.4, 500 mM NaCl, 0.4% SDS, 5 mM EDTA, 1 mM DTT, and fresh protease inhibitors - 1 µg/mL leupeptin, 1 µg/mL aprotinin, and 1 µg/mL pepstatin). Lysates were scraped into a 1.5 mL microfuge tube and sonicated on high for cycles of 30 s with a 30 s rest, for a total time of 5 min on ice using a BioRupter (Diogenode). Triton X-100 was added to a final volume of 2%, and the lysates were again sonicated as above. Lysates were then diluted in an equal volume of chilled 50 mM Tris pH 7.4 and subjected to a final round of sonication. Insoluble cellular debris was cleared by centrifugation at 16 000 x g for 10 min at 4℃. Cleared extracts were normalized by Bradford assay prior to loading on 125 µL slurry of washed Dynabeads MyOne Streptavidin C1 (Thermo

Fisher) and incubated overnight at 4℃. The following morning, beads were washed 2 times with Wash Buffer 1 (2% SDS), once with Wash Buffer 2 (0.1% sodium deoxycholate, 500 mM NaCl, 1 mM EDTA, 50 mM Hepes pH 7.5, and 1% Triton X-100), once in Wash Buffer 3 (10 mM Tris pH 8.1, 250 mM LiCl, 0.5% NP-40, 0.5% sodium deoxycholate, and 1 mM EDTA), and finally two times with Wash Buffer 4 (50 mM Tris pH 7.4 and 50 mM NaCl), pelleting beads using a magnetic rack. For western blotting, beads were resuspended in Laemelli sample buffer supplemented with 50 µM biotin and boiled for 10 min before loading on an SDS-PAGE gel.

Immunoprecipitation

Expression of stably-integrated or transiently transfected FKBP25 constructs was induced with 1 µg/mL tetracycline (Sigma) for 24 h before harvesting. For immunoprecipitation experiments performed with nuclear extract, the extracts were prepared by resuspending cell pellets ($\approx 3x10^7$ cells) in 1 mL buffer A (16.7 mM Tris pH 8, 50 mM NaCl, 1.67 mM $MgCl^2$, 0.1% Triton X-100, 1 µg/mL leupeptin, 1 µg/mL aprotinin, and 1 µg/mL pepstatin), vortexed for 10 s and incubated on ice for 5 min. Nuclei were centrifuged at 1000 x g for 5 min. Pellets were washed once more in buffer A as above. To extract the nuclear material, the pellet was sonicated using a BioRupter (Diogenode) on high power for cycles of 30 s with a 30 s rest, for a total time of 5 min on ice in 0.5 mL sonication buffer (25 mM Tris pH 8, 100 mM KCl, 2 mM EDTA, 1 mM DTT, 0.05% IGEPAL, and 1 µg/mL leupeptin, 1 µg/mL aprotinin, and 1 µg/mL pepstatin). Insoluble material was pelleted by centrifugation at 12 000 x g for 15 min. Extracts were normalized for total protein by Bradford assay. For immunoprecipitations using whole-cell extracts, cells were resuspended directly in immunoprecipitation wash buffer (50 mM Tris pH 8, 150 mM NaCl, 0.5% (w/v) NP-40, 0.5% (w/v) Triton X-100, 2 mM EDTA, and protease inhibitors) and sonicated on high power for cycles of 30 s with a 30 s rest, for a total time of 5 min on ice. Insoluble material was pelleted by centrifugation at 12 000 x g for 15 min and normalized by Bradford assay. For RNase A treatment, extracts (2-3 mg) were incubated with 100 µg RNase A (Qiagen) for 5 min at 37 ℃, followed by 1 h at 4 ℃. Nuclear and whole cell extracts were added to pre-washed EZ-view Red anti-FLAG M2 Affinity gel beads (Sigma), and incubated at 4 ℃ for 1.5-3 h with nutation. After binding, beads were washed three times with IP wash buffer, followed by addition of 0.75 mL wash buffer and nutation for 5 min, and then the beads centrifuged at 1000 rpm for 1 min. Bound FLAG-tagged FKBP25 and interacting proteins were eluted by competition with 3xFLAG peptide (Sigma), by nutating beads in 150 ng/µL peptide

in 1x TBS for 20 min at 4 ℃. Eluted material was resolved by NuPAGE Novex 4-12% Bis-Tris gradient gels (Thermo Fisher) at 150 V for approximately 1.5 h and either silver stained, transferred to nitrocellulose membrane for western blotting, or further processed for mass spectrometry analysis. For RNA-IPs, peptide-eluted immunoprecipitation material was TRIzol extracted to isolate RNA and samples were run on a 1% agarose-formaldehyde gel.

Protein identification by mass spectrometry

BioID samples were processed for mass spectrometry as outlined by Mojica et al. (2015). Briefly, streptavidin beads were washed with 50 mM NH_4HCO_3 and resuspended in 50 mM NH_4HCO_3 containing 5 mM dithiothreitol and heated at 75 ℃ for 10 min. Iodoacetamide was added to a final concentration of 10 mM to each sample followed by incubation in the dark at room temperature for 20 min. Afterward, 1 mM $CaCl_2$ and fresh 5 mM dithiothreitol were added and incubation continued overnight. The following morning, trifluoroacetic acid (TFA) was added to a final concentration of 0.5% (v/v). Beads were pelleted using a magnetic rack and the supernatant removed. A second elution of digested peptides with 0.5% TFA was performed and the supernatant pooled. To each sample, 1 µg of sequence grade trypsin was added and incubated overnight at 37℃. For 3x-FLAG peptide eluted material, in-solution trypsin digests were performed by incubating samples with 1 µg of sequence grade trypsin (Promega) at 37 ℃ in 1x TBS followed by lyophilization until dry. Digested peptides were passed over ZipTips (Millipore) and eluted with 0.1% TFA/50% acetonitrile. Peptides were analyzed by an Orbitrap LTQ mass spectrometer (Thermo Scientific) with result searches performed using the program MASCOT (Matrix Science). To identify protein interactors, peptide counts for sample versus control were submitted to the Crapome web server (Mellacheruvu et al., 2013). Proteins identified that had a fold change greater than two, and at least two peptides detected, were considered to be enriched.

Gene ontology & network analysis

For gene ontology analysis, lists of interacting proteins were submitted to the DAVID (Database for Annotation, Visualization and Integrated Discovery version 6.8) web server (Huang et al., 2009). Gene ontology terms with a p-value <0.05 were then summarized using the REVIGO (reduce and visualize gene ontologies) server with a similarity cut-off of 0.46 (Supek et al., 2011). Network visualizations were generated using Cytoscape software (Shannon et al., 2003) with protein-interaction data from

the APID (Agile Protein Interactomes DataServer) database (Alonso-López et al., 2016).

Western blot

For western blotting, eluted proteins were resolved by SDS-PAGE and transferred to a nitrocellulose membrane with phosphate transfer buffer (50 mM sodium phosphate buffer pH 6.8, 15% EtOH). Membranes were blocked in 10% skim milk for 30 min and probed with primary antibody for either 1 h at room temperature or overnight at 4℃. Followed by three 10 min washes in TBS-T (1x TBS containing 0.1% Tween 20). For the development of western blots, either a chemiluminescence or fluorescence biased detection system was used. For chemiluminescence, horseradish peroxidase conjugated anti-mouse (GE) or anti-rabbit (GE) secondary antibody was used at 1:5000 in 1% milk/TBS-T, incubating blots for 1 h at room temperature, followed by washing in TBS-T. Proteins were detected using chemiluminescence HRP substrate (Millipore) and exposed to film. For fluorescence based detection, blots were incubated with either IRdye 800CW anti-mouse (Mandel Scientific) or IRdye 680RD anti-rabbit (Mendel Scientific) at 1:5000 for 1 h at room temperature in 1% milk TBS-T, followed by washing in TBS-T and imaging on an Odyssey Clx (Li-Cor).

Antibodies

The following antibodies were used in this study; FKBP25 (Genscript, epitope residues 201-224 - IF 1:300, WB 1:2500), α-Tubulin (Rockland 600-401-880 - WB 1:10000), Ku86 (Santa Cruz sc-9034 - WB 1:5000), Ku70 (Millipore Q2187163 - WB 1:2500), TopoI (Abcam ab109374 - WB 1:10 000), Parp1 (Santa Cruz sc-8007 - WB 1:5000), Nucleolin (Abcam ab22758 - WB 1:5000), RPL3 (Santa Cruz sc-86828 - WB 1:500), RPS6 (Santa Cruz sc74459 - WB 1:500), FLAG (Sigma F3165 - WB 1:50000), RPL23a (Santa Cruz sc-135388 - 1:500), and UBF (Santa Cruz sc13125X - IF 1:500).

Immunofluorescence

Cells were seeded on 8-well glass slides (Millipore) at least 24 h before fixation. For pre-extraction, cells were washed first with 1x PBS and then incubated twice for 3 min at room temperature with CSK+T (10 mM Pipes pH 7.0, 100 mM NaCl, 300 mM sucrose, 3 mM $MgCl_2$, and 0.5% Triton X-100) or CSK+T+R (CSK+T with 0.3 mg/mL RNase A). CSK alone treated cells were washed with 1x PBS and CSK buffer without detergent or RNase A as above. To fix cells, they were first washed in 1x PBS and then incubated in a 3% paraformaldehyde (PFA) solution in PBS,

followed by three washes in 1x PBS. Before staining, cells were permeabilized for 10 min on ice using 0.5% Triton X-100 in 1x PBS and then blocked for 30 min in PBS-T (0.1% Tween 20 in PBS) containing 1% bovine serum albumin (BSA) at room temperature. Slides were then incubated with primary antibody diluted in PBS-T for 1 h at room temperature followed by three 5 min washes in PBS. After washing, the slides were then incubated with secondary antibodies, AlexaFluor 488 goat anti-mouse (Life Technologies) and goat anti-rabbit IgG-CFL 555 (Santa Cruz), in PBS-T for one hour and washed 3 times in 1x PBS. Coverslips were mounted in Fluoroshield with DAPI (Sigma) and sealed with clear nail polish. Slides were imaged on an SP8 confocal microscope (Leica) and images processed using the Fiji distribution of ImageJ (Schindelin et al., 2012).

In vitro protein expression and purification

Full-length human FKBP25$_{(1-224)}$, along with truncation mutants corresponding to the isolated BTHB domain$_{(1-74)}$ or FKBP domain$_{(108-224)}$, were expressed in *Escherichia coli* BL21 *LysY* (New England Biolabs) using LB medium or M9 minimum medium supplemented with $^{15}NH_4Cl$ (1 g liter^1), and for ^{13}C-labelled protein supplemented also with ^{13}C-glucose (2 g liter^1). Protein expression was initiated at an OD (600 nm) of 0.6 with 0.5 mM IPTG (final concentration) and was followed by overnight incubation at 25℃. Bacteria were collected by centrifugation and resuspended in 20 mL per litre culture media with 50 mM Tris (pH 7.5), 500 mM NaCl, 5% (v/v) glycerol and 5 mM imidazole. Cell lysate preparation used a combination of lysozyme and sonication followed by centrifugation at 20 000 x g for 30 mins. Protein purification from cell lysate was achieved by using Ni^{2+}-affinity chromatography with buffers composed of 50 mM Tris (pH 7.5), 500 mM NaCl, 5% (v/v) glycerol, and 5, 25, and 500 mM imidazole for the loading, wash and elution, respectively. Pooled fractions containing protein were exchanged to the low imidazole buffer by using a PD-10 column (GE Healthcare Life Sciences) and the His_6 tag was removed by addition of TEV protease and overnight incubation at 4℃, followed by a second Ni^{2+}-affinity chromatography step. The purified samples were concentrated by filter centrifugation, and the buffer exchanged by NAP-5 columns (GE Healthcare Life Sciences) into 20 mM sodium phosphate, pH 6.5 and 150 mM NaCl. Protein concentration was quantified by measuring the absorbance at 280 nm.

Oligonucleotide synthesis

The RNA was synthesized by using an Expedite 8909 (PerSeptive Biosystems). The

DNA oligonucleotides were commercially produced (Eurogentec). Concentrations were determined by measuring absorbance at 260 nm with extinction coefficients from OligoAnalyzer 3.1 (eu.idtdna.com/calc/analyzer).

NMR spectroscopy and chemical shift assignment

NMR spectra were recorded at 298 K using a Bruker Avance III 700 MHz or 800 MHz spectrometers equipped with a triple resonance gradient standard probe or cryoprobe, respectively. Topspin versions 2.1, 3.2 and 3.5 (Bruker BioSpin) were used for data collection. Spectra processing used NMRPipe followed by analysis with Sparky 3 (T. D. Goddard and D. G. Kneller, University of California) or NMRviewJ 8.0 (One Moon Scientific). Spectra for the assignment of backbone ^{1}H6N, ^{1}H, ^{13}C', ^{13}C, ^{13}C and ^{15}N^{H} nuclei of full-length FKBP25 were collected on a 200 µM ^{13}C,^{15}N-labelled sample in 20 mM sodium phosphate (pH 6.5) with 150 mM NaCl, and 10% D_2O added for the lock. NMR spectra include 2D ^{15}N-HSQC, 3D HNCO, 3D HNCACO, 3D HNCA. 3D HNCOCA, 3D CBCACONH, and 3D HNCACB. Chemical shifts for the full-length FKBP25 have been deposited in the Biological Magnetic Resonance Data Bank (bmrb.wisc.edu) under accession number 27070. ^{1}H^{N} and ^{15}NH assignments for the full-length protein were used to assign ^{15}N-HSQC spectra recorded for isolated BTHB and FKBP domains in the same buffer (20 mM sodium phosphate, pH 6.5, with 150 mM NaCl). For the BTHB domain, the assignments were confirmed by measuring additional 3D HNCO and 3D HNCACB spectra on a 310 µM sample of ^{13}C,^{15}N-labelled protein. Assignments of asparagine and glutamine sidechain amides were confirmed by using a 3D ^{15}N-HSQC-NOESY spectrum (150 ms mixing time). Chemical shifts for the BTHB domain of FKBP25 have been deposited in the Biological Magnetic Resonance Data Bank (bmrb.wisc.edu) under accession number 27071.

Titration experiments

Binding of FKBP25 constructs to oligonucleotide ligands were monitored by NMR spectroscopy on a Bruker Avance III 700 MHz spectrometer equipped with a triple-resonance gradient standard probe at 298 K. The buffer was the same as for the chemical shift assignment experiments: 20 mM sodium phosphate (pH 6.5), with 150 mM NaCl, and 10 % D_2O added for the lock. At the start of each titration the ^{15}N-labelled protein had a concentration of 100 µM in 20 mM sodium phosphate (pH 6.5), with 150 mM NaCl, and 10 % D_2O added for the lock. Following reference 1D 1H and 2D ^{15}N-HSQC spectra, the ligand was added from a concentrated stock to final concentrations of 25, 50, 75 and 100 µM, and at each point, 1D 1H and 2D

^{15}N-HSQC spectra were collected. The only exception was for the sample titrated with nucleolin-bound b2NRE stemloop. In this case, a final titration point (100 µM ligand) was first assembled stepwise with confirmation of nucleolin binding to b2NRE stemloop by 1D 1H NMR, before adding 100 µM final concentration of ^{15}N-labelled FKBP25$_{(1-74)}$. This sample was then serially diluted with free ^{15}N-FKBP25$_{(1-74)}$ (which was also used as the reference) to obtain all titration points.

Cross-linking immunoprecipitation (CLIP)

FKBP25 RNA CLIP experiments were performed as described previously (Konig et al., 2011). Briefly, 80% confluent HEK293-TRex cells were transfected in 6-well dishes and incubated overnight before being split to 10 cm^2 dishes. Cells were then induced with 0.1 µg/mL tetracycline and incubated for an additional 24 h to induce expression. Cells were washed once with 1x ice cold PBS and then irradiated with 150 mJ/cm6^2 UV at 254 nm using a Stratalinker 2400 (Stratagene). Irradiated cells were harvested by cell scraping, aliquoted into three equal volumes, and snap-frozen in liquid nitrogen to be stored at -80 ℃ until use. Thawed cell pellets were lysed in 1 mL lysis buffer (50 mM Tris-HCl pH 7.4, 100 mM NaCl, 1% NP-40, 0.1% SDS, and protease inhibitors). To remove DNA, 2 µL of Turbo DNase (Ambion) was added to each sample. To digest unprotected RNA, either a high (1:500), medium (1:10 000), or low (1:50 000) concentration of 100 mg/mL RNase A (Qiagen) was added and samples were incubated for 3 min at 37 ℃ followed by centrifugation at 22 000 x g for 20 min to pellet any insoluble material. Protein A/G agarose beads (Thermo Fisher) were prepared by washing three times in lysis buffer in between pelleting by centrifugation at 1000 rpm for 5 min, followed by incubation for 1 h at 4 ℃ with 5 µg mouse anti-FLAG antibody (Sigma). Unbound antibody was washed away with two additional washes in lysis buffer. Cleared nuclease treated cell lysates were added to prepared beads and rotated at 4 ℃ for 2 h. Beads were then washed twice with high-salt buffer (50 mM Tris-HCl pH 7.4, 1 M NaCl, 1 mM EDTA, 1% NP-20, 0.1% SDS, and 0.5% sodium deoxycholate) followed by two washes with wash buffer (20mM Tris-HCl pH7.4, 10 mM MgCl2, and 0.2 % Tween-20). The beads were then subjected to an additional three washes in high-salt wash buffer and three in wash buffer. The supernatant was removed and beads were then resuspended in 8 µl of 1x PNK buffer (70 mM Tris-HCl pH 7.6, 10 mM MgCl2, 5 mM DTT) containing 0.4 µl PNK (NEB) and 0.8 µl of 5 mCi/mL ^{32}P-γ-ATP (Perkin Elmer). The reaction was incubated at 37 ℃ for 5 min. The ^{32}P-labelled PNK mix was removed and beads were boiled in 1x Lamelli loading buffer and resolved on a 10% SDS-PAGE gel. Gels were dried

and exposed to a Phosphor screen (Molecular Dynamics) overnight and imaged with a Storm 820 scanner (Molecular Dynamics).

Chromatin immunoprecipitation (ChIP)

Cells were cross-linked with 1% formaldehyde for 10 mins at room temperature and the reaction quenched by the addition of glycine to 0.175 M with an additional 5 min incubation at room temperature. Cross-linked and washed cells were then harvested and resuspended in nuclei isolation buffer (5 mM PIPES pH 8.0, 85 mM KCl, 0.5% NP-40, and protease inhibitors - 1 µg/mL leupeptin, 1 µg/mL aprotinin, and 1 µg/mL pepstatin) and dounce homogenized to isolate nuclei. Nuclei were pelleted for 10 min at 1500 rpm in a swing bucket rotor and resuspended in micrococcal nuclease (MNase) digestion buffer (50 mM Tris-HCl pH 8.0, 5 mM $CaCl_2$, and protease inhibitors). Chromatin was digested by incubation with 50 U of MNase (Worthington) for 5 min at 37℃. Digestion was stopped by the addition of an equal volume of ice-cold 2x lysis buffer (100 mM Tris-HCl pH 8.0, 20 mM EDTA pH 8.0, and 2% SDS). Samples were then flash frozen in liquid nitrogen and stored at -80℃. A small aliquot was held and the cross-links reversed by heating at 65 ℃ overnight to assess the extent of MNase digestion and quantify the concentration of input chromatin. Prior to immunoprecipitation, chromatin samples were cleared of SDS and debris by centrifugation at 12 000 rpm for 10 min, diluted in dilution buffer (1% Triton X-100, 2 mM EDTA, 150 mM NaCl, 20 mM Tris-HCl pH 8.0, and protease inhibitors) to 0.1 µg/µl chromatin, and pre-cleared by mixing with protein A/G agarose beads (Thermo Scientific) for 2 h at 4℃. Pre-cleared solubilized chromatin samples were incubated with 5 µg of either anti-FKBP25 (raised against amino acids 3-18 of human FKBP25), anti-histone H3K4me3 (Abcam ab8580), anti-nucleolin (Abcam ab22758), or rabbit IgG (Rockland) for 2 h at 4 ℃. Protein A/G beads were added for 3 h at 4 ℃ to precipitate immune complexes. Beads were then washed three times with wash buffer (0.1% SDS, 1% Triton X-100, 2 mM EDTA, 150 mM NaCl, 20 mM Tris-HCl pH 8.0, and protease inhibitors) and once with a final high salt wash buffer (0.1% SDS, 1% Triton X-100, 2 mM EDTA, 500 mM NaCl, 20 mM Tris-HCl pH 8.0, and protease inhibitors), and eluted by incubation with elution buffer (50 mM Tris-HCl pH 8.0, 10 mM EDTA) for 30 min at 30℃. To reverse cross-links, samples were incubated overnight at 65 ℃ with 5 µg/ml RNase A (Qiagen). DNA was purified by PCR purification spin column (BioBasic) and quantitative PCR analysis performed using 2x MAXIMA SYBR green master mix (Thermo Fisher) and ran on an MX3000P qPCR system (Agilent Technologies). Primer sequences used in these experiments are listed

in Table A.6 of the appendix.

qPCR

RNA was isolated using TRIzol reagent (Thermo Fisher) and cDNA prepared using the High-Capacity cDNA Reverse Transcription kit (ThermoFisher). cDNA was diluted 1:200 and used as a template in reactions using 2x Maxima SYBR green master mix (Thermo Fisher). Samples were analyzed on a MX3000P qPCR system (Agilent Technologies) and fold change calculated by the $\Delta\Delta$ Ct method (Schmittgen and Livak, 2008). Primer sequences are listed in Table A.6 of the appendix.

Northern blot

Total RNA was extracted with TRIzol (Thermo Fisher). Northern blot analysis (adapted from PerkinElmer protocols) was performed by separation on a 1% agarose-formaldehyde gel, run at 200V for 1.5 h, and transferred overnight by capillary transfer to a Nylon membrane (Whatman, Inc.). The blot was rinsed in 2x SSPE (300 mM NaCl, 20 mM NaH_2PO_4-H_20, and 2 mM EDTA) and UV crosslinked (auto crosslink setting, 254 nm, Stratagene, Stratalinker). Membranes were prehybridized for 4-6 h at 42 ℃ in prehybridization solution (5x SSPE, 50% deionized formamide, 5x Denhardt's Solution, 1% SDS, 10% dextran sulfate, and 100 µg/mL sheared salmon sperm DNA). Oligonucleotides were end-labeled with γ-^{32}P (PerkinElmer) and T4 polynucleotide kinase (NEB) for 1 h at 37 ℃ and heat inactivated. Membranes were then incubated overnight with labeled probe. The blots were washed twice with 2x SSPE, 0.1% SDS for 10 min at room temperature and then with 0.2x SSPE, 0.1% SDS until background signal was minimal. Blots were then exposed to a phosphor screen (Molecular Dynamics) and imaged using a Phosphorimager (STORM, GE Healthcare). Probe sequences are listed in Table A.6 of the appendix.

Chapter 3

FKBP25 Regulates Microtubule Stability with Implitions on Cell Cycle Progression and Genome Stability

This chapter was adapted from a publition in preparation for submission:

Dilworth D, Gudavicius G, Boyce AKJ, Serpa JJ, Petrochenko EV, Borchers CH, Swayne LA, and Nelson, CJ. The prolyl isomerase FKBP25 regulates microtubule stability with implications on cell cycle progression and chromosome stability. *In preparation.*

Contributions: Experiments and data analysis performed by **DD** under the supervision of CJN with the following exceptions: GG, JJS, EVP, and CHB were involved in mass spectrometry sample preparation and instrument operation; AKJ and LAS provided technical support for confocal imaging of prepared slides; RNA-Seq libraries were prepared and sequenced at Canada's Michael Smith Genome Sciences Centre, Vancouver BC. **DD** and CJN wrote the manuscript.

3.1 Abstract

The FK506 binding protein FKBP25 is a nuclear chromatin-associated peptidyl-prolyl isomerase with nucleic acid binding properties – the biological function of this protein and its role in gene transcription remains largely uncharacterized. In an attempt to explore FKBP25's role in regulating transcript levels, I have discovered that FKBP25 is a novel microtubule-associated protein that stabilizes the microtubule network. I show that FKBP25 associates with the mitotic spindle apparatus and depletion of FKBP25 disrupts cell cycle progression in fitting with impaired microtubule dynamics. Consistent with a role in regulating the stability of the mitotic spindle, knockdown of FKBP25 leads to increased chromosomal instability, a hallmark of cancer. FKBP25's regulation during mitosis by multiple phosphorylation events is also examined – I observe that FKBP25 is multiply phosphorylated during mitosis by protein kinase C to regulate its activity, disrupting nucleic acid binding while maintaining its interaction with microtubules. Collectively, this data describes FKBP25 as a novel regulator of the microtubule network, adding FKBP25 to the list of isomerases known to regulate microtubule dynamics. This study highlights PPIs as potential therapeutic targets in microtubule-associated diseases.

3.2 Introduction

The microtubule (MT) cytoskeleton, primarily composed of α/β tubulin heterodimers, facilitates many functions within the cell, including cell motility, intracellular trafficking, and mitosis. A critical feature of microtubules is dynamic instability, the process of alternating between rapid polymerization, depolymerization, and catastrophe (Mitchison and Kirschner, 1984). Regulating this process is a host of microtubule-associated proteins (MAPs) that act to either stabilize or destabilize the MT network. Dynamic instability is most clearly demonstrated during mitosis as the interphase microtubule network rapidly disassembles and the mitotic spindle is formed, an MT structure responsible for the segregation of chromosomes during mitosis (Walczak et al., 2010). This carefully choreographed phenomenon ensures faithful segregation of sister chromatids. Failure to establish proper MT dynamics during mitosis can result in chromosomal instability, a hallmark of the cancer genome (Schvartzman et al., 2010).

I show here that FKBP25 is a novel MAP that acts to stabilize the MT network and is required for proper functioning of the mitotic spindle apparatus. I also present

a potential mechanism for its regulation during mitosis by protein kinase C (PKC) directed phosphorylation, which impairs its nucleic acid binding potential, likely displacing FKBP25 from chromatin to promote its localization to and stabilization of the mitotic spindle.

3.3 Results

3.3.1 Disruption of FKBP25 attenuates G1/S and G2/M transitions of the cell cycle

FKBP25 localizes to the nucleus, directly binds nucleic acids, and associates with chromatin modifying enzymes (Jin et al., 1992; Prakash et al., 2016; Yang et al., 2001) – the implications of these features on transcription remains an open question. To answer this question, I performed a single biological replicate exploratory RNA sequencing (RNA-Seq) experiment comparing transcriptomes from HEK293 cells transfected with either FKBP25 targeting siRNA or a GFP non-targeting control (Figure 22). Surprisingly, changes in overall gene expression were subtle in terms of the magnitude of the relative fold change, suggesting FKBP25's role in regulating transcript levels may be minimal (Figure 22B, a list of the top 100 genes with increased or decreased expression can be found in Tables A.7 and A.8 of the Appendix, respectively). Due to the modest changes in transcript levels, RNA-Seq experiments incorporating additional biological replicates were not pursued. However, I carried ahead with analysis of the dataset as an indicator of cell state when FKBP25 is depleted. To do so, I explored gene ontology and KEGG analysis of ranked differential expression, I found genes with altered expression were enriched in signaling factors involved in cell cycle regulation, including activation of MAPK and calcium stress response signaling (Figure 23), as well as decreased expression of genes associated with metabolic processes (Figure 22D). Several of these expression changes, including an increase in the levels of the GADD45 stress response genes, have been validated by RT-qPCR (data not shown). In agreement with this altered expression profile, there was a decrease in cellular proliferation when FKBP25 was disrupted (Figure 22E).

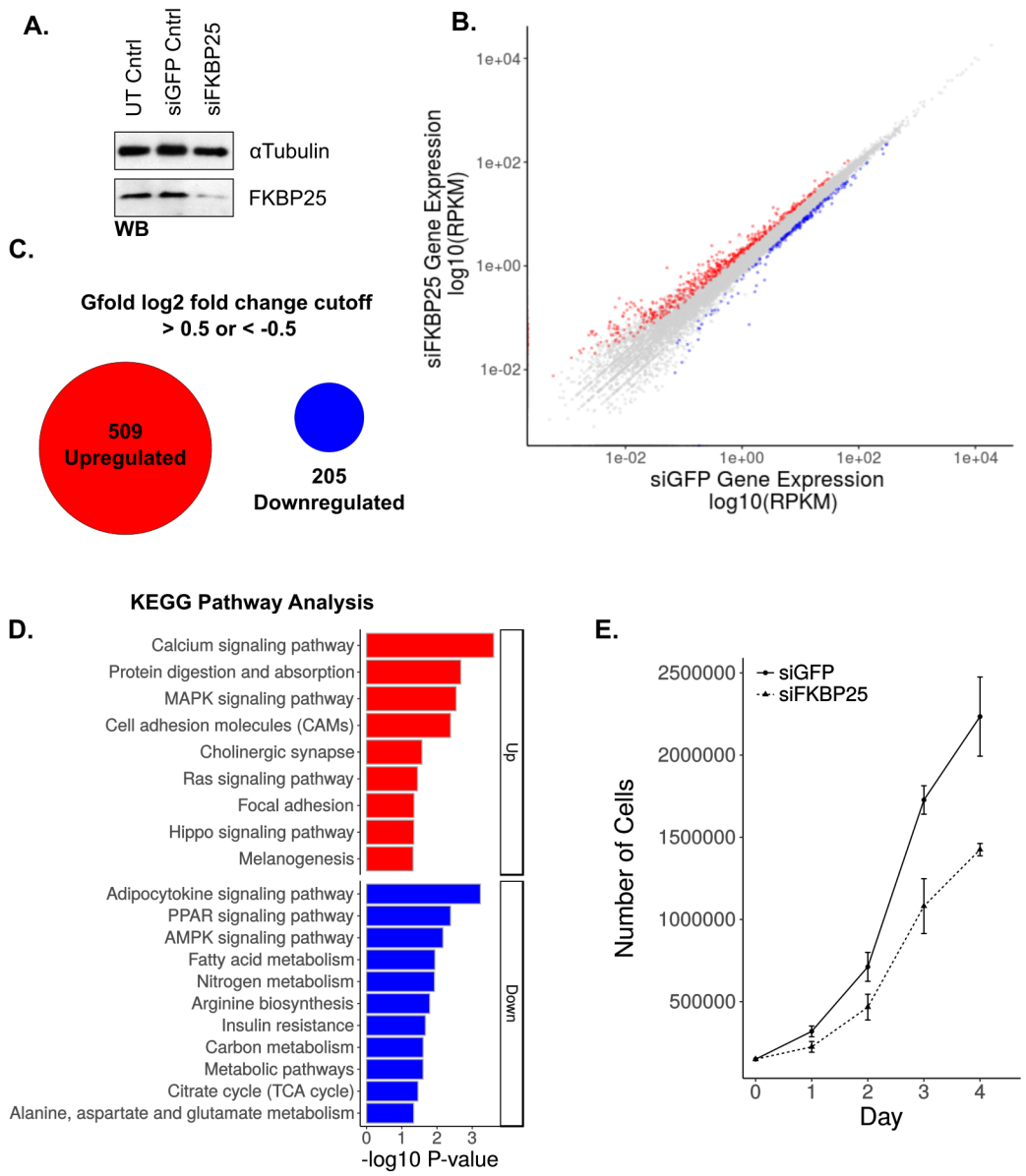

Figure 22. Transcriptome analysis of FKBP25 knockdown in HEK293 cells. (A) Western blot analysis of siRNA knockdown in HEK293 cells relative to untransfected (UT) and GFP targeting control. (B) RNA-Seq transcriptome analysis of cells treated with FKBP25 targeting siRNA vs. a GFP targeting control (n=1). Expression values are shown as log10 Read Per Kilobase of transcript per Million mapped reads (RPKM). Red data points indicate a log2 fold change greater than 0.5 and blue indicates less than -0.5. (C) Number of genes selected for gene ontology and KEGG analysis based on a Gfold log2 fold change of greater than 0.5 (upregulated expression) or less than -0.5 (downregulated expression). (D) KEGG pathway analysis of upregulated and downregulated gene sets. (E) Viable cell counts 1-4 days post-transfection with either FKBP25 targeting siRNA or siGFP control in HEK 293 cells. Shown are mean cell counts ± SD of three biological replicates.

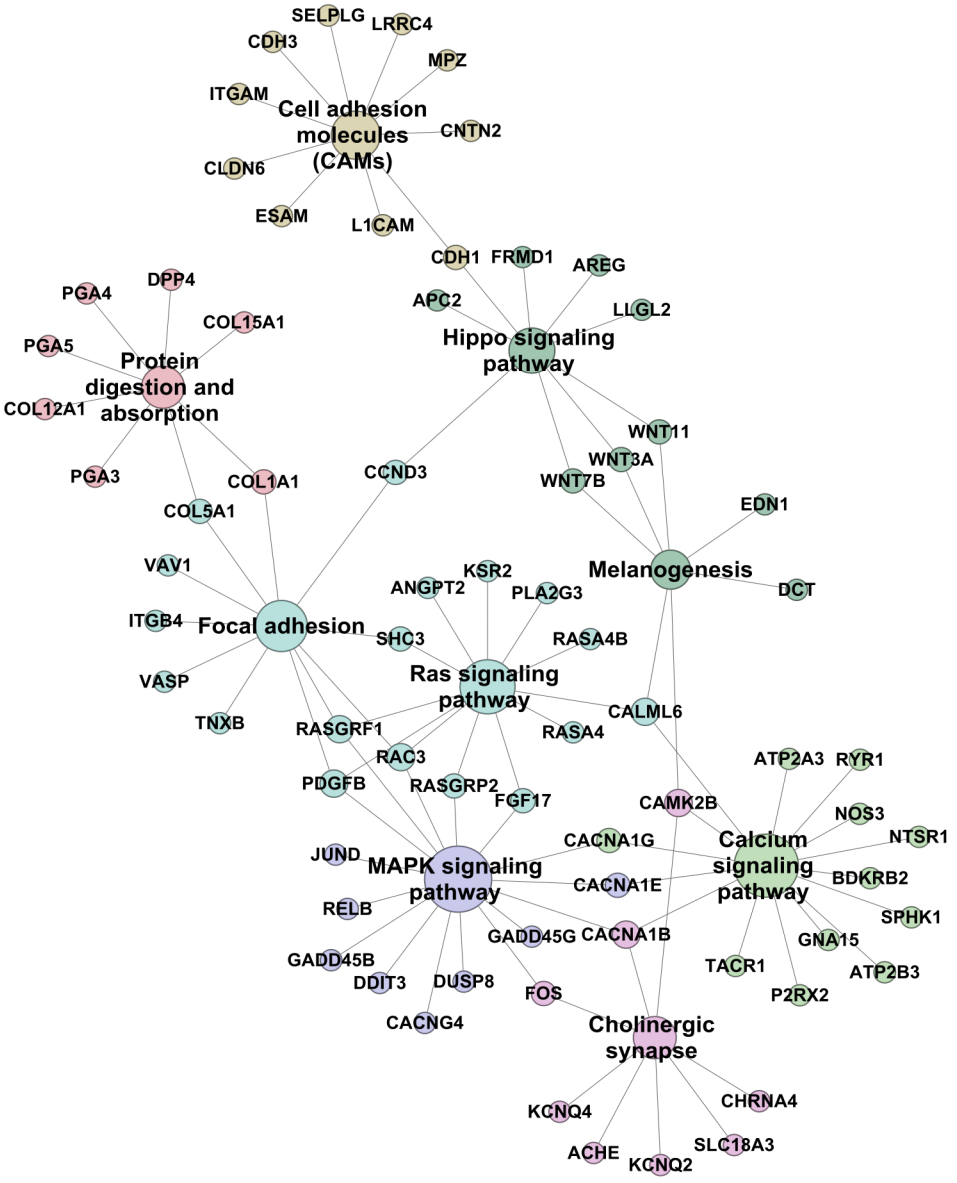

Figure 23. FKBP25 knockdown activates stress response signaling. Network analysis depicting the relationship between upregulated genes and enriched KEGG pathway terms. Network image was generated using the R package clusterProfiler (Yu et al., 2012)

To further explore a putative role for FKBP25 in cell cycle regulation I performed siRNA knockdowns in U2OS cells and quantified proliferation by the MTT assay, noting a significant decrease when FKBP25 expression was impaired (Figure 24AB). To characterize this phenotype cells were stained with the mitotic marker H3pS10 and propidium iodide (PI) 72 h post-transfection to measure changes in the cell cycle

(Figure 24CD). U2OS cells depleted in FKBP25 had a decreased S-phase content and increases in the G0/G1 and G2 populations, with fewer cells actively undergoing mitosis. I next performed nocodazole trap assays to further dissect and validate FKBP25 regulation of the cell cycle (Figure 24F-I). Cells were treated with nocodazole for 8 h to block progression through mitosis into G1 and the cell cycle distribution measured. I found that depletion of FKBP25 resulted in reduced entry into S phase and mitosis (Figure 24G-I). This observation suggests that cellular functions of FKBP25 play a role in G1/S and G2/M transitions of the cell cycle. I further validated this phenotype using stable cell lines expressing independent shRNAs targeting FKBP25 by nocodazole trap, and I again observed impaired entry into mitosis when FKBP25 expression was reduced, indicating the described phenotype results from on-target RNAi effects (Figure 24J). Interestingly, the tumor suppressor p53 has been shown to downregulate transcription of FKBP25 (Ahn et al., 1999), suggesting the halting of cell cycle progression by p53, which enforces both G1/S and G2/M checkpoints (Agarwal et al., 1995), may in part be facilitated by an FKBP25 mediated phenomenon. FKBP25 has also been shown to directly stimulate auto-ubiquitylation of MDM2 resulting in stabilization of p53 (Ochocka et al., 2009). However, I was unable to recapitulate this result (Figure 25), suggesting that FKBP25 regulation of p53 levels may be cell-type specific. In agreement with p53 regulation of FKBP25 expression, I found actinomycin D treatment, which promotes the accumulation of p53 (Zajkowicz et al., 2015; Ljungman et al., 1999), led to reduced expression of FKBP25 relative to the housekeeping gene GAPDH (Figure 25D).

To show that FKBP25 specifically influences entry into mitosis, cells were synchronized at the G2/M boundary by thymidine block followed by treatment with RO3306, a potent and selective inhibitor of CDK1 (Rizkallah and Hurt, 2009), and released (Figure 24K). By following H3pS10 in these cells, I observed that FKBP25 delayed entry into M-phase (Figure 24L). I further validated this observation with PI staining of stable shRNA knockdown cells, which progressed slower through mitosis and into G1 (Figure 24M). These results suggest that FKBP25 promotes entry into mitosis and its absence promotes an enhanced G2/M checkpoint. Collectively, these observations point to FKBP25 as an important contributor to the cell cycle and stress response.

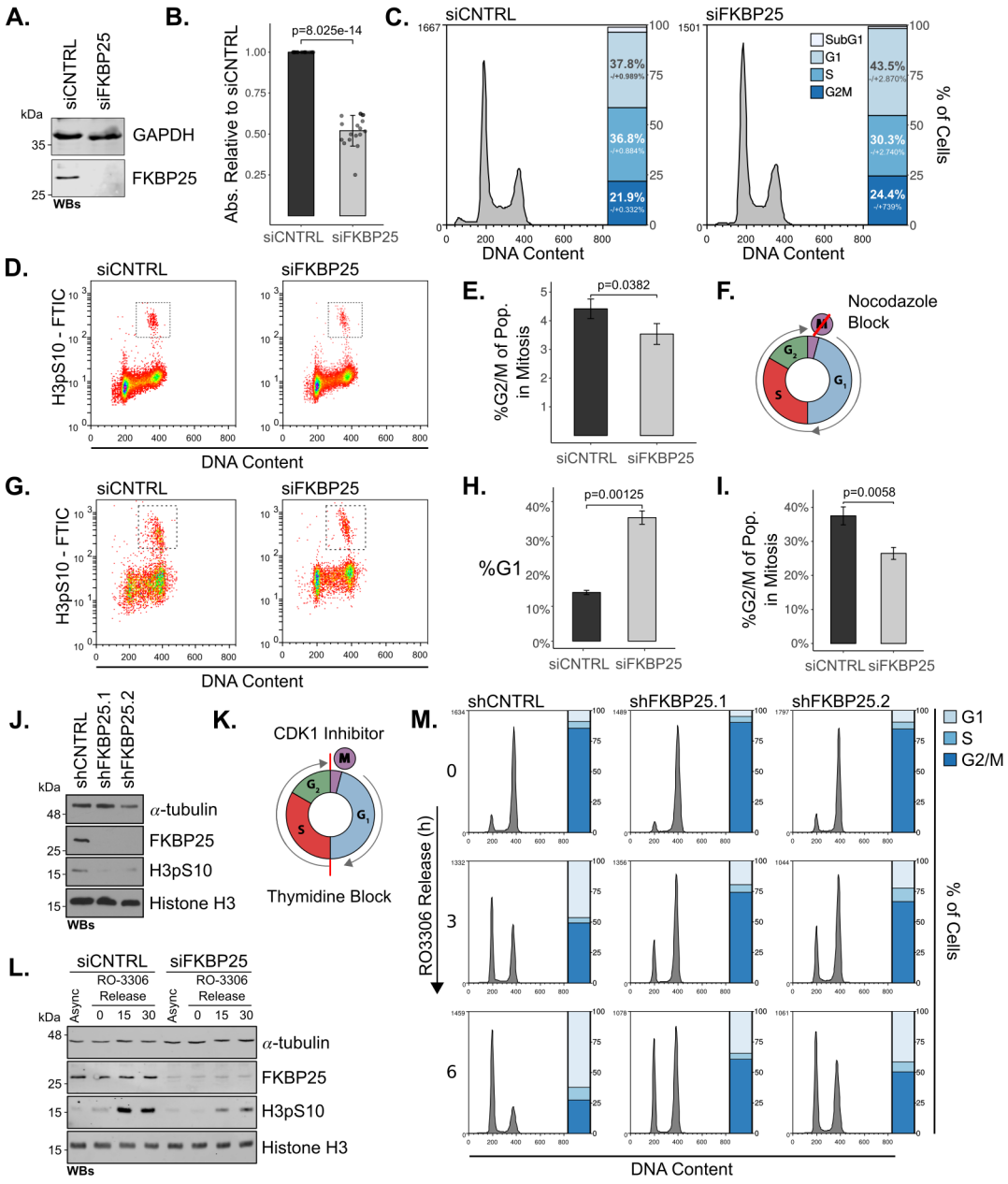

Figure 24. FKBP25 depletion disrupts cell cycle progression. (A) Western blot analysis of siRNA-mediated FKBP25 knockdown in U2OS cells. GAPDH is shown as a loading control. (B) MTT proliferation assay measuring cell viability 72 h post knockdown. Results shown are the mean ± SD of six independent transfections plated at three densities. (C) Flow cytometry analysis of PI stained cells showing cell cycle distribution in cells transfected with FKBP25 targeting siRNA or scrambled control, inlay bar graphs depict the mean ± SD of three replicates. (D) Flow cytometry analysis of mitotic marker H3pS10 and PI stained cells. (E) Quantification of H3pS10 positive mitotic cells as a percent of G2/M cells. Shown is the mean ± SD for three replicates.

Figure 24 ***(previous page).*** (F) Schematic representation of nocodazole trap. Cells were incubated for 8 h in nocodazole to halt progression into G1 of the cell cycle. (G) Flow cytometry analysis of mitotic marker H3pS10 and PI after 8 h nocodazole trap. (H) Quantification of cells remaining in G1 following 8 h nocodazole trap. Results are shown as the mean ± SD of three replicates. (I) Percentage of G2/M cells in mitosis following 8 h nocodazole trap. Results are shown as the mean ± SD of three replicates. (J) Western blot analysis of mitotic entry 8 h post-nocodazole trap of stable FKBP25 shRNA knockdown U2OS cells. Histone H3 and α-tubulin is shown as loading controls. (K) Schematic representation of synchronization at G2/M border by thymidine block followed by CDK1 inhibition (RO3306). (L) Western blot analysis of mitotic entry in FKBP25 siRNA knockdown cells released from G2/M transition block. (M) Flow cytometry analysis of PI stained stable shRNA FKBP25 knockdown cells released from G2/M transition block.

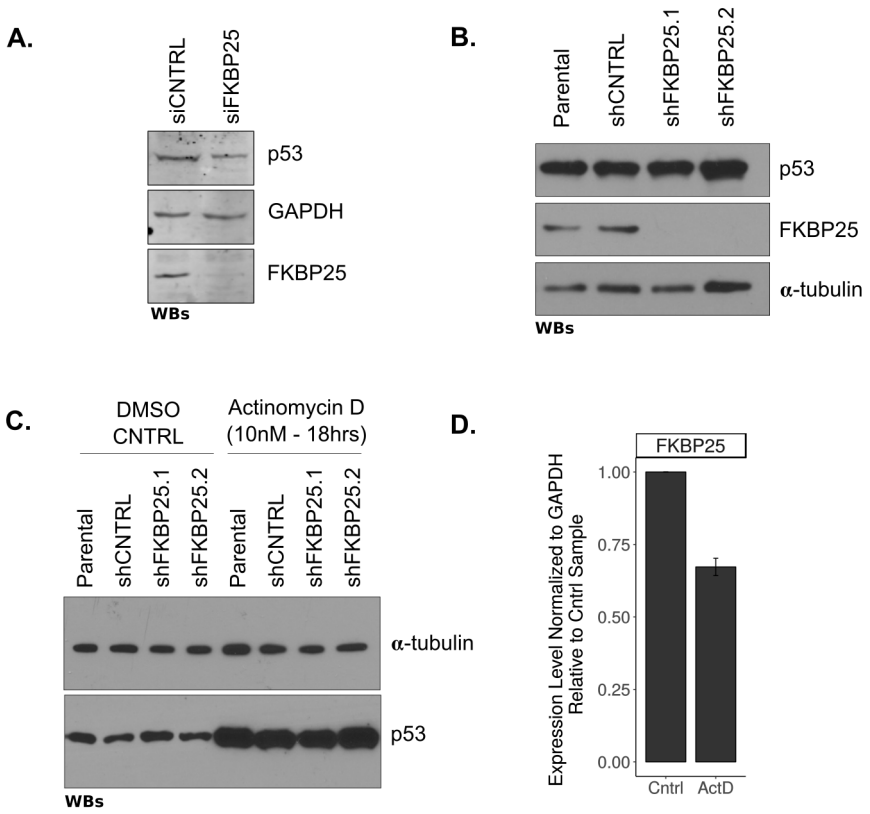

Figure 25. p53 status in FKBP25 knockdown cells. (A) Western blot analysis of p53 levels in U2OS cells depleted of FKBP25 by siRNA relative to a non-targeting control. GAPDH is shown as a loading control. (B) Western blot analysis of p53 levels in FKBP25 shRNA knockdown cells, α-Tubulin is shown as a loading control. (C) Western blot analysis of actinomycin D-mediated p53 induction in stable shRNA knockdown cells, α-Tubulin is shown as a loading control. (D) FKBP25 expression levels are relative to GAPDH in cells treated with Actinomycin D relative to a DMSO control. Results are shown as the mean $\pm$ SD of three replicates.

Given FKBP25's influence on cell cycle progression, I was next interested in testing the consequences of this phenotype on apoptosis. I found that FKBP25 knockdown reduced apoptosis and increased cell viability in cells treated with agents of genotoxic stress (Figure 26). I next wanted to test if this observation was connected to a block at the G2/M border. To do so, I synchronized stable shRNA cells at the G2/M border and treated with the DNA damage inducing drug etoposide before release and measured apoptosis by immunodetection of cleaved Parp-1. Indeed, FKBP25 knockdown cells showed decreased Parp1 cleavage (Figure 26GH). This phenotype is likely the result of a potentiated G2/M checkpoint, which prevents damaged cells from entering mitosis and undergoing apoptosis.

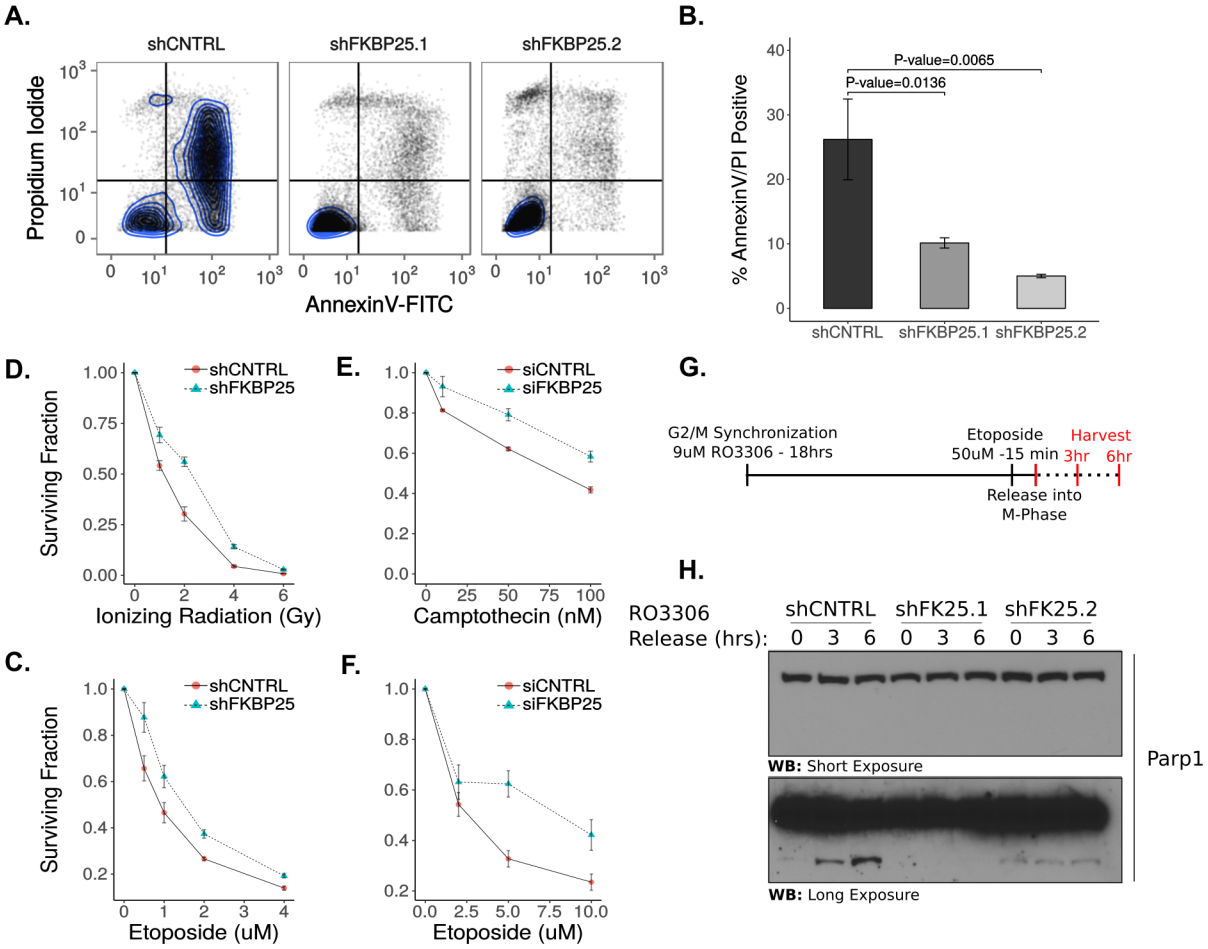

Figure 26. FKBP25 promotes M phase entry and apoptosis in cells exposed to genotoxic stress. (A) Flow cytometry analysis of apoptotic cell death measuring AnnexinV and PI staining after 24 h treatment with 100 µM etoposide in cells stably expressing shRNA. (B) Quantification of annexinV and PI positive cells. Results are shown as the mean ± SD of three replicates. (D-F) Clonogenic survival assays depicting cell survival in FKBP25 knockdown cells in the presence of several agents of genotoxic stress: ionizing radiation, camptothecin, and etoposide. . Results are shown as the mean ± SD of three replicates.(G) Schematic illustrating synchronization of cells and etoposide dosage for experiment in panel H. (H) Western blot of Parp1 cleavage, an indicator of apoptosis, following release from G2/M transition and brief treatment with etoposide in stable shRNA cells.

3.3.2 Subcellular distribution of FKBP25 during mitosis

To understand how FKBP25 may influence cellular proliferation and entry into mitosis, I set out to explore its localization during the cell cycle by immunofluorescence of asynchronous and M phase synchronized cells (Figure 27). FKBP25 has been shown to shuttle between the cytoplasm and nucleus (Ochocka et al., 2009). However, how the cell cycle may influence its localization has not been studied. By immunofluorescence analysis in U2OS cells, FKBP25 was primarily nuclear with a fraction present in the cytoplasm during interphase (Figure 27). In prophase, as visualized by DAPI stained condensed chromosomes, FKBP25 appeared to be dispersed from chromatin. The dispersed pattern was maintained as cells progressed through mitosis. FKBP25's mitotic localization was reminiscent of proteins that associate with the mitotic spindle apparatus and telophase midbody (Kim et al., 2009; Ishii et al., 2008; Tegha-Dunghu et al., 2008). These cytoskeletal structures, comprised primarily of microtubule polymers, are the macromolecular machines that segregate chromosomes and coordinate the orientation of the cleavage furrow. To explore this association further, I performed confocal imaging of cells stained for α-tubulin, a primary component of microtubules, and FKBP25 (Figure 28). Four key observations were made; (1) the cytoplasmic fraction of FKBP25 appeared to partially colocalize with α-tubulin, (2) FKBP25 was displaced from chromatin at the onset of mitosis, (3) FKBP25 partially colocalized with the mitotic spindle apparatus and midbody microtubules during cytokinesis, and finally (4) as telophase ends and daughter nuclei are formed FKBP25 returns to chromatin. These observations are supported by published proteomic datasets that have identified FKBP25 on purified mitotic spindles from Chinese hamster ovary cells (Bonner et al., 2011) and HeLa S3 cells (Ozlü et al., 2010). Interestingly, these reports also found a significant number of nucleolar and ribosomal proteins associated with the mitotic spindle, suggesting a link between the nucleolus and microtubule dynamics. We have recently identified a number of the same proteins as FKBP25 interacting partners (Gudavicius et al., 2014)(Chapter 2) and FKBP25 has long been known to associate with the multifunctional nucleolar protein nucleolin (Jin and Burakoff, 1993). Several of these factors have been further shown to regulate microtubule dynamics, including nucleolin, NPM1, and RPS3 (Jang et al., 2012; Gaume et al., 2015; Wang et al., 2010b). Furthermore, altered microtubule dynamics are known to activate the stress response and impair cell cycle progression, hinting at a potential mechanism for the cell cycle phenomenon I have uncovered here. Thus, I hypothesized that FKBP25 might play a similar role in the regulation of microtubule dynamics.

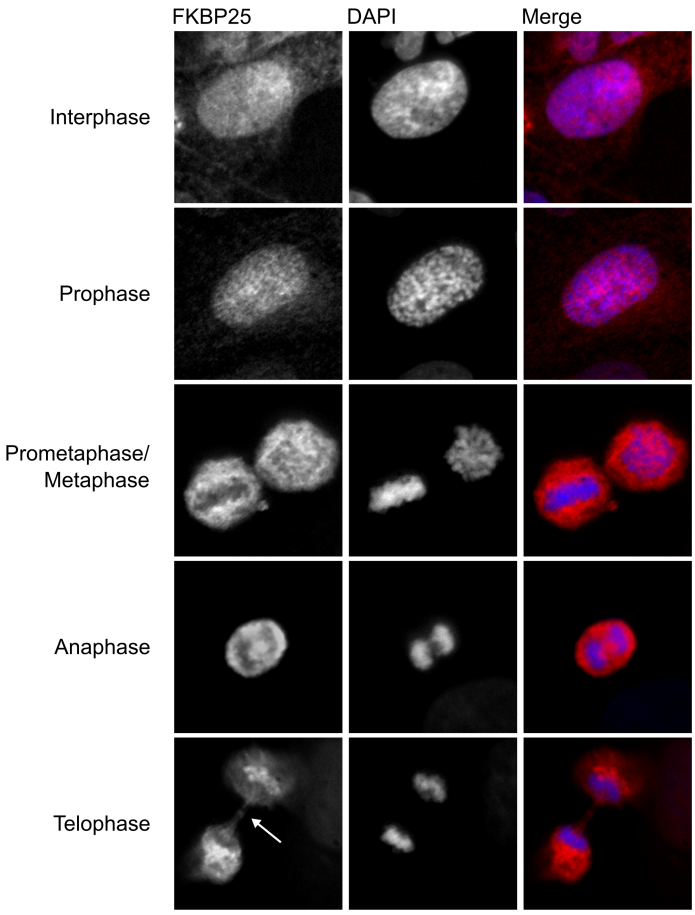

Figure 27. Epi-immunofluorescence analysis of FKBP25 localization throughout the cell cycle. Immunofluorescence staining of FKBP25 (red) in interphase cells and several stages of mitosis. Chromosomes are stained with DAPI (blue). A white arrow is drawn to indicate putative midbody microtubules.

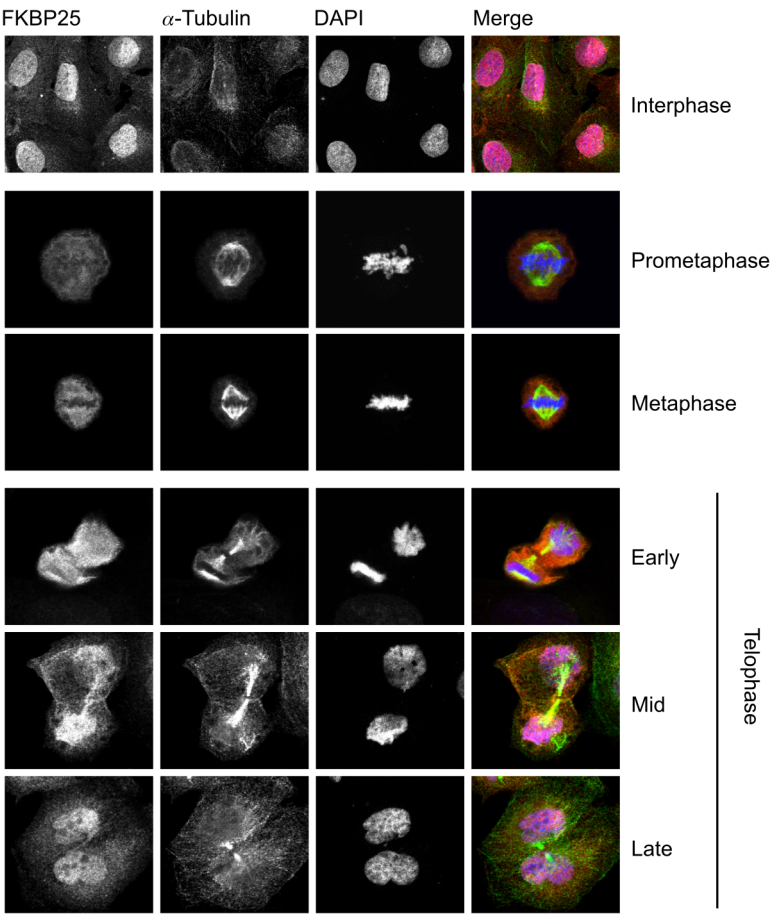

Figure 28. FKBP25 is displaced from chromatin during mitosis and associates with the mitotic spindle apparatus. Confocal imaging of the cellular distribution of FKBP25 and α-Tubulin during interphase and several stages of mitosis. Chromosomes are stained with DAPI.

3.3.3 FKBP25 influences microtubule dynamics independent of catalytic activity

To test for an interaction between FKBP25 and MTs, I performed microtubule spin-down assays to evaluate binding of FKBP25 to taxol-stabilized microtubules purified from asynchronous or mitotic HeLa S3 cells. I observed that FKBP25 interacts with microtubules independent of the cell cycle, as a fraction of recombinant FKBP25 pellets in the presence of MTs purified from either source (Figure 29). BSA was used as a negative control for binding. Next, I was interested in narrowing down the surface on FKBP25 that is involved in binding MTs. To do so, I repeated spin-down assays with domain constructs comprising either the N-terminal BTHB domain and linker region or the C-terminal FKBP isomerase domain (Figure 29B). Of the two domains, only the FKBP prolyl isomerase domain was able to bind. Interestingly, this is at odds with the majority of FKBP25's protein-protein interactions, which seem to be primarily mediated by RNA and the BTHB domain (Chapter 2). Given that the FKBP domain facilitates FKBP25's interaction with MTs; I was next interested if the catalytic pocket may be involved. To test this, I performed binding assays using a previously characterized Y198F catalytic null mutant (Gudavicius et al., 2013) or preincubation with rapamycin, a potent low nM affinity FKBP inhibitor (Jin et al., 1992). Neither mutational or chemical disruption of the catalytic pocket altered FKBP25 binding to microtubules, indicating it is an alternative surface on the isomerase domain involved in contact.

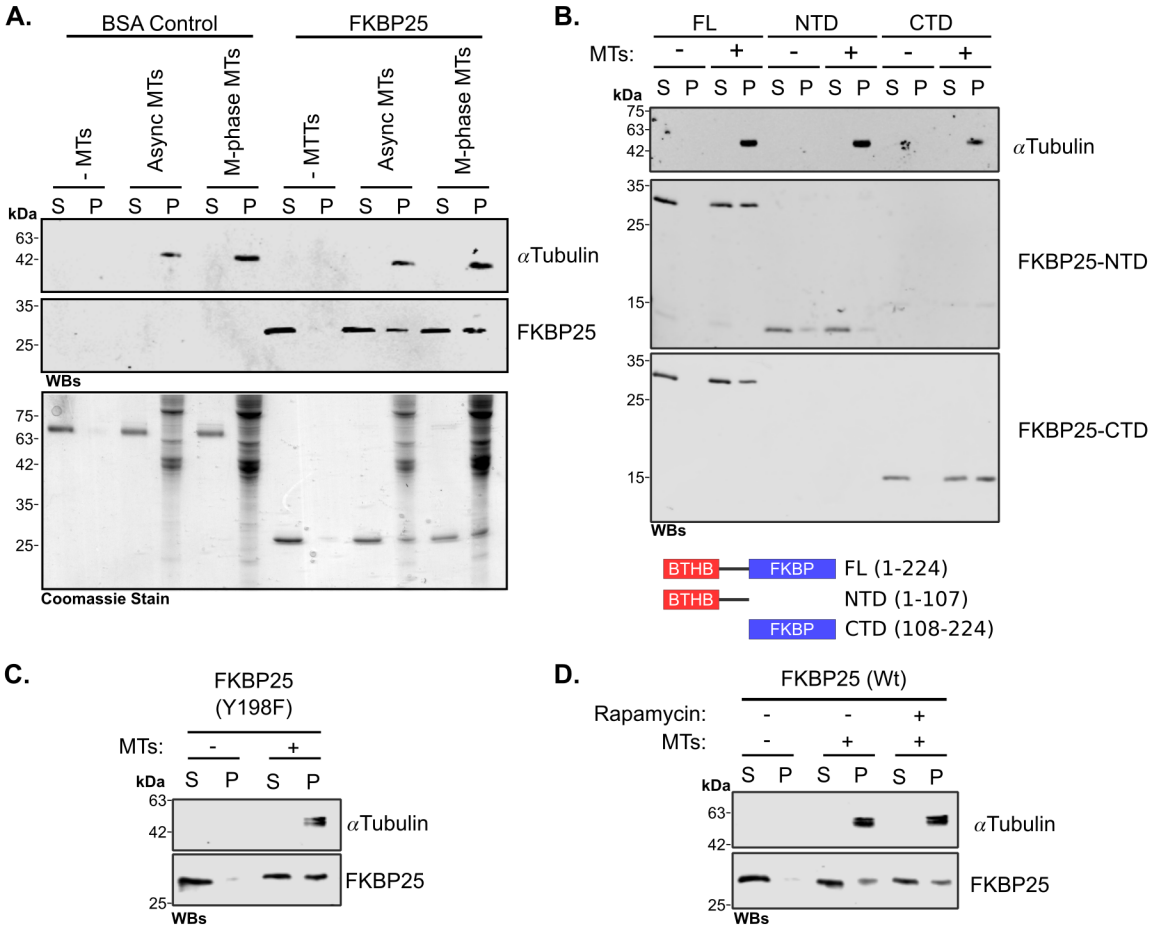

Figure 29. FKBP25 binds polymerized microtubules via its FKBP domain. (A) *In vitro* microtubule spin-down assay. Coomassie stained gels and western blots show supernatant (S) and pellet (P) in the absence or presence of microtubules purified from asynchronous or mitotic HeLa S3 cells incubated with recombinant FKBP25 or BSA control and centrifuged over a sucrose cushion. (B) Western blots analysis of MT spin-down assay with full-length, N-terminal, and C-terminal domains of FKBP25. (C) A catalytic-null FKBP25 mutant (Y198F) (D) and in the presence and or absence of 20 nM rapamycin.

Microtubule-associated proteins (MAPs) regulate the stability of microtubules. I next set out to explore whether FKBP25 alters the stability of microtubules *in vivo* by performing in cell tubulin polymerization assays. To confirm that any observed phenotypes were not a result of off-target RNAi effects and to test for a requirement for prolyl isomerase activity, I generated stable cell lines harboring either catalytically active or inactive tetracycline inducible transgenes with silent mutations in the siRNA

targeting sequence (Figure 30). I next assayed MT stability by immunostaining for α-tubulin in knockdown/rescue cells pre-extracted with detergent to release the dynamic MT fraction (Figure 30B). Quantification of fluorescence intensity per cell showed a significant disruption in the MT network in the absence of FKBP25, demonstrating that FKBP25 stabilizes MTs (Figure 30C). This phenotype was rescued by induction of either the wild-type or catalytic null transgenes, showing that while FKBP25 does influence MT dynamics, this function is not dependent on catalytic activity (Figure 30C). I further validated FKBP25's involvement in promoting MT stability using a pelleting assay to separate dynamic MTs (S - soluble fraction) from stable MTs (P - pelleted fraction). In agreement with the immunofluorescence-based assay, I found that stable shRNA knockdown cells had reduced levels of stabilized MTs relative to control shRNA cells (Figure 30DE). Together, these observations support a role for FKBP25 as an MT-stabilizing factor independent of catalytic activity. This is not particularly unusual as FKBP25 and members of the FKBP family have been shown to have non-catalytic functions (Arévalo-Rodríguez et al., 2004; Yang et al., 2001; Riggs et al., 2007; Ochocka et al., 2009). Indeed, no role for FKBP25's prolyl isomerase activity has yet been identified. These observations also provide a potential explanation for the delayed cell cycle phenotype. It has been shown in some breast cancer cell lines microtubule depolymerizing agents induce G1 and G2 cell cycle arrest (Blajeski et al., 2002) and delayed entry into M phase upon chemical disruption of microtubule networks has been described in rat kangaroo kidney (Rieder and Cole, 2000) and HEK 293 cells (Chang et al., 2011).

Formation of the mitotic spindle apparatus relies on the coordination of multiple pathways to ensure the faithful segregation of chromosomes and genomic integrity (Prosser and Pelletier, 2017). Misregulation of these pathways is associated with a number of pathologies, including cancer. One phenotype of aberrant division is an increase in micronuclei (MN), which result from chromosome segregation errors and promote complex chromosomal rearrangements (Holland and Cleveland, 2012). Given FKBP25's influence on MT stability, I quantified the frequency of micronuclei in stable shRNA knockdown cells by DAPI staining (Figure 30F). Disruption of FKBP25 led to a significant increase in MN frequency, suggesting FKBP25 is necessary for the proper segregation of chromosomes. Mitotic microtubule structures are not only required for segregation but also coordinate cytokinesis. Failure at this stage of cell division results in binucleated tetraploid cells, which have also been shown to contribute to carcinogenesis and chromosomal abnormalities (Fujiwara et al., 2005). I next looked at the relative number of bi-nucleated cells in knockdown versus control

cells and found FKBP25 represses their formation (Figure 30G). These results suggest that FKBP25's MT-stabilizing activities are essential for the formation and attachment of the mitotic spindle apparatus and coordination of cytokinesis by midbody microtubules. Importantly, FKBP25 suppresses chromosomal abnormalities.

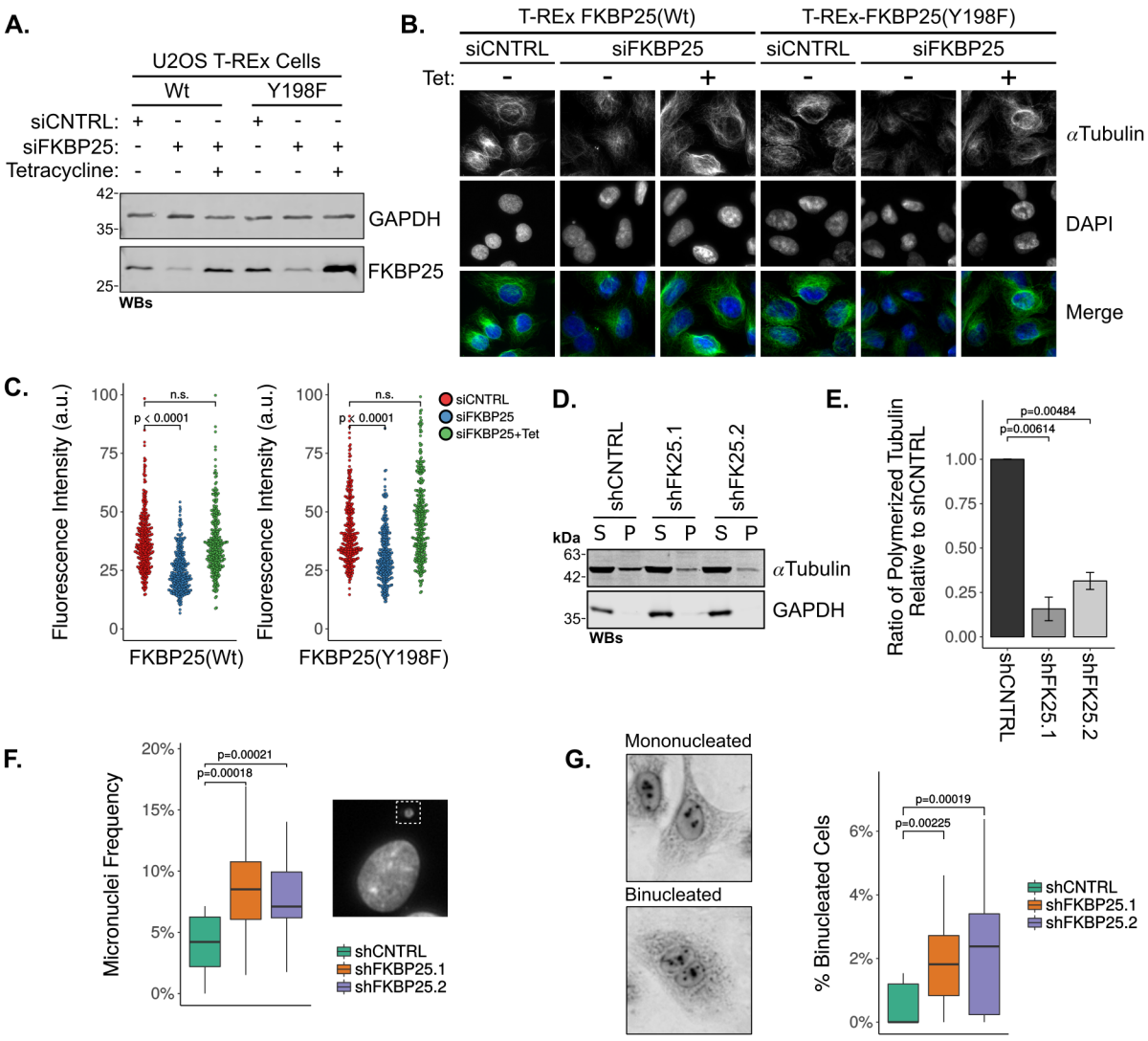

Figure 30. FKBP25 regulates the stability of microtubules independent of catalytic activity. (A) Western blot analysis of knockdown and tetracycline inducible rescue in stable Flp-In T-Rex U2OS cell lines expressing either wild-type or catalytic-null(Y198F) FKBP25 transgene. GAPDH is shown as a loading control. (B) In cell microtubule stability assay. Epi-fluorescence microscopy of α-tubulin (green), indicating polymerized microtubules, and DAPI (blue), indicating the nucleus in Flp-In T-Rex U2OS knockdown/rescue cells pre-extracted with PME buffer containing detergent. (C) Quantification of α-tubulin fluorescence intensity per cell (arbitrary units). Plots show the fluorescence intensity measurements of cells from at least 5 fields of view and greater than 250 cells per sample.

Figure 30 ***(previous page).*** FKBP25 regulates the stability of microtubules independent of catalytic activity. (D) In cell microtubule stability pelleting assay. Western blot analysis of supernatant and pellet of U2OS stable shRNA knockdown cells permeabilized with PEM buffer containing detergent and centrifuged. Pelleted fraction (P) represents stable polymerized microtubules and supernatant (S) unpolymerized tubulin. (E) Quantification of western blots in D. Results are shown as the mean ± SD for three replicates. (F) Micronuclei frequency assay. Boxplot showing the frequency of micronuclei in U2OS stable shRNA cells. Measurements are taken from three independent replicates each with at least 5 fields of view quantified. Inlay shown is a representative image of DAPI stained micronuclei relative to the cell nucleus. (G) Quantification of binucleated cells in U2OS stable shRNA-expressing cells. Binucleated cells were visualized by Giemsa staining as shown in representative images. Boxplot shows the percentage of binucleated cells in at least 5 fields of view from three replicate experiments.

3.3.4 FKBP25 is multiply phosphorylated upon entry into mitosis by PKC

I have shown here that FKBP25 regulates MT stability with implications on mitotic progression and genomic integrity. I was next interested in understanding how this process may be regulated. Entry into mitosis is largely co-ordinated by a wave of phosphorylation – large-scale proteomics screens have shown FKBP25 to be phosphorylated at several sites during mitosis (Olsen et al., 2010; Dephoure et al., 2008; Kettenbach et al., 2011), suggesting a putative regulatory mechanism. To first validate these findings, I purified FLAG-tagged FKBP25 from Flp-In HeLa S3 cells synchronized in various stages of the cell cycle and performed Phos-tag gel shift western blots probing for FKBP25 (Figure 31AB). Phos-tag is a commercially available phosphate binding compound that can be incorporated into SDS-PAGE gels, resulting in a mobility shift for phosphoproteins (Kinoshita, 2005). Only cells synchronized in M-phase by thymidine-nocodazole block showed a mobility shift when assayed, supporting published evidence of mitotic phosphorylation of FKBP25. To determine the timing of this phosphorylation event, Phos-tag gel shift assays were repeated on cells arrested at the G2/M border and released (Figure 31CD). The phosphorylated species was detected within 10 min of release, indicating that phosphorylation occurs upon entry into mitosis. FKBP25 phosphorylation seems to be temporally restricted, as detection of the phospho-species decreased at later time points. Mass spectrometry analysis of FLAG-tagged purified FKBP25 from mitotic cells identified several phosphorylation sites; S34, S36, T98, S100, T103, S152, and S163 (Figure 31E). Except T103, these sites have all been previously identified and are present in the phosphosite database (Hornbeck et al., 2004). It is important to note we did not

observe complete peptide coverage in this experiment. Therefore, this may not be a comprehensive list of all phospho-FKBP25 residues that occur during mitosis (Figure 32). Interestingly, several of the sites identified, lay proximal to residues characterized to be involved in nucleic acid binding by FKBP25 (Prakash et al., 2016), suggesting potential regulation of FKBP25's interaction with nucleic acids.

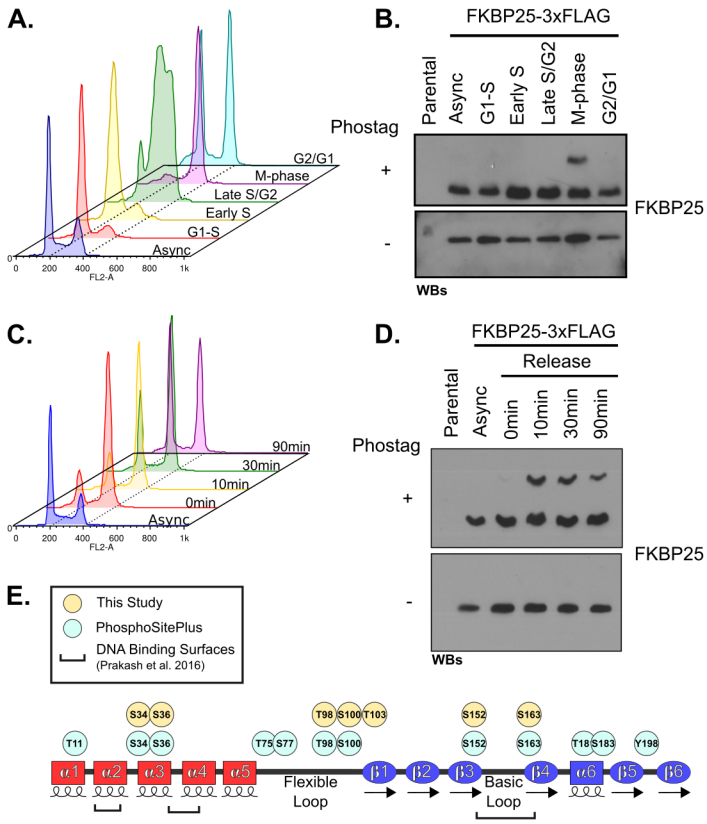

Figure 31. FKBP25 is multiply phosphorylated upon entry into mitosis. (A) Cell cycle distribution of synchronized cells. Flow cytometry analysis of PI stained synchronized Flp-In HeLa S3 cells expressing FLAG-tagged FKBP25. (B) Western blotting of immunoprecipitated FLAG-FKBP25 material from synchronized cells on SDS-PAGE gels with or without 50 µM Phos-tag. Parental cell line does not have an integrated FKBP25 transgene. (C) Flow cytometry analysis of cell cycle distribution of PI stained cells synchronized at G2/M border by thymidine/CDK1 block and released. (D) Western blot analysis of FLAG-FKBP25 IP material from cells synchronized and released at G2/M transition run on SDS-PAGE gels with or without 50 µM Phos-tag. (E) Schematic representation of mass spectrometry identified phosphoresidues in immunoprecipitated FLAG-FKBP25 from thymidine/nocodazole-synchronized mitotic cells (this study). Phosphoresidues previously detected as described on the PhosphoSite plus database are also shown (Hornbeck et al., 2004).

AspN coverage (57%):
MAAAVPQRAWTVEQLRSEQLPKKDIIKFLQEHGSDSFLAEHKLLGNIKNVAKTAN
KDHLVTAYNHLFETKRFKGTESISKVSEQVKNVKLNEDKPKETKSEETLDEGPPK
YTKSVLKKGDKTNFPKKGDVVHCWYTGTLQDGTVFDTNIQTSAKKKKNAKPLS
FKVGVGKVIRGWDEALLTMSKGEKARLEIEPEWAYGKKGQPDAKIPPNAKLTFE
VELVDID

Trypsin coverage (50%):
MAAAVPQRAWTVEQLRSEQLPKKDIIKFLQEHGSDSFLAEHKLLGNIKNVAKTAN
KDHLVTAYNHLFETKRFKGTESISKVSEQVKNVKLNEDKPKETKSEETLDEGPPK
YTKSVLKKGDKTNFPKKGDVVHCWYTGTLQDGTVFDTNIQTSAKKKKNAKPLS
FKVGVGKVIRGWDEALLTMSKGEKARLEIEPEWAYGKKGQPDAKIPPNAKLTFE
VELVDID

Total coverage (80%):
MAAAVPQRAWTVEQLRSEQLPKKDIIKFLQEHGSDSFLAEHKLLGNIKNVAKTAN
KDHLVTAYNHLFETKRFKGTESISKVSEQVKNVKLNEDKPKETKSEETLDEGPPK
YTKSVLKKGDKTNFPKKGDVVHCWYTGTLQDGTVFDTNIQTSAKKKKNAKPLS
FKVGVGKVIRGWDEALLTMSKGEKARLEIEPEWAYGKKGQPDAKIPPNAKLTFE
VELVDID

Figure 32. Peptide overage for purified mitotic FKBP25 digested with Asp-N or trypsin.

Multiple kinases coordinate mitosis to regulate nuclear envelope disassembly, chromatin condensation, and formation of the mitotic spindle (Tang and Poon, 2011). To identify the kinase that targets FKBP25 during mitosis, I first performed a bioinformatic analysis of putative kinase motifs within FKBP25. Unfortunately, this approach failed to elicit any high confidence hits. Thus, I turned to an unbiased approach utilizing recombinant FKBP25 as a substrate in *in vitro* kinase reactions with kinase-active mitotic extract and characterized selective inhibitors of mitotic kinases. I first tested purified extracts from thymidine-nocodazole synchronized HEK293 cells for activity by incubation with recombinant Histone H3 and ATP (Figure 33A). Western blot analysis for the mitotic marker H3pS10 indicated that the extract was active and could be inhibited by the Aurora kinase inhibitor MK-0457 (Figure 33A). Next, I incubated recombinant FKBP25 or its domains, with purified extract in the presence of $^{32}[\gamma]$-ATP and visualized phosphorylation by autoradiography (Figure 33B). All constructs showed some level of phosphorylation, in agreement with the mass spectrometry analysis, which identified multiple phosphorylation events on the BTHB domain, linker, and FKBP domains. This experiment was repeated in the presence of mitotic kinase inhibitors to decipher the kinase targeting FKBP25 (Figure 33C). For this experiment staurosporine was used as a positive control as it is a potent

broad spectrum inhibitor that targets many mitotic kinases (Karaman et al., 2008). Of the selective inhibitors tested, an inhibitor of protein kinase C (GO6983) had the most profound effect on FKBP25 phosphorylation. Inhibitors targeting CKII (tyrphostin AG1112), CDK1-Cyclin B1 (RO3306), and Aurora kinases (MK-0457) showed only modest reductions in phosphorylation, while roscovitine a multipotent cyclin-dependent kinase inhibitor had no effect.

Protein kinase C (PKC) is a family of serine/threonine protein kinases consisting of eight isozymes, the novel isoforms (PKC δ, ϵ, θ and η) are activated by increased diacylglycerol (DAG), a lipid second messenger, whereas the canonical PKC isozymes (PKCα, βI, βII and γ) also require Ca^{2+} (Mochly-Rosen et al., 2012). These proteins have a broad range of substrates and are implicated in diverse cellular functions. The PKCβII isozyme has been shown to translocate to the nucleus during G2/M (Deacon et al., 2002), where it aids in disassembly of nuclear envelope by phosphorylation of lamin B (Goss et al., 1994) and is required for G2/M transition of the cell cycle (Thompson and Fields, 1996). This coincides with a rise in nuclear levels of DAG (Deacon et al., 2002) and increased Ca^{2+} signaling (Machaca, 2011), suggesting activation of canonical PKC signaling during mitosis. Thus, I selected two canonical PKC isoforms, alpha and beta II, to validate PKC phosphorylation of FKBP25. Using *in vitro* kinase assays with recombinant proteins, I observed that FKBP25 is phosphorylated by canonical PKC isozymes, but not CDK1. Recombinant histone H1 is shown as a positive control – it is known to be robustly phosphorylated by both PKC and CDK1 (Mühlhäusser and Kutay, 2007). I next determined the sites on FKBP25 that are targeted by PKC using mass spectrometry analysis of *in vitro* phosphorylated FKBP25. PKC phosphorylated many of the phosphosites identified on FKBP25 purified from mitotic cells, with the exceptions of S36 in the BTHB domain and T98, S100, T103 in the linker region (Figure 33E). This result implies additional kinases target FKBP25 during mitosis. One possibility is CKII, which has been previously shown to associate with and phosphorylate FKBP25 (Jin and Burakoff, 1993), however, others have found CKII activity against FKBP25 to be minimal (Shi et al., 1994). In agreement with this finding, I also found only minimal activity against FKBP25 as compared to PKC *in vitro*(Figure 34). However, it is possible that other members of the complex containing CKII and FKBP25 may be required for full activity by stabilizing the interaction between CKII and FKBP25. Alternatively, phosphorylation at other sites in FKBP25 may participate in crosstalk with sites hit by CKII, priming FKBP25 for CKII mediated phosphorylation.

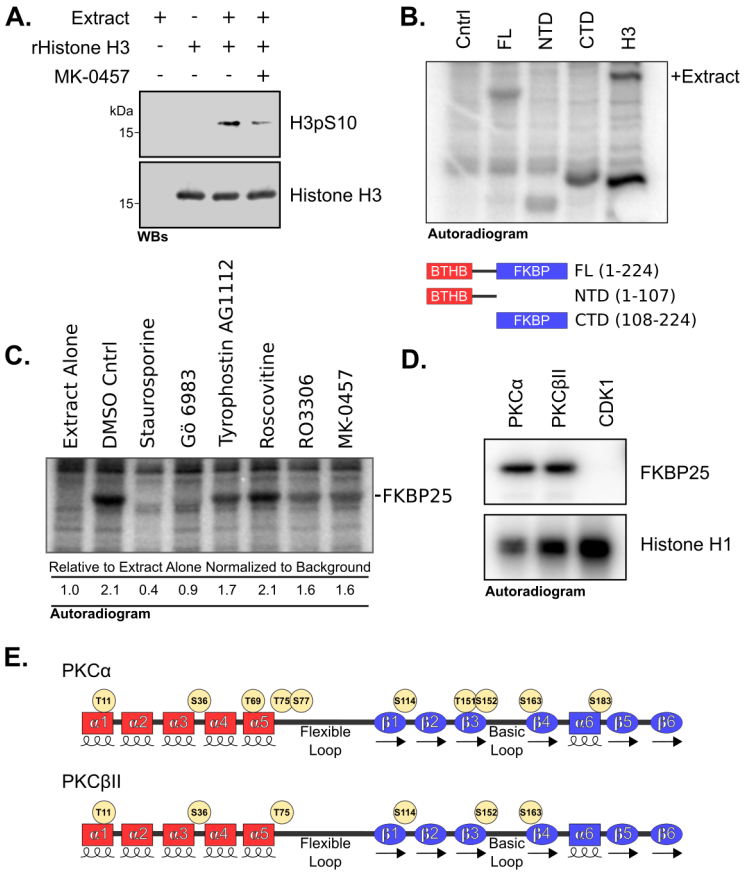

Figure 33. FKBP25 is phosphorylated by protein kinase C. (A) *In vitro* kinase assay with mitotic extract on recombinant histone H3. Western blot analysis of recombinant histone H3 untreated, treated with mitotic extract, or treated with mitotic extract and the Aurora kinase inhibitor MK-0457 (50 µM) (B) *In vitro* kinase assay with mitotic extract on recombinant FKBP25 constructs. Purified proteins were incubated with mitotic extract in the presence of $\gamma[^{32}\text{P}]$-ATP, resolved by SDS-PAGE, and visualized by autoradiography. For the Cntrl lane, no recombinant protein was included in the reaction. Histone H3 was included as a positive control. (C) Identification of putative mitotic kinase by *in vitro* kinase assay in the presence of mitotic kinase inhibitors. Assays were performed as in B with the inclusion of the kinase inhibitors staurosporine (broad range), Gö 6983 (PKC), Tyrphostin AG1112 (CKII), Roscovitine (CDKs), RO3306 (CDK1), and MK-0457(Aurora). (D) *In vitro* kinase assay with recombinant canonical PKC kinases and CDK1. Recombinant FKBP25 was incubated with purified PKCα (12.5 ng), PKCβII (12.5 ng), or CDK1-cyclinB1 (20 ng). (E) Schematic representation of mass spectrometry identified phosphoresidues on recombinant FKBP25 *in vitro* phosphorylated with either PKCα or PKCβII.

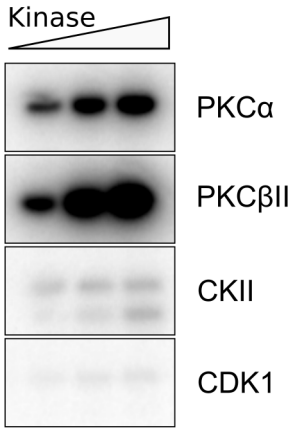

Figure 34. CKII has limited activity for FKBP25 in *in vitro* kinase assays. *In vitro* phosphorylation FKBP25 with increasing amounts of PKC*alpha* (12.5, 25, or 50 ng), PKCβII (25, 50, or 100 ng), CKII (125, 250, or 500 ng), and CDK1-CyclinB1 (10, 20, or 4 0ng). Kinase reactions were resolved by SDS-PAGE and visualized by autoradiography.

3.3.5 Phosphorylation of FKBP25 disrupts DNA Binding but not MT interaction

Immunofluorescence analysis of FKBP25's localization during mitosis showed that FKBP25 is displaced from chromatin early and then associates with the forming mitotic spindle. I also found that FKBP25 is phosphorylated, in part by PKC, at sites adjacent to key lysine residues involved in nucleic acid binding upon entry into mitosis. I next set out to test if phosphorylation during mitosis could influence either nucleic acid binding of FKBP25, as this is a determinant of its interactions with chromatin or the novel association with microtubules. To test this, I *in vitro* phosphorylated FKBP25 using either PKCα or PKCβII and performed microtubule spin-down assays as before and DNA mobility shift assays using a 1:100 DNA-FKBP25 molar ratio, as previously described (Prakash et al., 2016)(Figure 35). I observed that phosphorylation of FKBP25 reduced binding of FKBP25 to DNA (Figure 35B), as indicated by an increase in the unbound species when incubated with kinase and ATP. This result fits with the observation that several of the mitotic phosphosites identified lie adjacent to features implicated in the recognition of nucleic acids by FKBP25 (Prakash et al., 2016). In contrast, phosphorylation by PKC had little effect on FKBP25's interaction with polymerized microtubules (Figure 35A). I validated these results by repeating experiments with FKBP25 mutants containing phosphomimetic serine/threonine to glutamate mutations at the sites identified to be phosphorylated

by mass spectrometry in mitotic HeLa S3 cells. Starting with an 8x S/T to E mutant, I show that there is little influence on FKBP25 MT interactions (Figure 35C), but a dramatic reduction in DNA binding (Figure 35D). These observations support a model where different surfaces of the protein are required for mediating these interactions. Characterization of phosphomimetic mutations in either the BTHB domain, linker, or FKBP domain revealed that while all mutants showed decreased interaction with DNA, it is phosphorylation at sites flanking the basic loop of the FKBP domain that has the greatest influence on DNA binding. This is in agreement with the previous NMR characterization of FKBP25-DNA interactions, which showed several sites in the N and C-terminal to be involved in DNA binding (Prakash et al., 2016). Interestingly, a single mutation at either site flanking the basic loop showed similar decreases in DNA binding to the double mutant (Figure 35E), suggesting that a single phosphorylation event can substantially disrupt FKBP25-DNA interactions. Collectively, these results suggest that FKBP25's interactions with DNA are primarily mediated by the basic loop contained within the FKBP domain. In support, I find the FKBP domain alone showed greater binding to DNA than the BTHB domain + linker region (Figure 35F). Interestingly, this stretch of basic residues is unique to the FKBP domain of FKBP25 and is highly conserved in vertebrates (Figure 36). To validate that these sites are important for FKBP25's nucleic acid interactions in cells RNA-IP and ChIP experiments were performed using FLAG-tagged FKBP25 phosphomimetic mutants. In support of our *in vitro* experiments, these mutations disrupted FKBP25's interactions with nucleic acids in cells (Figure 37). These experiments support a model where mitotic phosphorylation of FKBP25 promotes its displacement from DNA without altering its association with microtubules and may serve to support FKBP25's role in stabilizing the mitotic spindle during mitosis (Figure 35G).

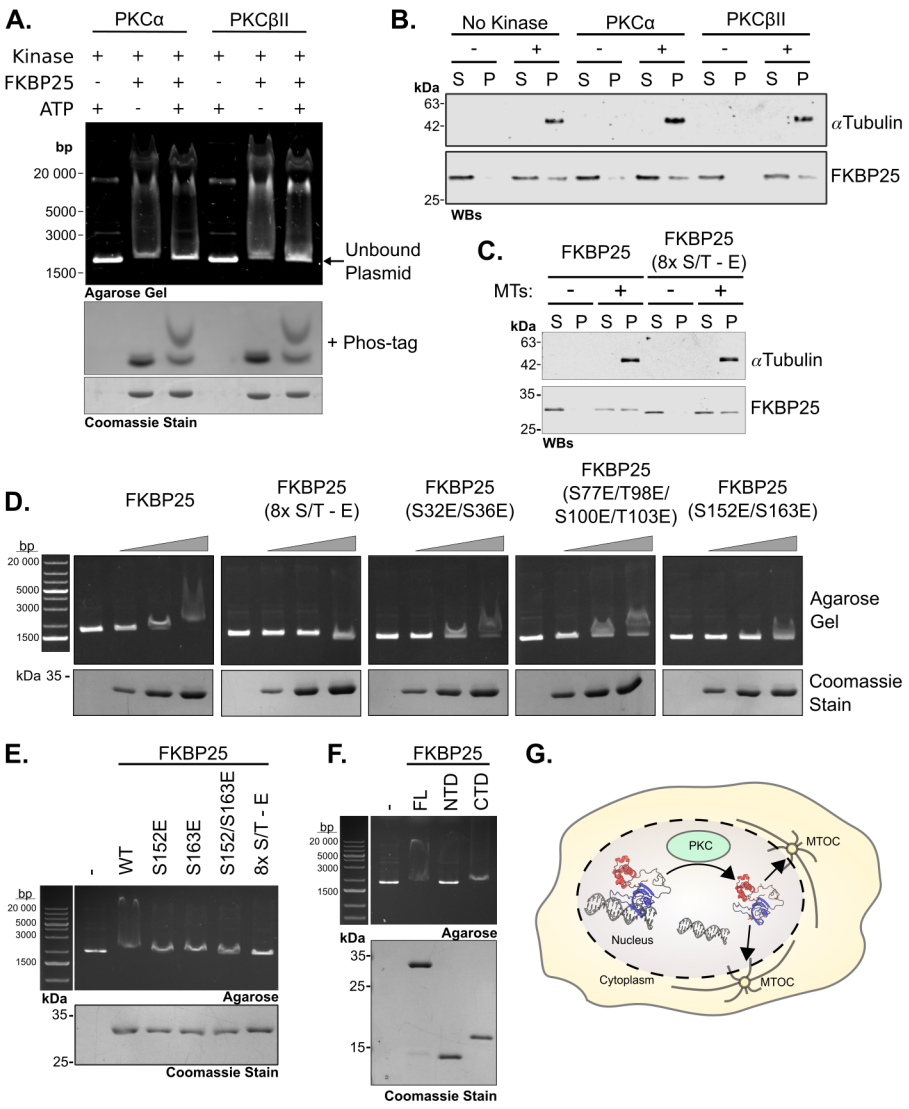

Figure 35. Phosphorylation of FKBP25 impairs DNA binding, but not its interaction with microtubules.(A) Gel retardation assay measuring DNA binding of FKBP25 with and without PKC phosphorylation. Coomassie stained SDS-PAGE gels with or without 50 µM Phos-tag show loading and phosphorylation status of FKBP25. (B) *In vitro* microtubule spin-down assay with recombinant FKBP25 *in vitro* phosphorylated with either PKCα or PKCβII. A no kinase sample is shown as a control.

Figure 35 ***(previous page).*** Phosphorylation of FKBP25 impairs DNA binding, but not its interaction with microtubules. (C) *In vitro* microtubule spin-down assay with phosphomimetic recombinant FKBP25 8xS/T to E mutant (S32, S36, S77, T98, S100, T103, S152, S163 mutated to glutamate). (D-E) Gel retardation assay measuring DNA binding of recombinant FKBP25 wild-type sequence and phosphomimetic S/T to E mutants,(F) and FKBP25 domains. (G) Model. FKBP25 (PDB ID: 2MPH) is phosphorylated by PKC during mitosis to promote its release from chromatin, freeing FKBP25 to function as a microtubule stabilizer in the formation of the mitotic spindle apparatus.

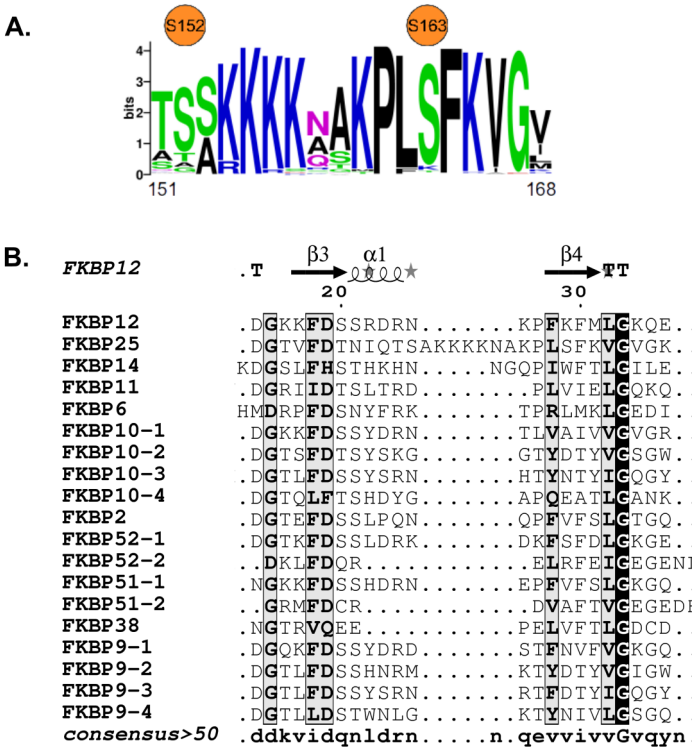

Figure 36. The basic loop in FKBP25's FKBP domain is unique and conserved in vertebrates. (A) Sequence logo analysis of FKBP25 from 142 vertebrate sequences generated using the WebLogo3 server (Crooks et al., 2004). (B) T coffee protein alignment of human FKBPs visualized using the ESPript server (http://espript.ibcp.fr) (Robert and Gouet, 2014; Notredame et al., 2000).

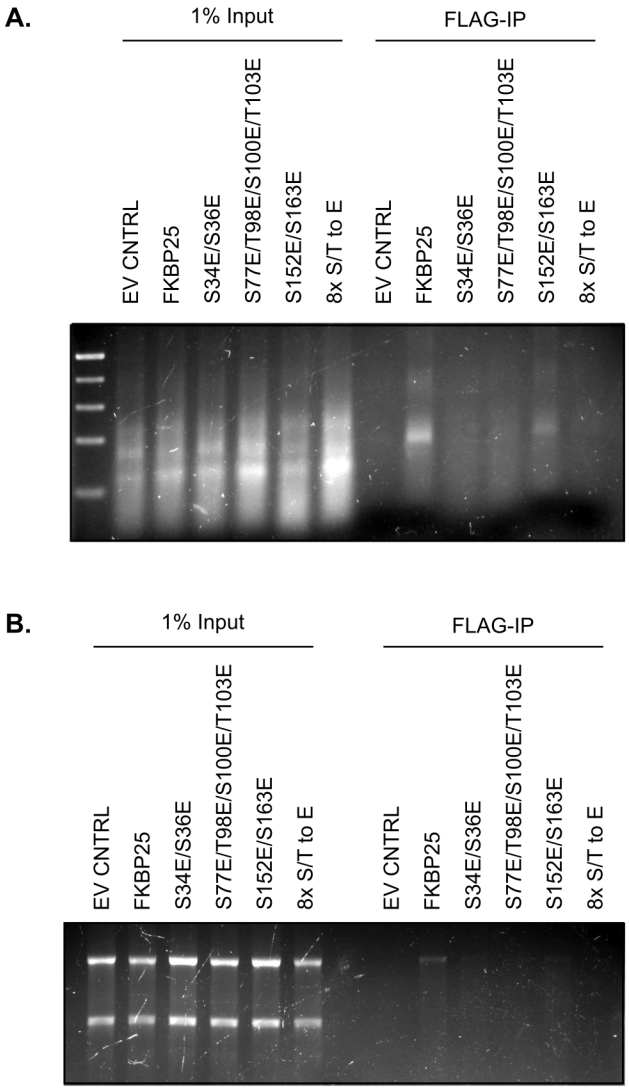

Figure 37. Phosphomemetic mutations disrupt FKBP25's interactions with chromatin and RNA in cells. (A) Purified DNA from ChIP of FKBP25-FLAG phosphomutants run on a 1.5% agrose gel and stained with ethidium bromide (EtBr)(B) RNA-IP of phosphomutants. RNA purified by trizol extraction and run on a 1% formaldehyde denaturing agrose gel.

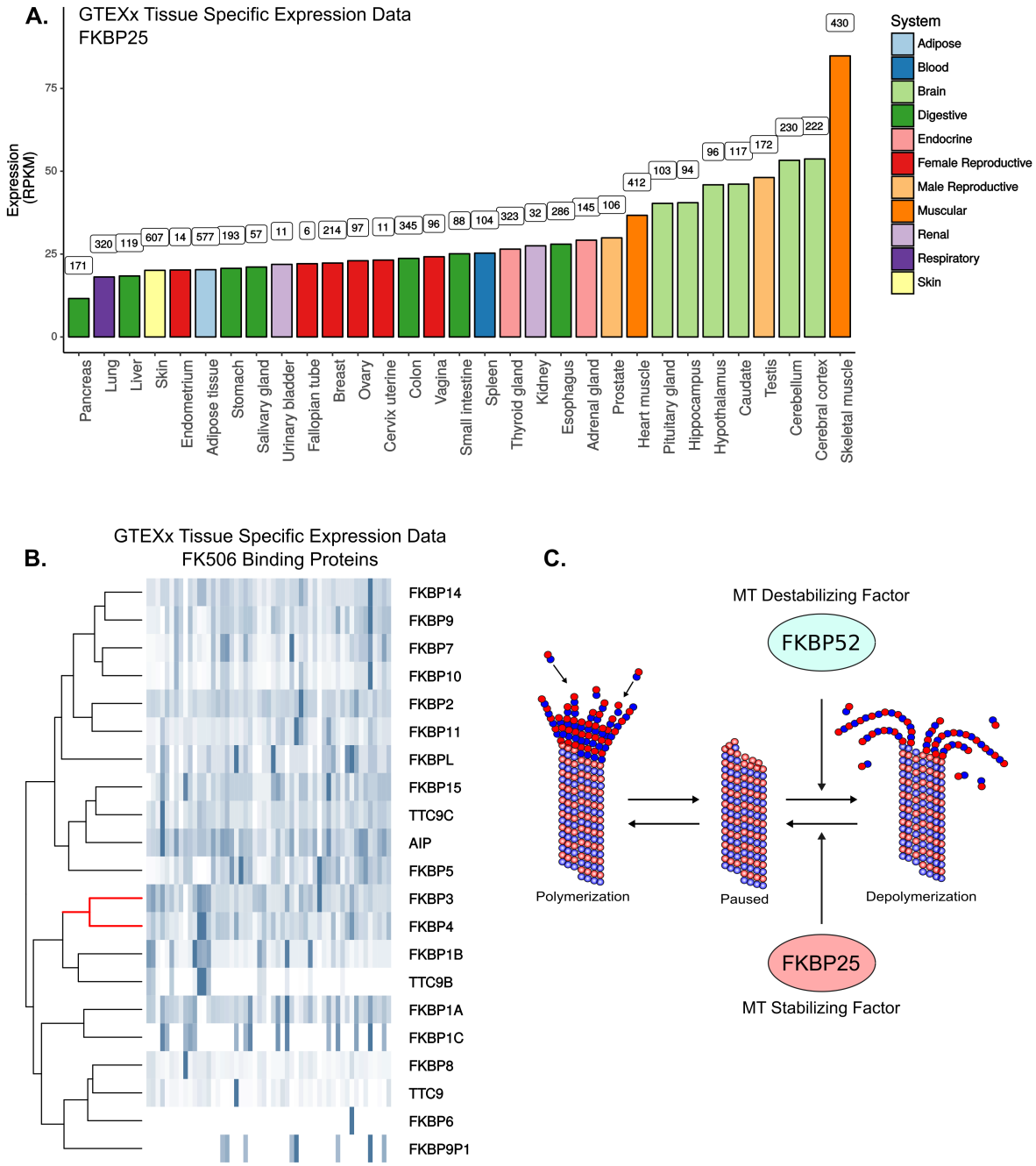

Figure 38. Tissue specific expression of FKBP25 relative to the FKBP family. (A) Publicly available tissue-specific RNA-Seq data for FKBP25 from the Genotype-Tissue Expression (GTEx) project (Lonsdale et al., 2013) shown as RPKM values by tissue. Numbers above bar graphs indicate the number of samples sequenced per tissue. (B) Heatmap of normalized tissue-specific gene expression from GTEx datasets for human FKBP domain containing proteins. FKBP52 (FKBP4) and FKBP25 (FKBP3) cluster together based on tissue-specific expression patterns, indicated in red. (C) Schematic representation of opposing functions of FKBP52 and FKBP25 on microtubule stability.

3.4 Discussion

Here I identify the nuclear PPI FKBP25 as a novel MT-stabilizing factor and propose a mechanism for its regulation during mitosis that promotes displacement from chromatin while maintaining access to the MT network. During mitosis microtubule dynamics increase, and the interphase MT network undergoes a dramatic rearrangement to form the mitotic spindle apparatus (Wittmann et al., 2001); a process tightly regulated by MAPs and critical to maintaining genomic stability. It has been shown that a significant cause of chromosomal instability is a failure of the mitotic spindle (Bakhoum et al., 2014). In line with FKBP25 regulating MT dynamics during mitosis, I found FKBP25 colocalized with both the mitotic spindle apparatus and midbody MTs. Also, I observed that decreased FKBP25 expression led to increased frequenct of formation micronuclei, presumably caused by missegregation of chromosomes, and binucleated cells, suggesting a failure to complete cytokinesis. Collectively, these observations suggest FKBP25's role in regulating MT dynamics during mitosis is required to maintain the stability of the genome.

Binding of nucleic acids by FKBP25 has long been appreciated (Rivière et al., 1993) – the functional significance of this feature of the protein is unclear. It has been proposed that nucleic acid recognition by FKBP25 may have a role in the regulation of chromatin and transcription (Yang et al., 2001; Prakash et al., 2016), however, this hypothesis has not been tested directly. I show here that depletion of FKBP25 had minimal effects on bulk transcription, indicating a more subtle and potentially indirect role. I did note the transcriptional activation of MAPK stress response signaling. MAPK signaling is intrinsically linked to the MT network, with an estimated one-third of MAPK proteins physically associating with the MT cytoskeleton (Reszka et al., 1995). It has been proposed that microtubule disassembly activates p38 MAPK signaling leading to inhibition of the cdc25B phosphatase and delayed entry into mitosis (Mikhailov et al., 2005), similarly to FKBP25 knockdown. These findings support the idea that the delayed cell cycle phenotype and transcriptional changes I describe here are likely the consequence of FKBP25's activity on microtubules; whereby disruption of FKBP25 results in a destabilized MT network, leading to activation of MAPK stress signaling and attenuated cell cycle checkpoints. However, based on these experiments alone I cannot rule out a direct role for FKBP25 in transcriptional control. Further research is required to determine exactly how FKBP25 acts on the chromatin template and the functional nature of its DNA-binding properties.

One potential explanation for FKBP25's conserved nucleic acid binding features

is as a means to sequester its MT-stabilizing activities to the nucleus during interphase. Similar to FKBP25, the mitotic spindle-associated proteins NuSAP, Numa, and TPX2 show a cell cycle-dependent localization, localizing to the nucleus during interphase to sequester their MT-stabilizing activities until the mitotic breakdown of the nuclear envelope (Wittmann et al., 2000; Merdes et al., 1996; Kahana, 2001; Raemaekers et al., 2003). Further, TPX2 mediated microtubule nucleation is inhibited nuclear import proteins (Roostalu et al., 2015). FKBP25 contains a putative nuclear localization signal (Jin and Burakoff, 1993), however direct binding to import proteins has not been shown. As FKBP25 is a relatively small protein (25kDa), it may enter the nucleus by diffusion and its nucleic acid binding properties would act to support its residency. I show here that FKBP25 is multiply phosphorylated during mitosis and identify protein kinase C as the putative mitotic kinase responsible – PKC-mediated phosphorylation of FKBP25 releases it from DNA while maintaining access to MT networks. Interestingly, PKC activity has been previously linked to the regulation of MT dynamics, where activation of PKC by DAG-lactone treatment increased MT dynamics and reduced MT catastrophe through phosphorylation of α-tubulin (De et al., 2014). FKBP25 could represent a secondary target of PKC that acts to promote MT stability upon phosphorylation by releasing FKBP25 from chromatin, to promote association with the forming mitotic spindle. This hypothesis is supported by our immunofluorescence data showing FKBP25's displacement from chromatin and mitotic phosphorylation occur early in mitosis. Thus, these events are at the least temporally related if not mechanistically connected.

Interestingly, it is the FKBP domain of FKBP25 that mediates its interaction with microtubules. This finding differs from the majority of FKBP25's protein-protein interactions, which seem to occur via the BTHB, as outlined in Chapter 2. As well, this result also challenges the generally held idea that it is accessory domains of prolyl isomerases that dictate substrate specificity and localization. The role of the BTHB domain in microtubule stability and its RNA binding features remains unclear. How these two domains may interact to coordinate microtubule function is an interesting question that warrants further characterization.

Cellular architecture is built upon microtubules. These structures give shape and movement to a cell, as well as provide a platform for the intracellular trafficking of nucleic acids, proteins, and vesicles. Interestingly, several members of the FKBP family are known to be required for MT-dependent transport. FKBP52, a large immunophilin, facilitates the nuclear localization of the transcription factor p53 and the glucocorticoid receptor by bridging their interactions with the motor protein dynein

and the MT network; like FKBP25, FKBP52 binds the MT network through its FKBP domain (Galigniana et al., 2002; Wochnik et al., 2005). FKBP52 also binds to tubulin directly through its tetratricopeptide repeat, inhibiting MT polymerization (Chambraud et al., 2007). FKBP52 and FKBP25 are co-expressed in multiple tissues and share a similar tissue-specific expression pattern, with high expression in neurons (Figure 37), supporting the idea that these two FKBPs may act antagonistically in the regulation of MT dynamics. Two catalytically inactive FKBPs, FKBPL and FKBP15, have also been shown to function similarly to FKBP52 in the transport of signaling molecules (McKeen et al., 2008; Viklund et al., 2009). These studies support the idea that the catalytic activity of FKBP domains is not a prerequisite for associating with the MT infrastructure, as I report for FKBP25.

RNA molecules are another important class of cellular cargo – mRNA transport along microtubule highways is essential for proper neuronal physiology (Buxbaum et al., 2015). I have shown that the BTHB domain of FKBP25 can bind RNA directly. Also, a large-scale screen identified FKBP25 as a direct mRNA binding protein, indicating that mRNA may be an additional substrate (Castello et al., 2016). These observations support the idea of a potential function for FKBP25 in the MT directed movement of mRNA. Whereby FKBP25 interacts with the dynein/dynactin motor complex through its FKBP domain and binds mRNA through its BTHB domain to facilitate transport. Interestingly, the adenomatous polyposis coli (APC) protein, an RNA binding MAP implicated in RNA localization, was shown to regulate microtubule stability through the transport of β2B-tubulin mRNA to the plus end where it is locally translated to promote growth cone expansion and neuron migration (Preitner et al., 2014). This study of APC suggests a self-organizing model for microtubule dynamics that relies on MT-dependent transport of mRNA encoding tubulin subunits (Preitner et al., 2014), hinting at a putative mechanism for FKBP25's MT-stabilizing activities. Interestingly, this form of regulation may also hold true for the mitotic spindle as well – mRNAs encoding mitotic spindle components have also been shown to associate with the mitotic spindle as a means to provide localized translation of spindle components (Sharp et al., 2011). Further characterization of FKBP25's role in regulating microtubule dynamics and the contribution of each domain would shed light on this fascinating area of cell biology.

The microtubule network is anchored by the centrosome, which serves as a platform for signaling and the nucleation of MTs (Conduit et al., 2015). Duplication of the centrosome occurs during interphase, allowing the formation of a bi-polar mitotic spindle during mitosis. Misregulation of this process results in centrosome amplifi-

cation causing aneuploidy and spontaneous tumorigenesis (Levine et al., 2017). Interestingly, the prolyl isomerases CypA and Pin1 are known to regulate centrosome duplication in a manner dependent on their isomerase activities (Suizu et al., 2006; Bannon et al., 2012), implicating prolyl isomerization as a regulatory mechanism. Notably, Nucleolin and NPM1, two proteins known to interact with FKBP25, are also involved in centrosome duplication – these proteins localize to the centrosome during interphase and knockdown of either leads to centrosome amplification (Okuda, 2002; Gaume et al., 2015; Ugrinova et al., 2007). As well, both proteins influence microtubules dynamics (Gaume et al., 2016; Wang et al., 2010b) and promote chromosomal stability during mitosis (Ugrinova et al., 2007; Amin et al., 2008). Given the striking similarities between the functions, localizations, and phenotypes of these proteins it seems plausible that FKBP25 may also regulate centrosome duplication, which would contribute to the chromosome instability phenotypes identified here. Also, of interest is the connection between nucleolar factors and microtubule dynamics. Again, the regulation of fundamental cell structures may be integrated at a systems-level.

The FKBP family has important roles in neuronal signaling and have become recognized as promising targets for the treatment of microtubule-associated neurological diseases such as Alzheimer's and Parkinsons (Blair et al., 2015; Hausch, 2015; Cao and Konsolaki, 2011). There remains a significant knowledge gap in our understanding of the individual functions of each member FKBP and how they individually contribute to health and disease. This is the first report to describe a cellular function for FKBP25 in microtubule dynamics and serves to clarify the involvement of FKBPs. As described here, FKBPs, like FKBP25 and FKBP52, may have antagonistic roles. Thus, understanding the individual functions of FKBP members will be important in the rational design of targeted therapeutics that can discriminate between FKBPs to elicit the most effective response in patients.

3.5 Materials & Methods

Cell culture, transfections, and generation of stable cell lines

U2OS (ATCC), Flp-In T-Rex HEK293 (Thermo Fisher), Flp-In T-Rex U2OS (a generous gift from Dr. Blerta Xhemalce, University of Texas at Austin), and Flp-In HeLa S3 (graciously provided by Dr. Till Bartke, Imperial College London) cells were cultured in DMEM containing 10% (v/v) FBS (Sigma) and antibiotics (10 units/ml penicillin and 10 µg/ml streptomycin, ThermoFisher) at 37℃ and 5% $C0_2$. For transient siRNA knockdown, reverse transfection of 10 nM targeting or non-targeting control siRNA was performed using jetPRIME (Polyplus-transfection) following the manufacturer's instruction, followed by incubation for 48-72 h before downstream analysis. Stable U2OS shRNA knockdown cells were generated by transfection with HuSH 29-mer shRNA expression vectors (Origene) using GenJet U2OS Transfection Reagent (SignaGen) followed by selection with puromycin (InvivoGen) 48 h post-transfection until colonies formed. Colonies were then isolated, expanded, and screened for knockdown by western blot and RT-qPCR. Flp-In stable cell lines were generated following the manufacturer's instruction (Thermo Fisher). siRNA and shRNA targeting sequences are presented in Table A.4 and A.5 of the appendix, respectively.

Rationale for cell line selection

The cell lines utilized in this chapter are common throughout biomedical research as a generalized model for human cell biology. RNA-Seq experiments were performed in HEK293 cells as this cell line was first utilized for optimization of siRNA-mediated knockdown. Initially, HEK293 cells were to be used throughout the study as a model system. However, due to their semi-adherent characteristics synchronization involving multiple wash steps made their use technically challenging. Therefore, for cell biology experiments U2OS cells were instead used throughout this study. HeLa S3 cell lines were used for synchronization and mass spectrometry analysis as they are easily grown in large volumes. This ensured adequate production of material for purification of FLAG-tagged FKBP25 and downstream analysis. HEK 293 Flp-In cells were used to generate phosphomemetic mutants for ChIP and RNA-IPs due to the relative ease of generating cell lines using the FRT/Flp-In system (Thermo Fisher).

Statistics

All numerical results are reported as mean ± standard deviation (SD). The number of replicates, technical or biological, are indicated in corresponding figure legends. The

R programming language for statistical analysis was used for the calculation of statistical significance. If not indicated otherwise in figure legends, two-tailed Students t test for unpaired data was used to evaluate single comparisons between different experimental groups.

Plasmids

FRT containing expression vectors for stable integration and tetracycline-inducible expression were generated by subcloning a synthesized FKBP25-3xFLAG-6xHIS gene containing (GenScript) into a modified pcDNA5/FRT/TO vector (Thermo Fisher). For plasmids used to generate Flp-In T-Rex U2OS Trex Flp lines used in siRNA rescue experiments, a stop codon was introduced before the 3xFLAG-6HIS tag to generate a tagless FKBP25 construct as well as silent mutations in the siRNA targeting sequence by site-directed mutagenesis. His-tag bacterial expression vectors were generated by cloning synthesized FKBP25 genes (GenScript) into a pET 6-His vector using standard techniques. Site-directed mutagenesis of pcDNA5 and pET 6-His vectors was accomplished by inverse PCR with mutagenic primers. All constructs were validated by sequencing.

Recombinant proteins

FKBP25 6-His proteins were expressed in *Eschericia coli* BL21 (DE3) cells grown overnight, diluted 1:20 and induced at an OD_{600} of ≈ 0.6 with 1 mM IPTG for 4 h. Cell pellets were resuspended in binding buffer (50 mM Tris pH 8, 150 mM NaCl, 0.5% NP-40, 5 mM EDTA, 1 µg/ml leupeptin, 1 µg/ml aprotinin, and 1 µg/ml pepstatin), sonicated, and cleared by centrifugation. Recombinant 6-His proteins from cleared lysates were purified using Nickel-NTA agarose (Qiagen) following the manufacturer's protocol and dialyzed overnight in 1x PBS containing 10% glycerol. Histone H3 was expressed in *Escherichia coli* BL21 (DE3) and purified to homogeneity through acid extraction, ion exchange (Macro-Prep Ion Exchange Media, BioRad), and reverse phase HPLC (C18-300, 250 mM x 4.5 mM, 5 µM, ACE). Histone H1 was sourced from Roche. PKCα and PKCβII kinases were purchased from SignalChem. CDK1-cyclinB1 and CKII kinases were purchased from New England Biolabs.

Antibodies

The following antibodies were used in this study: GAPDH (Santa Cruz, sc-47724 - WB 1:10 000), FKBP25(GeneScript WB 1:2000 IF 1:300), α-tubulin (Santa Cruz sc8035 WB 1:10 000, IF 1:1000), H3pS10 (abcam ab5176 - WB 1:10 000 Flow Cytom-

etry 1:5000), Annexin V (Santa Cruz, sc-4252 FITC Flow Cytometry 1:300), Histone H3 (abcam, ab1791 WB 1:50 000), Parp1 (Santa Cruz, sc-8007 WB 1:5000), and p53 (Santa Cruz, sc126 WB 1:5000).

SDS PAGE, Phos-tag SDS-PAGE, and western blotting

Western blots were performed by resolving proteins by SDS-PAGE and transferring to nitrocellulose membranes in phosphate transfer buffer (50 mM sodium phosphate buffer pH 6.8, 15% EtOH). For Phos-tag western blots, SDS-PAGE gels included 50 µM Phos-tag (MANAC inc.) and 10 mM $MnCl_2$. Phos-tag-SDS-PAGE gels were washed twice in a solution of transfer buffer containing 100 mM EDTA before transfer, as previously described (Kinoshita, 2005). Membranes were incubated in 10% skim milk for 30 min to block and probed with primary antibody for either 1 h at room temperature or overnight at 4℃ followed by three washes in TBS-T (1x TBS with 0.1% Tween 20). For chemiluminescence based detection, horseradish peroxidase conjugated anti-mouse (GE) or anti-rabbit (GE) secondary antibody was used at 1:5000 in 1% milk/TBS-T. Blots were then washed three times in TBS-T and proteins detected by incubation with a chemiluminescence HRP substrate (Millipore) and exposed to film. For fluorescence-based detection, blots were incubated with either IRdye 800CW anti-mouse (Mendel Scientific) or IRdye 680RD anti-rabbit (Mandel Scientific) at 1:5000 for 1 h at room temperature in 1% milk TBS-T, followed by three washes in TBS-T and one wash in 1x TBS, and imaging on an Odyssey Clx imaging system (Li-Cor).

MTT proliferation assay

Assays were performed as previously described (van de Loosdrecht et al., 1994). Briefly, cells reverse transfected with siRNA were incubated overnight, then trypsinized, counted by hemocytometer, and plated at densities ranging from 5000 to 15 000 cells per well of a 96-well plate. Plates were incubated for 72 h, and 20 µl of 5 mg/ml thiazolyl blue tetrazolium (Sigma) was added to each well and incubated for 2.5-3 h at 37℃. Media was removed and 150 µl of DMSO added per well to solubilize the precipitant. Plates were incubated for a further 15 min at room temperature with shaking and samples were read at OD 595 nm and OD 630 nm, as a reference, on an absorbance microplate reader (BioTek).

Cell cycle analysis

Cells were harvested by trypsinization and centrifugation at 1200 rpm for ten minutes at 4℃. Cell numbers were determined by counting with a hemocytometer and $1X10^6$ cells per sample were aliquoted in tubes, washed in 1 mL 1x PBS, and resuspended in 300 µl 1x PBS. Cells were then fixed with 700 µl of 100% ice cold ethanol added dropwise with gentle vortexing to a final concentration of 70% and incubated overnight at -20℃. For experiments where cells were co-stained for the mitotic marker H3pS10 and propidium iodide, fixed cells were resuspended in 1 ml of 0.25% Triton in 1x PBS (PBS-T) and incubated for 10 min on ice to permeabilize the membrane. Permeabilized cells were pelleted as above and incubated in 500 µl of 1x PBS containing 1% BSA to block non-specific binding. A polyclonal antibody for H3pS10 (Abcam, ab5176) was diluted 1:5000 in PBS-T and 150 µl was added to each sample and incubated for 1-1.5 h at room temperature. Cells were then washed one time in 1 ml of 1x PBS and resuspended in 150 µl of goat anti-rabbit AlexaFluor 488-conjugated antibody diluted 1:300 in PBS-T. Samples were incubated for 1 h in secondary antibody at room temperature before continuing with the protocol for PI (PI) staining. To stain DNA with PI, cells were washed once with 1x PBS and then resuspended in 0.25 ml 1x PBS with 0.5 mg/ml RNase A (Qiagen) and incubated for 1 hour at 37℃. Following RNase A treatment 10 µl of 1 mg/ml PI (Sigma) was added to each sample and incubated for 30 min in the dark at room temperature. Fixed and stained cells were washed, filtered, and analyzed by flow cytometry on a BD FacsCalibur.

Cell synchronization

Synchronization of cells was accomplished by treating cells with reversible cell cycle arresting agents, followed by two washes with warmed 1x PBS, and release into fresh media. Double thymidine blocks were used to arrest cells at early S phase, by treating cells with 2 mM thymidine (Sigma) for 18 h followed by release for 9 h and treatment with 2 mM thymidine for an additional 17 h before release into S phase. To arrest cells in M-phase, cells were first arrested at early S by a 24 h thymidine block as above followed by treatment with 100 ng/ml nocodazole (Sigma) for 12 h. To release from nocodazole cells were harvested by mitotic shake off, washed with 1x PBS and reseeded in fresh media. Synchronization of cells at G2/M was accomplished by first blocking cells in early S phase by 24 h treatment with 2 mM thymidine followed by 12 h treatment with 9 µM RO-3306 (Santa Cruz), a potent CDK1 inhibitor. Cells were then released into mitosis by two washes with 1x PBS and supplemented with fresh media.

Immunoprecipitation

Flp-In HeLa S3 cells stably expressing an FKBP25-3xFLAG transgene or a parental control were synchronized in various stages of the cell cycle as described, harvested by cell scraper, and pelleted by centrifugation at 1500 rpm in a swinging bucket rotor. Whole cell extracts were prepared by resuspending cell pellets directly in IP wash buffer with protease and phosphatase inhibitors (50 mM Tris pH8, 150 mM NaCl, 0.5% NP-40, 0.5% Triton X-100, 2 mM EDTA, 1 µg/ml aprotinin, 1 µg/ml leupeptin, 1 µg/ml pepstatin, 5 mM β-glycerophosphate, 10 mM NaF, 20 mM $Na_4P_2O_7$, and 2 mM Na_3VO_4) and sonicated on high for 5 min with 20 sec ON/OFF cycles on ice. Insoluble material was pelleted by centrifugation at 12 000 x g for 15 min and normalized by Bradford assay. Whole cell extracts were added to pre-washed EZ-view Red ANTIFLAG M2 Affinity gel beads (Sigma), and incubated at 4℃ for 1.5-3 h with nutating. After binding, beads were washed three times with IP wash buffer. Bound FLAG-tagged FKBP25 from synchronized cells was eluted by competition with 3xFLAG peptide (Sigma), by nutating beads in 150 ng/µl peptide in 1x TBS for 20 min at 4℃. Eluted material was run on SDS-PAGE gels with or without 50 µM Phos-tag and transferred by western blotting or further processed for mass spectrometry analysis of phosphorylated residues.

Immunoflorescence

For imaging of interphase and mitotic cells, U2OS cells were seeded on 8-well glass slides (Millipore) and either synchronized at the G2/M transition and released as described or grown asynchronously. Immunofluorescence staining was performed by first washing cells once with 1x PBS and fixing with a 3.7% PFA in PBS solution for 10 min at room temperature. Fixed cells were permeabilized for 10 min on ice using 0.5% Triton X-100 in 1x PBS and then blocked for 30 min in PBS-T (0.1% Tween 20 in PBS) containing 1% BSA at room temperature. Slides were then incubated with primary antibody diluted in PBS-T for 1 h at room temperature followed by three 5 min washes in PBS. After washing, the slides were then incubated with secondary antibodies, AlexaFluor 488 goat anti-mouse (Life Technologies) and goat anti-rabbit IgG-CFL 555 (Santa Cruz), in PBS-T for one hour and washed 3 times with 1x PBS. Coverslips were mounted using Fluoroshield with DAPI (Sigma) and sealed with clear nail polish. Slides were then imaged on an SP8 confocal microscope (Leica) or a DM IRE2 epi-fluorescence microscope (Leica) and images processed using the Fiji distribution of ImageJ (Schindelin et al., 2012).

Microtubule purification and spin-down binding experiments

Microtubules and microtubule-associated proteins were purified for binding experiments as previously described (Ozlü et al., 2010; Sloboda, 2015). Harvested asynchronous or thymidine-nocodazole arrested HeLa cells were weighed and homogenized in 1 mL of PME Buffer with detergent containing protease and phosphatase inhibitors (100 mM Pipes pH 6.9, 1 mM $MgCl_2$, 2 mM EGTA, 1 mM DTT, 0.5% NP-40, 1 µg/ml aprotinin, 1 µg/ml leupeptin, 1 µg/ml pepstatin, 5 mM β-glycerophosphate, 10 mM NaF, 20 mM Na4P2O7, and 2 mM 2 mM Na3VO4) per gram of cells. The homogenate was then centrifuged at 100 000 x g for 60 min at 4℃ in a TLA-100.3 rotor. Cleared supernatant was incubated at 37℃for 15-20 min with 20 µM paclitaxel (Sigma) and 0.1 mM GTP (Sigma). The sample was then underlain with PME containing 10% sucrose and 10 µM paclitaxel and centrifuged at 45 000xg for 30min at 25oC in a TLA-100.3 rotor (Beckman). Following pelleting of microtubules, the supernatant was removed, and the tube gently rinsed with room temperature PME buffer. The pellet was resuspended in PME buffer containing 10 µM paclitaxel and centrifuged over a second PME sucrose cushion as above before being resuspended in PME buffer and flash frozen. For microtubule spin-down binding experiments 5 µg of recombinant FKBP25 was added to 25 µg of purified microtubules and incubated at 37℃ for 30 min to allow binding to occur. The mixture was then underlay with a PME sucrose cushion as described and centrifuged at 45 000 x g for 30 min at 25℃ in a TLA-100.3 rotor. The supernatant (unbound fraction) was removed, and Laemelli sample buffer added. The pellet (bound fraction) was washed one time in warm PME buffer before being resuspended in Laemmeli sample buffer. Samples were resolved by SDS-PAGE and western blotting.

Mass spectrometry analysis of phosphorylated proteins

To identify phosphorylated sites on FKBP25 purified FLAG-tagged FKBP25 from mitotic HeLa S3 cells or *in vitro* phosphorylated recombinant FKBP25, samples were first digested overnight with either AspN or trypsin at 37℃ and lyophilized until dry. Peptides were resuspended in water and desalted/purified by passing through C18 ZipTips (Millipore). Samples were then analyzed on an Orbitrap LTQ mass spectrometer and phosphorylated peptides identified using the MASCOT server (Matrix Science).

In cell microtubule stability assays

In cell microtubule stability assays were performed as described previously (Wang et al., 2010a). For western blotting analysis of shRNA stable knockdown cells, cells were first harvested by trypsinization, washed twice in PME buffer and then incubated with PME buffer (100 mM Pipes pH 6.9, 1 mM $MgCl_2$, 2 mM EGTA) supplemented with 0.05% Triton X-100 (w/v) and protease inhibitors (1 µg/ml aprotinin, 1 µg/ml leupeptin, and 1 µg/ml pepstatin) at 37℃ for 30 min. Samples were then centrifuged at 15 000 x g for 30 min and the supernatant (S fraction) containing solubilized tubulin was removed and the pellet (P fraction) containing sedimented polymerized tubulin was washed once in PME buffer. Laemmli sample buffer was added to both samples to 1x at equal volumes and the samples were resolved by SDS-PAGE and western blotting. For knockdown/rescue immunofluorescence experiments, U2OS-T-Rex Flp-In cells harboring siRNA-resistant tagless FKBP25 transgenes (wild-type sequence or Y198F mutant) were cultured in the absence or presence of 0.1 µg/ml tetracycline (Sigma) for 24 h to induce expression of the rescue allele, transfected with 10 nM siRNA overnight as described, then seeded on 8-well glass slides (Millipore) in media with (transgene rescue) or without 0.1 µg/ml tetracycline (Sigma) and cultured for an additional 48 h. Cells were washed once with 1x PBS then incubated with PME buffer with protease inhibitors and 0.5% Triton X-100 for 5 min at room temperature and washed one time in 1x PBS before immunofluorescence staining and imaging as described.

Quantification of micronuclei and bi-nucleated Cells

To quantify the frequency of micronucleated cells, U2OS stably expressing FKBP25 targeting or control shRNA were seeded in 8-well glass slides (Millipore) and incubated overnight. The following day cells were washed 1 x with PBS and fixed with 3.7% PFA. Cells were mounted in FluroShield mounting media containing DAPI (Sigma) and slides sealed with nail polish. For each stable cell line at least 5 fields of view were imaged with a Leica DM IRE2 epi-florescent microscope. The number of micronuclei and intact nuclei was counted per image using ImageJ software. For the quantification of bi-nucleated cells, shRNA stable cells were seeded in 12 well plates at a low density to avoid clumping and reduce ambiguity between bi-nucleated and adjacent or overlapping cells. The following day cells were fixed in methanol for 5 min at room temperature and allowed to air dry. Next plates were stained with 1:20 diluted Giemsa stain (Sigma) for 1 h at room temperature and rinsed with deionized water. Plates were allowed to air dry prior to imaging on a Leica DM IRE2 micro-

scope and counting with ImageJ software. For both experiments, all image filenames were randomized prior to quantification.

In vitro kinase assays

For kinase assays using HEK293 cell extracts, extracts were prepared as previously described (Laurell et al., 2011; Mühlhäusser and Kutay, 2007). Thymidine/nocodazole-synchronized mitotic cells were harvested by mitotic shake off and resuspended and washed twice in EBS buffer containing protease inhibitors (40 mM β-glycerophosphate pH 7.3, 15 mM $MgCl_2$, 20 mM EGTA, 2 mM ATP, 1 mM glutathione, 1 µg/ml aprotinin, 1 µg/ml leupeptin, and 1 µ/ml pepstatin), and flash frozen in liquid nitrogen. After thawing, the suspension was passed through a 27 G needle 10 times, followed by ultracentrifugation (100 000 rpm for 10 min in a TLA100.3 rotor [Beckman]). The supernatant was again centrifuged at 100 000 rpm, removed, and supplemented with 250 mM sucrose. The protein concentration of extracts was measured by Bradford assay, adjusted to $\approx$ 15 mg/ml, and aliquots were flash frozen in liquid nitrogen and stored at -80℃. For *in vitro* phosphorylation with mitotic extract 3 µg of protein was incubated with 2 µl of extract in EBS buffer supplemented with 1 µCi γ[32P] ATP. Reactions were incubated for 30 min at 30℃and one-fourth of each reaction was resolved by SDS-PAGE. Gels were dried, exposed to a phosphor screen (Molecular Dynamics), and imaged on a Phosphorimager (STORM, GE Healthcare). For *in vitro* phosphorylation reactions with commercial recombinant kinases, 1 µg of recombinant protein was incubated with kinases following the manufacturer's recommendations and incubated for 30 min at 30℃.

Gel retardation assay

Plasmid-based *in vitro* DNA binding assay was performed as previously described (Prakash et al., 2016). Increasing amounts of FKBP25 were mixed at DNA: FKBP25 molar ratios of 1:0, 1:25, 1:50, 1:100. The mixture was incubated for 30 min at room temperature and loaded on a 1% agarose gel. Gels were visualized by ethidium bromide staining on an AlphaImager.

Annevin V Apoptosis Assay

To measure induction of apoptosis cells were treated with 50 mM etoposide (Sigma) for 24 h and processed using the Annexin V Apoptosis Kit from Santa Cruz (sc-4252 AK) following the manufacturer's protocol. Briefly, cells were trypsinized for 5 min at 37℃ and collected in 15 ml falcon tubes. To pellet, cells were spun at 1500 rpm

for 5 min and washed twice in ice-cold 1x PBS then resuspended in 1x Assay Buffer at a concentration of $1x10^6$ cells/ml. To each sample 1 µl of Annexin V FITC and 10 µl of PI was added per 100 µl of cells. Cells were then gently vortexed and incubated for 15 min at room temperature in the dark. 400 µl of Assay Buffer was added to each sample, which was then analyzed by flow cytometry on a BD FacsCalibur.

Clonogeneic survival assay

For clonogenic survival assays, performed as previously described (Franken et al., 2006), cells were plated at low density in 6-well plates (500-1500 cells /well) and incubated overnight. The following day cells were treated for 1 h with etoposide (Sigma), camptothecin (Sigma), or X-ray irradiated at the BC Cancer Agency, Royal Jubilee Hosptial. Plates were incubated for approximately 14 days until colonies of sufficient size were formed, changing media every 3-4 days. For fixation, media was removed and cells washed in 1x PBS and 2 ml of fixative solution (acetic acid: methanol 1:7) was added and left for 5 min at room temperature. Fixation solution was removed and 1 ml of 0.5% crystal violet was added per well and incubated for 2 h at room temperature. The crystal violet solution was removed by rinsing plates in tap water and the plates were allowed to air dry overnight. Plates were then imaged on a flatbed scanner and analyzed using the ColonyArea plugin for ImageJ (Guzman et al., 2014).

RT-qPCR measurement of FKBP25 expression following p53 induction

FKBP25 expression levels were measured in U2OS cells following treatment with 10 nM actinomycin D (Sigma) or a DMSO control for 18 h by RT-qPCR. RNA was isolated using the TRIzol reagent (Thermo Fisher) and cDNA prepared using the High-Capacity cDNA Reverse Transcription kit (ThermoFisher). cDNA was diluted 1:200 and used as a template in reactions using 2x Maxima SYBR green master mix (Thermo Fisher), and plates run on an MX3000P qPCR system (Agilent Technologies). Primer sequences are presented in Table A.6 of the appendix.

RNA-Seq, gene ontology, and network analysis

siRNA treated HEK293 samples were harvested at 80% confluency and stored at -80 ℃. Frozen cell pellets were processed and sequenced at the BC Cancer Agency Michael Smith Genome Sciences Centre following standard operating protocols. Briefly, oligo(dT) purification of mRNA was performed using the µMACs mRNA isolation kit (Miltenyl Biotec) and analyzed on an Agilent 2100 Bioanalyzer using Agilent 6000 RNA

Nano Kit (Agilent Technologies). cDNA was generated using the Superscript Double-Stranded cDNA Synthesis kit (Invitrogen), 75 bp paired-end libraries prepared using the Paired-End Sample Prep Kit (Illumina) and sequenced on a HiSeq 2000 sequencing system (Illumina). Paired-end reads ($\approx 12x10^6$/sample) were aligned to the UCSC hg19 human reference genome using the HISAT2 alignment program (Kim et al., 2015). Ranked lists of differentially expressed genes were generated using GFOLD (Feng et al., 2012). For gene ontology and KEGG analysis, ranked lists with a log fold change either $>$ or $<$ 0.5 were submitted to the DAVID (Database for Annotation, Visualization and Integrated Discovery version 6.8) web server(Huang et al., 2009). Gene ontology terms with a p-value < 0.05 were then summarized using the REVIGO (reduce and visualize gene ontologies) server using a similarity cut-off of 0.4 (Supek et al., 2011). Network analysis of RNA-Seq data was done using the R package clusterProfiler (Yu et al., 2012).

Chromatin immunoprecipitation (ChIP)

To crosslink chromatin 80% confluent cells in 15 cm dishes were incubated with 1% formaldehyde for 10 min at room temperature. Following crosslinking, 1.5ml of 2.5 M glycine was added to each dish and incubated for 5 min at room temperature to quench the reaction. Cells were washed twice in 1x ice-cold PBS and then scraped in 5 ml of 1x PBS and pelleted at 1500 rpm for 10 min in a swinging bucket centrifuge. Cells were then resuspended in 10 ml of nuclei isolation buffer (5 mM Pipes pH8.0, 85 mM KCl, 0.5% NP-40), incubated on ice for 10 min to swell and dounced for 10 strokes with a tight pestle. Nuclei were isolated by centrifugation at 1500 rpm for 10 min at 4℃. Isolated nuclei were then resuspended in 500 µl 1x MNase Buffer (50 mM Tris-HCl pH8.0, 5 mM $CaCl_2$) and 100 U of MNase (Worthington Biochemical Corporation) was added per 15 cm dish of crosslinked nuclei and incubated for 5 min in a 37℃ waterbath. To stop the reaction and lyse the nuclei 500 µl of 2x nuclei lysis buffer was added to each sample (100 mM Tris-HCl pH8.0, 20 mM EDTA pH8.0, 2% SDS), followed by flash freezing in liquid nitrogen and storage of pellets at -80℃. Prior to immunoprecipitation x-linked and digested nuclear lysates were thawed on ice and spun at 12 000 rpm for 20 min at 4℃ in a benchtop centrifuge. Cleared lysates were normalized by Bradford with ChIP Dilution Buffer (1% Triton X-100, 2mM EDTA, 150 mM NaCl, 20 mM Tris-HCl pH8.0) and a 50 µl input samples were taken from each sample. Lysates were then incubated with washed FLAG beads (Sigma) for 3 h to overnight at 4℃. The following morning, beads were washed three times for 5 min at 4℃ in Wash Buffer (0.1% SDS, 1% Triton X-100, 2 mM EDTA, 150 mM

NaCl, 20 mM Tris-HCl pH8.0). Followed by one additional wash in Final Wash Buffer (0.1% SDS, 1% TritonX-100, 2 mM EDTA, 150 mM NaCl, 20 mM TrisHCl pH8.0). Enriched material was eluted with 100 µl of elution buffer (50 mM Tris-HCl, 20 mM EDTA -pH8.0, 2% SDS) for 15 min at 30℃. Crosslinks were reversed by incubation at 65℃ overnight and DNA isolated by spin column purification (BioBasic). Purified DNA was run on a 1% agarose gel and visualized by EtBr staining.

Chapter 4

FKBP25 Participates in the Repair of DNA double-strand Breaks

This chapter was adapted from a publication in preparation for submission:

Dilworth D, Gong F, Miller K, and Nelson, CJ. The Prolyl Isomerase FKBP25 Regulates DNA Double-Strand Break Repair by Homologous Recombination *In preparation.*

Contributions: Experiments and data analysis performed by **DD** under the supervision of CJN except for laser micro-irradiation experiments (Figure 44CD), which were done by FD and KM. **DD** and CJN wrote the paper.

4.1 Introduction

The genome is under constant assault from environmental factors, such as UV radiation and as the strains of DNA replication. As such, cells have evolved several repair pathways to ensure genomic lesions do not go unfixed. Failure to repair results in genome instability, a contributing factor in tumorigenesis (Hanahan and Weinberg, 2011). Of the types of lesions that occur, double-strand breaks (DSB), which completely sever the DNA fiber, are the most severe. The DNA Damage Response (DDR) to DSBs involves a complex network of proteins that promote repair and cell cycle arrest or apoptosis. DDR networks are thoroughly integrated with the nucleolar stress response and chromatin regulatory pathways to mount a coordinated and effective reaction to genomic lesions. In Chapter 2, I have shown that FKBP25 interacts with several multifunctional factors known to regulate both ribosome biogenesis and DSB repair.

The DDR has long been exploited in the chemotherapeutic treatment of cancer and researchers are now looking to the DDR in the development of precision therapeutics, particularly in tumors with impaired repair pathways. Therefore, identifying novel proteins and mechanisms involved in DNA repair is essential not only to our understanding of a fundamental pathway but may elicit novel candidates for targeted cancer interventions. Here, I identify the prolyl isomerase FKBP25 as a novel participant in the repair of DNA double-stranded breaks. I show that FKBP25 influences DSB repair outcome downstream of DNA end resection, promoting homologous recombination (HR) and suppressing the mutagenic single-strand annealing (SSA) pathway. This role is in part mediated by FKBP25's prolyl isomerase activity and is the first description of a role for this activity. I also provide evidence that inhibition of FKBP25 in combination with targeting of Parp may be beneficial in disrupting the DDR as a therapeutic strategy in HR-proficient tumors.

4.2 Results

4.2.1 FKBP25 localizes and interacts with DSB repair factors

Our proteomic studies of FKBP25's interacting proteins identified a number of regulators of the DNA damage repair process, including: histone H1, Ku86, Ku70, MDC1, DNA-dependent protein kinase (DNA-PKcs), Kap1, Parp-1, topoisomerase enzymes, nucleophosmin, and nucleolin (Figure 1A-B, the roles of these proteins in the DDR have been summarized in Table 4.1). In support of our protein-protein interaction data, many of these DDR factors are known to localize to the nucleolus similarly to FKBP25 (O'Connor, 2015), often requiring RNA to mediate their localization. Two examples are the Ku proteins (Zhang et al., 2004) and Parp-1 (Guetg et al., 2012). To validate the RNA-dependent nucleolar localization of these factors and FKBP25, I performed *in situ* CSK extractions of U2OS cells in the presence and absence of RNase A and looked at the localization of Ku86, nucleolin, and FKBP25. UBF, a DNA associated nucleolar factor, is used here as a control, as RNA depletion should not alter its localization. In agreement with previous studies, Ku86 and nucleolin localize to the nucleolus in an RNA-dependent manner similar to FKBP25. I further validate these associations, showing an RNA-dependent chromatin association of nucleolin, Ku86, Ku70, and Parp-1 by *in situ* extraction followed by western blot analysis (Figure 1C-D). This observation supports the idea of crosstalk between RNA metabolism and DNA damage repair processes. Given that FKBP25 interacts and localizes with many DSB repair factors, I hypothesized that it may also have a role in the repair of DSBs.

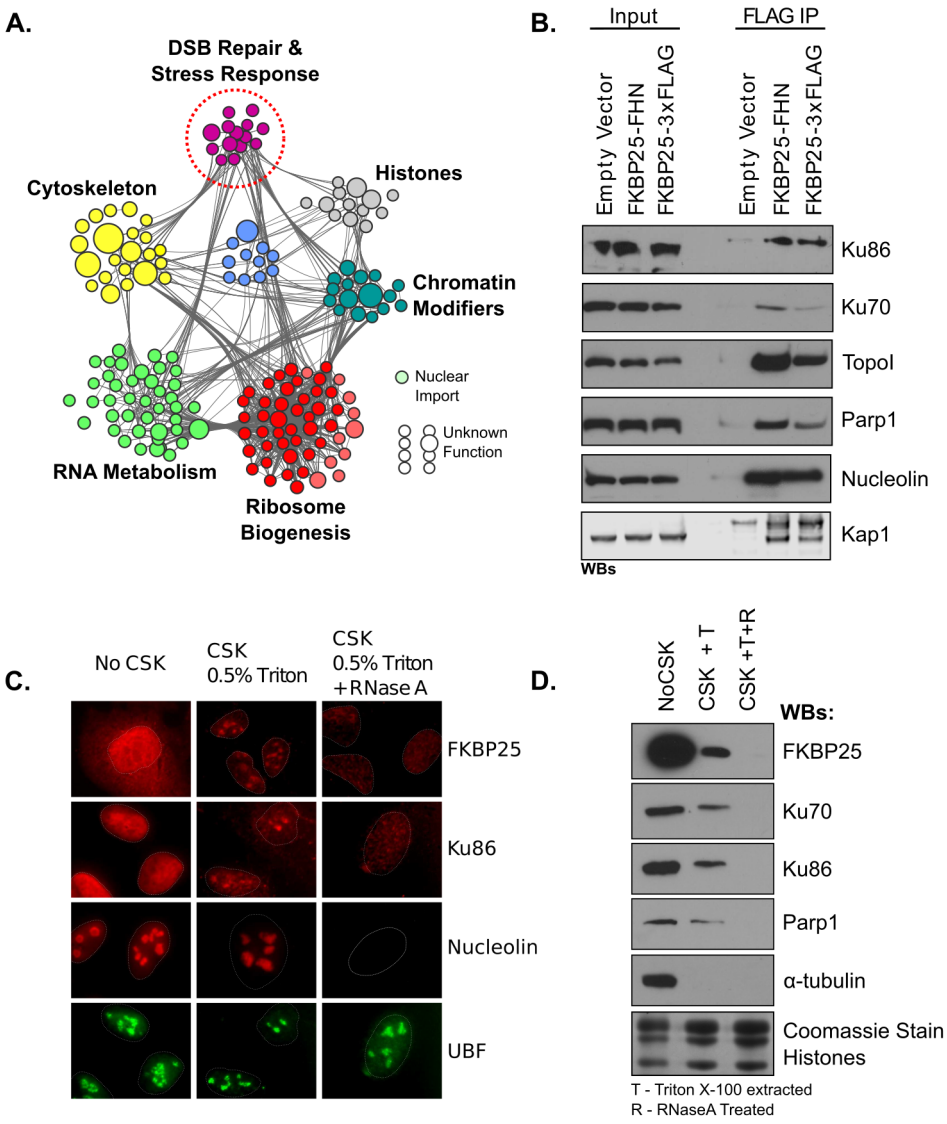

Figure 39. FKBP25 localizes and interacts with DNA DSB repair factors. (A) Network analysis of FKBP25 interactome highlighting factors involved in DSB repair and the cellular stress response. (B) FKBP25-FLAG Co-IP validation of FKBP25 interacting proteins known to participate in the DSB response (panel includes data also presented in Figure 12). (C) Immunofluorescence analysis of *in situ* CSK Triton pre-extraction of FKBP25, Ku86, nucleolin, UBF. Panels shown are without detergent pre-extraction (No CSK), with detergent pre-extraction(CSK 0.5% Triton), or with pre-extraction and RNase A treatment (CSK 0.5% Triton + RNaseA). (D) Western blot analysis of *in situ* CSK triton extraction as in C.

Table 4.1. The roles of FKBP25 interacting proteins in DSB repair

Protein & Function	**Ref.**
Nucleolin • nucleolin is directly recruited to DNA double-strand breaks • during the DNA damage response nucleolin's histone chaperone activity is utilized to establish a chromatin environment ammenable for repair	Goldstein et al. (2013); Kobayashi et al. (2012)
NPM1 • recruited to DSBs by RNF8-dependent ubquitylation • thought to act simiarly to nucleolin in the remodeling of chromatin around DSBs	Koike et al. (2010)
VCP • VCP forms a homo-hexameric complex with ATPase activity • promotes displacement of L3MBTL1 to recruit 53BP1	Acs et al. (2011)
H2AFZ • H2Az is a histone variant • it is exchanged at sites of DSBs to promote an open chromatin conformation amenable to ubquitin and acetyl DSB signaling	Xu et al. (2012)
SAFB • a chromatin associated scaffolding factor • faciltates spread of γH2Ax chromatin domains	Altmeyer et al. (2013)
ZMYND8 • recruits NuRD histone deactylase complex to damage chromatin • important for establishing the appropriate chromatin enivironment for repair	Gong et al. (2015); Spruijt et al. (2016)
TSPYL1 • interacts with ZMYND8	Spruijt et al. (2016)

The roles of FKBP25 interacting proteins in DSB repair

Protein & Function	**Ref.**
SMARCC2 • member of the SWI/SNF chromatin remodeling complex • SWI/SNF chromatin remodeling activity is important for establishing the proper chromatin environment for DSB repair	Park et al. (2006)
MDC1 • MDC1 binds γH2Ax in a phosphorylation dependent manner • MDC1 in turn recruits RNF8 to intiate non-proteosomal ubquitylation signaling	Stewart et al. (2003); Kolas et al. (2007)
Ku70-K86 • Ku proteins form a heterodimer complex that binds the ends of DNA double-stranded breaks sensing damage and activating repair by ligation during G1 of the cell cycle • absolutely required for c-NHEJ	Downs and Jackson (2004)
Parp-1 • Parp-1 is a sensor for DNA double-strand breaks • many downstream signaling pathways require Parp activity for initiation • Poly ADP ribosylation recruits downstream effectors including DNA-end resection factors	Beck et al. (2014)
Kap1 • phosphorylated by ATM during the DSB repair response to disrupt its interaction with chromatin • also shown to be recruited to DSB to establish transient heterochromatin marks that are required for efficent repair	White et al. (2012); Ayrapetov et al. (2014)
E2F7 • induced in response to DNA damage in a p53-dependent manner • effector of cell cycle signaling in response to DNA damage	Panagiotis Zalmas et al. (2008)

4.2.2 FKBP25 influences DSB repair pathway usage

I first set out to determine if FKBP25 can interact with damaged chromatin. Using HEK293-T-Rex cell lines stably expressing an FLAG-HA-NLS tagged FKBP25 transgene or empty vector control, I performed co-immunoprecipitation experiments probing for an interaction with γH2Ax in conditions of induced DNA damage. To induce damage I used etoposide, a potent topoisomerase II inhibitor that stabilizes the covalent topoisomerase-DNA cleavage complex by inhibiting the second transesterification reaction – resolution of the etoposide poisoned cleavage complex results in the formation of a DNA DSB (Montecucco et al., 2015). Using this approach, I observed that FKBP25 does indeed interact with chromatin originating from sites surrounding DSBs, supporting the hypothesis that FKBP25 may indeed play a role in DSB repair. I next set out to determine at what point in the DSB response FKBP25 may act.

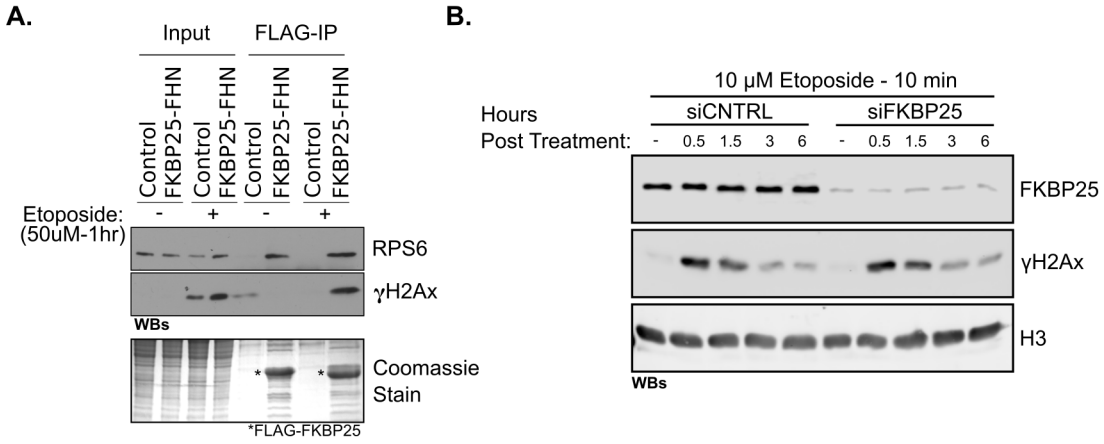

Figure 40. FKBP25 interacts with γH2Ax, however, does not influence the induction of the DSB response. (A) FLAG affinity capture from HEK293 cells expressing FKBP25-FLAG-HA-NLS or an empty vector control treated with 50 μM etoposide or a DMSO control for 1 h (B) Western blot analysis of FKBP25 knockdown cells treated with 10 μM etoposide for 10 min followed by recovery for 30 min, 1.5, 3, and 6 h.

I reasoned that given FKBP25's interaction with the DNA damage sensor Parp-1, it may also be involved in the detection of DSB breaks. As phosphorylation of the histone variant H2Ax is one of the earliest events in DDR – I followed phosphorylation kinetics of γH2Ax in response to a brief etoposide dose in FKBP25 depleted cells. I found little difference in the relative levels of γH2Ax, indicating that FKBP25 is

unlikely to influence the induction of the DNA damage response by the early responders ATM/ATR/DNA-PKcs. This experiment ruled out FKBP25 acting as a DNA damage sensor. Therefore, I next looked to function in downstream repair pathways.

Once initiated, repair of DSB can proceed through one of several pathways with distinct genetic outcomes (Chapman et al., 2012). To assay FKBP25's participation in the repair process, I used a standard in cell GFP-based reporter assay that provides a readout for repair by either c-NHEJ, HR, SSA or Alt-EJ. Each reporter cell line contains a unique integrated non-functional GFP cassette with recognition sequences for the rare-cutting nuclease I-SceI – expression of I-SceI results in site-specific breaks within the reporter, which will only lead to restoration and expression of the GFP cassette if repair proceeds through a specific pathway (Gunn and Stark, 2012). Expression of GFP is then measured by flow cytometry. To normalize for transfection efficiency under knockdown conditions a dsRed reporter was also co-transfected. Using this assay, I found that depletion of FKBP25 significantly impairs homologous recombination and promotes the error prone single-strand annealing pathway (Figure 41). FKBP25 depletion did not significantly alter end-joining repair by either c-NHEJ or Alt-EJ. The decision between HR and SSA repair events occurs downstream of DNA-end resection by CtIP. For HR to proceed Rad51 must displace RPA to form the presynaptic complex, a process critical for strand invasion (Krejci et al., 2012). Rad52, a mediator of SSA, can suppress RPA turnover and Rad51 loading onto ssDNA, in turn promoting repair by SSA (Gibb et al., 2014; Rothenberg et al., 2008). Therefore, the observation that FKBP25-depleted cells have reduced HR, and increased SSA, suggests that FKBP25 influences repair decisions downstream of DNA-end resection by CtIP and upstream of RPA turnover by Rad51.

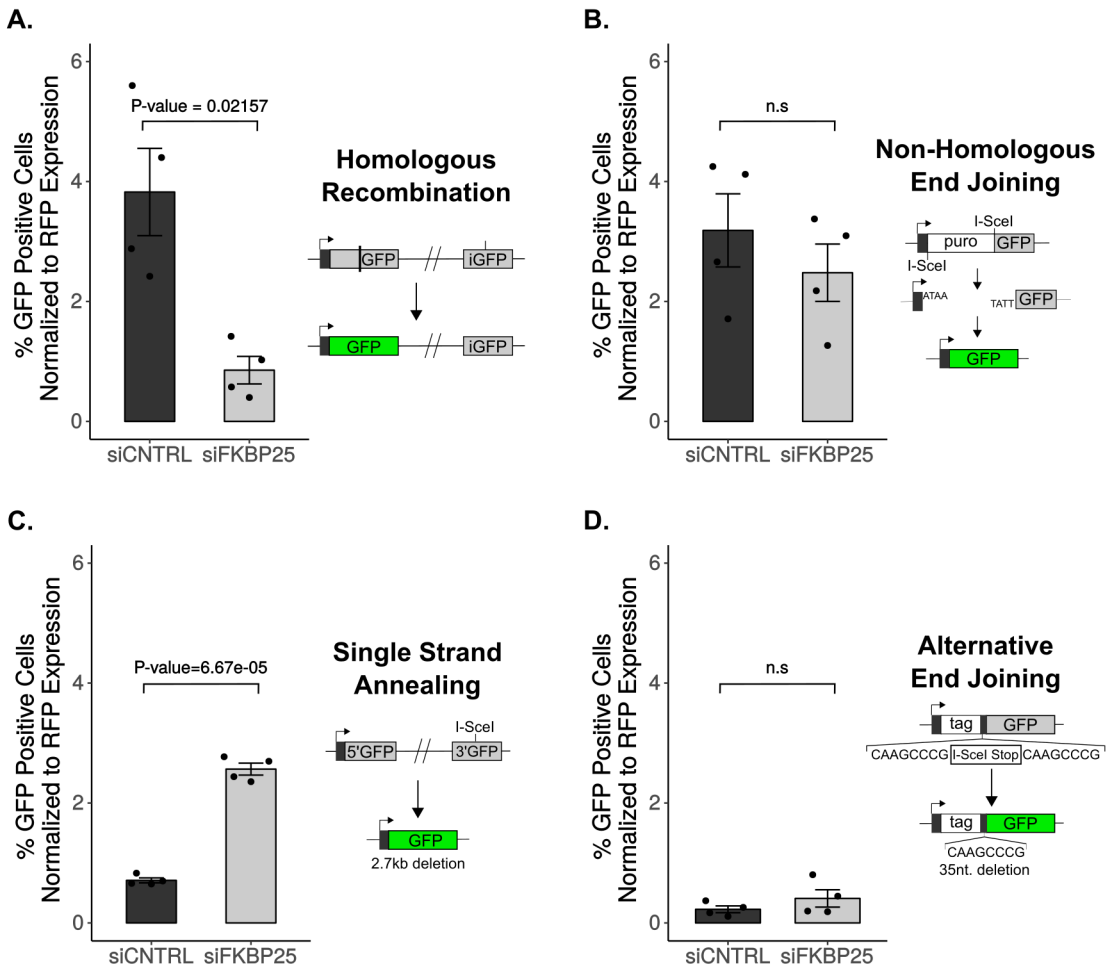

Figure 41. FKBP25 promotes homologous recombination, suppressing single-strand annealing DSB repair pathways. (A-D) Flow cytometry reporter assay measuring DSB repair pathway utilization in FKBP25 knockdown U2OS cells containing stably integrated reporters for (A) Homologous Recombination, (B) Non-Homologous End Joining, (C) single-strand annealing, and (D) Alternative End Joining. Error bars represent the standard error of four independent replicates.

To validate these results I first looked at Rad51 foci formation in response to etoposide-induced DNA damage by epi-immunofluorescence as a readout for HR. I found relative to control cells that express non-targeting shRNA, FKBP25-depleted cells display reduced Rad51 foci formation in response to the DNA-damaging agent etoposide. It is important to note that the shRNA targeting sequence differs from the siRNA used in the reporter cell line experiments, indicating that the HR deficit is unlikely to be the result of off-target effects. These results were independently validated through a collaboration with Dr. Kyle Miller's lab at the University of Texas at Austin, showing that Rad51 foci formation is also impaired in response to IR as well as etoposide-induced breaks (data presented in Appendix Figure A2). I further hypothesized that if cells have switched from HR-mediated repair to SSA when FKBP25 is depleted, they would become reliant on SSA for survival. To test this, I depleted Rad52, using a pooled siRNA approach, in combination with FKBP25 knockdown and evaluated viability by cell counts and the MTT proliferation assay. In support of our finding that FKBP25 suppresses SSA, I identify a synthetic sick relationship between FKBP25 and Rad52. Collectively, these results point to a role for FKBP25 promoting repair by homologous recombination downstream of DNA-end resection.

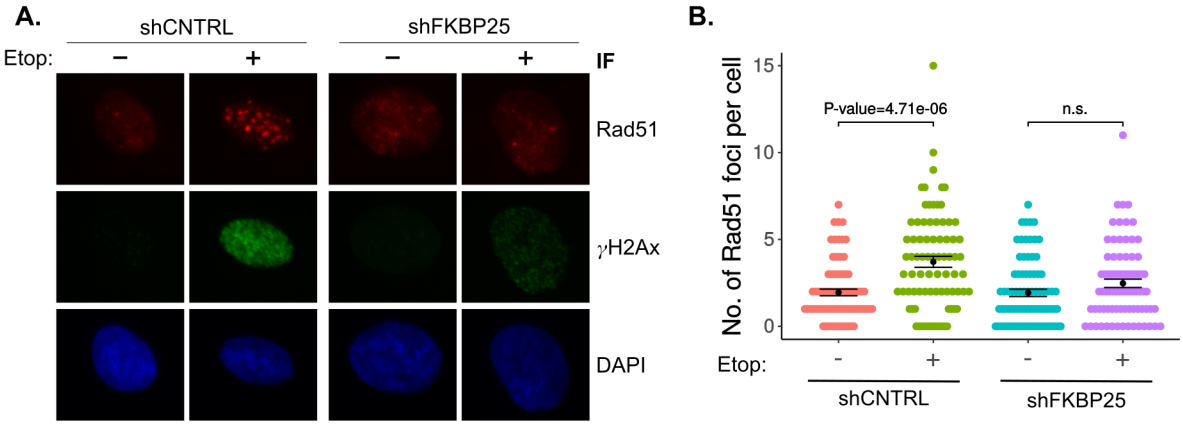

Figure 42. FKBP25 promotes Rad51 foci formation in etoposide treated U2OS cells. (A) Immunofluorescence based Rad51 foci formation assay in U2OS stable shRNA expressing cells treated with 10 µM etoposide or DMSO control. (B) Quantification of Rad51 foci per cell shown in A. Error bars represent the standard error of at least 80 measurements.

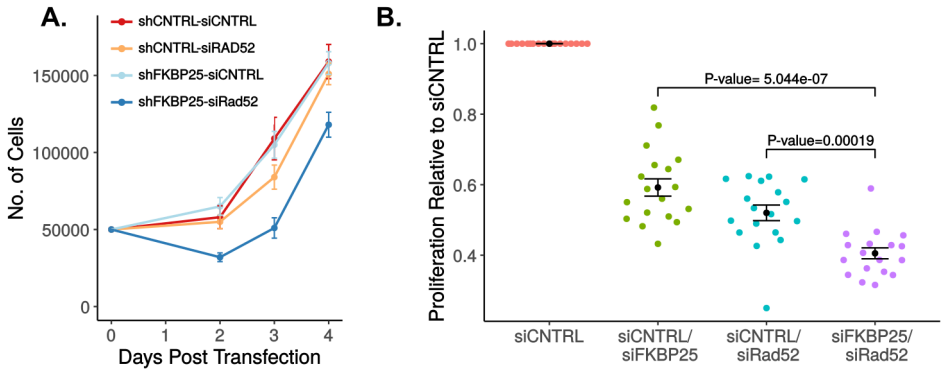

Figure 43. FKBP25 is synthetically sick with the SSA repair factor Rad52. (A) Cell counting assay quantifying proliferation in U2OS cells stably expressing shRNA targeting GFP or FKBP25 and transfected with pooled siRNA targeting Rad52 or a non-targeting control. Error bars represent the standard error of four replicates in two independent experiments. (B) MTT proliferation assay of U2OS cells transfected with different combinations of siRNA, targeting FKBP25, Rad52, or a non-targeting control. Assay performed 72 hours post-transfection. Data points shown are multiple measurements taken from two independent experiments. Error bars represent the standard error of four measurements across four independent transfections.

4.2.3 Mobilization of FKBP25 from laser micro-irradiation induced DSBs

By co-immunoprecipitation FKBP25 interacts with phosphorylated H2Ax (γH2Ax). As γH2Ax, and chromatin in general, is actively reorganized around sites of damage to facilitate repair, this does not necessarily mean FKBP25 localizes to sites of DNA damage. This interaction may take place off the chromatin template. To test if FKBP25 gets actively recruited to DNA double-strand breaks, I evaluated co-localization at an integrated lacO array, of an mCherry-LacI-FokI fusion and FKBP25-GFP. This approach generates site-specific breaks and allows visualization of the affected locus (Figure 44A)(Shanbhag and Greenberg, 2013). Unfortunately, a robust colocalization was not observed, thus from this experiments it was unclear whether FKBP25 is recrutied to DSBs (Figure 44B). While this approach provides a robust readout and requires only commonly available laboratory equipment to perform, transient events in DSB repair and more subtle redistributions of repair proteins may go undetected. Thus, we decided to try fluorescent imaging of micro-irradiated cells expressing FKBP25-GFP, which is a more sensitive technique that captures kinetic information of protein localization to sites of DNA damage. For these experiments,

we used an NLS-containing FKBP25-GFP construct, as the GFP construct used in Figure 44B primarily localized to the cytoplasm. Surprisingly, FKBP25 appeared to be evicted from damaged chromatin within minutes (Figure 44 C-D). A similar phenomenon has been observed for histone H1 as well as the heterochromatin-associated protein KAP-1, two FKBP25 interacting partners, which are both transiently displaced from IR-damaged chromatin in a Parp-1/ATM dependent manner (Guo et al., 1999; White et al., 2012; Strickfaden et al., 2016). It has recently become apparent that tight control over the chromatin environment surrounding DSBs is required for repair – during the DDR there is an initial expansion of chromatin followed by a phase of chromatin condensation (Khurana et al., 2014; Burgess et al., 2014; Li et al., 2014b). These results suggest that FKBP25 displacement at sites of DSB may play a role in the reorganization of the chromatin environment to promote repair by homologous recombination.

4.2.4 FKBP25's catalytic activity is required to promote HR

I have shown that FKBP25 can promote DSB repair by homologous recombination. Next, I set out to determine if this function is dependent on FKBP25's prolyl isomerization activity. Using the HR DSB reporter assay shown in in Figure 41, I over-expressed FKBP25-FLAG-HA-NLS constructs containing the wild-type sequence or a Y198F point mutation in the catalytic site, which ablates prolyl isomerase activity (Gudavicius et al., 2013). Over-expression of the wild-type sequence significantly increased repair by homologous recombination, while the catalytic null point mutant showed no difference from cells transfected with an empty vector control plasmid. While this indicates FKBP25's catalytic activity is required to promote repair by HR, the lack of a dominant negative phenotype for the Y198F mutant suggests catalytic activity is not absolutely required for HR to proceed. This is the first description of a catalytic function for FKBP25.

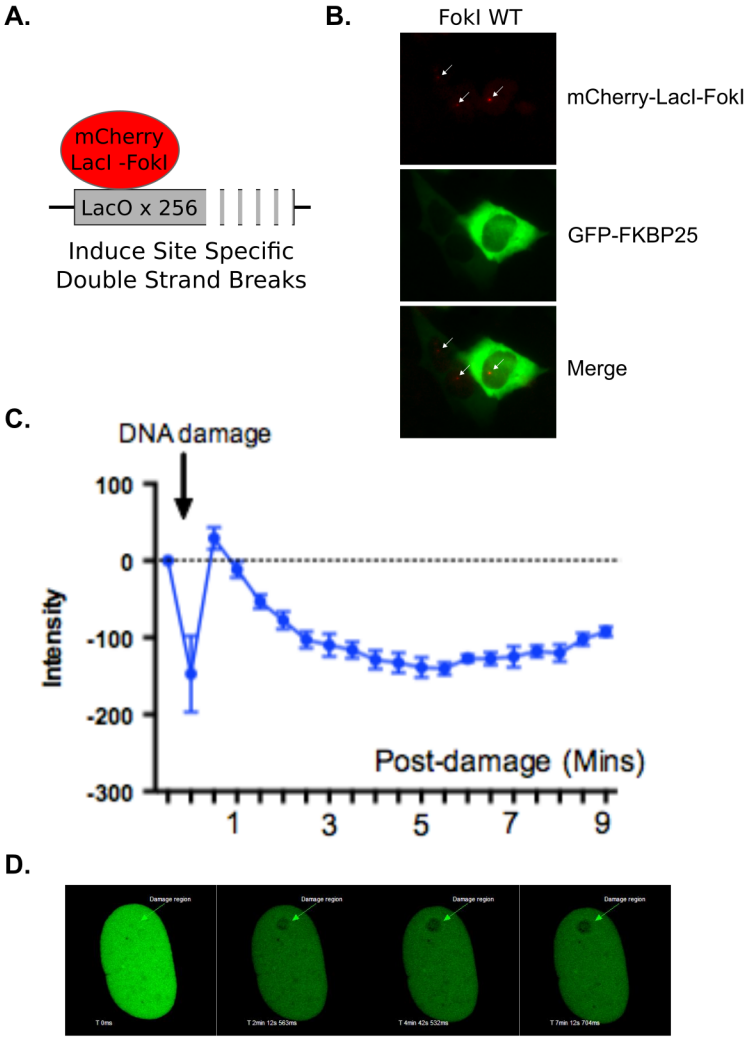

Figure 44. FKBP25 is displaced from laser micro-irradiation induced DNA double-strand breaks. (A) Schematic representation of mCherry LacI-FokI DSB localization assay. U2OS LacO reporter cells contain a stably integrated 256 tandem repeat of the lac operon. The transfected mCherry-LacI-FokI fusion localizes to the lac operon introducing site-specific DNA double-stranded breaks that can be visualized by mCherry fluorescence. By co-transfection of a GFP fusion protein of interest, active recruitment to DSBs can be evaluated. (B) Immunofluorescence of mCherry-LacI-FokI localization and an FKBP25-GFP indicating FKBP25 is not actively recruited to DSB sites. (C) Fluorescence intensity of FKBP25-FHN-GFP at sites of IR-induced breaks over time (D) Immunofluorescence of FKBP25-FHN-GFP in cells treated with localized ionizing radiation. Laser micro-irradiated area is indicated by an arrow.

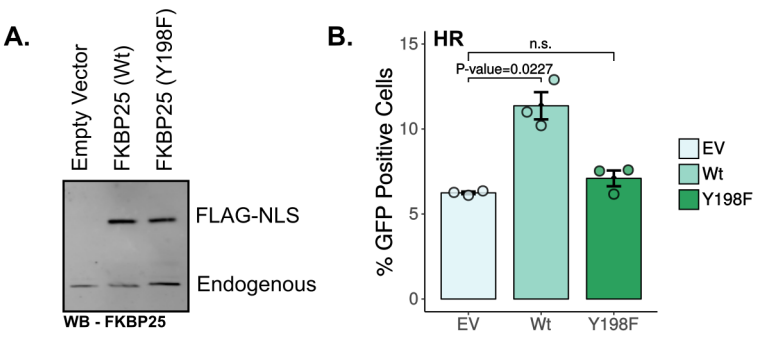

Figure 45. FKBP25's catalytic activity is required to promote HR. (A) Western blot analysis of the U2OS DR-GFP homologous recombination reporter cells transfected with I-SceI and either an empty vector control, FKBP25(Wt), or FKBP25(Y198F) expression vectors. (B) Quantification of GFP U2OS DR-GFP reporter cells transfected as in A by flow cytometry. Error bars represent standard error of three independent transfections.

4.2.5 Chemical inhibition of FKBPs disrupts HR

Therapeutic strategies targeting the DDR are now being used successfully in the treatment of cancer (O'Connor, 2015). For example, the Parp inhibitor olaparib has been shown to be successful as a maintenance treatment in recurrent hereditary BRCA-associated cancers, extending progression-free survival of patients (Kaufman et al., 2015). BRCA mutations disrupt repair by homologous recombination and are the most common cause of hereditary forms of breast and ovarian cancer (Petrucelli et al., 2010). While playing a role in the development of the disease, these mutations are also an Achilles' heel, sensitizing cells to therapies that target DSB repair. More generally, loss of DDR pathways, increased replication stress, and increased endogenous damage may leave other cancers susceptible to treatments that target the DDR as well. Thus, there is significant interest in extending the utility of Parp inhibitors, and other DDR targeted therapies, in BRCA proficient cells. The mTOR/FKBP inhibitor rapamycin has emerged as a potential candidate in this respect, as it has been shown to inhibit DNA double-strand break repair (Chen et al., 2011) and sensitize cells to Parp inhibition (Peng et al., 2014). While this activity has in part been attributed to downstream mTOR signaling events through the regulation of SUV39H1 expression, a histone methyltransferase involved in homologous repair (Mo et al., 2016; Chen et al., 2011). What isn't clear is whether the inhibition of FKBPs may also play a role.

Given that FKBP25 regulates HR, I decided to test if pharmacological inhibition

of FKBP25 could be used to sensitize cells to Parp inhibition. In contrast to most FKBPs, FKBP25 has a strong binding preference for rapamycin (K_i=0.9 nM) relative to FK506 (K_i = 200 nM)(Dejmek et al., 2009). Unfortunately, assessing FKBP mediated effects of rapamycin is convoluted by the fact that upon rapamycin treatment several FKBPs, including FKBP25, form a drug induced heteromeric complex with mTOR that allosterically inhibits its kinase activity (Galat, 2013; Chen et al., 1995). A recent report showed that it is possible to overcome mTor inhibition of rapamycin by treating cells with excess FK506, which does not inhibit mTOR – maintaining inhibition of FKBP25's catalytic activity (Figure 46A)(März et al., 2013). I decided to use this strategy to dissect the involvement of FKBPs in rapamycin inhibition of HR and sensitization of cells to Parp inhibition. I first show that indeed excess FK506 rescues a rapamycin proliferative phenotype, but not that of the mTOR catalytic inhibitor Torin1 (Figure 46B). This observation supports the idea that mTOR-independent rapamycin phenotypes can be explored in this way. Next, I looked at sensitivity to Parp inhibition in the presence of rapamycin or rapamycin and FK506 (Figure 46C). In contrast to previous studies, I observed modest effects of rapamycin treatment on the sensitivity to Parp inhibition. Because the assay used measures proliferation, without differentiating between cell death and senescence, I may not be observing the previously described synergism between treatments as proliferation is already greatly reduced in rapamycin-treated cells. When cells were treated with rapamycin and FK506, I observed that with increasing doses of the Parp inhibitor olaparib there is a synergistic effect on proliferation (Figure 46C). Indicating that inhibition of FKBP prolyl isomerase activity may provide a therapeutic route for potentiating Parp inhibitor activity in BRCA proficient cancer cells. I repeated this assay including the direct mTOR inhibitor Torin1 and Fk506 treatment alone and show that the rapamycin/FK506 combination shows the greatest decrease in proliferation with increasing concentrations of olaparib (Figure 46D). As Torin1 alone also sensitizes cells, the mechanism is at least in part mTOR-dependent, as has been previously suggested. To evaluate whether this phenotype is the result of impaired HR, I performed the HR and SSA GFP reporter assays in the presence of mTOR and FKBP inhibitors. In agreement with the previous literature, mTOR inhibition impairs HR (Figure 46E-F)(Mo et al., 2016; Chen et al., 2011). However, I also show a reduction in HR with the rapamycin/FK506 combination, which suggests that FKBP inhibition, most likely through FKBP25, may contribute at least in part to the synergistic mechanism described for Parp sensitization by rapamycin.

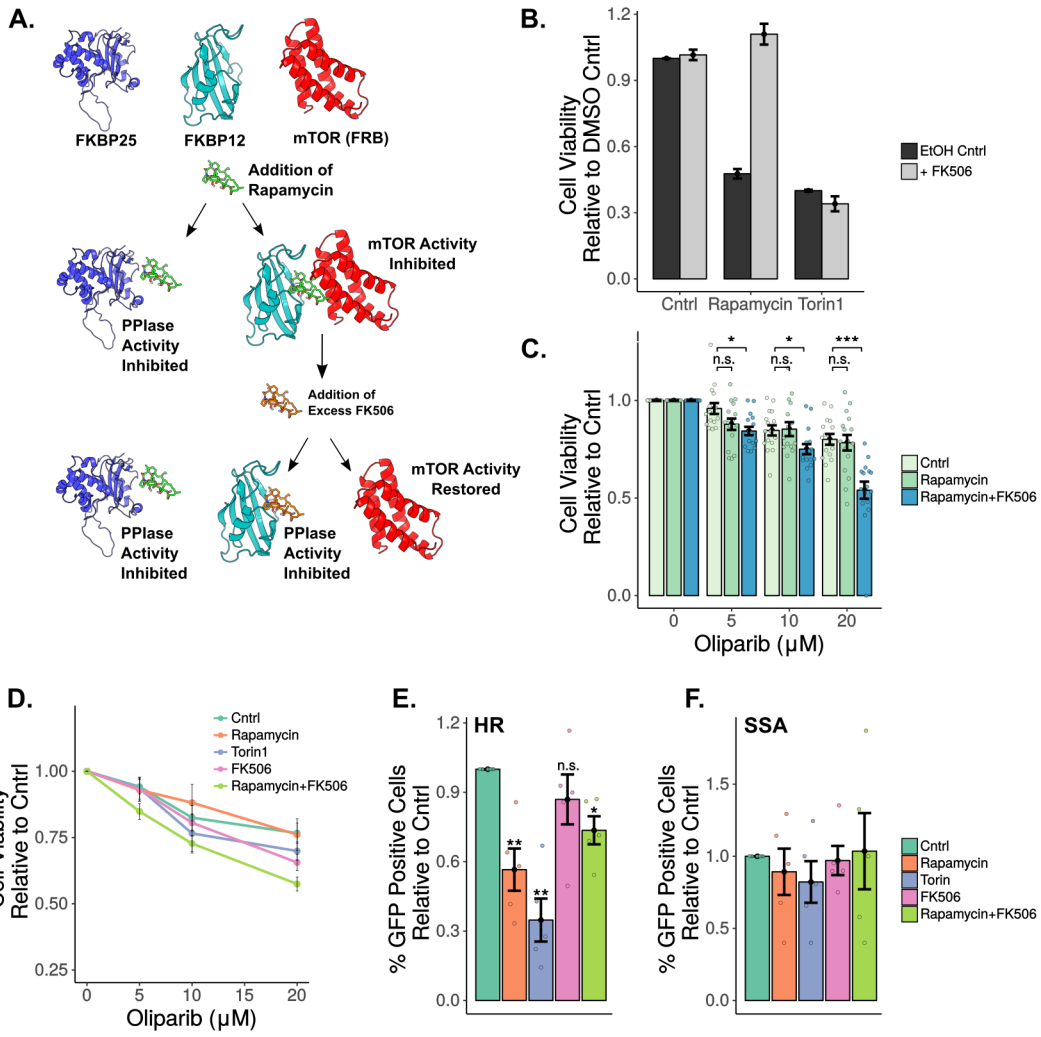

Figure 46. Inhibition of FKBPs impairs homologous recombination independently of mTOR. (A) A schematic presenting the strategy for chemical inhibition of FKBP25 by rapamycin without inhibiting mTOR. mTOR activity is restored by competition with FK506, which has a similar affinity for FKBP12 as rapamycin. (B) MTT proliferation assay as a proxy for the restoration of mTOR activity measuring proliferation. Cells were treated with either a DMSO control, 10 nM rapamycin, or 10 nM Torin1 in the absence or presence of 2 μM FK506. Error bars represent the standard error of four measurements across four independent experiments. (C) MTT proliferation assay of cells treated with increasing doses of the Parp inhibitor Olaparib in combination with 10 nM rapamycin or 10 nM rapamycin and 2 μM FK506. Error bars represent the standard error of four measurements across four independent experiments (D) MTT proliferation assay, cells treated as in E. Error bars represent standard error of four measurements from two independent experiments. (E-F) Flow cytometry reporter assay measuring HR(E) and SSA(F) DSB repair pathway utilization in cells treated with DMSO control, 10 nM rapamycin, 10 nM Torin 1, 2 μM FK506, or 10 nM rapamycin and 2 M FK506. Error bars represent standard error of four independent experiments. Significance relative to DMSO control treated cells is shown above each bar (* P-value <0.05, ** P-value <0.01).

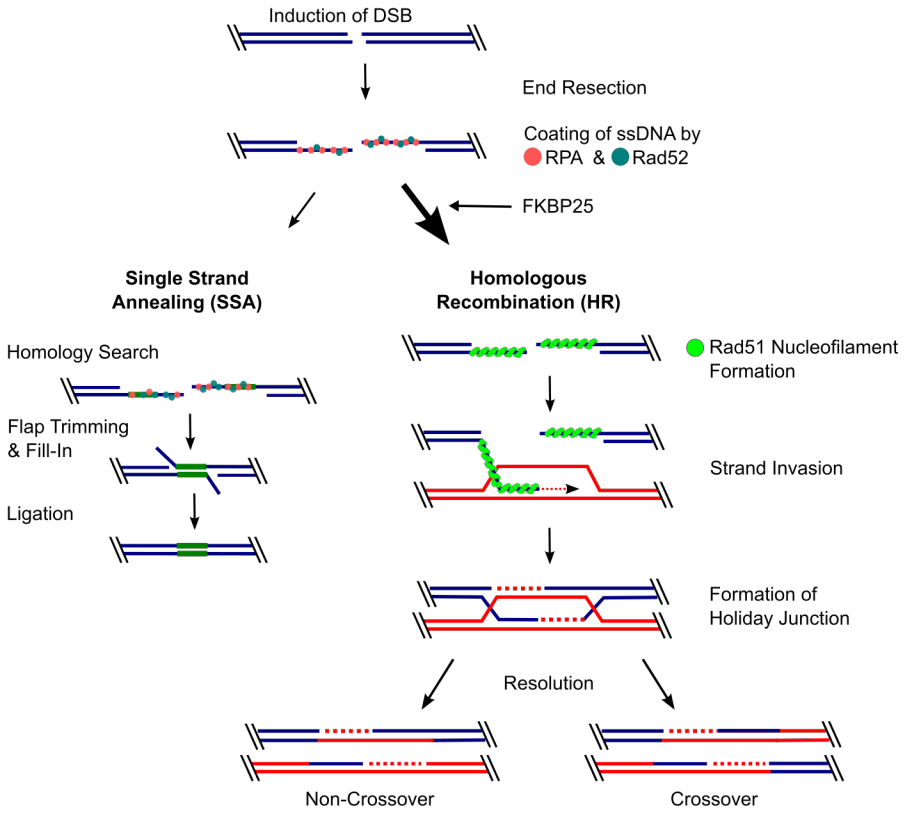

Figure 47. Schematic representation of FKBP25's involvement in DNA double-strand break repair. FKBP25 acts downstream of Ct-IP mediated end resection to promote homologous repair at the expense of single-strand annealing.

4.3 Discussion

I identify here a novel role for the prolyl isomerase FKBP25 in the regulation of DSB repair. Our data shows that FKBP25 physically interacts with a number of DSB repair factors and promotes homologous recombination dependent on catalytic activity. In the absence of FKBP25, there is a significant increase in repair by the error-prone single-strand annealing pathway. SSA can result in large deletions of the intervening sequence between stretches of homologous DNA, leading to genetic instability. Therefore, these results further implicate FKBP25 in maintaining the integrity of the genome in cycling cells.

Strikingly, I show FKBP25 to be displaced early from sites of induced double-

stranded breaks, similar to interacting partners Kap1 and histone H1. KAP-1, a KRAB zinc finger interactor, establishes heterochromatin environments by recruiting repressive histone methyltransferase enzymes and heterochromatin protein 1(HP1) (Iyengar and Farnham, 2011). KAP-1 is directly phosphorylated by ATM in response to DSBs, p-KAP-1 then diffuses to the nucleus resulting in relaxation of heterochromatin domains to facilitate access and repair (Geuting et al., 2013; White et al., 2012). Surprisingly, KAP-1 and HP1 depletion both disrupt recruitment of Rad51 within euchromatin and heterochromatin (Baldeyron et al., 2011) and KAP-1 knockdown up-regulated alternative error-prone repair pathways (Geuting et al., 2013). Indicating, that KAP-1 also plays an active role in DSB repair. Indeed, a complex containing KAP-1/HP1/SUV39H1 is recruited to DSBs, resulting in H3K9me3 dependent activation of ATM (Ayrapetov et al., 2014). Thus, the eviction of heterochromatin proteins occurs only transiently, suggesting dynamic cycles of relaxation and compaction of the chromatin template is vital for repair by HR. The same also seems to be true for the linker histone H1, which had the highest enrichment in our BioID proteomics screen. There is also a significant overlap in the protein-protein interactions of FKBP25 and histone H1 (Szerlong et al., 2015). Like KAP-1, histone H1 is initially evicted from chromatin in response to DSBs (Strickfaden et al., 2016) and its presence can prevent Rad51 loading (Machida et al., 2014). However, it is also important at break sites, initiating and amplifying ubiquitination signaling, which is required for the recruitment of downstream repair proteins (Thorslund et al., 2015). Interestingly, histone H1 has been shown to be a target for Pin1 mediated prolyl isomerization, with implications for its binding to chromatin (Raghuram et al., 2013). Given these findings, histone H1 may be a target for prolyl isomerization by FKBP25 in the regulation of DNA repair. Also of great interest is whether FKBP25's activities in regulating HR may be through influence over the chromatin environment. While further characterization is required, a role in DNA damage repair may explain FKBP25's, so far inexplicable, association with chromatin.

Alternatively, FKBP25 regulation of DNA damage may come as result of its regulation of microtubule dynamics (outlined in Chapter 3). Microtubule-dependent transport of the DNA damage repair proteins DNA-PK, NBS1, MRE11, and 53BP1 promotes their nuclear localization (Poruchynsky et al., 2015). Thus, disrupting the microtubule network may impair their function. The cytoskelton has recently been established as an important influencer of interphase chromosome movements, in part through connections mediated by the LINC complex (Spichal and Fabre, 2017). The mobility of chromatin plays a major role in repair, increasing the efficiency of homol-

ogous recombination (Dion and Gasser, 2013). While most studies of DSB dependent chromatin movements have been performed in yeast, an ATM-dependent increase in chromatin mobility has also been observed in mammalian cells (Becker et al., 2014). This process is dependent on the dynamic microtubule cytoskeleton (Lottersberger et al., 2015). Thus, a mechanistic connection between FKBP25's activity in stabilizing microtubules and roles in HR cannot be directly ruled out. However, the fact that overexpression of the FKBP25-NLS construct showed an increase in HR and is actively displaced from chromatin suggests that FKBP25's involvement in DNA repair is more likely a result of the nuclear pool. Uncovering the exact mechanism of FKBP25's role in repair and differentiating between these two putative modes of action will require further experimentation.

I also show here the potential for targeting FKBPs to potentiate the activity of the Parp inhibitor olaparib, presumably through FKBP25. While targeting of FKBPs may work to potentiate the action of DDR targeted therapies, a significant drawback is their immunoinhibitory effects. It is now well appreciated that the immune system plays a vital role in the body's own defense against cancer (Zitvogel et al., 2013). This, of course, is a significant drawback of directly targeting mTOR, as rapamycin's inhibition of the immune system acts through mTOR. Thus, future research should focus on exploring inhibitory molecules that do not engage the immune system, targeting only the catalytic pocket of selective FKBPs. Such chemical probes will also help dissect the contributions of individual FKBPs to processes such as DSB repair and their potential as therapeutic targets. While there is still much to be learned, this research provides preliminary evidence that inhibiting FKBPs may be an effective route to enhance targeting of the DDR.

4.4 Materials & Methods

Cell culture

U2OS cells (ATCC), U2OS DSB repair pathway reporter cells (DR-GFP, SA-GFP, EJ5-GFP, and EJ2-GFP were a gift from Dr. Jeremy Stark, City of Hope), and Lac-O U2OS cells (a gift from Dr. Daniel Durocher, Lunenfeld Institute and originally generated by Dr. Roger Greenberg, University of Pennsylvania) were cultured in DMEM containing 10% (v/v) FBS (Sigma) and antibiotics (10 units/ml penicillin and 10 µg/ml streptomycin, ThermoFisher) at 37℃ and 5% $C0_2$. Stable U2OS shRNA knockdown cells were generated by transfection with HuSH 29-mer shRNA expression vectors (Origene) using GenJet U2OS Transfection Reagent (SignaGen) followed by selection with puromycin (InvivoGen) 48 h posttransfection until colonies formed. Colonies were then isolated, expanded, and screened for knockdown by western blot and RT-qPCR. siRNA and shRNA targeting sequences are presented in Table A.4 and A.5 of the appendix, respectively.

Rationale for cell line selection

U2OS (human osteosarcoma) cells are one of the most commonly used cell lines in the study of DNA damage repair. Additionally, the reporter assay cell line generously provided by Dr. Jeremy Stark were in a U2OS background. Therefore additional experiments studying FKBP25s involvement in DNA damage repair were also performed in U2OS cells.

Statistics

All numerical results are reported as mean ± standard error (SEM). The number of replicates, technical or biological, are indicated in corresponding figure legends. The R programming language for statistical analysis was used for the calculation of statistical significance. If not indicated otherwise in figure legends, two-tailed Students t test for unpaired data was used to evaluate single comparisons between different experimental groups.

Plasmids

FKBP25 expression plasmids were generated by subcloning a synthesized FKBP25 gene (GenScript) into a modified pcDNA5/FRT/TO vector (Thermo Fisher). For the DSB repair pathway reporter assay, the I-SceI expression vector was used fo generating site-specific double-strand breaks (Addgene # 26477, a gift from Dr. Maria Jasin,

Memorial Sloan-Kettering Cancer Center) and a pIRES2-DsRed-Express was used as a transfection control (Clontech a kind gift from Dr. Bob Chow, University of Victoria). An mCherry-LacI-FokI fusion was used to generate site specific breaks at an integrated LacO array in U2OS cells to test for FKBP25 recruitment to DNA DSBs (provided by Dr. Daniel Durocher of Lunenfeld Institute, with permission from Dr. R Greenberg, University of Pennsylvania). FKBP25-GFP and FKBP25-NLS-GFP were generated by subcloning from pcDNA 5 FRT vectors into pGFP-N1 (Clonetech) using standard molecular biology techniques.

Antibodies

The following antibodies were used in this study: FKBP25 (GeneScript, epitope residues 201-224 - WB 1:2000, IF 1:300), α-tubulin (Santa Cruz sc8035 - WB 1:10 000), Histone H3 (abcam ab1791 - WB 1:50 000), Parp-1 (Santa Cruz sc-8007 - WB 1:5000), nucleolin (abcam ab22758 - IF 1:1000), Kap1 (abcam ab 10483 - 1:5000), γH2Ax (BioLegend 613402 - WB 1:5000), Rad51 (abcam ab133534 - IF 1:250), RPS6 (Santa Cruz sc74459 - WB 1:500), TopoI (abcam ab09374 - WB 1:5000), Ku86 (Santa Cruz sc-9034 - WB 1:5000 IF 1:500), and Ku70 (Millipore Q2187163 WB 1:2500).

DSB repair pathway reporter assay

Assays were performed as previously described by Gunn and Stark (2012). For siRNA knockdown, cells were reverse transfected with 10 nM siRNA in 12 well plates using the jetPRIME (Polyplus transfection). Cells were then incubated for 24 h and split to 6-well plates and incubated for a further 24 h. 48 h after the initial siRNA transfection cells were co-transfected with 0.8 µg of I-SceI expression plasmid, 0.4 µg dsRED expression vector, and 10 nM siRNA using Lipofectamine 2000 following the manufacturer's instructions. Cells were incubated with the transfection mix for 3 h, then washed in 1x PBS, and fresh growth media added. For over-expression studies, cells were co-transfected with 0.8 µg I-SceI and 0.4 µg FKBP25 expression vector using Lipofectamine 2000, for 3 h as above. For chemical treatments, compounds were added to fresh media after a three-hour transfection with 0.8 ug I-SceI as above. Three days following transfections cells were harvested by trypsinization by adding 200 µl 1x trypsin-EDTA (Thermo Fisher) per well, incubating for 3-5 min at room temperature, dispersing cells with the addition 200 µl growth medium and collecting in FACs tubes. After harvesting the cells, 200 µl 10% formaldehyde was added (1:2 ratio) to fix and samples immediately vortexed for 2-3 seconds at medium speed. Samples were then analyzed by flow cytometry on a BD FACS Calibur within 4 h of

harvesting.

Rad51 foci formation assay

To evaluate Rad51 recruitment U2OS cells expressing shRNA targeting FKBP25 or non-targeting control were plated on glass coverslips in 6-well plates and incubated overnight. The following day cells were treated with 100 µM etoposide for 20 min to induce DSB breaks. Cells were then washed twice with 1x PBS and allowed to recover for 2 h in fresh media. Immunofluorescence, staining for Rad51 and γH2Ax, was performed as described in Chapter 3 of this thesis. At least 80 cells were counted per condition.

Cell proliferation assays

MTT assays were performed as previously described (van de Loosdrecht et al., 1994). Briefly, for knockdowns cells were reverse transfected with siRNA, incubated O/N, then trypsinized, counted by hemocytometer, and plated at densities ranging from 5000 to 15 000 cells per well of a 96-well plate. For FKBP and mTOR inhibition, cells were counted and plated at different densities in media containing drugs at the indicated concentrations. Plates were incubated for 72-96 h and 20 µl of 5 mg/ml thiazolyl blue tetrazolium (Sigma) was added to each well and incubated for 2.5-3 h at 37℃. Media was removed and 150 µl of DMSO added per well to solubilize the precipitant. Plates were incubated for a further 15 min at room temperature with shaking and samples were read at OD 595 nm and OD 630 nm, as a reference, on an absorbance microplate reader (BioTek).

Laser micro-irradiation

FKBP25-NLS-GFP recruitment to IR-induced breaks was performed by Dr. Fade Gong from the laboratory of Dr. Kyle Miller at the University of Texas at Austin as described in their recent publication (Gong et al., 2015). Briefly, cells were seeded on glass-bottom dishes and incubated overnight. The following day, cells were transfected with an FKBP25-NLS-GFP construct using Fugene HD transfection and incubated for 24 h. Cells were then incubated for a further 24 h in the presence of 10 µM 5-bromo-2'-deoxyuridine (BrdU) at 37℃. A 405-nm solid-state laser was used to generate BrdU-dependent DNA damage. Following damage, GFP fluorescence was monitored by live confocal fluorescent microscopy using an Olympus FV1000 microscope.

mCherry LacI-FokI assay

Recruitment of FKBP25-GFP to mCherry-LacI-FokI induced DSBs at an integrated LacO array was performed as previously described (Shanbhag and Greenberg, 2013). Briefly, reporter cells were plated one day before transfection in 6-well plates containing HCl-treated glass coverslips to improve adherence. Cells were then transfected with a 0.6 µg FKBP25-GFP expression vector and 0.6 µg mCherry-LacI-FokI using Lipofectamine 3000 following the manufacturer's instructions. Transfected cells were incubated for 18- 24 h, washed once in cold 1x PBS and fixed for 10 min at room temperature in a formaldehyde fixation solution (3% paraformaldehyde/2% sucrose in 1x PBS). Fixed cells were mounted in Fluroshield containing DAPI (Sigma), sealed with nail polish, and imaged on a Leica IRES-DM2.

Western blotting

Western blots were performed by resolving proteins by SDS-PAGE and transferring to nitrocellulose membranes in phosphate transfer buffer (50 mM sodium phosphate buffer pH 6.8, 15% EtOH). Membranes were incubated in 10% skim milk for 30 min to block and probed in primary antibody for either 1 h at room temperature or overnight at 4℃ followed by three washes in TBS-T (1x TBS with 0.1% Tween 20). For chemiluminescence based detection, horseradish peroxidase conjugated anti-mouse (GE) or anti-rabbit (GE) secondary antibody was used at 1:5000 in 1% milk/TBS-T. Blots were then washed three times in TBS-T and proteins detected by incubation with a chemiluminescence HRP substrate (Millipore) and exposed to film. For fluorescence based detection, blots were incubated with either IRdye 800CW anti-mouse (Mendel Scientific) or IRdye 680RD anti-rabbit (Mendel Scientific) at 1:5000 for 1 h at room temperature in 1% milk TBS-T, followed by three washes in TBS-T and one wash in 1x TBS, and imaging on an Odyssey Clx imaging system (Li-Cor).

Chapter 5

Discussion & Future Directions

5.1 Summary of Research Objectives

Prolyl isomerases are a functionally diverse superfamily of non-covalent protein modifying enzymes. They influence proteins from the cradle to the grave; regulating protein folding, function, and turnover – PPIs are found throughout the cell, touching many aspects of cell biology. Since the first description of these enzymes almost 30 years ago, several fascinating examples of isomerization as a mechanism of protein regulation have been described. These include the parvulin Pin1 as a master regulator of cell signaling, targeting pS/T motifs downstream of MAPK and CDK (Zhou and Lu, 2016); the cyclophilin Cyp33 in the control of the chromatin modifying enzyme MLL1, altering its function from an activator of transcription to a repressor via a single proline switch (Wang et al., 2010b); and the yeast FKBP, Fpr4, which targets histone tails to influence the epigenetic state of chromatin (Nelson et al., 2006). These accounts support peptidyl-prolyl isomerization as an important regulatory mechanism. However, a significant knowledge gap remains; the substrates and functions of most PPIs are completely uncharacterized. Characterizing the role of these enzymes is not only important from a basic research standpoint – as their study will undoubtedly bring greater clarity to our understanding of the post-translational regulation of protein networks. It is also important in the context of human health. As the intracellular targets of immunosuppressant drugs, which may also be valuable in the treatment of cancer and neurodegenerative disease, the study of these enzymes may result in the discovery of novel targeted therapies for the treatment of these and other diseases. The work presented here is a significant step forward in the understanding of one such PPI, the nuclear prolyl isomerase FKBP25. This work uncovers FKBP25 as a multifunctional protein localized to the nucleolus by dsRNA

binding and involved in the regulation of microtubule dynamics and DSB repair. In these roles, FKBP25 suppresses genomic instability, a prominent feature of the cancer genome.

From "Omics" to Function

When I began this research, relatively little was known about FKBP25 beyond its interaction with several nuclear factors involved in ribosome biogenesis and the regulation of chromatin. This work was initiated by broadly defining the protein-protein interactions of FKBP25 in an unbiased manner, providing an increasingly complete picture of its interactome (Figure 12). First, using BioID, ribosome biogenesis and RNA metabolic proteins were identified as neighboring interactors, showing FKBP25 functions proximally to proteins that regulate the fate of RNA in the cell (Figure 10). Further characterization of the FKBP25 interactome by FKBP25-FLAG Co-IP also identified protein-protein interactions with components of the cytoskeleton, chromatin-associated proteins, and members of DNA DSB repair networks (Figure 11). I show here that these interactions and FKBP25's localization to the nucleolus is largely mediated by RNA. It was these discoveries that led directly to the hypothesis that FKBP25 itself may be an RNA binding protein. Indeed, through a collaboration with Dr. Cameron Mackereth's lab, we identified the enigmatic BTHB domain as a novel dsRNA binding module. We further defined the key determinants of binding, two lysine residues (K22 & K23) at the head of the BTHB domain that are required for efficient binding both *in vitro* and in cells (Figure 19). Collectively, these results describe the molecular mechanisms that recruit FKBP25 to clientele proteins and provide a stable footing for future studies of its role in RNA-centric processes, such as ribosome biogenesis. The proteomic datasets generated are also valuable resources for future inquiries on FKBP25's role within the cell and the identification of putative substrates.

Again starting from an unbiased "omic" perspective, RNA-Seq experiments to investigate the contributions of FKBP25 to transcriptional regulation were performed. The initial expectation was that results would point to a putative function in the regulation of chromatin. Instead, FKBP25 knockdown produced a transcript signature associated with the induction of the p38 MAPK stress response and impaired metabolic activity (Figure 22). The MAPK signaling network is activated by both internal and external stress to regulate the cell cycle, apoptosis, and senescence (Coulthard et al., 2009) (Figure 22). This result in connection with a proliferation defect in knockdown cells led us to perform a detailed characterization of the contributions of FKBP25 to the cell cycle (Figure 24). Here, I showed FKBP25 promotes cell cycle transi-

tions, as its depletion appeared to enhance G1/S and G2/M cell cycle checkpoints. Surprisingly, while exploring cell cycle regulation by FKBP25, a novel role in the stabilization of the microtubule cytoskeleton was uncovered. Immunofluorescence of FKBP25's localization during mitosis showed parital colocalization with the mitotic spindle apparatus and midbody microtubules (Figure 28); macromolecular structures critical for chromosome segregation. This association also turned out to be functionally important – FKBP25 is required for the maintenance of chromosome stability (Figure 30). Disruption of microtubule stability is known to prompt a p38 stress response (Mikhailov et al., 2005). Thus, this function may account for both the stress response signature and accompanying delays in cell cycle progression when FKBP25 is depleted. While FKBP25 is known to associate with chromatin, as well as interact with and regulate the transcription factor YY1 (Yang et al., 2001), at least *in vitro*, the transcriptional consequences of these properties remain unclear, as well as the influence of this protein on the chromatin fiber.

Functional Exploration of Novel FKBP25 Protein-Protein Interactions

The proteomics experiments undertaken identified novel interactions between DSB repair proteins and FKBP25 (Figure 39). This result provided the first indication that FKBP25 may be involved in the repair of genomic lesions. I first validated several of these interactions with DSB proteins, including Ku70, Ku86, Parp1, and γH2Ax, the involvement of FKP25 in repair was then established using field standard cell based reporter assays (Gunn and Stark, 2012)(Figure 41). These observations show for the first time that FKBP25 influences DSB repair downstream of CtIP-mediated end processing, promoting homologous recombination, dependent on catalytic activity, and suppressing error prone single-strand annealing. Given that SSA is largely mutagenic, FKBP25's role in DSB repair encourages the fidelity of repair by suppressing SSA. Importantly, this is the first description of a role for FKBP25's catalytic activity. However, the substrates targeted by FKBP25 in DNA repair still need to be identified. These results and FKBP25's association with the pre-ribosome also strengthen the notion of crosstalk between the nucleolus and DNA repair. However, many questions remain concerning the mechanism of FKBP25's involvement in DSB repair and how these two functions may relate.

Identifying Putative Substrates

The final aim of this research was to identify substrates of FKBP25. While falling short of pinpointing a specific proline residue, this study establishes several potential substrates for future investigation. Singling out functional enzyme-mediated prolyl

isomerization events is a formidable task – only a few have been identified to date. In the case of FKBPs, Fpr4 targeting of histone tail prolines is one of the only examples (Nelson et al., 2006). As prolyl isomerization is a non-covalent post-translational modification, it is hard to detect. Methodologies that allow unbiased screening, such as radiography and mass spectrometry are not possible. Identification must be made on a candidate basis, where mutational analysis can be used or conformer specific antibodies raised. The BioID experiments performed here provide a candidate list of substrates, as these proteins come into close physical contact with FKBP25 in the cell. Since, FKBP25's regulation of homologous recombination is dependent on its catalytic activity, focusing on DDR regulators as putative substrates will narrow this list. Repeating BioID experiments in the context of DNA damage may also provide increased confidence of the proteins targeted by FKBP25 during the DDR. Further strategies for identifying putative substrates are discussed in the Future Directions section below. Collectively, this work has made a significant movement towards defining a substrate for FKBP25 prolyl isomerization.

5.1.1 FKBP25's Role in Ribosome Biogenesis

Shortly after FKBP25's initial discovery as a high-affinity receptor of the immunosuppressant rapamycin in the early 1990s (Galat et al., 1992), it was also identified as a binding partner of the multifunctional nucleolar protein nucleolin (Jin and Burakoff, 1993). The primary function of nucleolin is the regulation of ribosome biogenesis (Tajrishi et al., 2011), implying FKBP25 may also be involved. Since these preliminary results were published, there have been no further reports of nucleolar regulation by FKBP25. The research presented here makes significant strides in understanding the role of FKBP25 in ribosome biogenesis, which has been otherwise lacking. This work has shown that FKBP25 is recruited to the nucleolus by an RNA polymerase I transcribed ribosomal RNA (Figure 14) and physically associates with a large number of proteins involved in RNA metabolism and ribosome biogenesis (Figure 12). Given these connections, I was surprised to find FKBP25 does not seem to play a significant role in either the transcription or processing of the 47S pre-rRNA (Figure 20). However, it remains a possibility that this is a false negative result and should be investigated further. One explanation is that compensatory mechanisms may be in place in the absence of FKBP25. Ribosome biogenesis involves hundreds of proteins, some having overlapping functions, providing a built-in redundancy that buffers against disruption, genetic or otherwise. For example, the ribosomal pro-

teins Rps0 and Rps21 in yeast have been shown to be functionally redundant in the maturation of the 3′ end of 18S rRNA. Interestingly, ribosomal genes are the largest class of conserved duplicated genes in mammals (Dharia et al., 2014). Exactly how many duplicated genes are involved in genetic buffering is still not clear. However, it does support the idea that evolution may favor the development of a robust and redundant ribosome synthesis pathway. In the case of PPIs, FKBP25 is not alone in its association with the nucleolus. Strikingly, the parvulin Par14 also interacts with NPM1, associates with the nucleolus in an RNA-dependent manner, and localizes to the spindle apparatus during mitosis (Fujiyama-Nakamura et al., 2009). Further similarities to FKBP25 include DNA binding activity and an association with chromatin (Saningong and Bayer, 2015). Par14 knockdown decreases the rate of pre-rRNA processing, however, does not seem to influence the absolute levels of 28S and 18S rRNA, as shown by pulse/chase experiments using [^{3}H]uridine incorporation (Fujiyama-Nakamura et al., 2009). As the northern blot experiments performed in this thesis did not measure the kinetics of pre-rRNA processing in the absence of FKBP25, more subtle effects on processing rates may not have been observed. This fact combined with the potential for functional redundancy on the part of another PPI, suggests a more detailed evaluation of FKBP25's involvement in processing events should be undertaken before any definitive conclusions regarding its participation can be made. Furthermore, a complete gene knockout of FKBP25 may be required to see a pronounced effect. Thus, future lines of experimentation should incorporate CRISPR-Cas9 gene editing technologies into experimental pipelines.

Ribosome biogenesis encompasses many steps beyond just transcription and processing, several of which are not directly tested in this work. The BioID proteomics screen performed here identified a number of ribosome biogenesis factors, including the RNA helicase DDX27. Interestingly, northern blotting in DDX27 cells was shown to have relatively little effect on processing events and 47S transcription using *in vivo* labeling and probes to ITS2, similar to FKBP25 (Kellner et al., 2015). However, when the authors used probes directed downstream of the 3′ ETS they found a significant increase in signal when DDX27 was knocked-down. This result suggested that DDX27 is important in 3′ end processing. In its absence, an extended form of the 47S transcript is generated, which may be caused by either a read-through event or impaired processing (Kellner et al., 2015). The work presented in this thesis did not directly address the possibility of a 47S read-through event. Thus, FKBP25 may function with DDX27 to regulate the termination or processing of the 3′ ends of 47S rRNA.

Finally, this work did not study events that take place downstream of transcription and major processing events. FKBP25, like nucleolin, may play a role in the export of ribosomal RNA. FKBP25 shuttles between the nucleus and cytoplasm and is retained in the nucleus in response to Crm1-mediated nuclear export inhibitor LMB (Ochocka et al., 2009). Similarly, this treatment also blocks the export of pre-ribosomal particles (Bai et al., 2013). Given FKBP25's interaction with pre-ribosomes in the nucleus, it may be exported with pre-ribosomal particles. Whether FKBP25 may influence this process remains to be determined. Clearly, further experimentation is required to understand the exact role FKBP25 may play in the synthesis of new ribosomes. This thesis presents several lines of evidence that will be helpful to the future study of FKBP25's function within the nucleolus.

5.1.2 A Novel Microtubule Binding Protein

An unexpected finding of this thesis is that FKBP25 is a microtubule-associated protein (MAP). While this is the first description of an interaction between FKBP25 and MTs, several FKBPs have been shown to interact with MTs through their FKBP domains, including FKBPL (McKeen et al., 2008), FKBP15 (Viklund et al., 2009), FKBP51 (Jinwal et al., 2010), and FKBP52 (Chambraud et al., 2007). Understanding how FKBP25 functions in the regulation of the cytoskeleton is important as cytoskeletal dysfunction is a contributing factor in neurodegenerative diseases (Cairns et al., 2004). As well, there is growing interest in FKBPs as potential targets in the treatment of such disease (Chattopadhaya et al., 2011; Hausch, 2015). Here I show that FKBP25 acts to stabilize the MT network, through an interaction mediated by its FKBP domain. This activity is critical for the proper function of the mitotic spindle during chromosome segregation. I propose that this activity may be aided by PKC-mediated phosphorylation at the onset of mitosis, disrupting FKBP25's interaction with nucleic acids to promote its binding to MTs. Interestingly, FKBP52 and FKBP25 share a similar expression pattern, both with higher expression in brain tissues, and have opposing functions in regulating MT stability. Notably, within the adult brain, FKBP25 is found exclusively in neurons (Uhlen et al., 2015). Further understanding of the individual contributions of FKBPs to MT dynamics will aid in the development of effective FKBP-targeted therapeutics.

Given FKBP25's involvement in MT dynamics and expression patterns in neuronal tissues, it may also play a major role in development. In support of this idea, FKBP25 has been shown to be differentially expressed in the developing mouse brain

(Mas et al., 2005). Researchers found FKP25 was maximally expressed during cortical neurogenesis, with expression levels falling in the adult brain (Mas et al., 2005). Further supporting a role for FKBP25 in neuronal development, our RNA-Seq dataset showed genes with increased transcription were enriched for neuron projection development and neurotransmitter transport in FKBP25 knockdown cells (Figure A2). These cells may be engaging pathways that promote neurite outgrowth to compensate for the loss of FKBP25. The exact function that FKBP25 may play in the developing brain is largely unclear. However, these results support further investigation.

The results of this thesis have defined functions for both the BTHB and FKBP domains of FKBP25 as a dsRNA and MT binder, respectively. How these two functions may come together is not known. As a result of a high-throughput screen, FKBP25 has been identified as an mRNA binding protein (Castello et al., 2016). Taken together these functions suggest a putative role in the MT-mediated transport of RNA. In further support of this hypothesis, the mRNA transport proteins staufen1 and staufen2 are identified here as proximal FKBP25 interactors by BioID (Figure 10). Staufen proteins also possess both dsRNA and tubulin binding domains and are well characterized in the MT-dependent movement of mRNA molecules (Roegiers and Jan, 2000). Like FKBP25, they also localize to stress induced RNP granules (Thomas et al., 2005). Identification of stauffens as proximal interactors suggest they likely bind to mRNA within a contiguous stretch of dsRNA. Staufen proteins are known to engage mRNA at long range duplexes in 3′UTRs (Sugimoto et al., 2015). Thus, these regions may also provide an interaction surface for FKBP25, where it can bind mRNA adjacent to staufen. A role for several other FKBPs in MT-dependent intracellular transport has also been shown. Whereby, these proteins interact with the motor protein complex dynactin through their FKBP domains and bind cargo through their accessory domains (described in more detail in the introduction of this thesis and discussion section of Chapter 3). Thus, FKBP25 may operate similarly, tethering mRNP complexes to the transport apparatus (Figure 48).

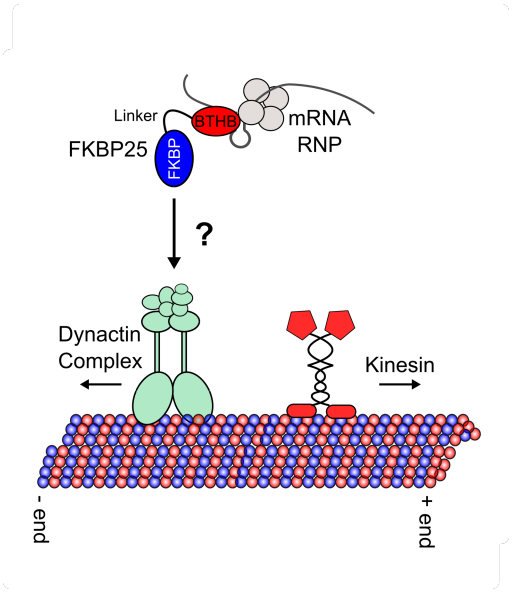

Figure 48. Model depicting FKBP25 mediated mRNA transport

5.1.3 DNA Damage-Dependent Mobilization of FKBP25

This research provides the first evidence of an FKBP protein being involved in the repair of DNA DSB breaks. Further, this activity is dependent on catalytic activity and is the first description of a catalytic function for FKBP25. Interestingly, I found that FKBP25 is evicted from sites of induced breaks shortly after their formation (Figure 44). This event may influence chromatin structure around DSBs to establish the proper environment for repair. Further experimentation will be required to define the molecular mechanisms at play. One important aspect will be to decipher what drives dissociation of FKBP25 from chromatin in response to DNA damage. We have shown here that FKBP25's displacement from chromatin during mitosis is likely regulated by phosphorylation. Suggesting its eviction from DSBs may also be driven by phosphorylation by disabling its nucleic acid binding properties. Interestingly, RPS3, which was found proximally associated with FKBP25 by BioID, is phosphorylated by PKCδ in response to DNA damage, resulting in mobilization from rRNA, switching from a function at the ribosome to repair of DNA breaks (Kim et al., 2009). Large-scale proteomic screens have also found that RBPs are a major class of ATM/ATR substrates in DNA damage response and also include several FKBPs (Matsuoka et al., 2007). While this may be primarily a way to halt cellular progression until DNA damage is repaired, many RNA-binding proteins are known to play active roles in DNA repair as well (Kai, 2016). This suggests phosphorylation may be a primary mechanism to alter the function of dsRNA binding proteins from roles in RNA metabolism to DNA

repair. Of interest will be to determine the mechanism of FKBP25 displacement from damaged chromatin, based on these findings, phosphorylation would be a reasonable starting point for future studies.

5.2 Future Directions

5.2.1 Identification of FKBP25 Bound RNAs in Cells

We have established the unique BTHB domain of FKBP25 as a novel dsRNA binding module. Using a CLIP based approach, I also validate RNA binding in cells (Figure 19). The RNA species bound directly by FKBP25 in cells is however still unclear. Ribosomal RNA seems a likely candidate – rRNA was enriched in FKBP25 RNA-IPs and in *in vitro* NMR titration experiments FKBP25 displayed tight binding to the b1NRE and b2NRE stemloop sequences found in pre-rRNA, strongly supporting direct binding of rRNA. Although FKBP25 dsRNA binding seemed to lack defined sequence specificity, it is likely to bind other RNAs in the cell. This is supported by the aforementioned proteomics screen which found FKBP25 enriched by mass spectrometry in UV-crosslinked oligo-dT enriched material, suggesting a direct interaction with mRNA (Castello et al., 2012). Performing next-generation sequencing of CLIP enriched RNase A trimmed RNAs will establish the exact RNA species FKBP25 binds, defining any real sequence preference. This experiment would also map the interaction surface of FKBP25 on ribosomal RNA, perhaps directing the identification of ribosomal proteins chaperoned by FKBP25 in ribosome biogenesis. Furthermore, it would identify any mRNA species that associate with FKBP25, shedding light on a role for FKBP25 in the cellular transport of RNA. This experiment may also inform on the mechanism of FKBP25's regulation of microtubule stability. As shown with the mRNA transport protein APC (Preitner et al., 2014), FKBP25 may also direct the localized translation of mRNA encoding microtubule components through the transport of mRNA. Thus the identification of FKBP25 bound cellular RNAs has the potential to aid understanding of the multiple functions this protein is involved in.

5.2.2 Probing the FKBP25 Interactome Throughout the Cell Cycle and Under Stress

FKBP25 is a cell cycle regulated protein. In chapter 3, I identified multiple residues that are phosphorylated on FKBP25 during mitosis. Additionally, I observed that

these modifications influence nucleic acid binding by FKBP25. However, how this regulatory event may alter FKBP25's protein-protein interactions is unclear. Therefore I suggest that BioId is used to further explore cell cycle-dependent changes in FKBP25's interactome. Starting with synchronized cells and using narrow biotin labelling windows at specific time points corresponding to the phases of the cell cycle will provide a snapshot of FKBP25's interactome throughout the cell cycle. This approach would also lead to mechanistic insight into FKBP25's function in cell cycle regulation. Additionally, BioID can be used to further study FKBP25's role in DNA damage repair and the stress response. Briefly treating FKBP25-BirA expressing cell lines with biotin to label and identify proximally interacting proteins following induction of DSBs or the stress response would clarify the involvement of FKBP25 in these processes and aid in the identification of putative substrates.

5.2.3 Involvement of FKBP25 in the Transport of RNA

As in the discussion above FKBP25 may be involved in the transport of mRNA. First, an interaction between FKBP25 and the motor complex dynactin should be established. If FKBP25 does not interact with the transport machinery, it is unlikely that it plays a role in transport, other than as an MT-stabilizing protein. Next, modern fluorescent microscopy technologies can be utilized to study the cellular movement of FKBP25 and the mRNAs it binds. By first identifying the precise mRNA molecules that FBKP25 may serve to transport, as described above, they can then be studied in the context of FKBP25-mediated mRNA transport. In the absence of experimental identification of putative FKBP25 bound RNAs, the mRNAs that stauffen binds have been well characterized and are good candidates for single gene studies (Ricci et al., 2013; Sugimoto et al., 2015). These can first be validated by RNA-IPs followed by qPCR before further characterization, analogously to a ChIP experiment.

There are a number of technologies that enable the visualization of RNA movement in live cells, including microinjected fluorescently labeled transcripts, transfection of labeled anti-sense probes, or utilizing transgenes that target fluorescently labeled bacteriophage components (Weil et al., 2010). The MS2-MCP system is well established in the real-time visualization of mRNAs in living cells (Peña et al., 2015; Bertrand et al., 1998). The system requires two components, genomic insertion of an MS2 stem-loop motif into the mRNA of interest and expression of an MCP domain fused to a fluorescent protein. The MCP fusion protein tightly binds the MS2 stem loop structure, allowing visualization of an mRNA molecule from transcription to degra-

dation. FKBP25 can also be fluorescently labeled to allow tracking of both protein and RNA. By using this approach in combination with live cell confocal imaging, the intracellular movements of FKBP25 and bound mRNA can be evaluated.

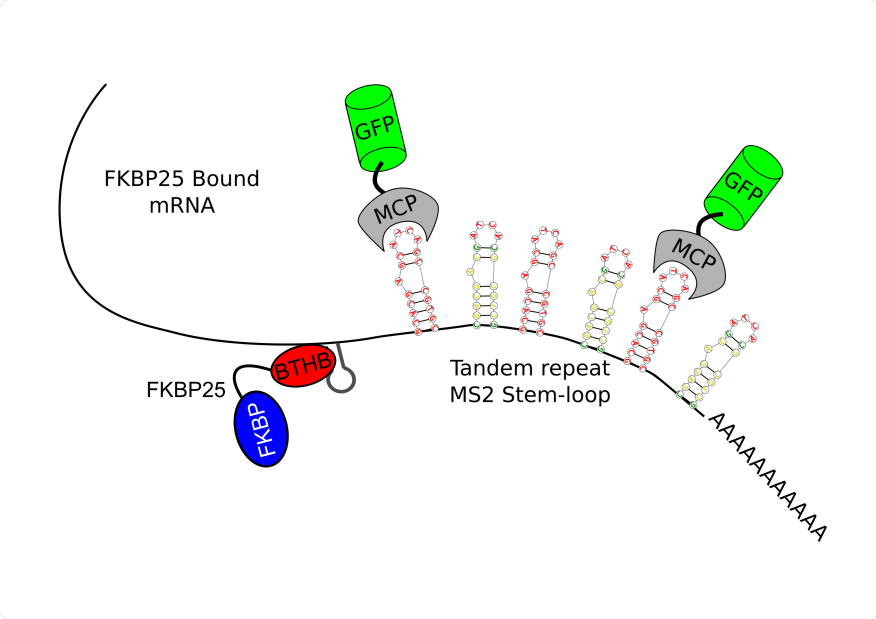

Figure 49. The MS2-MCP system for studying mRNA transport

5.2.4 Identifying FKBP25 Substrates in Homologous Recombination

In Chapter 4, a catalytic role for FKBP25 in the regulation of homologous recombination is identified. This is the first description of a function for FKBP25's prolyl isomerization activity. However, the substrate of this activity remains unknown. A strong candidate for this activity is the linker histone H1. In Chapter 2, histone H1 was the most enriched protein identified in our BioID screen. Also, prolyl isomerization of histone H1, albeit at the hands of Pin1, has been shown to alter its association with chromatin (Raghuram et al., 2013). As a first experiment, histone H1 mobilization from chromatin should be evaluated in the absence of FKBP25, using fluorescent microscopy and laser micro-irradiation. Given the advances in CRISPR mediated gene targeting (Sander and Joung, 2014), it would be valuable to create knockout cell lines for these experiments. These lines would also be useful in exploring other functions of FKBP25, including putative roles in ribosome biogenesis. Concurrently, other proteins involved in the DSB response can be screened in this way to gain further mechanistic insight into FKBP25's activities during DSB repair

and identify putative substrates. Once a suitable substrate has been identified, *in vitro* studies can be undertaken to establish whether there is a direct interaction. Structural NMR studies can then be used to determine putative prolines isomerized by FKBP25. The Nelson lab has an established collaboration with Dr. Cameron Mackereth's lab, experts in the field of NMR structural biology. They have successfully used NMR in this way to identify putative prolines isomerized by the yeast FKBP Fpr4 (Monneau et al., 2013). Finally, proline mutant proteins can be tested for function in HR assays using the in cell flow cytometry based HR cell reporter assay and Rad51 foci formation assays presented in Chapter 4.

5.2.5 Regulation of Chromatin by FKBP25 Prolyl Isomerization

In yeast, the post-translational modification of chromatin by prolyl isomerization is an established mechanism, with implications on the methylation status of H3K36 (Nelson et al., 2006). A recent study also showed that acetylation of lysine H3K14 can influence the conformational state of P16 in histone H3, with crosstalk at H3K4me3 (Howe et al., 2014). Thus, prolyl isomerization of the histone tails is an important mechanism in the epigenetic regulation of the genome. FKBP25 is the most likely functional orthologue of the responsible enzyme, Fpr4, in humans. Fpr4 modifies chromatin in two ways, through prolyl isomerization and histone chaperone activity of its N-terminal nucleophosmin like domain (Xiao et al., 2006; Edlich-Muth et al., 2015). Although FKBP25 and Fpr4 differ significantly in their NTD, established interactions between FKBP25 and nucleophosmin or nucleolin, may provide FKBP25 with access to chaperone functions found in Fpr4 (Figure 50). Our lab has shown that at least *in vitro*, FKBP25 can target prolines in the histone tail of H3 *in vitro* (data not shown). I have also performed ChIP-Seq experiments to characterize FKBP25's localization on the chromatin template (Figure A4 of the appendix). While I was able to significantly enrich chromatin from FLAG ChIPs of tagged FKBP25, as indicated by agarose gel and western blot (Figure A4), next-generation sequencing of this material did not generate any significant peaks relative to an empty-vector control. Thus, I was unable to determine where in the genome FKBP25 may be acting. Localization of FKBP25 activity on chromatin will be an important step in establishing a role in the modification of chromatin. One explanation is that the reference genomes used to align the ChIP-Seq datasets did not include repetitive regions. When assayed by qPCR, I found significant enrichment of FKBP25 on centromeric and rDNA repeats.

Thus, FKBP25 may regulate chromatin in the context of repetitive DNA sequences. Further bioinformatic interrogation of our existing ChIP-Seq datasets may reveal this relationship further. As well as performing experiments that define the epigenetic state of chromatin at the centromere and rDNA in FKBP25 knockout cells.

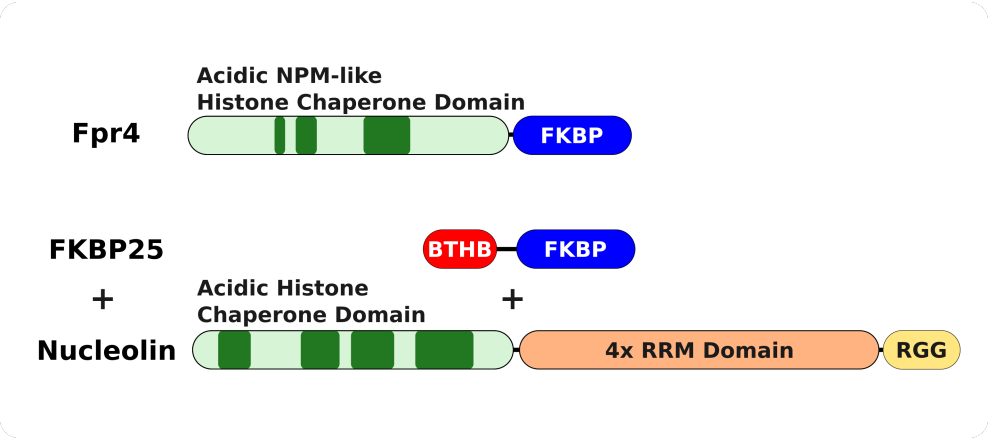

Figure 50. Comparison of domain architecture of Fpr4, FKBP25, and nucleolin

5.2.6 Targeting Prolyl Isomerases in Disease

The findings of this work significantly improve our understanding of PPI function, providing novel insights into the roles FKBP25 plays within the cell. A larger question remains: is there therapeutic value in targeting FKBP25? Indeed, the pan-FKBP inhibitors have shown promise in the treatment of disease, as discussed in the introduction of this thesis. And I have shown that mTOR-independent rapamycin effects sensitize cells to Parp inhibition, suggesting value in the treatment of cancer. However, a significant caveat is that this type of inhibition targets all FKBPs. It is entirely possible that beneficial effects become masked by countervailing mechanisms. Of great value to the PPI research community would be the development of chemical probes that can selectively and effectively impair the function of individual FKBPs. While the active sites of these enzymes are quite similar, selective inhibition of specific FKBPs has been shown, as in the case of FKBP38 (Edlich et al., 2006) and FKBP12 (März et al., 2013). Development of a panel of specific inhibitors will allow researchers to dissect the individual contributions of each FKBP in disease. Until we have this information, the true potential of these enzymes as therapeutic targets will likely remain elusive.

Bibliography

Acs, K., Luijsterburg, M. S., Ackermann, L., Salomons, F. a., Hoppe, T., and Dantuma, N. P. (2011). The AAA-ATPase VCP/p97 promotes 53BP1 recruitment by removing L3MBTL1 from DNA double-strand breaks. *Nature Structural & Molecular Biology*, 18(12):1345–1350.

Agarwal, M. L., Agarwal, A., Taylor, W. R., and Stark, G. R. (1995). p53 controls both the G2/M and the G1 cell cycle checkpoints and mediates reversible growth arrest in human fibroblasts. *Proceedings of the National Academy of Sciences of the United States of America*, 92(18):8493–8497.

Ahn, J., Murphy, M., Kratowicz, S., Wang, A., Levine, a. J., and George, D. L. (1999). Down-regulation of the stathmin/Op18 and FKBP25 genes following p53 induction. *Oncogene*, 18(43):5954–5958.

Alonso-López, D., Gutiérrez, M. A., Lopes, K. P., Prieto, C., Santamaría, R., and De Las Rivas, J. (2016). APID interactomes: providing proteome-based interactomes with controlled quality for multiple species and derived networks. *Nucleic Acids Research*, 44(April):gkw363.

Altmeyer, M., Toledo, L., Gudjonsson, T., Grøfte, M., Rask, M. B., Lukas, C., Akimov, V., Blagoev, B., Bartek, J., and Lukas, J. (2013). The chromatin scaffold protein SAFB1 renders chromatin permissive for DNA damage signaling. *Molecular Cell*, 52(2):206–220.

Amin, M. A., Matsunaga, S., Uchiyama, S., and Fukui, K. (2008). Nucleophosmin is required for chromosome congression, proper mitotic spindle formation, and kinetochore-microtubule attachment in HeLa cells. *FEBS Letters*, 582(27):3839–3844.

Andersen, J. S., Lam, Y. W., Leung, A. K. L., Ong, S.-E., Lyon, C. E., Lamond, A. I., and Mann, M. (2005). Nucleolar proteome dynamics. *Nature*, 433(7021):77–83.

Andreeva, L. and Crompton, M. (1994). An ADP-sensitive cyclosporin-A-binding protein in rat liver mitochondria. *European journal of biochemistry / FEBS*, 221(1):261–8.

Andreeva, L., Heads, R., and Green, C. J. (1999). Cyclophilins and their possible role in the stress response. *International journal of experimental pathology*, 80(6):305–15.

Apweiler, R. (2004). UniProt: the Universal Protein knowledgebase. *Nucleic Acids Research*, 32(90001):115D–119.

Arévalo-Rodríguez, M., Pan, X., Boeke, J. D., and Heitman, J. (2004). FKBP12 controls aspartate pathway flux in Saccharomyces cerevisiae to prevent toxic intermediate accumulation. *Eukaryotic Cell*, 3(5):1287–1296.

Audas, T. E., Jacob, M. D., and Lee, S. (2012). Immobilization of Proteins in the Nucleolus by Ribosomal Intergenic Spacer Noncoding RNA. *Molecular Cell*, 45(2):147–157.

Avramut, M., Zeevi, A., and Achim, C. L. (2001). The immunosuppressant drug FK506 is a potent trophic agent for human fetal neurons. *Developmental Brain Research*, 132(2):151–157.

Ayrapetov, M. K., Gursoy-Yuzugullu, O., Xu, C., Xu, Y., and Price, B. D. (2014). DNA double-strand breaks promote methylation of histone H3 on lysine 9 and transient formation of repressive chromatin. *Proceedings of the National Academy of Sciences of the United States of America*, 111(25):9169–74.

Bai, B., Moore, H. M., and Laiho, M. (2013). CRM1 and its ribosome export adaptor NMD3 localize to the nucleolus and affect rRNA synthesis. *Nucleus (Austin, Tex.)*, 4(4):315–325.

Baker, J. D., Shelton, L. B., Zheng, D., Favretto, F., Nordhues, B. A., Darling, A., Sullivan, L. E., Sun, Z., Solanki, P. K., Martin, M. D., Suntharalingam, A., Sabbagh, J. J., Becker, S., Mandelkow, E., Uversky, V. N., Zweckstetter, M., Dickey, C. A., Koren, J., and Blair, L. J. (2017). Human cyclophilin 40 unravels neurotoxic amyloids. *PLOS Biology*, 15(6):e2001336.

Bakhoum, S. F., Silkworth, W. T., Nardi, I. K., Nicholson, J. M., Compton, D. A., and Cimini, D. (2014). The mitotic origin of chromosomal instability. *Current Biology*, 24(4):R148–9.

Baldeyron, C., Soria, G., Roche, D., Cook, A. J. L., and Almouzni, G. (2011). HP1\$\alpha$lpha recruitment to DNA damage by p150CAF-1 promotes homologous recombination repair. *Journal of Cell Biology*, 193(1):81–95.

Bannikova, O., Zywicki, M., Marquez, Y., Skrahina, T., Kalyna, M., and Barta, A. (2013). Identification of RNA targets for the nuclear multidomain cyclophilin atCyp59 and their effect on PPIase activity. *Nucleic Acids Research*, 41(3):1783–1796.

Bannister, A. J. and Kouzarides, T. (2011). Regulation of chromatin by histone modifications. *Cell research*, 21(3):381–395.

Bannon, J. H., O'Donovan, D. S., Kennelly, S. M. E., and Mc Gee, M. M. (2012). The peptidyl prolyl isomerase cyclophilin A localizes at the centrosome and the midbody and is required for cytokinesis. *Cell Cycle*, 11(7):1340–1353.

Bartsch, I., Schoneberg, C., and Grummt, I. (1988). Purification and characterization of TTFI, a factor that mediates termination of mouse ribosomal DNA transcription. *Molecular and cellular biology*, 8(9):3891–7.

Beck, C., Robert, I., Reina-San-Martin, B., Schreiber, V., and Dantzer, F. (2014). Poly(ADP-ribose) polymerases in double-strand break repair: Focus on PARP1, PARP2 and PARP3. *Experimental Cell Research*, 329(1):18–25.

Becker, A., Durante, M., Taucher-Scholz, G., and Jakob, B. (2014). ATM alters the otherwise robust chromatin mobility at sites of DNA Double-Strand Breaks (DSBs) in human cells. *PLoS ONE*, 9(3):e92640.

Bennardo, N., Cheng, A., Huang, N., and Stark, J. M. (2008). Alternative-NHEJ is a mechanistically distinct pathway of mammalian chromosome break repair. *PLoS Genetics*, 4(6):e1000110.

Bertrand, E., Chartrand, P., Schaefer, M., Shenoy, S. M., Singer, R. H., and Long, R. M. (1998). Localization of ASH1 mRNA Particles in Living Yeast. *Molecular Cell*, 2(4):437–445.

Bhargava, R., Onyango, D. O., and Stark, J. M. (2016). Regulation of Single-Strand Annealing and its Role in Genome Maintenance. *Trends in Genetics*, 32(9):566–575.

Bhat, K. M. R. and Setaluri, V. (2007). Microtubule-associated proteins as targets in cancer chemotherapy. *Clinical Cancer Research*, 13(10):2849–2854.

Bieging, K. T., Mello, S. S., and Attardi, L. D. (2014). Unravelling mechanisms of p53-mediated tumour suppression. *Nature reviews. Cancer*, 14(5):359–70.

Bierer, B. E., Schreiber, S. L., and Burakoff, S. J. (1990). Mechanisms of Immunosuppression by Fk506 - Preservation of T-Cell Transmembrane Signal Transduction. *Transplantation*, 49(6):1168–1170.

Biffi, C. A. and Tuissi, A. (2017). Stato dell'arte sulle tecniche di produzione additiva per metalli. *Metallurgia Italiana*, 109(1):5–10.

Blair, L. J., Baker, J. D., Sabbagh, J. J., and Dickey, C. A. (2015). The emerging role of peptidyl-prolyl isomerase chaperones in tau oligomerization, amyloid processing, and Alzheimer's disease. *Journal of Neurochemistry*, 133(1):1–13.

Blajeski, A. L., Phan, V. a., Kottke, T. J., and Kaufmann, S. H. (2002). G 1 and G 2 cell-cycle arrest following microtubule depolymerization in human breast cancer cells. *The Journal of Clinical Investigation*, 110(1):91–99.

Boisvert, F.-m., Koningsbruggen, S. V., Navascués, J., Lamond, A. I., van Koningsbruggen, S., Navascués, J., and Lamond, A. I. (2007). The multifunctional nucleolus. *Nature reviews. Molecular cell biology*, 8(7):574–85.

Bonner, M. K., Poole, D. S., Xu, T., Sarkeshik, A., Yates, J. R., and Skop, A. R. (2011). Mitotic spindle proteomics in Chinese hamster ovary cells. *PLoS ONE*, 6(5):e20489.

Boulon, S., Westman, B. J., Hutten, S., Boisvert, F. M., and Lamond, A. I. (2010). The Nucleolus under Stress. *Molecular Cell*, 40(2):216–227.

Boulton, S. J. and Jackson, S. P. (1996). Identification of a Saccharomyces cerevisiae Ku80 homologue: roles in DNA double strand break rejoining and in telomeric maintenance. *Nucleic acids research*, 24(23):4639–48.

Bové, J., Martínez-Vicente, M., and Vila, M. (2011). Fighting neurodegeneration with rapamycin: mechanistic insights. *Nature reviews. Neuroscience*, 12(8):437–52.

Brandts, J. F., Halvorson, H. R., and Brennan, M. (1975). Consideration of the Possibility that the slow step in protein denaturation reactions is due to cis-trans isomerism of proline residues. *Biochemistry*, 14(22):4953–4963.

Brenkman, A. B., De Keizer, P. L. J., Van Den Broek, N. J. F., Van Groep, P. D., Van Diest, P. J., Van Der Horst, A., Smits, A. M. M., and Burgering, B. M. T. (2008). The peptidyl-isomerase Pin1 regulates p27kip1 expression through inhibition of Forkhead box O tumor suppressors. *Cancer Research*, 68(18):7597–7605.

Britton, S., Coates, J., and Jackson, S. P. (2013). A new method for high-resolution imaging of Ku foci to decipher mechanisms of DNA double-strand break repair. *Journal of Cell Biology*, 202(3):579–595.

Brondani, V., Schefer, Q., Hamy, F., and Klimkait, T. (2005). The peptidyl-prolyl isomerase Pin1 regulates phospho-Ser77 retinoic acid receptor α stability. *Biochemical and Biophysical Research Communications*, 328(1):6–13.

Burgess, R. C., Burman, B., Kruhlak, M. J., and Misteli, T. (2014). Activation of DNA Damage Response Signaling by Condensed Chromatin. *Cell Reports*, 9(5):1703–1718.

Burma, S., Chen, B. P., Murphy, M., Kurimasa, A., and Chen, D. J. (2001). ATM Phosphorylates Histone H2AX in Response to DNA Double-strand Breaks. *Journal of Biological Chemistry*, 276(45):42462–42467.

Buxbaum, A. R., Yoon, Y. J., Singer, R. H., and Park, H. Y. (2015). Single-molecule insights into mRNA dynamics in neurons. *Trends in Cell Biology*, 25(8):468–475.

Cairns, N. J., Lee, V. M. Y., and Trojanowski, J. Q. (2004). The cytoskeleton in neurodegenerative diseases. *Journal of Pathology*, 204(4):438–449.

Camilloni, C., Sahakyan, A. B., Holliday, M. J., Isern, N. G., Zhang, F., Eisenmesser, E. Z., and Vendruscolo, M. (2014). Cyclophilin A catalyzes proline isomerization by an electrostatic handle mechanism. *Proceedings of the National Academy of Sciences of the United States of America*, 111(28):10203–8.

Cao, W. and Konsolaki, M. (2011). FKBP immunophilins and Alzheimer's disease: A chaperoned affair. *Journal of Biosciences*, 36(3):493–498.

Cary, R. B., Peterson, S. R., Wang, J., Bear, D. G., Bradbury, E. M., and Chen, D. J. (1997). DNA looping by Ku and the DNA-dependent protein kinase. *Proc Natl Acad Sci U S A*, 94(9):4267–4272.

Castello, A., Fischer, B., Eichelbaum, K., Horos, R., Beckmann, B. M., Strein, C., Davey, N. E., Humphreys, D. T., Preiss, T., Steinmetz, L. M., Krijgsveld, J., and

Hentze, M. W. (2012). Insights into RNA Biology from an Atlas of Mammalian mRNA-Binding Proteins. *Cell*, 149(6):1393–1406.

Castello, A., Fischer, B., Frese, C. K., Horos, R., Alleaume, A. M., Foehr, S., Curk, T., Krijgsveld, J., and Hentze, M. W. (2016). Comprehensive Identification of RNA-Binding Domains in Human Cells. *Molecular Cell*, 63(4):696–710.

Ceccaldi, R., Rondinelli, B., and D'Andrea, A. D. (2016). Repair Pathway Choices and Consequences at the Double-Strand Break. *Trends in Cell Biology*, 26(1):52–64.

Chambraud, B., Belabes, H., Fontaine-Lenoir, V., Fellous, A., and Baulieu, E. E. (2007). The immunophilin FKBP52 specifically binds to tubulin and prevents microtubule formation. *FASEB journal : official publication of the Federation of American Societies for Experimental Biology*, 21(11):2787–97.

Chambraud, B., Sardin, E., Giustiniani, J., Dounane, O., Schumacher, M., Goedert, M., and Baulieu, E.-E. (2010). A role for FKBP52 in Tau protein function. *Proceedings of the National Academy of Sciences of the United States of America*, 107(6):2658–63.

Chandramouly, G., McDevitt, S., Sullivan, K., Kent, T., Luz, A., Glickman, J. F., Andrake, M., Skorski, T., and Pomerantz, R. T. (2015). Small-Molecule Disruption of RAD52 Rings as a Mechanism for Precision Medicine in BRCA-Deficient Cancers. *Chemistry and Biology*, 22(11):1491–1504.

Chang, C. H., Yu, F. Y., Wu, T. S., Wang, L. T., and Liu, B. H. (2011). Mycotoxin citrinin induced cell cycle G2/M arrest and numerical chromosomal aberration associated with disruption of microtubule formation in human cells. *Toxicological Sciences*, 119(1):84–92.

Chanut, P., Britton, S., Coates, J., Jackson, S. P., and Calsou, P. (2016). Coordinated nuclease activities counteract Ku at single-ended DNA double-strand breaks. *Nature Communications*, 7:12889.

Chapman, J. R., Taylor, M. R. G., and Boulton, S. J. (2012). Playing the End Game: DNA Double-Strand Break Repair Pathway Choice. *Molecular Cell*, 47(4):497–510.

Chatterji, U., Bobardt, M., Selvarajah, S., Yang, F., Tang, H., Sakamoto, N., Vuagniaux, G., Parkinson, T., and Gallay, P. (2009). The isomerase active site of

cyclophilin A is critical for hepatitis C virus replication. *Journal of Biological Chemistry*, 284(25):16998–17005.

Chattopadhaya, S., Harikishore, A., and S. Yoon, H. (2011). Role of FK506 Binding Proteins in Neurodegenerative Disorders. *Current Medicinal Chemistry*, 18(35):5380–5397.

Chelu, M. G., Danila, C. I., Gilman, C. P., and Hamilton, S. L. (2004). Regulation of ryanodine receptors by FK506 binding proteins. *Trends in Cardiovascular Medicine*, 14(6):227–234.

Chen, H., Lisby, M., and Symington, L. (2013). RPA Coordinates DNA End Resection and Prevents Formation of DNA Hairpins. *Molecular Cell*, 50(4):589–600.

Chen, H., Ma, Z., Vanderwaal, R. P., Feng, Z., Gonzalez-Suarez, I., Wang, S., Zhang, J., Roti Roti, J. L., Gonzalo, S., and Zhang, J. (2011). The mTOR inhibitor rapamycin suppresses DNA double-strand break repair. *Radiation research*, 175(2):214–24.

Chen, J., Zheng, X. F., Brown, E. J., and Schreiber, S. L. (1995). Identification of an 11-kDa FKBP12-rapamycin-binding domain within the 289-kDa FKBP12-rapamycin-associated protein and characterization of a critical serine residue. *Proceedings of the National Academy of Sciences of the United States of America*, 92(11):4947–51.

Chen, Z., Zang, J., Whetstine, J., Hong, X., Davrazou, F., Kutateladze, T. G., Simpson, M., Mao, Q., Pan, C. H., Dai, S., Hagman, J., Hansen, K., Shi, Y., and Zhang, G. (2006). Structural Insights into Histone Demethylation by JMJD2 Family Members. *Cell*, 125(4):691–702.

Cheung, P., Tanner, K. G., Cheung, W. L., Sassone-Corsi, P., Denu, J. M., and Allis, C. (2000). Synergistic Coupling of Histone H3 Phosphorylation and Acetylation in Response to Epidermal Growth Factor Stimulation. *Molecular Cell*, 5(6):905–915.

Cheung-Ong, K., Giaever, G., and Nislow, C. (2013). DNA-Damaging Agents in Cancer Chemotherapy: Serendipity and Chemical Biology. *Chemistry & Biology*, 20(5):648–659.

Chou, D. M., Adamson, B., Dephoure, N. E., Tan, X., Nottke, A. C., Hurov, K. E., Gygi, S. P., Colaiacovo, M. P., and Elledge, S. J. (2010). A chromatin localization

screen reveals poly (ADP ribose)-regulated recruitment of the repressive polycomb and NuRD complexes to sites of DNA damage. *Proceedings of the National Academy of Sciences*, 107(43):18475–18480.

Conduit, P. T., Wainman, A., and Raff, J. W. (2015). Centrosome function and assembly in animal cells. *Nature reviews. Molecular cell biology*, 16(10):611–624.

Cook, K. H., Schmid, F. X., and Baldwin, R. L. (1979). Role of proline isomerization in folding of ribonuclease A at low temperatures. *Proceedings of the National Academy of Sciences of the United States of America*, 76(12):6157–61.

Cooper, G. M. (2014). Translation of mRNA. *The Cell*, pages 1–9.

Cortajarena, A. L. and Regan, L. (2006). Ligand binding by TPR domains. *Protein Science*, 15(5):1193–1198.

Coulthard, L. R., White, D. E., Jones, D. L., McDermott, M. F., and Burchill, S. A. (2009). p38MAPK: stress responses from molecular mechanisms to therapeutics. *Trends in Molecular Medicine*, 15(8):369–379.

Crooks, G. E., Hon, G., Chandonia, J. M., and Brenner, S. E. (2004). WebLogo: A sequence logo generator. *Genome Research*, 14(6):1188–1190.

Cruz-García, A., López-Saavedra, A., and Huertas, P. (2014). BRCA1 accelerates CtIP-ediated DNA-end resection.

De, S., Tsimounis, A., Chen, X., and Rotenberg, S. A. (2014). Phosphorylation of alpha -tubulin by protein kinase C stimulates microtubule dynamics in human breast cells. *Cytoskeleton*, 71(4):257–272.

De Nicola, F., Bruno, T., Iezzi, S., Di Padova, M., Floridi, A., Passananti, C., Del Sal, G., and Fanciulli, M. (2007). The prolyl isomerase Pin1 affects Che-1 stability in response to apoptotic DNA damage. *Journal of Biological Chemistry*, 282(27):19685–19691.

Deacon, E. M., Pettitt, T. R., Webb, P., Cross, T., Chahal, H., Wakelam, M. J. O., and Lord, J. M. (2002). Generation of diacylglycerol molecular species through the cell cycle: a role for 1-stearoyl, 2-arachidonyl glycerol in the activation of nuclear protein kinase C-betaII at G2/M. *Journal of cell science*, 115(Pt 5):983–989.

Dejmek, J., Iglehart, J. D., and Lazaro, J. B. (2009). DNA-dependent protein kinase (DNA-PK)-dependent cisplatin-induced loss of nucleolar facilitator of chromatin transcription (FACT) and regulation of cisplatin sensitivity by DNA-PK and FACT. *Mol Cancer Res*, 7(4):581–591.

Dephoure, N., Zhou, C., Villén, J., Beausoleil, S. A., Bakalarski, C. E., Elledge, S. J., and Gygi, S. P. (2008). A quantitative atlas of mitotic phosphorylation. *Proc Natl Acad Sci U S A*, 105(31):10762–10767.

Dharia, A. P., Obla, A., Gajdosik, M. D., Simon, A., and Nelson, C. E. (2014). Tempo and Mode of Gene Duplication in Mammalian Ribosomal Protein Evolution. *PLoS ONE*, 9(11):e111721.

Dickerson, R., Drew, H., Conner, B., Wing, R., Fratini, A., and Kopka, M. (1982). The anatomy of A-, B-, and Z-DNA. *Science*, 216(4545):475–485.

Diehl, R., Ferrara, F., Müller, C., Dreyer, A. Y., Mcleod, D. D., Fricke, S., and Boltze, J. (2016). Immunosuppression for in vivo research: state-of-the-art protocols and experimental approaches. *Nature Publishing Group*, 14(2):146–179.

Dilworth, D., Gudavicius, G., Leung, A., and Nelson, C. J. (2012). The roles of peptidyl-proline isomerases in gene regulation. *Biochem Cell Biol*, 90(1):55–69.

Dion, V. and Gasser, S. M. (2013). Chromatin movement in the maintenance of genome stability. *Cell*, 152(6):1355–1364.

Domañska-Janik, K., Buzañska, L., Dłuzniewska, J., Kozłowska, H., Sarnowska, A., and Zabłocka, B. (2004). Neuroprotection by cyclosporin A following transient brain ischemia correlates with the inhibition of the early efflux of cytochrome C to cytoplasm. *Molecular Brain Research*, 121(1-2):50–59.

Dominguez, C., Boelens, R., and Bonvin, A. M. J. J. (2003). HADDOCK: A protein-protein docking approach based on biochemical or biophysical information. *Journal of the American Chemical Society*, 125(7):1731–1737.

Downs, J. A. and Jackson, S. P. (2004). A means to a DNA end: the many roles of Ku. *Nature Reviews Molecular Cell Biology*, 5(5):367–378.

Dubey, J., Ratnakaran, N., and Koushika, S. P. (2015). Neurodegeneration and microtubule dynamics: death by a thousand cuts. *Frontiers in Cellular Neuroscience*, 9(September):343.

Dumontet, C. and Jordan, M. A. (2010). Microtubule-binding agents: a dynamic field of cancer therapeutics. *Nat Rev Drug Discov*, 9(10):790–803.

Dunyak, B. M. and Gestwicki, J. E. (2016). Peptidyl-Proline Isomerases (PPIases): Targets for Natural Products and Natural Product-Inspired Compounds. *Journal of Medicinal Chemistry*, 59(21):9622–9644.

Edlich, F., Weiwad, M., Erdmann, F., Rg, J., Nel, F., Jarczowski, F., Rahfeld, J.-U., and Fischer, G. (2005). Bcl-2 regulator FKBP38 is activated by Ca 2 /calmodulin. *The EMBO Journal*, 24(14):2688–2699.

Edlich, F., Weiwad, M., Wildemann, D., Jarczowski, F., Kilka, S., Moutty, M. C., Jahreis, G., Lücke, C., Schmidt, W., Striggow, F., and Fischer, G. (2006). The specific FKBP38 inhibitor N-(N,N- dimethylcarboxamidomethyl)cycloheximide has potent neuroprotective and neurotrophic properties in brain ischemia. *Journal of Biological Chemistry*, 281(21):14961–14970.

Edlich-Muth, C., Artero, J. B., Callow, P., Przewloka, M. R., Watson, A. A., Zhang, W., Glover, D. M., Debski, J., Dadlez, M., Round, A. R., Forsyth, V. T., and Laue, E. D. (2015). The pentameric nucleoplasmin fold is present in Drosophila FKBP39 and a large number of chromatin-related proteins. *Journal of Molecular Biology*, 427(10):1949–1963.

Elvira, G. (2005). Characterization of an RNA granule from developing brain. *Molecular & Cellular Proteomics*, 5(4):635–651.

Fanghänel, J. and Fischer, G. (2004). Insights into the catalytic mechanism of peptidyl prolyl cis/trans isomerases. *Frontiers in bioscience : a journal and virtual library*, 9:3453–78.

Farber, S., Diamond, L. K., Mercer, R. D., Sylvester, R. F., and Wolff, J. A. (1948). Temporary Remissions in Acute Leukemia in Children Produced by Folic Acid Antagonist, 4-Aminopteroyl-Glutamic Acid (Aminopterin). *New England Journal of Medicine*, 238(23):787–793.

Feng, F. Y., de Bono, J. S., Rubin, M. A., and Knudsen, K. E. (2015a). Chromatin to Clinic: The Molecular Rationale for PARP1 Inhibitor Function. *Molecular Cell*, 58(6):925–934.

Feng, J., Meyer, C. A., Wang, Q., Liu, J. S., Liu, X. S., and Zhang, Y. (2012). GFOLD: A generalized fold change for ranking differentially expressed genes from RNA-seq data. *Bioinformatics*, 28(21):2782–2788.

Feng, L., Li, N., Li, Y., Wang, J., Gao, M., Wang, W., and Chen, J. (2015b). Cell cycle-dependent inhibition of 53BP1 signaling by BRCA1. *Cell discovery*, 1:15019.

Feng, W., Yonezawa, M., Ye, J., Jenuwein, T., and Grummt, I. (2010). PHF8 activates transcription of rRNA genes through H3K4me3 binding and H3K9me1/2 demethylation. *Nature structural & molecular biology*, 17(4):445–450.

Ferlay, J., Soerjomataram, I., Dikshit, R., Eser, S., Mathers, C., Rebelo, M., Parkin, D. M., Forman, D., and Bray, F. (2015). Cancer incidence and mortality worldwide: Sources, methods and major patterns in GLOBOCAN 2012. *International Journal of Cancer*, 136(5):E359–E386.

Fill, M. and Copello, J. A. (2002). Ryanodine receptor calcium release channels. *Physiol Rev*, 82(4):893–922.

Finger, L. D., Trantirek, L., Johansson, C., and Feigon, J. (2003). Solution structures of stem-loop RNAs that bind to the two N-terminal RNA-binding domains of nucleolin. *Nucleic Acids Research*, 31(22):6461–6472.

Fischer, G., Bang, H., and Mech, C. (1984). [Determination of enzymatic catalysis for the cis-trans-isomerization of peptide binding in proline-containing peptides]. *Biomedica biochimica acta*, 43(10):1101–11.

Fischer, G., Wittmann-Liebold, B., Lang, K., Kiefhaber, T., and Schmid, F. X. (1989). Cyclophilin and peptidyl-prolyl cis-trans isomerase are probably identical proteins. *Nature*, 337(6206):476–478.

Foulger, L. E., Sin, C. G. T., Zhuang, Q. Q., Smallman, H., Nicholson, J. M., Lambert, S. J., Reynolds, C. D., Dickman, M. J., Wood, C. M., Baldwin, J. P., and Evans, K. (2012). Efficient purification of chromatin architectural proteins: histones, HMGB proteins and FKBP3 (FKBP25) immunophilin. *RSC Advances*, 2(28):10598.

Franken, N. a. P., Rodermond, H. M., Stap, J., Haveman, J., and van Bree, C. (2006). Clonogenic assay of cells in vitro. *Nature protocols*, 1(5):2315–9.

Fujimoto, Y., Shiraki, T., Horiuchi, Y., Waku, T., Shigenaga, A., Otaka, A., Ikura, T., Igarashi, K., Aimoto, S., Tate, S. I., and Morikawa, K. (2010). Proline cis/trans-isomerase Pin1 regulates peroxisome proliferator- activated receptor γactivity through the direct binding to the activation function-1 domain. *Journal of Biological Chemistry*, 285(5):3126–3132.

Fujisawa, T. and Filippakopoulos, P. (2017). Functions of bromodomain-containing proteins and their roles in homeostasis and cancer. *Nature Reviews Molecular Cell Biology*, 18(4):246–262.

Fujiwara, T., Bandi, M., Nitta, M., Ivanova, E. V., Bronson, R. T., and Pellman, D. (2005). Cytokinesis failure generating tetraploids promotes tumorigenesis in p53-null cells. *Nature*, 437(7061):1043–7.

Fujiyama, S., Yanagida, M., Hayano, T., Miura, Y., Isobe, T., Fujimori, F., Uchida, T., and Takahashi, N. (2002). Isolation and proteomic characterization of human parvulin-associating preribosomal ribonucleoprotein complexes. *Journal of Biological Chemistry*, 277(26):23773–23780.

Fujiyama-Nakamura, S., Yoshikawa, H., Homma, K., Hayano, T., Tsujimura-Takahashi, T., Izumikawa, K., Ishikawa, H., Miyazawa, N., Yanagida, M., Miura, Y., Shinkawa, T., Yamauchi, Y., Isobe, T., and Takahashi, N. (2009). Parvulin (Par14), a peptidyl-prolyl cis-trans isomerase, is a novel rRNA processing factor that evolved in the metazoan lineage. *Molecular & cellular proteomics : MCP*, 8(7):1552–1565.

Galat, A. (2004). A note on clustering the functionally-related paralogues and orthologues of proteins: A case of the FK506-binding proteins (FKBPs). *Computational Biology and Chemistry*, 28(2):129–140.

Galat, A. (2013). Functional diversity and pharmacological profiles of the FKBPs and their complexes with small natural ligands. *Cellular and Molecular Life Sciences*, 70(18):3243–3275.

Galat, A., Lane, W. S., Standaert, R. F., and Schreiber, S. L. (1992). A rapamycin-selective 25-kDa immunophilin. *Biochemistry*, 31(8):2427–34.

Galat, A. and Thai, R. (2014). Rapamycin-binding FKBP25 associates with diverse proteins that form large intracellular entities. *Biochemical and Biophysical Research Communications*, 450(4):1255–1260.

Galigniana, M. D., Harrell, J. M., Murphy, P. J. M., Chinkers, M., Radanyi, C., Renoir, J. M., Zhang, M., and Pratt, W. B. (2002). Binding of hsp90-associated immunophilins to cytoplasmic dynein: Direct binding and in vivo evidence that the peptidylprolyl isomerase domain is a dynein interaction domain. *Biochemistry*, 41(46):13602–13610.

Galigniana, M. D., Harrell, J. M., O'Hagen, H. M., Ljungman, M., and Pratt, W. B. (2004). Hsp90-binding immunophilins link p53 to dynein during p53 transport to the nucleus. *Journal of Biological Chemistry*, 279(21):22483–22489.

Garel, J. R. and Baldwin, R. L. (1973). Both the fast and slow refolding reactions of ribonuclease A yield native enzyme. *Proceedings of the National Academy of Sciences of the United States of America*, 70(12):3347–3351.

Gaume, X., Place, C., Delage, H., Mongelard, F., Monier, K., and Bouvet, P. (2016). Expression of nucleolin affects microtubule dynamics. *PLoS ONE*, 11(6):e0157534.

Gaume, X., Tassin, A. M., Ugrinova, I., Mongelard, F., Monier, K., and Bouvet, P. (2015). Centrosomal nucleolin is required for microtubule network organization. *Cell Cycle*, 14(6):902–919.

Geuting, V., Reul, C., and Löbrich, M. (2013). ATM Release at Resected Double-Strand Breaks Provides Heterochromatin Reconstitution to Facilitate Homologous Recombination. *PLoS Genetics*, 9(8):e1003667.

Gibb, B., Ye, L. F., Kwon, Y., Niu, H., Sung, P., and Greene, E. C. (2014). Protein dynamics during presynaptic-complex assembly on individual single-stranded DNA molecules. *Nature structural & molecular biology*, 21(10):893–900.

Gold, B. G. (1999). Fk506 and the Role of the Immunophilin Fkbp-52 in Nerve Regeneration*. *Drug Metabolism Reviews*, 31(3):649–663.

Gold, B. G., Katoh, K., and Storm-Dickerson, T. (1995). The immunosuppressant FK506 increases the rate of axonal regeneration in rat sciatic nerve. *The Journal of neuroscience : the official journal of the Society for Neuroscience*, 15(11):7509–16.

Goldstein, M., Derheimer, F. A., Tait-Mulder, J., and Kastan, M. B. (2013). Nucleolin mediates nucleosome disruption critical for DNA double-strand break repair. *Proceedings of the National Academy of Sciences*, 110(42):16874–16879.

Gong, F., Chiu, L. Y., Cox, B., Aymard, F., Clouaire, T., Leung, J. W., Cammarata, M., Perez, M., Agarwal, P., Brodbelt, J. S., Legube, G., and Miller, K. M. (2015). Screen identifies bromodomain protein ZMYND8 in chromatin recognition of transcription-associated DNA damage that promotes homologous recombination. *Genes & development*, 29(2):197–211.

Gonzalez, I. L. and Sylvester, J. E. (1995). Complete sequence of the 43-kb human ribosomal DNA repeat: analysis of the intergenic spacer. *Genomics*, 27(2):320–8.

Goss, V. L., Hocevar, B. A., Thompson, L. J., Stratton, C. A., Burns, D. J., and Fields, A. P. (1994). Identification of nuclear beta II protein kinase C as a mitotic lamin kinase. *The Journal of biological chemistry*, 269(29):19074–80.

Gudavicius, G., Dilworth, D., Serpa, J. J., Sessler, N., Petrotchenko, E. V., Borchers, C. H., and Nelson, C. J. (2014). The prolyl isomerase, FKBP25, interacts with RNA-engaged nucleolin and the pre-60S ribosomal subunit. *Rna*, 20(7):1014–1022.

Gudavicius, G., Soufari, H., Upadhyay, S. K., Upadhyay, S., Mackereth, C. D., and Nelson, C. J. (2013). Resolving the functions of peptidylprolyl isomerases: insights from the mutagenesis of the nuclear FKBP25 enzyme. *Biochemical Society transactions*, 41(3):761–8.

Guetg, C., Scheifele, F., Rosenthal, F., Hottiger, M. O., and Santoro, R. (2012). Inheritance of Silent rDNA Chromatin Is Mediated by PARP1 via Noncoding RNA. *Molecular Cell*, 45(6):790–800.

Gullerova, M., Barta, A., and Lorkovic, Z. J. (2006). AtCyp59 is a multidomain cyclophilin from Arabidopsis thaliana that interacts with SR proteins and the C-terminal domain of the RNA polymerase II. *RNA (New York, N.Y.)*, 12(4):631–643.

Gunn, A. and Stark, J. M. (2012). I-SceI-based assays to examine distinct repair outcomes of mammalian chromosomal double strand breaks. In *Methods in Molecular Biology*, volume 920, pages 379–391. Springer.

Guo, C. Y., Wang, Y., Brautigan, D. L., and Larner, J. M. (1999). Histone H1 dephosphorylation is mediated through a radiation-induced signal transduction pathway dependent on ATM. *Journal of Biological Chemistry*, 274(26):18715–18720.

Guzman, C., Bagga, M., Kaur, A., Westermarck, J., and Abankwa, D. (2014). ColonyArea: An ImageJ plugin to automatically quantify colony formation in clonogenic assays. *PLoS ONE*, 9(3):e92444.

Haince, J. F., McDonald, D., Rodrigue, A., Déry, U., Masson, J. Y., Hendzel, M. J., and Poirier, G. G. (2008). PARP1-dependent kinetics of recruitment of MRE11 and NBS1 proteins to multiple DNA damage sites. *Journal of Biological Chemistry*, 283(2):1197–1208.

Hanahan, D. and Weinberg, R. A. (2011). Hallmarks of cancer: The next generation. *Cell*, 144(5):646–674.

Hancock, W. O. (2014). Bidirectional cargo transport: moving beyond tug of war. *Nature Reviews Molecular Cell Biology*, 15(9):615–628.

Handschumacher, R. E., Harding, M. W., Rice, J., Drugge, R. J., and Speicher, D. W. (1984). Cyclophilin: a specific cytosolic binding protein for cyclosporin A. *Science (New York, N.Y.)*, 226(4674):544–7.

Harding, M. W., Galat, a., Uehling, D. E., and Schreiber, S. L. (1989). A receptor for the immunosuppressant FK506 is a cis-trans peptidyl-prolyl isomerase. *Nature*, 341(6244):758–760.

Harding, S. M., Boiarsky, J. A., and Greenberg, R. A. (2015). ATM Dependent Silencing Links Nucleolar Chromatin Reorganization to DNA Damage Recognition. *Cell Reports*, 13(2):251–259.

Harrison, D. E., Strong, R., Sharp, Z. D., Nelson, J. F., Astle, C. M., Flurkey, K., Nadon, N. L., Wilkinson, J. E., Frenkel, K., Carter, C. S., Pahor, M., Javors, M. A., Fernandez, E., and Miller, R. A. (2010). Rapamycin fed late in life extends lifespan in genetically heterogeneous mice. *Nature*, 460(7253):392–395.

Hausch, F. (2015). FKBPs and their role in neuronal signaling. *Biochimica et Biophysica Acta - General Subjects*, 1850(10):2035–2040.

Havugimana, P. C., Hart, G. T., Nepusz, T., Yang, H., Turinsky, A. L., Li, Z., Wang, P. I., Boutz, D. R., Fong, V., Phanse, S., Babu, M., Craig, S. A., Hu, P., Wan, C., Vlasblom, J., Dar, V. U. N., Bezginov, A., Clark, G. W., Wu, G. C., Wodak, S. J., Tillier, E. R., Paccanaro, A., Marcotte, E. M., and Emili, A. (2012). A census of human soluble protein complexes. *Cell*, 150(5):1068–1081.

Heitman, J., Movva, N. R., and Hall, M. N. (1991). Targets for cell cycle arrest by the immunosuppressant rapamycin in yeast. *Science*, 253(5022):905–909.

Heitman, J., Movva, N. R., and Hall, M. N. (1992). Proline isomerases at the crossroads of protein folding, signal transduction, and immunosuppression. *The New biologist*, 4(5):448–60.

Helander, S., Montecchio, M., Lemak, A., Farès, C., Almlöf, J., Li, Y., Yee, A., Arrowsmith, C. H., Dhe-Paganon, S., and Sunnerhagen, M. (2014). Basic Tilted Helix Bundle - A new protein fold in human FKBP25/FKBP3 and HectD1. *Biochemical and Biophysical Research Communications*, 447(1):26–31.

Henderson, S. and Sollner-Webb, B. (1986). A transcriptional terminator is a novel element of the promoter of the mouse ribosomal RNA gene. *Cell*, 47(6):891–900.

Henras, A. K., Plisson-Chastang, C., O'Donohue, M. F., Chakraborty, A., and Gleizes, P. E. (2015). An overview of pre-ribosomal RNA processing in eukaryotes. *Wiley Interdisciplinary Reviews: RNA*, 6(2):225–242.

Ho, S., Clipstone, N., Timmermann, L., Northrop, J., Graef, I., Fiorentino, D., Nourse, J., and Crabtree, G. R. (1992). The mechanism of action of cyclosporin A and FK506. *Clinical immunology and immunopathology*, 13(4):136–142.

Ho, Y., Gruhler, A., Heilbut, A., Bader, G. D., Moore, L., Adams, S.-L., Millar, A., Taylor, P., Bennett, K., Boutilier, K., Yang, L., Wolting, C., Donaldson, I., Schandorff, S., Shewnarane, J., Vo, M., Taggart, J., Goudreault, M., Muskat, B., Alfarano, C., Dewar, D., Lin, Z., Michalickova, K., Willems, A. R., Sassi, H., Nielsen, P. A., Rasmussen, K. J., Andersen, J. R., Johansen, L. E., Hansen, L. H., Jespersen, H., Podtelejnikov, A., Nielsen, E., Crawford, J., Poulsen, V., Sørensen, B. D., Matthiesen, J., Hendrickson, R. C., Gleeson, F., Pawson, T., Moran, M. F., Durocher, D., Mann, M., Hogue, C. W. V., Figeys, D., and Tyers, M. (2002). Systematic identification of protein complexes in Saccharomyces cerevisiae by mass spectrometry. *Nature*, 415(6868):180–183.

Holland, A. J. and Cleveland, D. W. (2012). Chromoanagenesis and cancer: mechanisms and consequences of localized, complex chromosomal rearrangements. *Nature medicine*, 18(11):1630–8.

Hom, R. A., Chang, P. Y., Roy, S., Musselman, C. A., Glass, K. C., Selezneva, A. I., Gozani, O., Ismagilov, R. F., Cleary, M. L., and Kutateladze, T. G. (2010). Molecular Mechanism of MLL PHD3 and RNA Recognition by the Cyp33 RRM Domain. *Journal of Molecular Biology*, 400(2):145–154.

Hornbeck, P. V., Chabra, I., Kornhauser, J. M., Skrzypek, E., and Zhang, B. (2004). PhosphoSite: A bioinformatics resource dedicated to physiological protein phosphorylation. *Proteomics*, 4(6):1551–1561.

Horton, J. K., Houghton, P. J., and Houghton, J. A. (1988). Relationships between tumor responsiveness, vincristine pharmacokinetics and arrest of mitosis in human tumor xenografts. *Biochemical Pharmacology*, 37(20):3995–4000.

Howe, F., Boubriak, I., Sale, M., Nair, A., Clynes, D., Grijzenhout, A., Murray, S., Woloszczuk, R., and Mellor, J. (2014). Lysine Acetylation Controls Local Protein Conformation by Influencing Proline Isomerization. *Molecular Cell*, 55(5):733–744.

Huang, D. W., Lempicki, R. a., and Sherman, B. T. (2009). Systematic and integrative analysis of large gene lists using DAVID bioinformatics resources. *Nature Protocols*, 4(1):44–57.

Hunter, T. (2007). The Age of Crosstalk: Phosphorylation, Ubiquitination, and Beyond. *Molecular Cell*, 28(5):730–738.

Iadevaia, V., Zhang, Z., Jan, E., and Proud, C. G. (2012). MTOR signaling regulates the processing of pre-rRNA in human cells. *Nucleic Acids Research*, 40(6):2527–2539.

Inoué, S. and Bajer, A. (1961). Birefringence in endosperm mitosis. *Chromosoma*, 12(1):48–63.

Iqbal, K., Liu, F., and Gong, C.-X. (2016). Tau and neurodegenerative disease: the story so far. *Nature reviews. Neurology*, 12(1):15–27.

Ishibashi, K., Fukumoto, Y., Hasegawa, H., Abe, K., Kubota, S., Aoyama, K., Kubota, S., Nakayama, Y., and Yamaguchi, N. (2013). Nuclear ErbB4 signaling through H3K9me3 is antagonized by EGFR-activated c-Src. *Journal of cell science*, 126(Pt 2):625–37.

Ishii, S., Kurasawa, Y., Wong, J., and Yu-Lee, L.-Y. (2008). Histone deacetylase 3 localizes to the mitotic spindle and is required for kinetochore-microtubule attachment. *Proceedings of the National Academy of Sciences of the United States of America*, 105(11):4179–4184.

Iyengar, S. and Farnham, P. J. (2011). KAP1 protein: An enigmatic master regulator of the genome. *Journal of Biological Chemistry*, 286(30):26267–26276.

Jang, C. Y., Kim, H. D., Zhang, X., Chang, J. S., and Kim, J. (2012). Ribosomal protein S3 localizes on the mitotic spindle and functions as a microtubule associated protein in mitosis. *Biochemical and Biophysical Research Communications*, 429(1-2):57–62.

Javed, A., Zaidi, S. K., Gutierrez, S. E., Lengner, C. J., Harrington, K. S., Hovhannisyan, H., Cho, B. C., Pratap, J., Pockwinse, S. M., Montecino, M., van Wijnen, A. J., Lian, J. B., Stein, J. L., and Stein, G. S. (2004). <I>In Situ</I> Immunofluorescence Analysis: Immunofluorescence Microscopy. In *Cell Cycle Control and Dysregulation Protocols*, volume 285, pages 023–028. Humana Press, New Jersey.

Jia, K., Chen, D., and Riddle, D. L. (2004). The TOR pathway interacts with the insulin signaling pathway to regulate C. elegans larval development, metabolism and life span. *Development (Cambridge, England)*, 131(16):3897–906.

Jin, Y. J. and Burakoff, S. J. (1993). The 25-kDa FK506-binding protein is localized in the nucleus and associates with casein kinase II and nucleolin. *Proceedings of the National Academy of Sciences of the United States of America*, 90(16):7769–73.

Jin, Y. J., Burakoff, S. J., and Bierer, B. E. (1992). Molecular cloning of a 25-kDa high affinity rapamycin binding protein, FKBP25. *Journal of Biological Chemistry*, 267(16):10942–10945.

Jinwal, U. K., Koren, J., Borysov, S. I., Schmid, A. B., Abisambra, J. F., Blair, L. J., Johnson, A. G., Jones, J. R., Shults, C. L., O'Leary, J. C., Jin, Y., Buchner, J., Cox, M. B., and Dickey, C. a. (2010). The Hsp90 cochaperone, FKBP51, increases Tau stability and polymerizes microtubules. *The Journal of neuroscience : the official journal of the Society for Neuroscience*, 30(2):591–599.

Jost, S. C., Doolabh, V. B., Mackinnon, S. E., Lee, M., and Hunter, D. (2000). Acceleration of peripheral nerve regeneration following FK506 administration. *Restorative neurology and neuroscience*, 17(1):39–44.

Kaeberlein, M. (2005). Response to Nutrients Regulation of Yeast Replicative Life Span by TOR and Sch9 in Response to Nutrients. *Science (New York, N.Y.)*, 1193(2005):1193–1196.

Kahana, J. A. (2001). CELL CYCLE: Some Importin News About Spindle Assembly. *Science*, 291(5509):1718–1719.

Kai, M. (2016). Roles of RNA-binding proteins in DNA damage response. *International Journal of Molecular Sciences*, 17(3):310.

Kakarougkas, A. and Jeggo, P. A. (2014). DNA DSB repair pathway choice: An orchestrated handover mechanism. *British Journal of Radiology*, 87(1035):20130685.

Kallen, J., Spitzfaden, C., Zurini, M. G., Wider, G., Widmer, H., Wüthrich, K., and Walkinshaw, M. D. (1991). Structure of human cyclphilin and its binding site for cyclosporin A determined by X-ray crystallography and NMR spectroscopy. *Nature*, 353(6341):276–279.

Kapahi, P., Zid, B. M., Harper, T., Koslover, D., Sapin, V., and Benzer, S. (2004). Regulation of lifespan in Drosophila by modulation of genes in the TOR signaling pathway. *Current Biology*, 14(10):885–890.

Karaman, M. W., Herrgard, S., Treiber, D. K., Gallant, P., Atteridge, C. E., Campbell, B. T., Chan, K. W., Ciceri, P., Davis, M. I., Edeen, P. T., Faraoni, R., Floyd, M., Hunt, J. P., Lockhart, D. J., Milanov, Z. V., Morrison, M. J., Pallares, G., Patel, H. K., Pritchard, S., Wodicka, L. M., and Zarrinkar, P. P. (2008). A quantitative analysis of kinase inhibitor selectivity. *Nature Biotechnology*, 26(1):127–132.

Kaufman, B., Shapira-Frommer, R., Schmutzler, R. K., Audeh, M. W., Friedlander, M., Balma{\˜n}a, J., Mitchell, G., Fried, G., Stemmer, S. M., Hubert, A., Rosengarten, O., Steiner, M., Loman, N., Bowen, K., Fielding, A., and Domchek, S. M. (2015). Olaparib monotherapy in patients with advanced cancer and a germline BRCA1/2 mutation. *Journal of Clinical Oncology*, 33(3):244–250.

Kellner, M., Rohrmoser, M., Forné, I., Voss, K., Burger, K., Mühl, B., Gruber-Eber, A., Kremmer, E., Imhof, A., and Eick, D. (2015). DEAD-box helicase DDX27 regulates 3 end formation of ribosomal 47S RNA and stably associates with the PeBoW-complex. *Experimental Cell Research*, 334(1):146–159.

Kettenbach, A. N., Schweppe, D. K., Faherty, B. K., Pechenick, D., Pletnev, A. a., and Gerber, S. a. (2011). Quantitative phosphoproteomics identifies substrates and functional modules of Aurora and Polo-like kinase activities in mitotic cells. *Science signaling*, 4(179):rs5.

Khurana, S., Kruhlak, M. J., Kim, J., Tran, A. D., Liu, J., Nyswaner, K., Shi, L., Jailwala, P., Sung, M. H., Hakim, O., and Oberdoerffer, P. (2014). A macrohi-

stone variant links dynamic chromatin compaction to BRCA1-dependent genome maintenance. *Cell Reports*, 8(4):1049–1062.

Kiebler, M. A. and Bassell, G. J. (2006). Neuronal RNA Granules: Movers and Makers. *Neuron*, 51(6):685–690.

Kiefhaber, T., Kohler, H. H., and Schmid, F. X. (1992). Kinetic coupling between protein folding and prolyl isomerization. I. Theoretical models. *Journal of molecular biology*, 224(1):217–29.

Kim, D., Langmead, B., and Salzberg, S. L. (2015). HISAT: a fast spliced aligner with low memory requirements. *Nature methods*, 12(4):357–60.

Kim, S. M., Choi, E. J., Song, K. J., Kim, S., Seo, E., Jho, E. H., and Kee, S. H. (2009). Axin localizes to mitotic spindles and centrosomes in mitotic cells. *Experimental Cell Research*, 315(6):943–954.

Kinoshita, E. (2005). Phosphate-binding Tag, a New Tool to Visualize Phosphorylated Proteins. *Molecular & Cellular Proteomics*, 5(4):749–757.

Klettner, A., Baumgrass, R., Zhang, Y., Fischer, G., Bürger, E., Herdegen, T., and Mielke, K. (2001). The neuroprotective actions of FK506 binding protein ligands: Neuronal survival is triggered by de novo RNA synthesis, but is independent of inhibition of JNK and calcineurin. *Molecular Brain Research*, 97(1):21–31.

Kobayashi, J., Fujimoto, H., Sato, J., Hayashi, I., Burma, S., Matsuura, S., Chen, D. J., and Komatsu, K. (2012). Nucleolin Participates in DNA Double-Strand Break-Induced Damage Response through MDC1-Dependent Pathway. *PLoS ONE*, 7(11):e49245.

Kofron, J. L., Kuzmic, P., Kishore, V., Colon-Bonilla, E., and Rich, D. H. (1991). Determination of kinetic constants for peptidyl prolyl cis trans isomerases by an improved spectrophotometric assay. *Biochemistry*, 30(25):6127–6134.

Koike, A., Nishikawa, H., Wu, W., Okada, Y., Venkitaraman, A. R., and Ohta, T. (2010). Recruitment of phosphorylated NPM1 to sites of DNA damage through RNF8-dependent ubiquitin conjugates. *Cancer Research*, 70(17):6746–6756.

Kolas, N. K., Chapman, J. R., Nakada, S., Ylanko, J., Chahwan, R., Sweeney, F. D., Panier, S., Mendez, M., Wildenhain, J., Thomson, T. M., Pelletier, L., Jackson,

S. P., and Durocher, D. (2007). Orchestration of the DNA-Damage Response by the RNF8 Ubiquitin Ligase. *Science*, 318(5856):1637–1640.

Komlodi-Pasztor, E., Sackett, D., Wilkerson, J., and Fojo, T. (2011). Mitosis is not a key target of microtubule agents in patient tumors. *Nature Reviews Clinical Oncology*, 8(4):244–250.

König, J., Zarnack, K., Luscombe, N. M., and Ule, J. (2011). Protein-RNA interactions: new genomic technologies and perspectives. *Nature reviews. Genetics*, 13(2):77–83.

Konig, J., Zarnack, K., Rot, G., Curk, T., Kayikci, M., Zupan, B., Turner, D. J., Luscombe, N. M., and Ule, J. (2011). iCLIP–transcriptome-wide mapping of protein-RNA interactions with individual nucleotide resolution. *Journal of visualized experiments : JoVE*, -(April):1–7.

Koren, J., Jinwal, U. K., Davey, Z., Kiray, J., Arulselvam, K., and Dickey, C. A. (2011). Bending tau into shape: The emerging role of peptidyl-prolyl isomerases in tauopathies. *Molecular Neurobiology*, 44(1):65–70.

Korgaonkar, C., Hagen, J., Tompkins, V., Frazier, A. A., Allamargot, C., Quelle, F. W., and Quelle, D. E. (2005). Nucleophosmin (B23) targets ARF to nucleoli and inhibits its function. *Molecular and cellular biology*, 25(4):1258–71.

Koutelou, E., Hirsch, C. L., and Dent, S. Y. R. (2010). Multiple faces of the SAGA complex. *Current Opinion in Cell Biology*, 22(3):374–382.

Krejci, L., Altmannova, V., Spirek, M., and Zhao, X. (2012). Homologous recombination and its regulation. *Nucleic Acids Research*, 40(13):5795–5818.

Krogan, N. J., Cagney, G., Yu, H., Zhong, G., Guo, X., Ignatchenko, A., Li, J., Pu, S., Datta, N., Tikuisis, A. P., Punna, T., Peregrín-Alvarez, J. M., Shales, M., Zhang, X., Davey, M., Robinson, M. D., Paccanaro, A., Bray, J. E., Sheung, A., Beattie, B., Richards, D. P., Canadien, V., Lalev, A., Mena, F., Wong, P., Starostine, A., Canete, M. M., Vlasblom, J., Wu, S., Orsi, C., Collins, S. R., Chandran, S., Haw, R., Rilstone, J. J., Gandi, K., Thompson, N. J., Musso, G., St Onge, P., Ghanny, S., Lam, M. H. Y., Butland, G., Altaf-Ul, A. M., Kanaya, S., Shilatifard, A., O'Shea, E., Weissman, J. S., Ingles, C. J., Hughes, T. R., Parkinson, J., Gerstein, M., Wodak, S. J., Emili, A., and Greenblatt, J. F. (2006). Global landscape of protein complexes in the yeast Saccharomyces cerevisiae. *Nature*, 440(7084):637–643.

Kruhlak, M., Crouch, E. E., Orlov, M., Montaño, C., Gorski, S. A., Nussenzweig, A., Misteli, T., Phair, R. D., Casellas, R., Montano, C., Gorski, S. A., Nussenzweig, A., Misteli, T., Phair, R. D., and Casellas, R. (2007). The ATM repair pathway inhibits RNA polymerase I transcription in response to chromosome breaks. *Nature*, 447(7145):730–734.

Kuzuhara, T. and Horikoshi, M. (2004). A nuclear FK506-binding protein is a histone chaperone regulating rDNA silencing. *Nature structural & molecular biology*, 11(3):275–83.

Landrieu, I., Odaert, B., Wieruszeski, J. M., Drobecq, H., Rousselot-Pailley, P., Inzé, D., and Lippens, G. (2001). p13SUC1 and the WW domain of PIN1 bind to the same phosphothreonine-proline epitope. *Journal of Biological Chemistry*, 276(2):1434–1438.

Lang, K., Schmid, F. X., and Fischer, G. (1987). Catalysis of protein folding by prolyl isomerase. *Nature*, 329(6136):268–270.

Längst, G., Becker, P. B., and Grummt, I. (1998). TTF-I determines the chromatin architecture of the active rDNA promoter. *EMBO Journal*, 17(11):3135–3145.

Larsen, D. H. and Stucki, M. (2016). Nucleolar responses to DNA double-strand breaks. *Nucleic Acids Research*, 44(2):538–544.

Laurell, E., Beck, K., Krupina, K., Theerthagiri, G., Bodenmiller, B., Horvath, P., Aebersold, R., Antonin, W., and Kutay, U. (2011). Phosphorylation of Nup98 by multiple kinases is crucial for NPC disassembly during mitotic entry. *Cell*, 144(4):539–550.

Leclercq, M., Vinci, F., and Galat, A. (2000). Mammalian FKBP-25 and its associated proteins. *Arch Biochem Biophys*, 380(1):20–28.

Lee, J. S., Smith, E., and Shilatifard, A. (2010). The Language of Histone Crosstalk. *Cell*, 142(5):682–685.

Lee, S.-Y., Lee, H., Lee, H.-K., Lee, S.-W., Ha, S. C., Kwon, T., Seo, J. K., Lee, C., and Rhee, H.-W. (2016). Proximity-Directed Labeling Reveals a New Rapamycin-Induced Heterodimer of FKBP25 and FRB in Live Cells. *ACS Central Science*, 2(8):506–516.

Lessard, F., Morin, F., Ivanchuk, S., Langlois, F., Stefanovsky, V., Rutka, J., and Moss, T. (2010). The ARF Tumor Suppressor Controls Ribosome Biogenesis by Regulating the RNA Polymerase I Transcription Factor TTF-I. *Molecular Cell*, 38(4):539–550.

Levine, M. S., Bakker, B., Boeckx, B., Moyett, J., Lu, J., Vitre, B., Spierings, D. C., Lansdorp, P. M., Cleveland, D. W., Lambrechts, D., Foijer, F., and Holland, A. J. (2017). Centrosome amplification is sufficient to promote spontaneous tumorigenesis in mammals. *Developmental cell*, in press(3):313–322.e5.

Li, H., He, Z., Lu, G., Lee, S. C., Alonso, J., Ecker, J. R., and Luan, S. (2007). A WD40 domain cyclophilin interacts with histone H3 and functions in gene repression and organogenesis in Arabidopsis. *The Plant cell*, 19(8):2403–16.

Li, H. and Luan, S. (2010). AtFKBP53 is a histone chaperone required for repression of ribosomal RNA gene expression in Arabidopsis. *Cell Research*, 20(3):357–366.

Li, J., Kim, S. G., and Blenis, J. (2014a). Rapamycin: One drug, many effects. *Cell Metabolism*, 19(3):373–379.

Li, J., Langst, G., and Grummt, I. (2006). NoRC-dependent nucleosome positioning silences rRNA genes. *Embo J*, 25(24):5735–5741.

Li, M. L., Yuan, G., and Greenberg, R. A. (2014b). Chromatin yo-yo: Expansion and condensation during DNA repair. *Trends in Cell Biology*, 24(11):616–618.

Liang, J., Hung, D. T., Schreiber, S. L., and Clardy, J. (1996). Structure of the human 25 kDa FK506 binding protein complexed with rapamycin. *Journal of the American Chemical Society*, 118(5):1231–1232.

Liou, Y.-C., Ryo, A., Huang, H.-K., Lu, P.-J., Bronson, R., Fujimori, F., Uchida, T., Hunter, T., and Lu, K. P. (2002). Loss of Pin1 function in the mouse causes phenotypes resembling cyclin D1-null phenotypes. *Proceedings of the National Academy of Sciences of the United States of America*, 99(3):1335–40.

Liu, J., Doty, T., Gibson, B., and Heyer, W.-D. (2010). Human BRCA2 protein promotes RAD51 filament formation on RPA-covered single-stranded DNA. *Nature structural & molecular biology*, 17(10):1260–2.

Liu, J., Farmer, J. D., Lane, W. S., Friedman, J., Weissman, I., and Schreiber, S. L. (1991). Calcineurin is a common target of cyclophilin-cyclosporin A and FKBP-FK506 complexes. *Cell*, 66(4):807–815.

Liu, W., Youn, H. D., Zhou, X. Z., Lu, K. P., and Liu, J. O. (2001). Binding and regulation of the transcription factor NFAT by the peptidyl prolyl cis-trans isomerase Pin1. *FEBS Letters*, 496(2-3):105–108.

Ljungman, M., Zhang, F., Chen, F., Rainbow, a. J., and McKay, B. C. (1999). Inhibition of RNA polymerase II as a trigger for the p53 response. *Oncogene*, 18(3):583–592.

Lo, W.-S., Trievel, R. C., Rojas, J. R., Duggan, L., Hsu, J.-Y., Allis, C., Marmorstein, R., and Berger, S. L. (2000). Phosphorylation of Serine 10 in Histone H3 Is Functionally Linked In Vitro and In Vivo to Gcn5-Mediated Acetylation at Lysine 14. *Molecular Cell*, 5(6):917–926.

Lonsdale, J., Thomas, J., Salvatore, M., Phillips, R., Lo, E., Shad, S., Hasz, R., Walters, G., Garcia, F., Young, N., Foster, B., Moser, M., Karasik, E., Gillard, B., Ramsey, K., Sullivan, S., Bridge, J., Magazine, H., Syron, J., Fleming, J., Siminoff, L., Traino, H., Mosavel, M., Barker, L., Jewell, S., Rohrer, D., Maxim, D., Filkins, D., Harbach, P., Cortadillo, E., Berghuis, B., Turner, L., Hudson, E., Feenstra, K., Sobin, L., Robb, J., Branton, P., Korzeniewski, G., Shive, C., Tabor, D., Qi, L., Groch, K., Nampally, S., Buia, S., Zimmerman, A., Smith, A., Burges, R., Robinson, K., Valentino, K., Bradbury, D., Cosentino, M., Diaz-Mayoral, N., Kennedy, M., Engel, T., Williams, P., Erickson, K., Ardlie, K., Winckler, W., Getz, G., DeLuca, D., MacArthur, D., Kellis, M., Thomson, A., Young, T., Gelfand, E., Donovan, M., Meng, Y., Grant, G., Mash, D., Marcus, Y., Basile, M., Liu, J., Zhu, J., Tu, Z., Cox, N. J., Nicolae, D. L., Gamazon, E. R., Im, H. K., Konkashbaev, A., Pritchard, J., Stevens, M., Flutre, T., Wen, X., Dermitzakis, E. T., Lappalainen, T., Guigo, R., Monlong, J., Sammeth, M., Koller, D., Battle, A., Mostafavi, S., McCarthy, M., Rivas, M., Maller, J., Rusyn, I., Nobel, A., Wright, F., Shabalin, A., Feolo, M., Sharopova, N., Sturcke, A., Paschal, J., Anderson, J. M., Wilder, E. L., Derr, L. K., Green, E. D., Struewing, J. P., Temple, G., Volpi, S., Boyer, J. T., Thomson, E. J., Guyer, M. S., Ng, C., Abdallah, A., Colantuoni, D., Insel, T. R., Koester, S. E., Little, A. R., Bender, P. K., Lehner, T., Yao, Y., Compton, C. C., Vaught, J. B., Sawyer, S., Lockhart, N. C., Demchok, J., and Moore, H. F. (2013). The Genotype-Tissue Expression (GTEx) project. *Nature Genetics*, 45(6):580–585.

Lottersberger, F., Karssemeijer, R. A., Dimitrova, N., and De Lange, T. (2015). 53BP1 and the LINC Complex Promote Microtubule-Dependent DSB Mobility and DNA Repair. *Cell*, 163(4):880–893.

Lu, C. T., Huang, K. Y., Su, M. G., Lee, T. Y., Bretaña, N. A., Chang, W. C., Chen, Y. J., Chen, Y. J., and Huang, H. D. (2013). DbPTM 3.0: An informative resource for investigating substrate site specificity and functional association of protein post-translational modifications. *Nucleic Acids Research*, 41(D1):D295–D305.

Lu, K. P., Finn, G., Lee, T. H., and Nicholson, L. K. (2007). Prolyl cis-trans isomerization as a molecular timer. *Nature Chemical Biology*, 3(10):619–629.

Lu, K. P., Hanes, S. D., and Hunter, T. (1996). A human peptidyl-prolyl isomerase essential for regulation of mitosis. *Nature*, 380(6574):544–547.

Lu, P. J., Wulf, G., Zhou, X. Z., Davies, P., and Lu, K. P. (1999). The prolyl isomerase Pin1 restores the function of Alzheimer-associated phosphorylated tau protein. *Nature*, 399(6738):784–8.

Lufei, C., Koh, T. H., Uchida, T., and Cao, X. (2007). Pin1 is required for the Ser727 phosphorylation-dependent Stat3 activity. *Oncogene*, 26(55):7656–64.

Luger, K., Mäder, a. W., Richmond, R. K., Sargent, D. F., and Richmond, T. J. (1997). Crystal structure of the nucleosome core particle at 2.8 A resolution. *Nature*, 389(6648):251–260.

Luo, Z., Wijeweera, A., Oh, Y., Liou, Y.-C., and Melamed, P. (2010). Pin1 Facilitates the Phosphorylation-Dependent Ubiquitination of SF-1 To Regulate Gonadotropin -Subunit Gene Transcription. *Molecular and Cellular Biology*, 30(3):745–763.

Machaca, K. (2011). Ca2+ signaling, genes and the cell cycle. *Cell Calcium*, 49(5):323–330.

Machida, S., Takaku, M., Ikura, M., Sun, J., Suzuki, H., Kobayashi, W., Kinomura, A., Osakabe, A., Tachiwana, H., Horikoshi, Y., Fukuto, A., Matsuda, R., Ura, K., Tashiro, S., Ikura, T., and Kurumizaka, H. (2014). Nap1 stimulates homologous recombination by RAD51 and RAD54 in higher-ordered chromatin containing histone H1. *Scientific reports*, 4(1):4863.

Magli, A., Angelelli, C., Ganassi, M., Baruffaldi, F., Matafora, V., Battini, R., Bachi, A., Messina, G., Rustighi, A., Del Sal, G., Ferrari, S., and Molinari, S. (2010). Proline isomerase pin1 represses terminal differentiation and myocyte enhancer factor 2C function in skeletal muscle cells. *Journal of Biological Chemistry*, 285(45):34518–34527.

Mahaney, B., Meek, K., and Lees-Miller, S. (2009). Repair of ionizing radiation-induced DNA double-strand breaks by non-homologous end-joining. *Biochemical Journal*, 417(3):639–650.

Maison, C., Bailly, D., Peters, A. H. F. M., Quivy, J.-P., Roche, D., Taddei, A., Lachner, M., Jenuwein, T., and Almouzni, G. (2002). Higher-order structure in pericentric heterochromatin involves a distinct pattern of histone modification and an RNA component. *Nature genetics*, 30(3):329–334.

Makkonen, H., Kauhanen, M., Paakinaho, V., Jääskeläinen, T., and Palvimo, J. J. (2009). Long-range activation of FKBP51 transcription by the androgen receptor via distal intronic enhancers. *Nucleic Acids Research*, 37(12):4135–4148.

Mantovani, F., Piazza, S., Gostissa, M., Strano, S., Zacchi, P., Mantovani, R., Blandino, G., and Del Sal, G. (2004). Pin1 links the activities of c-Abl and p300 in regulating p73 function. *Molecular Cell*, 14(5):625–636.

März, A. M., Fabian, A.-K., Kozany, C., Bracher, A., and Hausch, F. (2013). Large FK506-binding proteins shape the pharmacology of rapamycin. *Molecular and cellular biology*, 33(7):1357–67.

Mas, C., Guimiot-Maloum, I., Guimiot, F., Khelfaoui, M., Nepote, V., Bourgeois, F., Boda, B., Levacher, B., Galat, A., Moalic, J. M., and Simonneau, M. (2005). Molecular cloning and expression pattern of the Fkbp25 gene during cerebral cortical neurogenesis. *Gene Expression Patterns*, 5(5):577–585.

Masliah, G., Barraud, P., and Allain, F. H. T. (2013). RNA recognition by double-stranded RNA binding domains: A matter of shape and sequence. *Cellular and Molecular Life Sciences*, 70(11):1875–1895.

Matamoros, A. J. and Baas, P. W. (2016). Microtubules in health and degenerative disease of the nervous system. *Brain Research Bulletin*, 126(Pt 3):217–225.

Matsuoka, S., Ballif, B. A., Smogorzewska, A., McDonald, E. R., Hurov, K. E., Luo, J., Bakalarski, C. E., Zhao, Z., Solimini, N., Lerenthal, Y., Shiloh, Y., Gygi, S. P., and Elledge, S. J. (2007). ATM and ATR Substrate Analysis Reveals Extensive Protein Networks Responsive to DNA Damage. *Science*, 316(5828):1160–1166.

Mayer, C., Bierhoff, H., and Grummt, I. (2005). The nucleolus as a stress sensor: JNK2 inactivates the transcription factor TIF-IA and down-regulates rRNA synthesis. *Genes and Development*, 19(8):933–941.

McClintock, B. (1934). The relation of a particular chromosomal element to the development of the nucleoli in Zea mays. *Zeitschrift f{\"u}r Zellforschung und Mikroskopische Anatomie*, 21(2):294–326.

McElhinny, S. A. N., Havener, J. M., Garcia-Diaz, M., Juárez, R., Bebenek, K., Kee, B. L., Blanco, L., Kunkel, T. A., and Ramsden, D. A. (2005). A gradient of template dependence defines distinct biological roles for family X polymerases in nonhomologous end joining. *Molecular Cell*, 19(3):357–366.

McKeen, H. D., McAlpine, K., Valentine, A., Quinn, D. J., McClelland, K., Byrne, C., O'Rourke, M., Young, S., Scott, C. J., McCarthy, H. O., Hirst, D. G., and Robson, T. (2008). A novel FK506-like binding protein interacts with the glucocorticoid receptor and regulates steroid receptor signaling. *Endocrinology*, 149(11):5724–5734.

McStay, B. and Grummt, I. (2008). The epigenetics of rRNA genes: from molecular to chromosome biology. *Annual review of cell and developmental biology*, 24(1):131–157.

Mellacheruvu, D., Wright, Z., Couzens, A. L., Lambert, J.-P., St-Denis, N. A., Li, T., Miteva, Y. V., Hauri, S., Sardiu, M. E., Low, T. Y., Halim, V. A., Bagshaw, R. D., Hubner, N. C., Al-Hakim, A., Bouchard, A., Faubert, D., Fermin, D., Dunham, W. H., Goudreault, M., Lin, Z.-Y., Badillo, B. G., Pawson, T., Durocher, D., Coulombe, B., Aebersold, R., Superti-Furga, G., Colinge, J., Heck, A. J. R., Choi, H., Gstaiger, M., Mohammed, S., Cristea, I. M., Bennett, K. L., Washburn, M. P., Raught, B., Ewing, R. M., Gingras, A.-C., and Nesvizhskii, A. I. (2013). The CRAPome: a contaminant repository for affinity purification-mass spectrometry data. *Nature methods*, 10(8):730–6.

Merdes, A., Ramyar, K., Vechio, J. D., and Cleveland, D. W. (1996). A complex of NuMA and cytoplasmic dynein is essential for mitotic spindle assembly. *Cell*, 87(3):447–458.

Mesa, A., Somarelli, J. A., and Herrera, R. J. (2008). Spliceosomal immunophilins. *FEBS Letters*, 582(16):2345–2351.

Mi, H., Kops, O., Zimmermann, E., Jäschke, A., and Tropschug, M. (1996). A nuclear RNA-binding cyclophilin in human T cells. *FEBS Letters*, 398(2-3):201–205.

Mikhailov, A., Shinohara, M., and Rieder, C. L. (2005). The p38-mediated stress-activated checkpoint: A rapid response system for delaying progression through antephase and entry into mitosis. *Cell Cycle*, 4(1):57–62.

Miki, H., Okada, Y., and Hirokawa, N. (2005). Analysis of the kinesin superfamily: Insights into structure and function. *Trends in Cell Biology*, 15(9):467–476.

Miller, O. L. and Beatty, B. R. (1969). Visualization of nucleolar genes. *Science (New York, N.Y.)*, 164(882):955–957.

Miné-Hattab, J. and Rothstein, R. (2013). DNA in motion during double-strand break repair. *Trends in Cell Biology*, 23(11):529–536.

Mitchison, T. and Kirschner, M. (1984). Dynamic instability of microtubule growth. *Nature*, 312(5991):237–42.

Mo, W., Liu, Q., Lin, C. C. J., Dai, H., Peng, Y., Liang, Y., Peng, G., Meric-Bernstam, F., Mills, G. B., Li, K., and Lin, S. Y. (2016). mTOR inhibitors suppress homologous recombination repair and synergize with PARP inhibitors via regulating SUV39H1 in BRCA-proficient triple-negative breast cancer. *Clinical Cancer Research*, 22(7):1699–1712.

Mochly-Rosen, D., Das, K., and Grimes, K. V. (2012). Protein kinase C, an elusive therapeutic target? *Nature reviews.Drug discovery*, 11(12):937–957.

Mojica, S. A., Hovis, K. M., Frieman, M. B., Tran, B., Hsia, R.-c., Ravel, J., Jenkins-Houk, C., Wilson, K. L., and Bavoil, P. M. (2015). SINC, a type III secreted protein of Chlamydia psittaci, targets the inner nuclear membrane of infected cells and uninfected neighbors. *Molecular biology of the cell*, 26(10):1918–34.

Monje, P., Hernández-Losa, J., Lyons, R. J., Castellone, M. D., and Gutkind, J. S. (2005). Regulation of the transcriptional activity of c-Fos by ERK: A novel role for the prolyl isomerase Pin1. *Journal of Biological Chemistry*, 280(42):35081–35084.

Monneau, Y. R., Soufari, H., Nelson, C. J., and Mackereth, C. D. (2013). Structure and Activity of the Peptidyl-Prolyl Isomerase Domain from the Histone Chaperone Fpr4 toward Histone H3 Proline Isomerization. *Journal of Biological Chemistry*, 288(36):25826–25837.

Montecucco, A., Zanetta, F., and Biamonti, G. (2015). Molecular mechanisms of etoposide. *EXCLI Journal*, 14:95–108.

Montgomery, T. S. H. (1898). Comparative cytological studies, with especial regard to the morphology of the nucleolus. *Journal of Morphology*, 15(2):265–582.

Moretto-Zita, M., Jin, H., Shen, Z., Zhao, T., Briggs, S. P., and Xu, Y. (2010). Phosphorylation stabilizes Nanog by promoting its interaction with Pin1. *Proceedings of the National Academy of Sciences of the United States of America*, 107(30):13312–7.

Morgan, M. A. and Shilatifard, A. (2015). Chromatin signatures of cancer. *Genes and Development*, 29(3):238–249.

Motycka, T. A., Bessho, T., Post, S. M., Sung, P., and Tomkinson, A. E. (2004). Physical and Functional Interaction between the XPF/ERCC1 Endonuclease and hRad52. *Journal of Biological Chemistry*, 279(14):13634–13639.

Mueller, J. W., Kessler, D., Neumann, D., Stratmann, T., Papatheodorou, P., Hartmann-Fatu, C., and Bayer, P. (2006). Characterization of novel elongated Parvulin isoforms that are ubiquitously expressed in human tissues and originate from alternative transcription initiation. *BMC molecular biology*, 7(1):9.

Mühlhäusser, P. and Kutay, U. (2007). An in vitro nuclear disassembly system reveals a role for the RanGTPase system and microtubule-dependent steps in nuclear envelope breakdown. *Journal of Cell Biology*, 178(4):595–610.

Nakamura, K., Greenwood, A., Binder, L., Bigio, E. H., Denial, S., Nicholson, L., Zhou, X. Z., and Lu, K. P. (2012). Proline isomer-specific antibodies reveal the early pathogenic tau conformation in Alzheimer's disease. *Cell*, 149(1):232–244.

Nakano, A., Koinuma, D., Miyazawa, K., Uchida, T., Saitoh, M., Kawabata, M., Hanai, J. I., Akiyama, H., Abe, M., Miyazono, K., Matsumoto, T., and Imamura, T. (2009). Pin1 down-regulates transforming growth factor-beta (TGF-beta) signaling by inducing degradation of Smad proteins. *Journal of Biological Chemistry*, 284(10):6109–6115.

Nakatsu, Y., Sakoda, H., Kushiyama, A., Ono, H., Fujishiro, M., Horike, N., Yoneda, M., Ohno, H., Tsuchiya, Y., Kamata, H., Tahara, H., Isobe, T., Nishimura, F., Katagiri, H., Oka, Y., Fukushima, T., Takahashi, S. I., Kurihara, H., Uchida, T., and Asano, T. (2010). Pin1 associates with and induces translocation of CRTC2 to the cytosol, thereby suppressing cAMP-responsive element transcriptional activity. *Journal of Biological Chemistry*, 285(43):33018–33027.

Neal, C. L. and Yu, D. (2006). Microtubule-associated protein tau: A marker of paclitaxel sensitivity in breast cancer. *Breast Diseases*, 16(4):374–375.

Nelson, C. J., Santos-Rosa, H., and Kouzarides, T. (2006). Proline Isomerization of Histone H3 Regulates Lysine Methylation and Gene Expression. *Cell*, 126(5):905–916.

Neumaier, T., Swenson, J., Pham, C., Polyzos, A., Lo, A. T., Yang, P., Dyball, J., Asaithamby, A., Chen, D. J., Bissell, M. J., Thalhammer, S., and Costes, S. V. (2012). Evidence for formation of DNA repair centers and dose-response nonlinearity in human cells. *Proceedings of the National Academy of Sciences*, 109(2):443–448.

Nigro, P., Pompilio, G., and Capogrossi, M. C. (2013). Cyclophilin A: a key player for human disease. *Cell death & disease*, 4(10):e888.

Nishi, M., Akutsu, H., Masui, S., Kondo, A., Nagashima, Y., Kimura, H., Perrem, K., Shigeri, Y., Toyoda, M., Okayama, A., Hirano, H., Umezawa, A., Yamamoto, N., Lee, S. W., and Ryoa, A. (2011). A distinct role for pin 1 in the induction and maintenance of pluripotency. *Journal of Biological Chemistry*, 286(13):11593–11603.

Notredame, C., Higgins, D., and Heringa, J. (2000). T-Coffee: A novel method for fast and accurate multiple sequence alignment. *Journal of Molecular Biology*, 302(1):205–217.

Ochocka, A. M., Kampanis, P., Nicol, S., Allende-Vega, N., Cox, M., Marcar, L., Milne, D., Fuller-Pace, F., and Meek, D. (2009). FKBP25, a novel regulator of the p53 pathway, induces the degradation of MDM2 and activation of p53. *FEBS Letters*, 583(4):621–626.

O'Connor, M. J. (2015). Targeting the DNA Damage Response in Cancer. *Molecular Cell*, 60(4):547–560.

Ogawa, L. M. and Baserga, S. J. (2017). Crosstalk between the nucleolus and the DNA damage response. *Mol. BioSyst.*, 13(3):443–455.

Okuda, M. (2002). The role of nucleophosmin in centrosome duplication. *Oncogene*, 21(40):6170–6174.

Olsen, J. V., Vermeulen, M., Santamaria, A., Kumar, C., Miller, M. L., Jensen, L. J., Gnad, F., Cox, J., Jensen, T. S., Nigg, E. A., Brunak, S., and Mann, M. (2010). Quantitative Phosphoproteomics Reveals Widespread Full Phosphorylation Site Occupancy During Mitosis – Olsen et al. 3 (104): ra3 – Science Signaling. *Science signaling*, 3(104):ra3.

Ozlü, N., Monigatti, F., Renard, B. Y., Field, C. M., Steen, H., Mitchison, T. J., and Steen, J. J. (2010). Binding partner switching on microtubules and aurora-B in the mitosis to cytokinesis transition. *Molecular & cellular proteomics : MCP*, 9(2):336–50.

Pahlke, D., Freund, C., Leitner, D., and Labudde, D. (2005). Statistically significant dependence of the Xaa-Pro peptide bond conformation on secondary structure and amino acid sequence. *BMC structural biology*, 5(1):8.

Panagiotis Zalmas, L., Zhao, X., Graham, A. L., Fisher, R., Reilly, C., Coutts, A. S., and Thangue, N. B. L. (2008). DNA-damage response control of E2F7 and E2F8. *EMBO reports*, 9(3):252–259.

Pani, E., Menigatti, M., Schubert, S., Hess, D., Gerrits, B., Klempnauer, K. H., and Ferrari, S. (2008). Pin1 interacts with c-Myb in a phosphorylation-dependent manner and regulates its transactivation activity. *Biochimica et Biophysica Acta - Molecular Cell Research*, 1783(6):1121–1128.

Park, J.-H., Park, E.-J., Lee, H.-S., Kim, S. J., Hur, S.-K., Imbalzano, A. N., and Kwon, J. (2006). Mammalian SWI/SNF complexes facilitate DNA double-strand break repair by promoting gamma-H2AX induction. *The EMBO Journal*, 25(17):3986–3997.

Park, S., Osmers, U., Raman, G., Schwantes, R. H., Diaz, M. O., and Bushweller, J. H. (2010). The PHD3 domain of MLL Acts as a CYP33-regulated switch between MLL-mediated activation and repression. *Biochemistry*, 49(31):6576–6586.

Parker, A. L., Kavallaris, M., and McCarroll, J. A. (2014). Microtubules and their role in cellular stress in cancer. *Frontiers in oncology*, 4(June):153.

Paull, T. T., Haykinson, M. J., and Johnson, R. C. (1993). The nonspecific DNA-binding and -bending proteins HMG1 and HMG2 promote the assembly of complex nucleoprotein structures. *Genes and Development*, 7(8):1521–1534.

Pederson, T. (2011). The nucleolus. *Cold Spring Harbor Perspectives in Biology*, 3(3):1–15.

Pederson, T. and Tsai, R. Y. L. (2009). In search of nonribosomal nucleolar protein function and regulation. *Journal of Cell Biology*, 184(6):771–776.

Peña, E., Heinlein, M., and Sambade, A. (2015). In vivo RNA labeling using MS2. In *Methods in Molecular Biology*, volume 1217, pages 329–341. Springer New York.

Peng, G., Chun-Jen Lin, C., Mo, W., Dai, H., Park, Y.-Y., Kim, S. M., Peng, Y., Mo, Q., Siwko, S., Hu, R., Lee, J.-S., Hennessy, B., Hanash, S., Mills, G. B., and Lin, S.-Y. (2014). Genome-wide transcriptome profiling of homologous recombination DNA repair. *Nature communications*, 5:3361.

Petrucelli, N., Daly, M. B., and Feldman, G. L. (2010). Hereditary breast and ovarian cancer due to mutations in BRCA1 and BRCA2. *Genetics in medicine : official journal of the American College of Medical Genetics*, 12(5):245–259.

Pfister, K. K., Shah, P. R., Hummerich, H., Russ, A., Cotton, J., Annuar, A. A., King, S. M., and Fisher, E. M. C. (2006). Genetic analysis of the cytoplasmic dynein subunit families. *PLoS Genetics*, 2(1):11–26.

Poruchynsky, M. S., Komlodi-Pasztor, E., Trostel, S., Wilkerson, J., Regairaz, M., Pommier, Y., Zhang, X., Kumar Maity, T., Robey, R., Burotto, M., Sackett, D., Guha, U., and Fojo, A. T. (2015). Microtubule-targeting agents augment the toxicity of DNA-damaging agents by disrupting intracellular trafficking of DNA repair proteins. *Proceedings of the National Academy of Sciences of the United States of America*, 112(5):1571–6.

Powell, S. N. and Kachnic, L. A. (2003). Roles of BRCA1 and BRCA2 in homologous recombination, DNA replication fidelity and the cellular response to ionizing radiation. *Oncogene*, 22(37):5784–5791.

Powers, R. W., Kaeberlein, M., Caldwell, S. D., Kennedy, B. K., and Fields, S. (2006). Extension of chronological life span in yeast by decreased TOR pathway signaling. *Genes and Development*, 20(2):174–184.

Prabakaran, S., Lippens, G., Steen, H., and Gunawardena, J. (2012). Post-translational modification: Nature's escape from genetic imprisonment and the basis for dynamic information encoding. *Wiley Interdisciplinary Reviews: Systems Biology and Medicine*, 4(6):565–583.

Prakash, A., Shin, J., Rajan, S., and Yoon, H. S. (2016). Structural basis of nucleic acid recognition by FK506-binding protein 25 (FKBP25), a nuclear immunophilin. *Nucleic Acids Research*, 44(6):2909–2925.

Preitner, N., Quan, J., Nowakowski, D. W., Hancock, M. L., Shi, J., Tcherkezian, J., Young-Pearse, T. L., and Flanagan, J. G. (2014). APC is an RNA-binding protein, and its interactome provides a link to neural development and microtubule assembly. *Cell*, 158(2):368–382.

Prosser, S. L. and Pelletier, L. (2017). Mitotic spindle assembly in animal cells: a fine balancing act. *Nature Reviews Molecular Cell Biology*, 18(3):187–201.

Pulikkan, J. a., Dengler, V., Peer Zada, a. a., Kawasaki, a., Geletu, M., Pasalic, Z., Bohlander, S. K., Ryo, a., Tenen, D. G., and Behre, G. (2010). Elevated PIN1 expression by C/EBPalpha-p30 blocks C/EBPalpha-induced granulocytic differentiation through c-Jun in AML. *Leukemia : official journal of the Leukemia Society of America, Leukemia Research Fund, U.K*, 24(5):914–923.

Raemaekers, T., Ribbeck, K., Beaudouin, J., Annaert, W., Van Camp, M., Stockmans, I., Smets, N., Bouillon, R., Ellenberg, J., and Carmeliet, G. (2003). NuSAP, a novel microtubule-associated protein involved in mitotic spindle organization. *Journal of Cell Biology*, 162(6):1017–1029.

Raghuram, N., Strickfaden, H., McDonald, D., Williams, K., Fang, H., Mizzen, C., Hayes, J. J., Th'ng, J., and Hendzel, M. J. (2013). Pin1 promotes histone H1 dephosphorylation and stabilizes its binding to chromatin. *Journal of Cell Biology*, 203(1):57–71.

Rahfeld, J. U., Rücknagel, K. P., Schelbert, B., Ludwig, B., Hacker, J., Mann, K., and Fischer, G. (1994). Confirmation of the existence of a third family among peptidyl-prolyl cis/trans isomerases Amino acid sequence and recombinant production of parvulin. *FEBS Letters*, 352(2):180–184.

Ramachandran, G. and Sasisekharan, V. (1968). Conformation of Polypeptides and Proteins. *Advances in Protein Chemistry*, 23:283–437.

Ramachandran, G. N. and Mitra, A. K. (1976). An explanation for the rare occurrence of cis peptide units in proteins and polypeptides. *Journal of Molecular Biology*, 107(1):85–92.

Ranganathan, R., Lu, K. P., Hunter, T., and Noel, J. P. (1997). Structural and functional analysis of the mitotic rotamase Pin1 suggests substrate recognition is phosphorylation dependent. *Cell*, 89(6):875–886.

Reeves, R. (2010). Nuclear functions of the HMG proteins. *Biochimica et Biophysica Acta - Gene Regulatory Mechanisms*, 1799(1-2):3–14.

Reiken, S., Lacampagne, A., Zhou, H., Kherani, A., Lehnart, S. E., Ward, C., Huang, F., Gaburjakova, M., Gaburjakova, J., Rosemblit, N., Warren, M. S., lun He, K., hua Yi, G., Wang, J., Burkhoff, D., Vassort, G., and Marks, A. R. (2003). PKA phosphorylation activates the calcium release channel (ryanodine receptor)-in skeletal muscle: Defective regulation in heart failure. *Journal of Cell Biology*, 160(6):919–928.

Reszka, A. A., Seger, R., Diltz, C. D., Krebs, E. G., and Fischer, E. H. (1995). Association of mitogen-activated protein kinase with the microtubule cytoskeleton. *Proceedings of the National Academy of Sciences of the United States of America*, 92(19):8881–5.

Ricci, E. P., Kucukural, A., Cenik, C., Mercier, B. C., Singh, G., Heyer, E. E., Ashar-Patel, A., Peng, L., and Moore, M. J. (2013). Staufen1 senses overall transcript secondary structure to regulate translation. *Nature Structural & Molecular Biology*, 21(1):26–35.

Rieder, C. L. and Cole, R. (2000). Microtubule disassembly delays the G2-M transition in vertebrates. *Current Biology*, 10(17):1067–1070.

Riggs, D. L., Cox, M. B., Tardif, H. L., Hessling, M., Buchner, J., and Smith, D. F. (2007). Noncatalytic role of the FKBP52 peptidyl-prolyl isomerase domain in the regulation of steroid hormone signaling. *Molecular and cellular biology*, 27(24):8658–69.

Rivière, S., Ménez, A., and Galat, A. (1993). On the localization of FKBP25 in T-lymphocytes. *FEBS Letters*, 315(3):247–251.

Rizkallah, R. and Hurt, M. M. (2009). Regulation of the Transcription Factor YY1 in Mitosis through Phosphorylation of Its DNA-binding Domain. *Molecular Biology of the Cell*, 20(22):4766–4776.

Robert, X. and Gouet, P. (2014). Deciphering key features in protein structures with the new ENDscript server. *Nucleic Acids Research*, 42(W1):W320–W324.

Roegiers, F. and Jan, Y. N. (2000). Staufen: a common component of mRNA transport in oocytes and neurons? *Trends in cell biology*, 10(6):220–4.

Roostalu, J., Cade, N. I., and Surrey, T. (2015). Complementary activities of TPX2 and chTOG constitute an efficient importin-regulated microtubule nucleation module. *Nature Cell Biology*, 17(11):1422–1434.

Rothenberg, E., Grimme, J. M., Spies, M., and Ha, T. (2008). Human Rad52-mediated homology search and annealing occurs by continuous interactions between overlapping nucleoprotein complexes. *Proceedings of the National Academy of Sciences of the United States of America*, 105(51):20274–9.

Roux, K. J., Kim, D. I., Raida, M., and Burke, B. (2012). A promiscuous biotin ligase fusion protein identifies proximal and interacting proteins in mammalian cells. *Journal of Cell Biology*, 196(6):801–810.

Rustighi, A., Tiberi, L., Soldano, A., Napoli, M., Nuciforo, P., Rosato, A., Kaplan, F., Capobianco, A., Pece, S., Di Fiore, P. P., and Del Sal, G. (2009). The prolyl-isomerase Pin1 is a Notch1 target that enhances Notch1 activation in cancer. *Nat Cell Biol*, 11(2):133–142.

Ryo, a., Nakamura, M., Wulf, G., Liou, Y. C., and Lu, K. P. (2001). Pin1 regulates turnover and subcellular localization of beta-catenin by inhibiting its interaction with APC. *Nature cell biology*, 3(9):793–801.

Ryo, A., Suizu, F., Yoshida, Y., Perrem, K., Liou, Y. C., Wulf, G., Rottapel, R., Yamaoka, S., and Lu, K. P. (2003). Regulation of NF-KB Signaling by Pin1-Dependent Prolyl Isomerization and Ubiquitin-Mediated Proteolysis of p65/RelA. *Molecular Cell*, 12(6):1413–1426.

Saitoh, T., Tun-Kyi, A., Ryo, A., Yamamoto, M., Finn, G., Fujita, T., Akira, S., Yamamoto, N., Lu, K. P., and Yamaoka, S. (2006). Negative regulation of interferon-regulatory factor 3dependent innate antiviral response by the prolyl isomerase Pin1. *Nature Immunology*, 7(6):598–605.

Sander, J. D. and Joung, J. K. (2014). CRISPR-Cas systems for editing, regulating and targeting genomes. *Nature Biotechnology*, 32(4):347–355.

Sanij, E., Poortinga, G., Sharkey, K., Hung, S., Holloway, T. P., Quin, J., Robb, E., Wong, L. H., Thomas, W. G., Stefanovsky, V., Moss, T., Rothblum, L., Hannan,

K. M., McArthur, G. A., Pearson, R. B., and Hannan, R. D. (2008). UBF levels determine the number of active ribosomal RNA genes in mammals. *Journal of Cell Biology*, 183(7):1259–1274.

Saningong, A. D. and Bayer, P. (2015). Human DNA-binding peptidyl-prolyl cis/trans isomerase Par14 is cell cycle dependently expressed and associates with chromatin in vivo. *BMC biochemistry*, 16(1):4.

Sarkar, P., Reichman, C., Saleh, T., Birge, R. B., and Kalodimos, C. G. (2007). Proline cis-trans Isomerization Controls Autoinhibition of a Signaling Protein. *Molecular Cell*, 25(3):413–426.

Sarkar, P., Saleh, T., Tzeng, S.-R., Birge, R. B., and Kalodimos, C. G. (2011). Structural basis for regulation of the Crk signaling protein by a proline switch. *Nature chemical biology*, 7(1):51–7.

Saveanu, C., Namane, A., Gleizes, P.-E., Lebreton, A., Rousselle, J.-C., Noaillac-Depeyre, J., Gas, N., Jacquier, A., and Fromont-Racine, M. (2003). Sequential protein association with nascent 60S ribosomal particles. *Molecular and Cellular Biology*, 23(13):4449–60.

Saxena, U. H., Owens, L., Graham, J. R., Cooper, G. M., and Hansen, U. (2010). Prolyl isomerase Pin1 regulates transcription factor LSF (TFCP2) by facilitating dephosphorylation at two serine-proline motifs. *Journal of Biological Chemistry*, 285(41):31139–31147.

Schiene-Fischer, C. (2015). Multidomain Peptidyl Prolyl cis/trans Isomerases. *Biochimica et Biophysica Acta - General Subjects*, 1850(10):2005–2016.

Schindelin, J., Arganda-Carreras, I., Frise, E., Kaynig, V., Longair, M., Pietzsch, T., Preibisch, S., Rueden, C., Saalfeld, S., Schmid, B., Tinevez, J.-Y., White, D. J., Hartenstein, V., Eliceiri, K., Tomancak, P., and Cardona, A. (2012). Fiji: an open-source platform for biological-image analysis. *Nature Methods*, 9(7):676–682.

Schmid, F. X. (1995). Protein folding: Prolyl isomerases join the fold. *Current Biology*, 5(9):993–994.

Schmidpeter, P. A. M., Jahreis, G., Geitner, A. J., and Schmid, F. X. (2011). Prolyl isomerases show low sequence specificity toward the residue following the proline. *Biochemistry*, 50(21):4796–4803.

Schmidt, W. J. (1939). Doppelbrechung der Kernspindel und Zugfasertheorie der Chromosomenbewegung. *Chromosoma*, 1(1):253–264.

Schmittgen, T. D. and Livak, K. J. (2008). Analyzing real-time PCR data by the comparative CT method. *Nature Protocols*, 3(6):1101–1108.

Schönbrunner, E. R. and Schmid, F. X. (1992). Peptidyl-prolyl cis-trans isomerase improves the efficiency of protein disulfide isomerase as a catalyst of protein folding. *Proceedings of the National Academy of Sciences of the United States of America*, 89(10):4510–4513.

Schreiber, K. H., Ortiz, D., Academia, E. C., Anies, A. C., Liao, C. Y., and Kennedy, B. K. (2015). Rapamycin-mediated mTORC2 inhibition is determined by the relative expression of FK506-binding proteins. *Aging Cell*, 14(2):265–273.

Schroer, T. A. (2004). Dynactin. *Annual Review of Cell and Developmental Biology*, 20(1):759–779.

Schvartzman, J.-M., Sotillo, R., and Benezra, R. (2010). Mitotic chromosomal instability and cancer: mouse modelling of the human disease. *Nature reviews. Cancer*, 10(2):102–15.

Schwertman, P., Bekker-Jensen, S., and Mailand, N. (2016). Regulation of DNA double-strand break repair by ubiquitin and ubiquitin-like modifiers. *Nature Reviews Molecular Cell Biology*, 17(6):379–394.

Scott, D. D. and Oeffinger, M. (2016). Nucleolin and Nucleophosmin: nucleolar proteins with multiple functions in DNA repair. *Biochemistry and Cell Biology*, 432(June):bcb–2016–0068.

Sengupta, J., Bussiere, C., Pallesen, J., West, M., Johnson, A. W., and Frank, J. (2010). Characterization of the nuclear export adaptor protein Nmd3 in association with the 60S ribosomal subunit. *Journal of Cell Biology*, 189(7):1079–1086.

Shanbhag, N. M. and Greenberg, R. A. (2013). The dynamics of DNA damage repair and transcription. *Methods in Molecular Biology*, 1042:227–235.

Shannon, P., Markiel, A., Ozier, O., Baliga, N. S., Wang, J. T., Ramage, D., Amin, N., Schwikowski, B., and Ideker, T. (2003). Cytoscape: A software Environment for integrated models of biomolecular interaction networks. *Genome Research*, 13(11):2498–2504.

Sharp, J. A., Plant, J. J., Ohsumi, T. K., Borowsky, M., and Blower, M. D. (2011). Functional analysis of the microtubule-interacting transcriptome. *Molecular biology of the cell*, 22(22):4312–23.

Shi, Y., Brown, E. D., and Walsh, C. T. (1994). Expression of recombinant human casein kinase II and recombinant heat shock protein 90 in Escherichia coli and characterization of their interactions. *Proc. Natl Acad. Sci. USA*, 91(March):2767–2771.

Siekierka, J. J., Hung, S. H., Poe, M., Lin, C. S., and Sigal, N. H. (1989). A cytosolic binding protein for the immunosuppressant FK506 has peptidyl-prolyl isomerase activity but is distinct from cyclophilin. *Nature*, 341(6244):755–757.

Siepe, D. and Jentsch, S. (2009). Prolyl isomerase Pin1 acts as a switch to control the degree of substrate ubiquitylation. *Nature cell biology*, 11(8):967–72.

Sinigaglia-Coimbra, R., Cavalheiro, E. A., and Coimbra, C. (2002). Protective effect of systemic treatment with cyclosporine A after global ischemia in rats. *J Neurol Sci.*, 203-204(0022-510X (Print)):273–276.

Sloboda, R. D. (2015). Isolation of Microtubules and Microtubule-Associated Proteins Using Paclitaxel. *Cold Spring Harbor Protocols*, 2015(1):pdb.prot081190.

Smeenk, G., Wiegant, W. W., Vrolijk, H., Solari, A. P., Pastink, A., and Van Attikum, H. (2010). The NuRD chromatin-remodeling complex regulates signaling and repair of DNA damage. *Journal of Cell Biology*, 190(5):741–749.

Smoter, M., Bodnar, L., Duchnowska, R., Stec, R., Grala, B., and Szczylik, C. (2011). The role of Tau protein in resistance to paclitaxel. *Cancer Chemotherapy and Pharmacology*, 68(3):553–557.

Solassol, J., Mange, A., and Maudelonde, T. (2011). FKBP family proteins as promising new biomarkers for cancer. *Current Opinion in Pharmacology*, 11(4):320–325.

Soto, C. and Sigurdsson, E. M. (1998). β-sheet breaker peptides inhibit fibrillogenesis in a rat brain model of amyloidosis: Implications for Alzherimer's therapy. *Nature Medicine*, 4(7):623–6.

Spichal, M. and Fabre, E. (2017). The Emerging Role of the Cytoskeleton in Chromosome Dynamics. *Frontiers in Genetics*, 8:60.

Spruijt, C. G., Luijsterburg, M. S., Menafra, R., Lindeboom, R. G. H., Jansen, P. W. T. C., Edupuganti, R. R., Baltissen, M. P., Wiegant, W. W., Voelker-Albert, M. C., Matarese, F., Mensinga, A., Poser, I., Vos, H. R., Stunnenberg, H. G., van Attikum, H., and Vermeulen, M. (2016). ZMYND8 Co-localizes with NuRD on Target Genes and Regulates Poly(ADP-Ribose)-Dependent Recruitment of GATAD2A/NuRD to Sites of DNA Damage. *Cell Reports*, 17(3):783–798.

Stanya, K. J., Liu, Y., Means, A. R., and Kao, H. Y. (2008). Cdk2 and Pin1 negatively regulate the transcriptional corepressor SMRT. *Journal of Cell Biology*, 183(1):49–61.

Stark, J. M., Pierce, A. J., Oh, J., Pastink, A., and Jasin, M. (2004). Genetic steps of mammalian homologous repair with distinct mutagenic consequences. *Molecular and cellular biology*, 24(21):9305–16.

Stewart, G. S., Wang, B., Bignell, C. R., Taylor, A. M. R., and Elledge, S. J. (2003). MDC1 is a mediator of the mammalian DNA damage checkpoint. *Nature*, 421(6926):961–966.

Stiff, T., O'Driscoll, M., Rief, N., Iwabuchi, K., Löbrich, M., and Jeggo, P. A. (2004). ATM and DNA-PK Function Redundantly to Phosphorylate H2AX after Exposure to Ionizing Radiation. *Cancer Research*, 64(7):2390–2396.

Stivala, A., Wybrow, M., Wirth, A., Whisstock, J. C., and Stuckey, P. J. (2011). Automatic generation of protein structure cartoons with pro-origami. *Bioinformatics*, 27(23):3315–3316.

Storer, C. L., Dickey, C. A., Galigniana, M. D., Rein, T., and Cox, M. B. (2011). FKBP51 and FKBP52 in signaling and disease. *Trends in Endocrinology and Metabolism*, 22(12):481–490.

Strahl, B. D. and Allis, C. D. (2000). The language of covalent histone modifications. *Nature*, 403(6765):41–45.

Strickfaden, H., McDonald, D., Kruhlak, M. J., Haince, J. F., Th'Ng, J. P. H., Rouleau, M., Ishibashi, T., Corry, G. N., Ausio, J., Underhill, D. A., Poirier, G. G., and Hendzel, M. J. (2016). Poly(ADP-ribosyl)ation-dependent transient chromatin decondensation and histone displacement following laser microirradiation. *Journal of Biological Chemistry*, 291(4):1789–1802.

Strohner, R., Nemeth, A., Jansa, P., Hofmann-Rohrer, U., Santoro, R., Längst, G., and Grummt, I. (2001). NoRC - A novel member of mammalian ISWI-containing chromatin remodeling machines. *EMBO Journal*, 20(17):4892–4900.

Sugimoto, Y., Vigilante, A., Darbo, E., Zirra, A., Militti, C., D'Ambrogio, A., Luscombe, N. M., and Ule, J. (2015). hiCLIP reveals the in vivo atlas of mRNA secondary structures recognized by Staufen 1. *Nature*, 519(7544):491–494.

Suizu, F., Ryo, A., Wulf, G., Lim, J., and Lu, K. P. (2006). Pin1 Regulates Centrosome Duplication, and Its Overexpression Induces Centrosome Amplification, Chromosome Instability, and Oncogenesis. *Molecular and Cellular Biology*, 26(4):1463–1479.

Supek, F., Bošnjak, M., Škunca, N., and Šmuc, T. (2011). Revigo summarizes and visualizes long lists of gene ontology terms. *PLoS ONE*, 6(7):e21800.

Swann, M. M. (1951). Protoplasmic Structure and Mitosis. *Journal of Experimental Biology*, 28(4).

Szerlong, H. J., Herman, J. A., Krause, C. M., Deluca, J. G., Skoultchi, A., Winger, Q. A., Prenni, J. E., and Hansen, J. C. (2015). Proteomic Characterization of the Nucleolar Linker Histone H1 Interaction Network. *Journal of Molecular Biology*, 427(11):2056–2071.

Tafforeau, L., Zorbas, C., Langhendries, J. L., Mullineux, S. T., Stamatopoulou, V., Mullier, R., Wacheul, L., and Lafontaine, D. J. (2013). The complexity of human ribosome biogenesis revealed by systematic nucleolar screening of pre-rRNA processing factors. *Molecular Cell*, 51(4):539–551.

Tajrishi, M. M., Tuteja, R., and Tuteja, N. (2011). Nucleolin: The most abundant multifunctional phosphoprotein of nucleolus. *Communicative and Integrative Biology*, 4(3):267–275.

Takahashi, N., Hayano, T., and Suzuki, M. (1989). Peptidyl-prolyl cis-trans isomerase is the cyclosporin A-binding protein cyclophilin. *Nature*, 337(6206):473–5.

Tang, H. M. and Poon, R. Y. (2011). How protein kinases co-ordinate mitosis in animal cells. *Biochem. J*, 435(1):17–31.

Tanveer, a., Virji, S., Andreeva, L., Totty, N. F., Hsuan, J. J., Ward, J. M., and Crompton, M. (1996). Involvement of cyclophilin D in the activation of a mitochondrial pore by Ca2+ and oxidant stress. *European journal of biochemistry / FEBS*, 238(1):166–72.

Tegha-Dunghu, J., Neumann, B., Reber, S., Krause, R., Erfle, H., Walter, T., Held, M., Rogers, P., Hupfeld, K., Ruppert, T., Ellenberg, J., Gruss, O. J. O., Erfie, H., Walter, T., Held, M., Rogers, P., Hupfeld, K., Ruppert, T., Ellenberg, J., and Gruss, O. J. O. (2008). Eml3 is a nuclear microtubule-binding protein required for the correct alignment of chromosomes in metaphase. *Journal of Cell Science*, 121(Pt 10):jcs–019174.

Thiele, A., Krentzlin, K., Erdmann, F., Rauh, D., Hause, G., Zerweck, J., Kilka, S., Pösel, S., Fischer, G., Schutkowski, M., and Weiwad, M. (2011). Parvulin 17 promotes microtubule assembly by its peptidyl-prolyl cis/trans isomerase activity. *Journal of Molecular Biology*, 411(4):896–909.

Thomas, M. G., Martinez Tosar, L. J., Loschi, M., Pasquini, J. M., Correale, J., Kindler, S., and Boccaccio, G. L. (2005). Staufen recruitment into stress granules does not affect early mRNA transport in oligodendrocytes. *Molecular biology of the cell*, 16(1):405–20.

Thompson, L. J. and Fields, A. P. (1996). beta II protein kinase C is required for the G2/M phase transition of cell cycle. *The Journal of biological chemistry*, 271(25):15045–15053.

Thomson, E., Ferreira-Cerca, S., and Hurt, E. (2013). Eukaryotic ribosome biogenesis at a glance. *Journal of cell science*, 126(Pt 21):4815–21.

Thorslund, T., Ripplinger, A., Hoffmann, S., Wild, T., Uckelmann, M., Villumsen, B., Narita, T., Sixma, T. K., Choudhary, C., Bekker-Jensen, S., and Mailand, N. (2015). Histone H1 couples initiation and amplification of ubiquitin signalling after DNA damage. *Nature*, 527(7578):389–93.

Uchida, M., Shiraishi, H., Ohta, S., Arima, K., Taniguchi, K., Suzuki, S., Okamoto, M., Ahlfeld, S. K., Ohshima, K., Kato, S., Toda, S., Sagara, H., Aizawa, H., Hoshino, T., Conway, S. J., Hayashi, S., and Izuhara, K. (2012). Periostin, a matricellular protein, plays a role in the induction of chemokines in pulmonary fibrosis. *American Journal of Respiratory Cell and Molecular Biology*, 46(5):677–686.

Ugrinova, I., Monier, K., Ivaldi, C., Thiry, M., Storck, S., Mongelard, F., and Bouvet, P. (2007). Inactivation of nucleolin leads to nucleolar disruption, cell cycle arrest and defects in centrosome duplication. *BMC Molecular Biology*, 8(1):66.

Uhlen, M., Fagerberg, L., Hallstrom, B. M., Lindskog, C., Oksvold, P., Mardinoglu, A., Sivertsson, A., Kampf, C., Sjostedt, E., Asplund, A., Olsson, I., Edlund, K., Lundberg, E., Navani, S., Szigyarto, C. A.-K., Odeberg, J., Djureinovic, D., Takanen, J. O., Hober, S., Alm, T., Edqvist, P.-H., Berling, H., Tegel, H., Mulder, J., Rockberg, J., Nilsson, P., Schwenk, J. M., Hamsten, M., von Feilitzen, K., Forsberg, M., Persson, L., Johansson, F., Zwahlen, M., von Heijne, G., Nielsen, J., and Ponten, F. (2015). Tissue-based map of the human proteome. *Science*, 347(6220):1260419–1260419.

Urfer, S. R., Kaeberlein, T. L., Mailheau, S., Bergman, P. J., Creevy, K. E., Promislow, D. E. L., and Kaeberlein, M. (2017). A randomized controlled trial to establish effects of short-term rapamycin treatment in 24 middle-aged companion dogs. *GeroScience*.

van de Loosdrecht, A. A., Beelen, R. H. J., Ossenkoppele, G. J., Broekhoven, M. G., and Langenhuijsen, M. M. A. C. (1994). A tetrazolium-based colorimetric MTT assay to quantitate human monocyte mediated cytotoxicity against leukemic cells from cell lines and patients with acute myeloid leukemia. *Journal of Immunological Methods*, 174(1-2):311–320.

Van Duyne, G. D., Standaert, R. F., Karplus, P. A., Schreiber, S. L., and Clardy, J. (1991). Atomic structure of FKBP-FK506, an immunophilin-immunosuppressant complex. *Science (New York, N.Y.)*, 252(5007):839–42.

Van Zundert, G. C. P., Rodrigues, J. P. G. L. M., Trellet, M., Schmitz, C., Kastritis, P. L., Karaca, E., Melquiond, A. S. J., Van Dijk, M., De Vries, S. J., and Bonvin, A. M. J. J. (2016). The HADDOCK2.2 Web Server: User-Friendly Integrative Modeling of Biomolecular Complexes. *Journal of Molecular Biology*, 428(4):720–725.

Vellai, T., Takacs-Vellai, K., Zhang, Y., Kovacs, A. L., Orosz, L., and Müller, F. (2003). Genetics: influence of TOR kinase on lifespan in C. elegans. *Nature*, 426(December):620.

Verdecia, M. A., Bowman, M. E., Lu, K. P., Hunter, T., and Noel, J. P. (2000).

Structural basis for phosphoserine-proline recognition by group IV WW domains. *Nature structural biology*, 7(8):639–643.

Viklund, I. M., Aspenström, P., Meas-Yedid, V., Zhang, B., Kopec, J., Ågren, D., Schneider, G., D'Amato, M., Olivo-Marin, J. C., Sansonetti, P., Van Nhieu, G. T., and Pettersson, S. (2009). WAFL, a new protein involved in regulation of early endocytic transport at the intersection of actin and microtubule dynamics. *Experimental Cell Research*, 315(6):1040–1052.

Villoria, M. T., Ramos, F., Dueñas, E., Faull, P., Cutillas, P. R., and Clemente-Blanco, A. (2017). Stabilization of the metaphase spindle by Cdc14 is required for recombinational DNA repair. *The EMBO Journal*, 36(1):79–101.

Walczak, C. E., Cai, S., and Khodjakov, A. (2010). Mechanisms of chromosome behaviour during mitosis. *Nature reviews. Molecular cell biology*, 11(2):91–102.

Walczak, C. E. and Heald, R. (2008). Mechanisms of Mitotic Spindle Assembly and Function. *International Review of Cytology*, 265:111–158.

Walker, J. R., Corpina, R. A., and Goldberg, J. (2001). Structure of the Ku heterodimer bound to DNA and its implications for double-strand break repair. *Nature*, 412(6847):607–14.

Wang, G., Gao, X., Huang, Y., Yao, Z., Shi, Q., and Wu, M. (2010a). Nucleophosmin/B23 inhibits Eg5-mediated microtubule depolymerization by inactivating its ATPase activity. *Journal of Biological Chemistry*, 285(25):19060–19067.

Wang, M., Wu, W., Wu, W., Rosidi, B., Zhang, L., Wang, H., and Iliakis, G. (2006). PARP-1 and Ku compete for repair of DNA double strand breaks by distinct NHEJ pathways. *Nucleic Acids Research*, 34(21):6170–6182.

Wang, P. and Heitman, J. (2005). The cyclophilins. *Genome biology*, 6(7):226.

Wang, Y., Han, R., Zhang, W., Yuan, Y., Zhang, X., Long, Y., and Mi, H. (2008). Human CyP33 binds specifically to mRNA and binding stimulates PPIase activity of hCyP33. *FEBS Letters*, 582(5):835–839.

Wang, Y. and Mandelkow, E. (2015). Tau in physiology and pathology. *Nature reviews. Neuroscience*, 17(1):22–35.

Wang, Z., Song, J., Milne, T. A., Wang, G. G., Li, H., Allis, C. D., and Patel, D. J. (2010b). Pro isomerization in MLL1 PHD3-Bromo cassette connects H3K4me readout to CyP33 and HDAC-mediated repression. *Cell*, 141(7):1183–1194.

Ward, B. K., Mark, P. J., Ingram, D. M., Minchin, R. F., and Ratajczak, T. (1999). Expression of the estrogen receptor-associated immunophilins, cyclophilin 40 and FKBP52, in breast cancer. *Breast cancer research and treatment*, 58(3):267–80.

Ward, I. M. and Chen, J. (2001). Histone H2AX Is Phosphorylated in an ATR-dependent Manner in Response to Replicational Stress. *Journal of Biological Chemistry*, 276(51):47759–47762.

Wassenaar, T. A., van Dijk, M., Loureiro-Ferreira, N., van der Schot, G., de Vries, S. J., Schmitz, C., van der Zwan, J., Boelens, R., Giachetti, A., Ferella, L., Rosato, A., Bertini, I., Herrmann, T., Jonker, H. R. A., Bagaria, A., Jaravine, V., Güntert, P., Schwalbe, H., Vranken, W. F., Doreleijers, J. F., Vriend, G., Vuister, G. W., Franke, D., Kikhney, A., Svergun, D. I., Fogh, R. H., Ionides, J., Laue, E. D., Spronk, C., Jurkša, S., Verlato, M., Badoer, S., Dal Pra, S., Mazzucato, M., Frizziero, E., and Bonvin, A. M. J. J. (2012). WeNMR: Structural Biology on the Grid. *Journal of Grid Computing*, 10(4):743–767.

Watashi, K., Ishii, N., Hijikata, M., Inoue, D., Murata, T., Miyanari, Y., and Shimotohno, K. (2005). Cyclophilin B is a functional regulator of hepatitis C virus RNA polymerase. *Molecular Cell*, 19(1):111–122.

Wehrens, X. H. T., Lehnart, S. E., Reiken, S. R., Deng, S. X., Vest, J. A., Cervantes, D., Coromilas, J., Landry, D. W., and Marks, A. R. (2004). Protection from Cardiac Arrhythmia Through Ryanodine Receptor-Stabilizing Protein Calstabin2. *Science*, 304(5668):292–296.

Wei, H. and Yu, X. (2016). Functions of PARylation in DNA Damage Repair Pathways. *Genomics, Proteomics & Bioinformatics*, 14(3):131–139.

Weil, T. T., Parton, R. M., and Davis, I. (2010). Making the message clear: visualizing mRNA localization. *Trends in cell biology*, 20(7):380–90.

Weiss, M. S., Jabs, a., and Hilgenfeld, R. (1998). Peptide bonds revisited. *Nature structural biology*, 5(8):676.

White, D., Rafalska-Metcalf, I. U., Ivanov, A. V., Corsinotti, A., Peng, H., Lee, S. C., Trono, D., Janicki, S. M., and Rauscher 3rd, F. J. (2012). The ATM substrate

KAP1 controls DNA repair in heterochromatin: regulation by HP1 proteins and serine 473/824 phosphorylation. *Mol Cancer Res*, 10(3):401–414.

Wilcox, C. B., Rossettini, A., and Hanes, S. D. (2004). Genetic interactions with C-terminal domain (CTD) kinases and the CTD of RNA pol II suggest a role for ESS1 in transcription initiation and elongation in Saccharomyces cerevisiae. *Genetics*, 167(1):93–105.

Wilson, T. E., Grawunder, U., and Lieber, M. R. (1997). Yeast DNA ligase IV mediates non-homologous DNA end joining. *Nature*, 388(6641):495–8.

Wittmann, T., Hyman, A., and Desai, A. (2001). The spindle: a dynamic assembly of microtubules and motors. *Nature cell biology*, 3(1):E28–34.

Wittmann, T., Wilm, M., Karsenti, E., and Vernos, I. (2000). TPX2, a novel Xenopus MAP involved in spindle pole organization. *Journal of Cell Biology*, 149(7):1405–1418.

Wochnik, G. M., Rüegg, J., Abel, G. A., Schmidt, U., Holsboer, F., and Rein, T. (2005). FK506-binding proteins 51 and 52 differentially regulate dynein interaction and nuclear translocation of the glucocorticoid receptor in mammalian cells. *Journal of Biological Chemistry*, 280(6):4609–4616.

Wulf, G. M., Ryo, A., Wulf, G. G., Lee, S. W., Niu, T., Petkova, V., and Lu, K. P. (2001). Pin1 is overexpressed in breast cancer and cooperates with Ras signaling in increasing the transcriptional activity of c-Jun towards cyclin D1. *EMBO Journal*, 20(13):3459–3472.

Xiao, H., Jackson, V., and Lei, M. (2006). The FK506-binding protein, Fpr4, is an acidic histone chaperone. *FEBS Letters*, 580(18):4357–4364.

Xu, G. G., Zhang, Y., Mercedes-Camacho, A. Y., and Etzkorn, F. A. (2011). A reduced-amide inhibitor of pin1 binds in a conformation resembling a twisted-amide transition state. *Biochemistry*, 50(44):9545–9550.

Xu, Y., Ayrapetov, M. K., Xu, C., Gursoy-Yuzugullu, O., Hu, Y., and Price, B. D. (2012). Histone H2A.Z Controls a Critical Chromatin Remodeling Step Required for DNA Double-Strand Break Repair. *Molecular Cell*, 48(5):723–733.

Xu, Y., Hirose, Y., Zhou, X., and Lu, K. (2003). Pin1 modulates the structure and function of human RNA polymerase II. *Genes & development*, 17(22):2765–2776.

Xu, Y. X. and Manley, J. L. (2007). Pin1 modulates RNA polymerase II activity during the transcription cycle. *Genes and Development*, 21(22):2950–2962.

Yaffe, M. B. (1997). Sequence-Specific and Phosphorylation-Dependent Proline Isomerization: A Potential Mitotic Regulatory Mechanism. *Science*, 278(5345):1957–1960.

Yang, W. M., Yao, Y. L., and Seto, E. (2001). The Fk506-binding protein 25 functionally associates with histone deacetylases and with transcription factor YY1. *EMBO Journal*, 20(17):4814–4825.

Yao, Y. L., Liang, Y. C., Huang, H. H., and Yang, W. M. (2011). FKBPs in chromatin modification and cancer. *Current Opinion in Pharmacology*, 11(4):301–307.

Yeh, E., Cunningham, M., Arnold, H., Chasse, D., Monteith, T., Ivaldi, G., Hahn, W. C., Stukenberg, P. T., Shenolikar, S., Uchida, T., Counter, C. M., Nevins, J. R., Means, A. R., and Sears, R. (2004). A signalling pathway controlling c-Myc degradation that impacts oncogenic transformation of human cells. *Nature cell biology*, 6(4):308–18.

Yi, P., Wu, R.-C., Sandquist, J., Wong, J., Tsai, S. Y., Tsai, M.-J., Means, A. R., and O'Malley, B. W. (2005). Peptidyl-prolyl isomerase 1 (Pin1) serves as a coactivator of steroid receptor by regulating the activity of phosphorylated steroid receptor coactivator 3 (SRC-3/AIB1). *Molecular and cellular biology*, 25(21):9687–99.

Yu, A. M. and McVey, M. (2010). Synthesis-dependent microhomology-mediated end joining accounts for multiple types of repair junctions. *Nucleic Acids Research*, 38(17):5706–5717.

Yu, G., Wang, L.-G., Han, Y., and He, Q.-Y. (2012). clusterProfiler: an R Package for Comparing Biological Themes Among Gene Clusters. *OMICS: A Journal of Integrative Biology*, 16(5):284–287.

Yuan, X., Feng, W., Imhof, A., Grummt, I., and Zhou, Y. (2007). Activation of RNA Polymerase I Transcription by Cockayne Syndrome Group B Protein and Histone Methyltransferase G9a. *Molecular Cell*, 27(4):585–595.

Zajkowicz, A., Gdowicz-Kłosok, A., Krześniak, M., Ścieglińska, D., and Rusin, M. (2015). Actinomycin D and nutlin-3a synergistically promote phosphorylation of p53 on serine 46 in cancer cell lines of different origin. *Cellular Signalling*, 27(9):1677–1687.

Zemp, I. and Kutay, U. (2007). Nuclear export and cytoplasmic maturation of ribosomal subunits. *FEBS Letters*, 581(15):2783–2793.

Zhang, S., Schlott, B., Görlach, M., and Grosse, F. (2004). DNA-dependent protein kinase (DNA-PK) phosphorylates nuclear DNA helicase II/RNA helicase A and hnRNP proteins in an RNA-dependent manner. *Nucleic Acids Research*, 32(1):1–10.

Zhang, Y. and Lu, H. (2009). Signaling to p53: Ribosomal Proteins Find Their Way. *Cancer Cell*, 16(5):369–377.

Zhou, X. Z. and Lu, K. P. (2016). The isomerase Pin1 controls numerous cancer-driving pathways acting as a unique drug target. *Nature Reviews Cancer*, 16(7):463–478.

Zimmermann, M., Lottersberger, F., Buonomo, S. B., Sfeir, A., and de Lange, T. (2013). 53BP1 regulates DSB repair using Rif1 to control 5' end resection. *Science (New York, N.Y.)*, 339(6120):700–4.

Zitvogel, L., Galluzzi, L., Smyth, M., Kroemer, G., Rizvi, N., Lesokhin, A., Segal, N., Ariyan, C., Gordon, R., Reed, K., and et Al. (2013). Mechanism of action of conventional and targeted anticancer therapies: reinstating immunosurveillance. *Immunity*, 39(1):74–88.

Zoldák, G., Aumüller, T., Lücke, C., Hritz, J., Oostenbrink, C., Fischer, G., and Schmid, F. X. (2009). A library of fluorescent peptides for exploring the substrate specificities of prolyl isomerases. *Biochemistry*, 48(43):10423–10436.

Appendix A

This appendix contains additional figures and tables that support the results discussed in the main body of this thesis.

A.1 Supplementary Figures

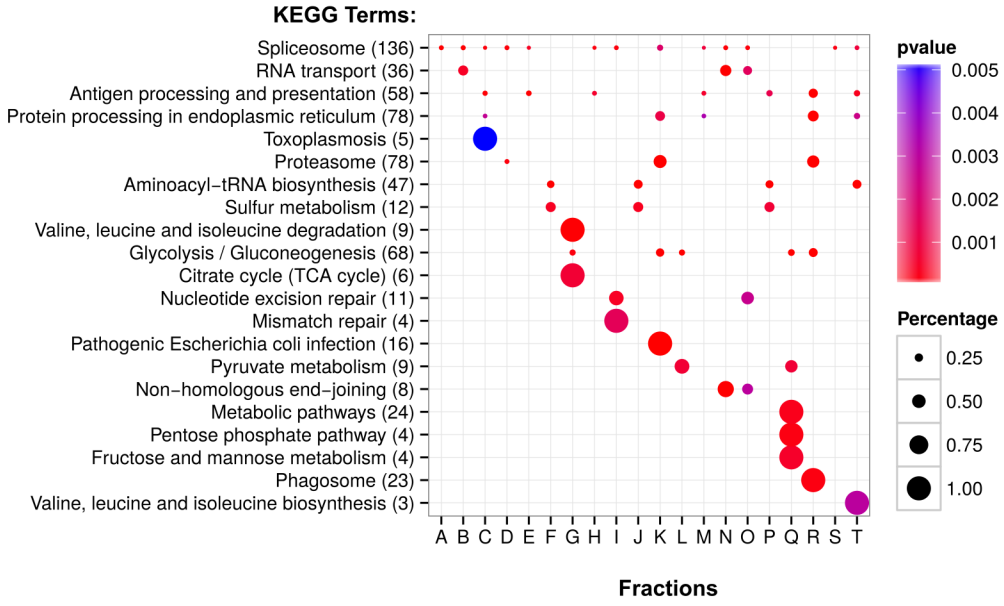

Figure A1. KEGG pathway analysis of FKBP25 co-fractionating proteins identified in Havugimana et al. (2012). In this study, Havugimana et al. quantitatively analyzed the protein composition of over 1000 biochemical fractions. The analysis performed here took into consideration all biological fractions with greater than 5 FKBP25 peptides identified. Each of these fractions was than than analyzed for enriched of KEGG pathway terms using the R package clusterProfiler (Yu et al., 2012).

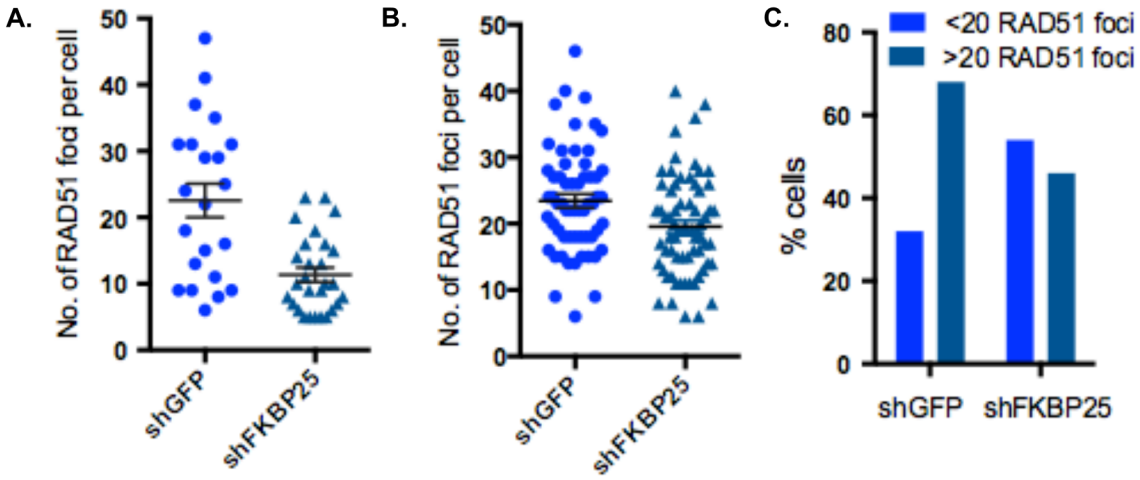

Figure A2. FKBP25 impairs Rad51 foci formation in response to DNA damage. An independent validation peformed by Dr. Fade Gong in the labratory of Dr Kyle Miller at the University of Texas at Austin (A) Rad51 foci formation in response to etoposide. shRNA knockdown cells treated with 100 µM washed and incubated for 2 h. 20 cells counted per sample. (B) Rad51 requirement in response to IR. Cells treated with 5 Gy of radiation and incubated for 2 h. 60 cells counted per condition. Both A-B imaged on a Olympus FV1000 confocal microscope. (C) Quantification of cells with greater or less than 20 Rad51 foci per cell from panel B.

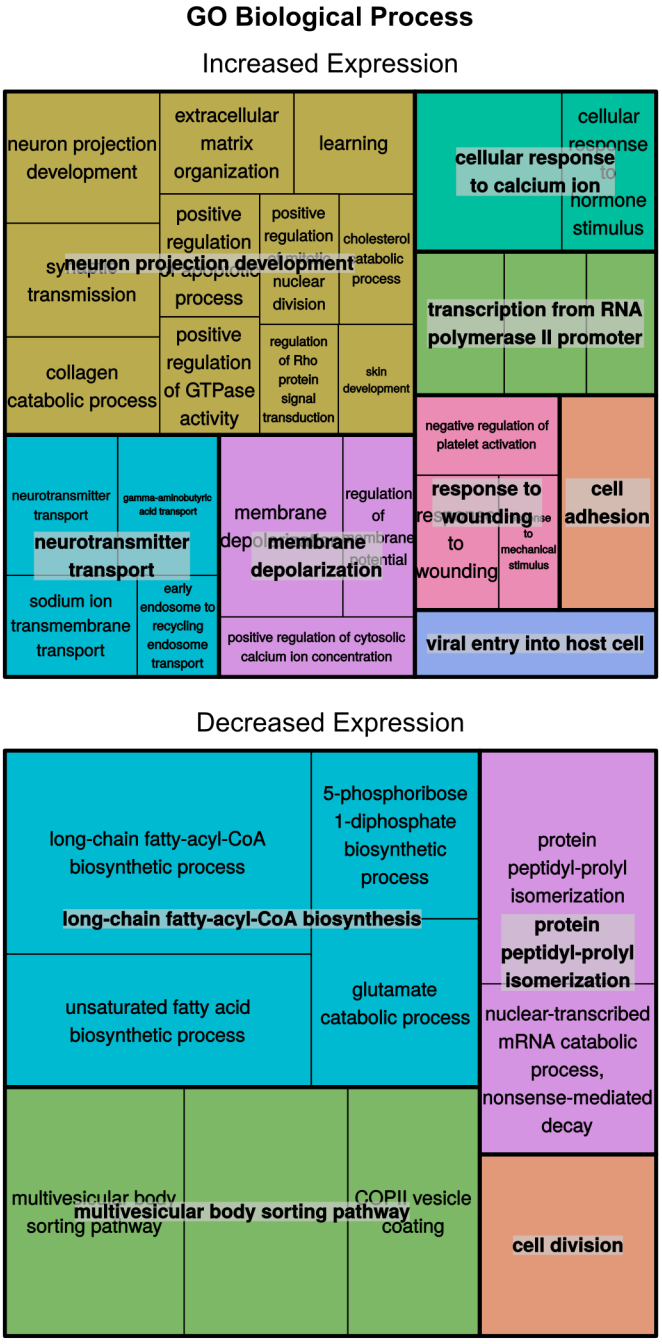

Figure A3. Treemap depicting enriched gene ontology terms associated with altered gene expression in FKBP25 knockdown cells

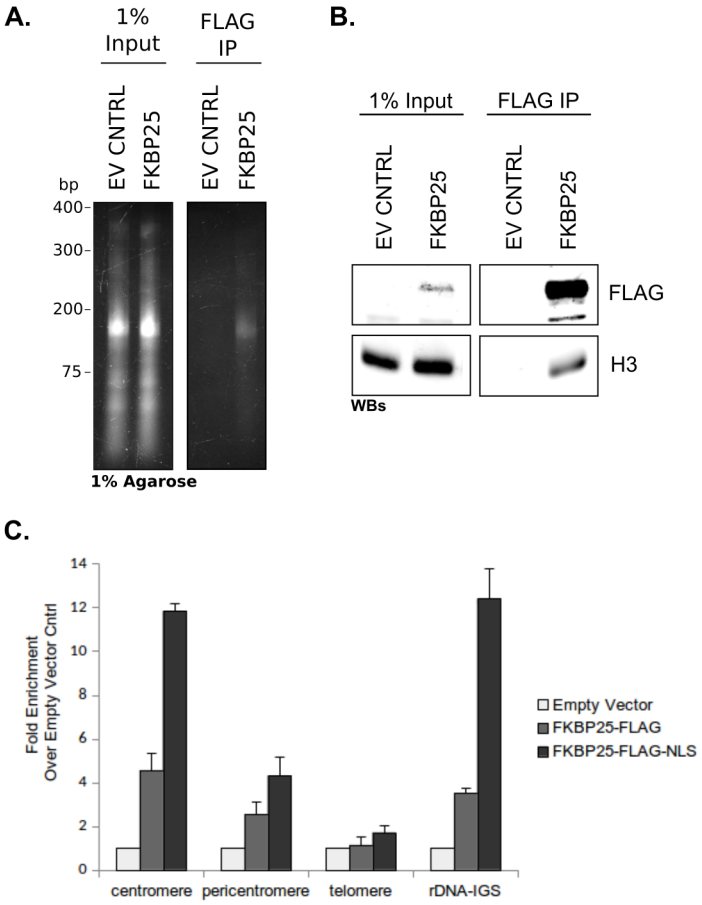

Figure A4. FKBP25 associates with repetitive elements by chromatin immunoprecipitation. (A) Agarose gel showing enrichment of DNA by chromatin immunoprecipitation of FKBP25. This material was sent for sequencing at the BC Genome Science Center on a MiSeq system (Illumina) (B) Western blot analysis of FKBP25 ChIP material showing FKBP25 interacts with histone H3 (C) qPCR analysis of ChIP DNA, showing FKBP25 is associated with repetitive elements in the genome. Results shown as mean ± of three technical replicates.

A.2 Supplementary Tables

Table A.1. Overview of Pin1-associated transcription factors. [1]

Target	Site of Recog.	Upstream Kinase	Mechanism	PPI Activity	Ref.
cJun	pSer63-Pro pSer73-Pro	JNK/ SAPKs	Promotes stability - inhibits ubiquitylation (+)	Y	Wulf et al. (2001); Pulikkan et al. (2010)
p73	pSer412-Pro pThr442-Pro pThr482-Pro	p38mapk	Promotes Stability stimulates acetylation via p300 (+)	Y	Mantovani et al. (2004)
RAR	pSer77-Pro	Cdk7	Promotes ubiquitin-mediated degradation (-)	ND	Brondani et al. (2005)
IRF3	pSer339-Pro	ND	Promotes ubiquitin-mediated degradation (-)	Y	Saitoh et al. (2006)
Che-1	pThr144-Pro	ATM/ ATR and Chk2	Promotes ubiquitin-mediated degradation (-)	Y	De Nicola et al. (2007)
SMRT	pSer1241-Pro T1445-Pro	Cdk2	Facilitates degradation exact mechanism unclear (-)	Y	Stanya et al. (2008)
PPAR	pSer84-Pro	ND	Promotes stability - inhibits ubiquitylation (+)	N	Fujimoto et al. (2010)
Smad2/ Smad3	pThr179-Pro pSer204-Pro pSer 208-Pro pSer213-Pro	TR-I	Promotes degradation (-)	Y	Nakano et al. (2009)
Spt23	pSer654-Pro	casein kinase 2	Inhibits ubiquiyltation promotes stabilty (+)	Y	Siepe and Jentsch (2009)
MEF2	pSer98-Pro pSer110-Pro pSer240-Pro pSer388 -Pro	ND	Decreases stability/activity exact mechanism unclear (-)	Y	Magli et al. (2010)
Nanog	pSer52-Pro pSer65-Pro	ND	Promotes stability - inhibits ubiquitylation (+)	Y	Moretto-Zita et al. (2010)
Oct4	pSer12-Pro	ND	Promotes stability - inhibits ubiquitylation (+)	Y	Nishi et al. (2011)
SRC-3/ AIB1	ND	ND	Promotes formation of co-activator complex/increases protein turn-over (+/-)	Y	Yi et al. (2005)
STAT3	pSer727-Pro	ND	Recruitement of co-activator (+)	N	Lufei et al. (2007)
c-Myb	pSer528-Pro	MAPK	Transactivation potenitally facilitates interaction with co-activators (+)	Y	Pani et al. (2008)
SF-1	pSer203-Pro	ERK1/2 or CDK7	Promotes ubiquitylation facilitating SF-1-Pitx1 interaction/increases protein-turn-over (+/-)	Y	Luo et al. (2010)
β-catenin	pSer246-Pro	ND	Increases translocation inhibits degradation (+)	Y	Ryo et al. (2001)
p65/ RelA	pThr254-Pro	ND	Inhibits p65 binding to IkBa enhances nuclear localization and protein stability (+)	Y	Ryo et al. (2003)
FoxO	ND	ND	Prevents monoubiquitination inhibiting translocation into the nucleus (-)	Y	Brenkman et al. (2008)

Overview of Pin1-associated transcription factors.

Target	Site of Recog.	Upstream Kinase	Mechanism	PPI Activity	Ref.
CRTC2	pSer136-Pro	ND	Induces translocation to cytosol (-)	ND	Nakatsu et al. (2010)
nFAT	ND	ND	Inhibits dephosphorylation translocation in nucleus (-)	Y	Liu et al. (2001)
c-Myc	pThr58-Pro pSer62-Pro	ERKs	Dephosphorylation of Ser62 by PP2A promotes turnover by ubquitin-proteasome pathway (-)	ND	Yeh et al. (2004)
Rpb1	pSer2-Pro pSer5-Pro	Cdk7 Cdk9	Dephosphorylation by Fcp1	Y	Xu et al. (2003); Wilcox et al. (2004)
LSF	pSer291-Pro pSer309-Pro pThr329-Pro	Erk cyclin C/Cdk2	Promotes Dephosphorylation (+)	Y	Saxena et al. (2010)
Notch1	Ser-Thr-rich region (STR)	ND	Promotes cleavage by-secretas postive feedback on Pin1 (+)	Y	Rustighi et al. (2009)
cFos	pThr232-Pro pThr325-Pro pThr331-Pro pSer374-Pro	ERKs	Transactivation exact mechanism unclear (+)	Y	Monje et al. (2005)

Table A.2. FKBP25-BirA enriched proteins relative to BirA control identified by streptavidin capture and mass spectrometry

Uniprot Accession	Gene Name	Fold Change	Mass (Da)	BirA Cntrl No. of Significant Peptides	BirA Cntrl No. of Significant Sequences	FKBP25-BirA No. of Significant Peptides	FKBP25-BirA No. of Significant Sequences
Q00688	FKBP3	32.85	25161	2	2	84	14
P08779	KRT16	14.94	51236	0	0	12	7
P16402	HIST1H1D	14.94	22336	0	0	12	6
P02538	KRT6A	12.61	60008	0	0	10	8
Q96GQ7	DDX27	9.13	89779	0	0	7	7
O60814	HIST1H2BK	9.13	13882	0	0	7	5
P26373	RPL13	7.97	24247	0	0	6	5
P62266	RPS23	6.89	15798	1	1	11	5
O43790	KRT86	6.81	53466	0	0	5	5
P62917	RPL8	6.81	28007	0	0	5	4
P39023	RPL3	6.81	46080	0	0	5	5
O95793	STAU1	5.75	63143	2	2	14	9
P61254	RPL26	5.65	17248	0	0	4	4
Q14157	UBAP2L	5.65	114465	0	0	4	4
P84098	RPL19	5.15	23451	1	1	8	5
Q03001	DST	4.48	860127	0	0	3	3
Q9NUQ6	SPATS2L	4.48	61691	0	0	3	3
P62979	RPS27A	4.48	17953	0	0	3	3
Q86UP2	KTN1	4.48	156179	0	0	3	3
O75683	SURF6	4.48	41426	0	0	3	2
Q8NE71	ABCF1	4.48	95866	0	0	3	3
Q13283	G3BP1	4.48	52132	0	0	3	3
Q86UE4	MTDH	4.48	63799	0	0	3	3
Q8IZH2	XRN1	4.48	193985	0	0	3	2
Q9UHB9	SRP68	4.48	70686	0	0	3	3
P05388	RPLP0	4.48	34252	0	0	3	3
Q9NUL3	STAU2	4.2	62601	2	2	10	8
P02751	FN1	4.2	262460	2	2	10	8
Q8NC51	SERBP1	4.15	44938	4	4	17	11
P62424	RPL7A	3.98	29977	1	1	6	5
Q9Y3U8	RPL36	3.4	12246	1	1	5	4
P46060	RANGAP1	3.4	63502	1	1	5	5
Q8NDW8	TTC21A	3.32	150847	0	0	2	1
Q9H0P0	NT5C3A	3.32	37924	0	0	2	1
P57087	JAM2	3.32	33186	0	0	2	1
Q7Z739	Q7Z739	3.32	63822	0	0	2	2
Q86UR5	RIMS1	3.32	188956	0	0	2	2
P58417	NXPH1	3.32	31063	0	0	2	1
Q8TCU4	ALMS1	3.32	460683	0	0	2	1
P02452	COL1A1	3.32	138857	0	0	2	2
P05556	ITGB1	3.32	88357	0	0	2	2
O60841	EIF5B	3.32	138742	0	0	2	2
Q86Y07	VRK2	3.32	58104	0	0	2	2
Q7Z406	MYH14	3.32	227732	0	0	2	2
Q9BRP8	WIBG	3.32	22642	0	0	2	2
P50914	RPL14	3.32	23417	0	0	2	2

FKBP25-BirA enriched proteins relative to BirA control identified by streptavidin capture and mass spectrometry

Uniprot Accession	Gene Name	Fold Change	Mass (Da)	BirA Cntrl No. of Significant Peptides	BirA Cntrl No. of Significant Sequences	FKBP25-BirA No. of Significant Peptides	FKBP25-BirA No. of Significant Sequences
Q9HAV0	GNB4	3.32	37543	0	0	2	2
O76021	RSL1D1	3.32	54939	0	0	2	2
P18621	RPL17	3.32	21383	0	0	2	2
Q14498	RBM39	3.32	59343	0	0	2	2
P46776	RPL27A	3.32	16551	0	0	2	2
Q9Y520	PRRC2C	3.32	316718	0	0	2	2
P62854	RPS26	3.32	13007	0	0	2	2
Q99733	NAP1L4	3.32	42797	0	0	2	2
P60866	RPS20	3.32	13364	0	0	2	2
Q8TEQ6	GEMIN5	3.32	168483	0	0	2	2
Q8WWM7	ATXN2L	3.32	113304	0	0	2	2
P45880	VDAC2	3.32	31547	0	0	2	2
P23396	RPS3	3.32	26671	0	0	2	2
Q9BVA1	TUBB2B	3.32	49921	0	0	2	2
P61247	RPS3A	3.15	29926	3	3	10	7
O00571	DDX3X	2.82	73198	1	1	4	4
Q9P2E9	RRBP1	2.66	152381	2	2	6	6
P0C0S8	HIST1H2AG	2.66	14083	2	2	6	3
Q04637	EIF4G1	2.29	175382	4	4	9	9
P61353	RPL27	2.28	15788	3	3	7	5
P50479	PDLIM4	2.27	35376	2	2	5	4
Q9Y6M1	IGF2BP2	2.27	66081	2	2	5	5
P61313	RPL15	2.27	24131	2	2	5	4
P49207	RPL34	2.24	13284	1	1	3	2
P46779	RPL28	2.24	15738	1	1	3	2
Q13442	PDAP1	2.24	20618	1	1	3	3
P83731	RPL24	2.24	17768	1	1	3	2
Q8IY81	FTSJ3	2.24	96499	1	1	3	3
P23588	EIF4B	2.06	69110	4	4	8	7

Table A.3. FKBP25-FLAG Co-IP enriched interacting proteins identified by mass spectrometry relative to empty vector control

RNase A Treated	Uniprot Accession	Gene Name	Fold Change	Mass (Da)	EV Cntrl No. of Significant Peptides	EV Cntrl No. of Significant Sequences	FKBP25-FLAG No. of Significant Peptides	FKBP25-FLAG No. of Significant Sequences
-	Q00688	FKBP3	56.2	25161	4	2	231	10
-	P11388	TOP2A	51.9	174276	0	0	42	18
-	Q9BQE3	TUBA1C	24.03	49863	0	0	19	9
-	Q9BQ39	DDX50	16.76	82514	0	0	13	4
-	P06899	HIST1H2BJ	15.54	13896	0	0	12	3
-	P11387	TOP1	14.33	90669	0	0	11	5
-	Q9BQG0	MYBBP1A	13.23	148762	1	1	21	12
-	Q9NR30	DDX21	12.05	87290	2	1	29	13
-	P46778	RPL21	11.91	18553	0	0	9	4
-	P17066	HSPA6	11.91	70984	0	0	9	4
-	P46087	NOP2	10.7	89247	0	0	8	5
-	Q02880	TOP2B	9.48	183152	0	0	7	4
-	P78527	PRKDC	9.48	468788	0	0	7	4
-	P61313	RPL15	9.48	24131	0	0	7	4
-	P39023	RPL3	9.34	46080	3	2	30	6
-	Q49A26	GLYR1	8.27	60518	0	0	6	3
-	P62263	RPS14	8.27	16263	0	0	6	3
-	P0C0S5	H2AFZ	8.27	13545	0	0	6	3
-	P04908	HIST1H2AB	8.27	14127	0	0	6	3
-	Q9NRI5	DISC1	7.06	93552	0	0	5	1
-	Q96SB4	SRPK1	7.06	74278	0	0	5	2
-	Q5SSJ5	HP1BP3	7.06	61169	0	0	5	4
-	P19013	KRT4	7.06	57250	0	0	5	4
-	Q9Y3U8	RPL36	5.85	12246	0	0	4	1
-	Q9NW13	RBM28	5.85	85685	0	0	4	1
-	Q92922	SMARCC1	5.85	122790	0	0	4	1
-	Q13868	EXOSC2	5.85	32768	0	0	4	1
-	P62937	PPIA	5.85	18001	0	0	4	2
-	P46783	RPS10	5.85	18886	0	0	4	2
-	P07237	P4HB	4.74	57081	1	1	7	3
-	Q9NZI8	IGF2BP1	4.64	63441	0	0	3	2
-	Q8TAQ2	SMARCC2	4.64	132797	0	0	3	1
-	Q86U86	PBRM1	4.64	192825	0	0	3	1
-	Q5RKV6	EXOSC6	4.64	28218	0	0	3	2
-	Q02388	COL7A1	4.64	295041	0	0	3	1
-	P84243	H3F3A	4.64	15318	0	0	3	2
-	P58107	P58107	4.64	555279	0	0	3	1
-	P27635	RPL10	4.64	24588	0	0	3	3
-	P12956	XRCC6	4.64	69799	0	0	3	1
-	P09874	PARP1	4.64	113012	0	0	3	2
-	O15131	KPNA5	4.64	60311	0	0	3	1
-	O00303	EIF3F	4.64	37540	0	0	3	1
-	P32969	RPL9	4.49	21850	3	2	14	4
-	Q9Y2X3	NOP58	4.14	59541	1	1	6	2
-	P46782	RPS5	3.58	22862	3	2	11	3
-	Q92522	H1FX	3.57	22474	2	1	8	4

FKBP25-FLAG Co-IP enriched interacting proteins identified by mass spectrometry relative to empty vector control

RNase A Treated	Uniprot Accession	Gene Name	Fold Change	Mass (Da)	EV Cntrl No. of Significant Peptides	EV Cntrl No. of Significant Sequences	FKBP25-FLAG No. of Significant Peptides	FKBP25-FLAG No. of Significant Sequences
-	Q9ULU4	ZMYND8	3.42	131610	0	0	2	1
-	Q9UJV9	DDX41	3.42	69793	0	0	2	2
-	Q9NZK5	CECR1	3.42	58895	0	0	2	1
-	Q9NX58	LYAR	3.42	43588	0	0	2	1
-	Q9NQT4	EXOSC5	3.42	25233	0	0	2	1
-	Q9H0U9	TSPYL1	3.42	49162	0	0	2	1
-	Q96P11	NSUN5	3.42	46662	0	0	2	1
-	Q8WW22	DNAJA4	3.42	44769	0	0	2	1
-	Q8N684	CPSF7	3.42	52018	0	0	2	1
-	Q4ADV7	KIAA1432	3.42	159199	0	0	2	1
-	Q13247	SRSF6	3.42	39563	0	0	2	1
-	P63162	SNRPN	3.42	24598	0	0	2	1
-	P62987	UBA52	3.42	14719	0	0	2	1
-	P62888	RPL30	3.42	12776	0	0	2	1
-	P62829	RPL23	3.42	14856	0	0	2	1
-	P49137	MAPKAPK2	3.42	45538	0	0	2	1
-	P46779	RPL28	3.42	15738	0	0	2	1
-	P46776	RPL27A	3.42	16551	0	0	2	1
-	P46013	MKI67	3.42	358474	0	0	2	1
-	P42285	SKIV2L2	3.42	117729	0	0	2	1
-	P40227	CCT6A	3.42	57988	0	0	2	1
-	P26196	DDX6	3.42	54382	0	0	2	1
-	P07305	H1F0	3.42	20850	0	0	2	1
-	P06748	NPM1	3.42	32555	0	0	2	1
-	P06493	CDK1	3.42	34074	0	0	2	1
-	P04085	PDGFA	3.42	24028	0	0	2	1
-	O75475	PSIP1	3.42	60067	0	0	2	1
-	O00629	KPNA4	3.42	57851	0	0	2	1
-	O00567	NOP56	3.42	66009	0	0	2	1
-	P62081	RPS7	3.28	22113	3	2	10	4
-	P46777	RPL5	3.16	34341	2	1	7	5
-	P78347	GTF2I	3.1	112346	13	6	35	16
-	Q9UKN8	GTF3C4	2.92	91923	1	1	4	1
-	Q8NC51	SERBP1	2.92	44938	1	1	4	3
-	Q6NVV1	Q6NVV1	2.92	12127	1	1	4	2
-	P62266	RPS23	2.92	15798	1	1	4	2
-	P18124	RPL7	2.87	29207	4	2	11	5
-	Q5QNW6	HIST2H2BF	2.79	13912	5	2	13	4
-	Q92499	DDX1	2.76	82380	2	1	6	2
-	P46781	RPS9	2.74	22578	6	3	15	8
-	P19338	NCL	2.64	76568	15	8	34	14
-	P61247	RPS3A	2.62	29926	4	2	10	5
-	P26373	RPL13	2.62	24247	4	2	10	4
-	Q02878	RPL6	2.52	32708	9	5	20	9
-	Q96AV8	E2F7	2.35	99826	2	1	5	3
-	P83731	RPL24	2.35	17768	2	1	5	2

FKBP25-FLAG Co-IP enriched interacting proteins identified by mass spectrometry relative to empty vector control

RNase A Treated	Uniprot Accession	Gene Name	Fold Change	Mass (Da)	EV Cntrl No. of Significant Peptides	EV Cntrl No. of Significant Sequences	FKBP25-FLAG No. of Significant Peptides	FKBP25-FLAG No. of Significant Sequences
-	P05386	RPLP1	2.35	11507	2	1	5	2
-	P62917	RPL8	2.14	28007	4	2	8	4
-	P61353	RPL27	2.14	15788	4	2	8	4
-	P62851	RPS25	2.07	13734	3	2	6	3
-	P30050	RPL12	2.07	17808	3	1	6	2
+	Q00688	FKBP3	199.71	25161	1	1	210	13
+	P60709	ACTB	33.25	41710	0	0	17	7
+	P04259	KRT6B	25.66	60030	0	0	13	6
+	P11388	TOP2A	23.77	174276	0	0	12	6
+	Q9Y250	LZTS1	19.97	66572	0	0	10	1
+	Q8IUE6	HIST2H2AB	19.97	13987	0	0	10	3
+	Q13509	Q13509	18.07	50400	0	0	9	4
+	P08779	KRT16	18.07	51236	0	0	9	6
+	O75367	H2AFY	16.18	39592	0	0	8	4
+	P81605	DCD	12.38	11277	0	0	6	3
+	Q9NRI5	DISC1	8.59	93552	0	0	4	1
+	Q15424	SAFB	8.59	102580	0	0	4	2
+	Q14676	MDC1	8.59	226529	0	0	4	2
+	P09874	PARP1	6.47	113012	10	6	37	17
+	Q86YZ3	HRNR	5.39	282228	2	1	8	3
+	Q9P1Z9	CCDC180	4.79	190979	0	0	2	1
+	Q8TAQ2	SMARCC2	4.79	132797	0	0	2	1
+	Q8NHM4	Q8NHM4	4.79	26522	0	0	2	1
+	Q7RTV0	PHF5A	4.79	12397	0	0	2	1
+	Q56NI9	ESCO2	4.79	68264	0	0	2	2
+	Q14980	NUMA1	4.79	238115	0	0	2	1
+	Q13247	SRSF6	4.79	39563	0	0	2	1
+	Q08945	SSRP1	4.79	81024	0	0	2	1
+	Q02388	COL7A1	4.79	295041	0	0	2	1
+	P14625	HSP90B1	4.79	92411	0	0	2	1
+	P12956	XRCC6	4.79	69799	0	0	2	1
+	P04085	PDGFA	4.79	24028	0	0	2	1
+	Q16695	HIST3H3	4.76	15499	2	1	7	3
+	Q96AV8	E2F7	4.29	99826	1	1	4	2
+	P78527	PRKDC	3.99	468788	4	3	10	5
+	P62805	HIST1H4A	3.62	11360	15	4	30	7
+	Q92522	H1FX	3.35	22474	1	1	3	2
+	P0C0S5	H2AFZ	2.58	13545	6	4	9	4
+	P35813	PPM1A	2.48	42421	4	2	6	3
+	P55072	VCP	2.4	89266	1	1	2	1
+	P13010	XRCC5	2.4	82652	1	1	2	2
+	P06899	HIST1H2BJ	2.32	13896	15	3	19	4
+	Q5QNW6	HIST2H2BF	2.29	13912	16	4	20	5
+	Q9C005	DPY30	2.23	11243	2	1	3	1
+	P07237	P4HB	2.23	57081	2	1	3	2
+	P01614	P01614	2.23	12668	2	1	3	1

FKBP25-FLAG Co-IP enriched interacting proteins identified by mass spectrometry relative to empty vector control

RNase A Treated	Uniprot Accession	Gene Name	Fold Change	Mass (Da)	EV Cntrl No. of Significant Peptides	EV Cntrl No. of Significant Sequences	FKBP25-FLAG No. of Significant Peptides	FKBP25-FLAG No. of Significant Sequences
+	Q08211	DHX9	2.22	140869	8	5	10	6

Table A.4. siRNA sense strand sequences

siRNA	**Sense Strand Sequence**	**Manufacturer**
siCNTRL	5′-GAUCAUACGUGCGAUCAGAtt-3′	Eurofins Genomics
siGFP	5′-GGCUACCAGGAGCGCACCtt-3′	Eurofins Genomics
siFKBP25	5′-CCACUUGGUUACAGCCUAUtt-3′	Eurofins Genomics
siFKBP25.2	5′-GCUCUAAGGAUAUUAGCAACAAUGA-3′	Integrated DNA Technologies (HSC.RNAi.N002013.12.2)
siRad52	SMARTpool pooled siRNA 5′-CAGAAGGUGUGCUACAUUG-3′ 5′-GGUCAUCGGGUAAUUAAUC-3′ 5′-GGAAGAGCCAGGACAUGAA-3′	Dharmacon (SO-2496476G)

Table A.5. shRNA targeting sequence

shRNA	**Targeting Sequence**	**Manufacturer**
shCNTRL(GFP)	5′-CACAAGCTGGAGTACAACTACAACAGCCA-3′	OriGene (TR30001)
shFKBP25.1	5′-CAGGAACACGGTTCAGATTCGTTTCTTGC-3′	OriGene (TR319727B)
shFKBP25.2	5′-TCGGAGTAGGCAAAGTTATCAGAGGATG-3′	OriGene (TR319727D)

Table A.6. DNA oligos used

Target	Type	Sequence	Application
GAPDH	Fwd	TGCACCACCAACTGCTTAGC	RT-qPCR
	Rev	GGCATGGACTGTGGTCATGAG	RT-qPCR
Pre-rRNA	Fwd	TGTCAGGCGTTCTCGTCTC	RT-qPCR
	Rev	AGCACGACGTCACCACATC	RT-qPCR
RN18S	Fwd	CGACGACCCATTCGAACGTC-	RT-qPCR
	Rev	CTCTCCGGAATCGAACCCTG	RT-qPCR
FKBP25	Fwd	CAAGGACCACTTGGTTACAGC	RT-qPCR
	Rev	CCAGCAGTGAACAACATCTCC	RT-qPCR
A-1 kb upstream	Fwd	CCGTGGGTTGTCTTCTGAC	ChIP
	Rev	AAGCGAAACCGTGAGTCG	ChIP
B- 5ETS	Fwd	CCTCCAGTGGTTGTCGACTT	ChIP
	Rev	GAACGACACACCACCGTTC	ChIP
C- ITS1	Fwd	CCCGTGGTGTGAAACCTTC	ChIP
	Rev	AAGAGGAGAGGGGGTTGC	ChIP
D- 28S	Fwd	AGTCGGGTTGCTTGGGAATGC	ChIP
	Rev	CCCTTACGGTACTTGTTGACT	ChIP
centromere	Fwd	CATCGAATGGAAATGAAAGGAGTC	ChIP
	Rev	ACCATTGGATGATTGCAGTCAA	ChIP
pericentromere	Fwd	ACGATCCTTTACAGAGCAGA	ChIP
	Rev	ATTGACCTCAAAGCGGCTGA	ChIP
telomere	Fwd	GGTTTTTGAGGGTGAGGGTGAGGGTGAGGGTGAGGGT	ChIP
	Rev	TCCCGACTATCCCTATCCCTATCCCTATCCCTATCCCTA	ChIP
rDNA-IGS	Fwd	GTGTGCCTCCGTCTTCTCTC	ChIP
	Rev	GTCAAGGGGCTATGCCATC	ChIP
ITS1	Probe	CCTCGCCCTCCGGGCTCCGTTAATTGATC	Northern
ITS2	Probe	CGCACCCCGAGGAGCCCGGAGGCACCCCCGG	Northern

Table A.7. RNA-Seq FKBP25 KD vs Control - top 100 upregulated genes ranked ranked by fold change.

Gene Symbol	Gene Name	GFOLD (0.01)	log2 Fold Change	siGFP (RPKM)	siFKBP25 (RPKM)
ENSG00000205922.4	ONECUT3	3.55476	4.0469	0.0517175	0.921808
ENSG00000060558.3	GNA15	2.58948	4.28829	0.00783967	0.238042
ENSG00000205867.2	KRTAP5-2	2.33536	2.90917	0.30287	2.46248
ENSG00000158525.11	CPA5	2.21681	3.94037	0.00669884	0.159023
ENSG00000164867.6	NOS3	2.10178	2.51606	0.12044	0.735199
ENSG00000153303.12	FRMD1	2.04226	3.44837	0.0106177	0.14068
ENSG00000183570.12	PCBP3	1.9634	2.21826	0.302935	1.49269
ENSG00000171219.8	CDC42BPG	1.90803	2.06723	0.901583	3.99114
ENSG00000140538.12	NTRK3	1.87759	4.76634	0	0.0311444
ENSG00000167195.7	GOLGA6C	1.85627	2.41788	0.182024	1.04835
ENSG00000129965.9	INS-IGF2	1.84317	2.14235	0.61973	2.9011
ENSG00000169896.12	ITGAM	1.80771	3.45821	0.00542411	0.0818491
ENSG00000072182.8	ASIC4	1.79745	2.63575	0.0292644	0.202488
ENSG00000167244.13	IGF2	1.73942	1.85617	1.53073	5.84984
ENSG00000006327.9	TNFRSF12A	1.73473	1.88591	3.40863	13.3042
ENSG00000162949.12	CAPN13	1.6799	4.58946	0	0.0478188
ENSG00000140478.10	GOLGA6D	1.67663	2.2034	0.21228	1.04941
ENSG00000181333.11	HEPHL1	1.65996	2.38782	0.0402419	0.230626
ENSG00000126895.9	AVPR2	1.64847	3.31382	0.013773	0.187556
ENSG00000165370.1	GPR101	1.63883	2.09469	0.409164	1.86634
ENSG00000103490.13	PYCARD	1.61036	3.38782	0.012333	0.197451
ENSG00000232423.3	PRAMEF6	1.60755	4.52533	0	0.0618791
ENSG00000108242.8	CYP2C18	1.60578	3.27535	0.0120737	0.159972
ENSG00000116014.5	KISS1R	1.60536	2.0659	0.365804	1.63579
ENSG00000149124.6	GLYAT	1.58887	3.17023	0.0145905	0.169154
ENSG00000168477.13	TNXB	1.58086	1.91068	0.0837448	0.33407
ENSG00000132698.9	RAB25	1.56624	2.09761	0.266827	1.22533
ENSG00000167103.7	PIP5KL1	1.56331	1.8625	0.469053	1.80757
ENSG00000215186.6	GOLGA6B	1.56186	2.12922	0.174224	0.82009
ENSG00000130287.9	NCAN	1.55559	3.33891	0.0029667	0.045859
ENSG00000165841.5	CYP2C19	1.55559	3.33891	0.0054729	0.0845996
ENSG00000198670.7	LPA	1.55559	3.33891	0.0031564	0.0487914
ENSG00000169429.6	IL8	1.51181	2.11798	0.148638	0.696254
ENSG00000157335.15	CLEC18C	1.47276	1.94938	0.119294	0.492204
ENSG00000170091.6	NSG2	1.45113	3.38782	0.00259567	0.0544536
ENSG00000142235.4	LMTK3	1.45	1.72137	0.380896	1.32959
ENSG00000164188.4	RANBP3L	1.42301	2.03372	0.100506	0.443892

RNA-Seq FKBP25 KD vs Control - top 100 upregulated genes ranked ranked by fold change.

Gene Symbol	Gene Name	GFOLD (0.01)	log2 Fold Change	siGFP (RPKM)	siFKBP25 (RPKM)
ENSG00000136931.5	NR5A1	1.42131	3.11029	0.00898204	0.105786
ENSG00000120738.7	EGR1	1.41705	1.52658	4.10941	12.4948
ENSG00000268470.1	DNAH17-AS1	1.41324	2.03273	0.0775215	0.342377
ENSG00000205869.2	KRTAP5-1	1.40684	2.10854	0.260956	1.22456
ENSG00000162426.10	SLC45A1	1.40138	2.0215	0.113491	0.497321
ENSG00000100336.13	APOL4	1.36614	3.31382	0.00234115	0.0465291
ENSG00000188263.6	IL17REL	1.36614	3.31382	0.00277125	0.055077
ENSG00000101188.4	NTSR1	1.35747	2.76634	0.0169218	0.136126
ENSG00000116254.13	CHD5	1.35406	1.55921	0.363511	1.13206
ENSG00000187775.12	DNAH17	1.34649	1.4954	0.432112	1.28631
ENSG00000175463.7	TBC1D10C	1.3409	1.98206	0.0613325	0.261849
ENSG00000243709.1	LEFTY1	1.32607	2.16826	0.0866633	0.430597
ENSG00000164256.5	PRDM9	1.31338	3.12479	0.00530151	0.0702432
ENSG00000148082.5	SHC3	1.30963	1.84222	0.184406	0.708205
ENSG00000171124.8	FUT3	1.30348	2.83849	0.0164724	0.145502
ENSG00000113389.11	NPR3	1.28764	1.93188	0.0311797	0.128526
ENSG00000124391.4	IL17C	1.27593	4.23582	0	0.139417
ENSG00000167011.4	NAT16	1.27593	3.23582	0.00264596	0.0496656
ENSG00000204539.3	CDSN	1.27593	4.23582	0	0.0753352
ENSG00000179603.13	GRM8	1.27083	2.18137	0.0222698	0.112407
ENSG00000073150.9	PANX2	1.26554	1.38157	3.8104	10.4779
ENSG00000136531.9	SCN2A	1.25978	1.72411	0.0523001	0.184239
ENSG00000181652.14	ATG9B	1.23718	1.70252	0.100762	0.349658
ENSG00000229859.4	PGA3	1.23421	2.33891	0.0223592	0.127926
ENSG00000140839.7	CLEC18B	1.23307	1.83849	0.137352	0.528627
ENSG00000177374.8	HIC1	1.22066	1.5213	0.364359	1.10757
ENSG00000167680.11	SEMA6B	1.21703	1.3717	1.49828	4.09359
ENSG00000144821.5	MYH15	1.19097	1.74602	0.0572431	0.205781
ENSG00000167711.9	SERPINF2	1.17981	4.15336	0	0.077064
ENSG00000175877.3	WBSCR28	1.17981	3.15336	0.0104836	0.185206
ENSG00000205108.5	FAM205A	1.17981	4.15336	0	0.0428275
ENSG00000157322.12	CLEC18A	1.17877	1.64344	0.111218	0.37032
ENSG00000178078.7	STAP2	1.17791	1.9072	0.0851692	0.347533
ENSG00000173714.7	WFIKKN2	1.17538	3.0045	0.00515866	0.0626546
ENSG00000110169.6	HPX	1.17436	2.0045	0.0479545	0.211793
ENSG00000153294.7	GPR115	1.1728	1.55874	0.289968	0.907133
ENSG00000108753.8	HNF1B	1.16918	1.72541	0.0738974	0.261856
ENSG00000131386.13	GALNT15	1.16024	2.78836	0.00721813	0.0637584

RNA-Seq FKBP25 KD vs Control - top 100 upregulated genes ranked ranked by fold change.

Gene Symbol	Gene Name	GFOLD (0.01)	log2 Fold Change	siGFP (RPKM)	siFKBP25 (RPKM)
ENSG00000122733.11	KIAA1045	1.1553	1.81722	0.0500561	0.190582
ENSG00000058335.11	RASGRF1	1.15334	1.74871	0.0436454	0.157596
ENSG00000169750.4	RAC3	1.15173	1.22981	17.7483	43.9183
ENSG00000116299.12	KIAA1324	1.14514	1.8284	0.0297428	0.114332
ENSG00000187583.6	PLEKHN1	1.14268	1.63418	0.20608	0.682621
ENSG00000015413.5	DPEP1	1.14006	2.17281	0.0453209	0.229352
ENSG00000100290.2	BIK	1.13776	1.48688	1.28972	3.83301
ENSG00000267335.2	CTB-60B18.6	1.13435	1.84119	0.32578	1.26616
ENSG00000049249.4	TNFRSF9	1.11659	1.72886	0.156956	0.559516
ENSG00000159871.10	LYPD5	1.11133	1.46279	0.239415	0.699741
ENSG00000184545.6	DUSP8	1.10958	1.21886	2.99332	7.35242
ENSG00000172264.12	MACROD2	1.10674	1.53187	0.0713419	0.219363
ENSG00000261359.2	C16orf98	1.10117	2.94037	0.0187078	0.216888
ENSG00000189052.6	CGB5	1.09723	1.84611	0.267938	1.04889
ENSG00000161082.8	CELF5	1.09231	1.35195	0.385965	1.04193
ENSG00000166828.2	SCNN1G	1.09131	2.65086	0.014603	0.112866
ENSG00000117983.13	MUC5B	1.09039	2.01699	0.00770487	0.0346366
ENSG00000137090.7	DMRT1	1.09023	1.65086	0.135391	0.455425
ENSG00000183914.10	DNAH2	1.08713	1.62111	0.0285324	0.0938546
ENSG00000099860.4	GADD45B	1.08306	1.22206	3.97628	9.79104
ENSG00000130518.12	KIAA1683	1.079	1.35006	0.232759	0.627668
ENSG00000244242.1	IFITM10	1.07812	1.5348	0.145588	0.449151
ENSG00000134765.5	DSC1	1.07695	4.0659	0	0.0397184
ENSG00000164877.14	MICALL2	1.07541	1.28711	0.404234	1.04229
ENSG00000101204.11	CHRNA4	1.07234	1.49176	0.0961849	0.287521

Table A.8. RNA-Seq FKBP25 KD vs Control - top 100 downregulated genes ranked ranked by fold change.

Gene Symbol	Gene Name	GFOLD (0.01)	log2 Fold Change	siGFP (RPKM)	siFKBP25 (RPKM)
ENSG00000206177.2	HBM	-2.6573	-4.02157	1.31945	0.0740774
ENSG00000255963.1	PPIAL4A	-1.70584	-2.41054	1.65707	0.316944
ENSG00000255854.1	PPIAL4B	-1.6773	-2.24077	2.43994	0.533043
ENSG00000198161.5	PPIAL4C	-1.47839	-2.11468	1.76145	0.41779
ENSG00000205642.5	VCX3B	-1.47576	-4.39354	0.183214	0
ENSG00000100442.6	FKBP3	-1.14302	-1.2137	34.667	15.7638
ENSG00000187537.9	POTEM	-1.08146	-1.65337	0.186329	0.0614127
ENSG00000231738.6	TSPAN19	-1.04811	-2.59707	0.0928629	0.0138559
ENSG00000196604.7	POTEF	-1.03036	-2.36706	0.12428	0.0233018
ENSG00000102934.5	PLLP	-1.01077	-1.37889	1.85251	0.746962
ENSG00000154079.5	C6orf57	-0.985917	-1.31585	2.53218	1.06809
ENSG00000222036.3	POTEG	-0.98177	-1.55301	0.177962	0.0629395
ENSG00000213366.8	GSTM2	-0.91948	-1.40425	0.293442	0.115714
ENSG00000231500.2	RPS18	-0.914805	-0.941191	262.069	143.968
ENSG00000198937.8	CCDC167	-0.883927	-1.04702	21.7426	11.0899
ENSG00000196950.9	SLC39A10	-0.877288	-0.933694	15.6311	8.63105
ENSG00000162378.8	ZYG11B	-0.876294	-0.941857	9.7735	5.36603
ENSG00000113328.14	CCNG1	-0.875739	-0.91106	88.3484	49.5579
ENSG00000185097.2	OR4F16	-0.866945	-1.57153	0.854401	0.295515
ENSG00000135821.12	GLUL	-0.865133	-0.890744	57.1254	32.4988
ENSG00000268800.1	AC112205.1	-0.860742	-1.08385	73.353	36.4406
ENSG00000171517.5	LPAR3	-0.831948	-0.981158	4.41154	2.35567
ENSG00000172340.10	SUCLG2	-0.820612	-0.926373	9.86796	5.47524
ENSG00000068366.15	ACSL4	-0.803402	-0.863253	14.4944	8.40385
ENSG00000163807.4	KIAA1143	-0.801195	-0.863872	16.1285	9.3472
ENSG00000165410.10	CFL2	-0.800605	-0.85233	34.8177	20.3412
ENSG00000170035.11	UBE2E3	-0.794833	-0.862439	24.2322	14.0574
ENSG00000168542.8	COL3A1	-0.790222	-1.21421	0.305052	0.137714
ENSG00000163347.5	CLDN1	-0.786462	-0.915377	5.56167	3.10901
ENSG00000188219.10	POTEE	-0.78499	-1.4843	0.204296	0.0751901
ENSG00000105810.5	CDK6	-0.776545	-0.821588	13.1624	7.85552
ENSG00000165983.10	PTER	-0.773634	-0.86356	10.2733	5.95442
ENSG00000181804.10	SLC9A9	-0.761949	-1.90373	0.115282	0.0304381
ENSG00000106070.13	GRB10	-0.759324	-0.822439	8.25458	4.9233
ENSG00000155629.10	PIK3AP1	-0.757759	-0.929006	2.03195	1.12475
ENSG00000091317.7	CMTM6	-0.755869	-0.819617	18.2082	10.8812
ENSG00000185238.8	PRMT3	-0.752816	-0.846571	6.85708	4.0214

RNA-Seq FKBP25 KD vs Control - top 100 downregulated genes ranked ranked by fold change.

Gene Symbol	Gene Name	GFOLD (0.01)	log2 Fold Change	siGFP (RPKM)	siFKBP25 (RPKM)
ENSG00000106460.14	TMEM106B	-0.748448	-0.82629	3.89256	2.31533
ENSG00000152332.11	UHMK1	-0.748009	-0.795767	15.3438	9.32277
ENSG00000257093.2	KIAA1147	-0.746448	-0.807999	11.66	7.0244
ENSG00000230178.1	OR4F3	-0.741327	-1.59707	0.576464	0.193222
ENSG00000148672.7	GLUD1	-0.738114	-0.780686	44.0655	27.0555
ENSG00000136444.5	RSAD1	-0.736424	-0.828056	9.2739	5.5091
ENSG00000104419.10	NDRG1	-0.731031	-0.777799	14.9431	9.19307
ENSG00000186960.6	C14orf23	-0.721288	-2.59707	0.0709098	0.00869935
ENSG00000176105.9	YES1	-0.719253	-0.789159	12.9196	7.88536
ENSG00000102409.9	BEX4	-0.714275	-0.791554	40.6153	24.7473
ENSG00000189266.7	PNRC2	-0.709286	-0.758525	51.2046	31.925
ENSG00000096060.10	FKBP5	-0.709142	-0.764703	9.72211	6.03552
ENSG00000181929.7	PRKAG1	-0.706574	-0.773881	15.5009	9.56164
ENSG00000196586.9	MYO6	-0.705579	-0.758497	12.9334	8.0638
ENSG00000100522.4	GNPNAT1	-0.705294	-0.783219	13.1832	8.07917
ENSG00000088986.6	DYNLL1	-0.692078	-0.735609	56.2629	35.6408
ENSG00000138760.4	SCARB2	-0.692071	-0.756325	13.5306	8.44854
ENSG00000165476.8	REEP3	-0.690033	-0.762116	11.7637	7.31564
ENSG00000136997.10	MYC	-0.687656	-0.729709	59.3827	37.7714
ENSG00000121361.3	KCNJ8	-0.683315	-0.90948	2.63073	1.47511
ENSG00000187772.6	LIN28B	-0.679653	-0.732116	20.7604	13.1827
ENSG00000178904.14	DPY19L3	-0.676498	-0.724367	12.6946	8.10449
ENSG00000164294.9	GPX8	-0.67503	-0.760869	11.1428	6.93519
ENSG00000187109.9	NAP1L1	-0.674797	-0.697932	64.138	41.7059
ENSG00000151090.13	THRB	-0.666081	-0.760623	4.07631	2.53738
ENSG00000212999.1	AC117834.1	-0.664989	-0.846993	4.58983	2.68915
ENSG00000163541.7	SUCLG1	-0.661596	-0.736407	13.1126	8.30112
ENSG00000086062.8	B4GALT1	-0.660426	-0.730125	12.7541	8.10954
ENSG00000148516.17	ZEB1	-0.659333	-0.73057	7.22396	4.59182
ENSG00000154734.10	ADAMTS1	-0.655466	-0.682923	57.9501	38.0761
ENSG00000107679.10	PLEKHA1	-0.652992	-0.72824	4.01673	2.55728
ENSG00000024526.12	DEPDC1	-0.651584	-0.698986	23.384	15.1938
ENSG00000160307.5	S100B	-0.650933	-1.49353	0.389046	0.140583
ENSG00000178031.11	ADAMTSL1	-0.649762	-1.22956	0.083203	0.0369187
ENSG00000100503.19	NIN	-0.647652	-0.699703	8.36664	5.43348
ENSG00000170779.10	CDCA4	-0.64586	-0.71001	30.0958	19.4051
ENSG00000143416.16	SELENBP1	-0.641855	-0.726242	12.5401	7.99451
ENSG00000128872.5	TMOD2	-0.636609	-0.710454	4.90208	3.15968

RNA-Seq FKBP25 KD vs Control - top 100 downregulated genes ranked ranked by fold change.

Gene Symbol	Gene Name	GFOLD (0.01)	log2 Fold Change	siGFP (RPKM)	siFKBP25 (RPKM)
ENSG00000178202.8	KDELC2	-0.635008	-0.692113	18.9814	12.3918
ENSG00000116678.14	LEPR	-0.634273	-0.706141	5.24776	3.39265
ENSG00000151414.10	NEK7	-0.630726	-0.695337	13.5067	8.79784
ENSG00000010292.8	NCAPD2	-0.630512	-0.658846	58.6383	39.1767
ENSG00000241399.2	CD302	-0.625574	-0.722079	8.72709	5.57945
ENSG00000159352.11	PSMD4	-0.625393	-0.672196	46.2487	30.6135
ENSG00000128694.7	OSGEPL1	-0.622984	-0.786306	3.33604	2.03899
ENSG00000256043.2	CTSO	-0.615449	-1.14143	0.436885	0.206735
ENSG00000155850.7	SLC26A2	-0.615192	-0.704644	4.5	2.91205
ENSG00000198814.8	GK	-0.614364	-0.653146	44.8596	30.0892
ENSG00000103319.7	EEF2K	-0.612572	-0.696353	6.92341	4.50623
ENSG00000198729.4	PPP1R14C	-0.61224	-0.696867	20.0472	13.0434
ENSG00000116288.8	PARK7	-0.607769	-0.648071	78.0004	52.5024
ENSG00000143179.8	UCK2	-0.607379	-0.657784	17.7516	11.8682
ENSG00000035141.3	FAM136A	-0.6069	-0.66481	29.5128	19.6353
ENSG00000123570.3	RAB9B	-0.606683	-0.906397	0.983807	0.552181
ENSG00000166479.5	TMX3	-0.606534	-0.673447	8.95902	5.92483
ENSG00000170043.7	TRAPPC1	-0.60537	-0.669994	62.5572	41.4701
ENSG00000099194.5	SCD	-0.604682	-0.624978	136.35	93.2615
ENSG00000091651.4	ORC6	-0.602476	-0.673947	13.915	9.19902
ENSG00000151468.9	CCDC3	-0.601187	-0.688085	11.0717	7.24756
ENSG00000141449.10	GREB1L	-0.600517	-0.671393	5.76166	3.81571
ENSG00000164181.9	ELOVL7	-0.595815	-0.691607	7.31896	4.77914
ENSG00000173698.13	GPR64	-0.594762	-0.766477	1.05304	0.652494
ENSG00000256977.6	LIMS3	-0.594632	-0.724868	8.87191	5.66004